

ИЗВЕСТИЯ ВЫСШИХ УЧЕБНЫХ ЗАВЕДЕНИЙ ЧЕРНАЯ МЕТАЛЛУРГИЯ

IZVESTIYA. FERROUS METALLURGY

fermet.misis.ru

2024 Том 67 № 5
Vol. No.

МЕТАЛЛУРГИЧЕСКИЕ ТЕХНОЛОГИИ

Оценка результативности применения технологических мероприятий по продлению кампании доменной печи № 5 ПАО «Северсталь» 2006 – 2024 гг. при исследовании ее рабочего пространства в период проведения капитального ремонта I разряда

МАТЕРИАЛОВЕДЕНИЕ

Деформация и разрушение термически обработанных лент аморфного сплава системы Co – Fe – Cr – Si – В при индентировании

ФИЗИКО-ХИМИЧЕСКИЕ ОСНОВЫ МЕТАЛЛУРГИЧЕСКИХ ПРОЦЕССОВ

Микрогетерогенное строение жидких чугунов ИЧХ28Н2, ИЧ310Х24М2Ф4ТР



ISSN 0368-0797
eISSN 2410-2091

ИЗВЕСТИЯ ВЫСШИХ УЧЕБНЫХ ЗАВЕДЕНИЙ ЧЕРНАЯ МЕТАЛЛУРГИЯ

Научно-технический журнал

Издается с января 1958 г. Выпускается 6 раз в год

2024 Том 67 № 5
Vol. No.

IZVESTIYA FERROUS METALLURGY

Scientific and Technical Journal

Published since January 1958. Issued 6 times a year

IZVESTIYA FERROUS METALLURGY

www.fermet.misis.ru

ISSN 0368-0797 (Print) ISSN 2410-2091 (Online)

Alternative title:

Izvestiya vuzov. Chernaya metallurgiya

Founders:



Editorial Board:

Sailaubai O. Baisanov, Dr. Sci. (Eng.), Prof., Abishev Chemical-Metallurgical Institute, Karaganda, Republic of Kazakhstan
Vladimir D. Belov, Dr. Sci. (Eng.), Prof., NUST MISIS, Moscow
Anatolii A. Brodov, Cand. Sci. (Econ.), Bardin Central Research Institute for Ferrous Metallurgy, Moscow
Il'ya V. Chumanov, Dr. Sci. (Eng.), Prof., South Ural State Research University, Chelyabinsk
Andrei N. Dmitriev, Dr. Sci. (Eng.), Prof., Academician, RANS, A.M. Prokhorov Academy of Engineering Sciences, Institute of Metallurgy, Ural Branch of RAS, Ural Federal University, Yekaterinburg
Aleksei V. Dub, Dr. Sci. (Eng.), Prof., JSC "Science and Innovations", Moscow
Mikhail R. Filonov, Dr. Sci. (Eng.), Prof., NUST MISIS, Moscow
Sergei M. Gorbatyuk, Dr. Sci. (Eng.), Prof., NUST MISIS, Moscow
Konstantin V. Grigorovich, Academician of RAS, Dr. Sci. (Eng.), Baikov Institute of Metallurgy and Materials Science of RAS, Moscow
Victor E. Gromov, Dr. Sci. (Eng.), Prof., Siberian State Industrial University, Novokuznetsk
Aleksei G. Kolmakov, Dr. Sci. (Eng.), Corresponding Member of RAS, Baikov Institute of Metallurgy and Materials Science of RAS, Moscow
Valerii M. Kolokol'tsev, Dr. Sci. (Eng.), Prof., Magnitogorsk State Technical University, Magnitogorsk
Mariya V. Kostina, Dr. Sci. (Eng.), Baikov Institute of Metallurgy and Materials Science of RAS, Moscow
Konstantin L. Kosyrev, Dr. Sci. (Eng.), Academician of RANS, Electrosteel Heavy Engineering Works JSC, Moscow
Yuliya A. Kurganova, Dr. Sci. (Eng.), Prof., Bauman Moscow State Technical University, Moscow
Linn Horst, Linn High Therm GmbH, Hirschbach, Germany
Vladimir I. Lysak, Academician of RAS, Dr. Sci. (Eng.), Prof., Rector, Volgograd State Technical University, Volgograd
Valerii P. Meshalkin, Dr. Sci. (Eng.), Academician of RAS, Prof., D.I. Mendeleev Russian Chemical-Technological University, Moscow
Radik R. Mulyukov, Dr. Sci. (Phys.-Chem.), Prof., Corresponding Member of RAS, Institute of Metals Superplasticity Problems of RAS, Ufa

In accordance with paragraph 5 of the Rules for the formation of the Higher Attestation Commission list journal "Izvestiya. Ferrous metallurgy" is included in the list of leading peer-reviewed scientific journals, publication in which is taken into account in the defense of candidate and doctoral dissertations, as indexed in international data bases.

Editor-in-Chief:

Leopol'd I. Leont'ev, Academician, Adviser of the Russian Academy of Sciences; Dr. Sci. (Eng.), Prof., NUST "MISIS"; Chief Researcher, Institute of Metallurgy UB RAS, Moscow
4 Leninskii Ave., Moscow 119049, Russian Federation
National University of Science and Technology "MISIS"

Deputy Editor-in-Chief:

Evgenii V. Protopopov, Dr. Sci. (Eng.), Prof., Siberian State Industrial University, Novokuznetsk

Publisher:

National University of Science and Technology "MISIS"

Editorial Office Address:

in Moscow
4 Leninskii Ave., Moscow 119049, Russian Federation
National University of Science and Technology "MISIS"
Tel.: +7 (495) 638-44-11
E-mail: fermet.misis@mail.ru, ferrous@misis.ru

in Novokuznetsk
42 Kirova Str., Novokuznetsk, Kemerovo Region – Kuzbass
654007, Russian Federation
Siberian State Industrial University
Tel.: +7 (3843) 74-86-28 E-mail: redjizvz@sibsiu.ru

Sergei A. Nikulin, Dr. Sci. (Eng.), Prof., Corresponding Member of RANS, NUST MISIS, Moscow
Asylbek Kh. Nurumgaliev, Dr. Sci. (Eng.), Prof., Karaganda State Industrial University, Karaganda, Republic of Kazakhstan
Oleg I. Ostrovski, Dr. Sci. (Eng.), Prof., University of New South Wales, Sydney, Australia
Loris Pietrelli, Dr., Scientist, Italian National Agency for New Technologies, Energy and Sustainable Economic Development, Rome, Italy
Igor' Yu. Pyshmintsev, Dr. Sci. (Eng.), Russian Research Institute of the Pipe Industry, Chelyabinsk
Andrei I. Rudskoi, Academician of RAS, Dr. Sci. (Eng.), Prof., Rector, Peter the Great Saint-Petersburg Polytechnic University, Saint-Petersburg
Oleg Yu. Sheshukov, Dr. Sci. (Eng.), Prof., Ural Federal University, Yekaterinburg
Laura M. Simonyan, Dr. Sci. (Eng.), Prof., NUST MISIS, Moscow
Robert F. Singer, Dr. Sci. (Eng.), Prof., Friedrich-Alexander University, Germany
Boris A. Sivak, Cand. Sci. (Eng.), Prof., VNIIMETMASH Holding Company, Moscow
Leonid A. Smirnov, Dr. Sci. (Eng.), Prof., Academician of RAS, OJSC "Ural Institute of Metals", Yekaterinburg
Sergei V. Solodov, Cand. Sci. (Eng.), NUST MISIS, Moscow
Marcus Speidel, Dr. Natur. Sci., Prof., Swiss Academy of Materials, Switzerland
Nikolai A. Spirin, Dr. Sci. (Eng.), Prof., Ural Federal University, Yekaterinburg
Guoi Tang, Institute of Advanced Materials of Tsinghua University, Shenzhen, China
Mikhail V. Temlyantsev, Dr. Sci. (Eng.), Prof., Siberian State Industrial University, Novokuznetsk
Ekaterina P. Volynkina, Dr. Sci. (Eng.), Advisor, ALE "Kuzbass Association of Waste Processors", Novokuznetsk
Aleksei B. Yur'ev, Dr. Sci. (Eng.), Rector, Siberian State Industrial University, Novokuznetsk
Vladimir S. Yusufov, Dr. Sci. (Eng.), Prof., Baikov Institute of Metallurgy and Materials Science of RAS, Moscow
Vladimir I. Zhuchkov, Dr. Sci. (Eng.), Prof., Institute of Metallurgy, Ural Branch of RAS, Ural Federal University, Yekaterinburg
Michael Zinigrad, Dr. Sci. (Physical Chemistry), Prof., Rector, Ariel University, Israel
Vladimir I. Zolotukhin, Dr. Sci. (Eng.), Prof., Tula State University, Tula

Indexed: Scopus, Russian Science Citation Index (RSCI), Research Bible, Chemical Abstracts, OCLC and Google Scholar

Registered in Federal Service for Supervision in the Sphere of Mass Communications **PI number FS77-35456.**



Articles are available under Creative Commons Attribution 4.0 License.

ИЗВЕСТИЯ ВЫСШИХ УЧЕБНЫХ ЗАВЕДЕНИЙ ЧЕРНАЯ МЕТАЛЛУРГИЯ

www.fermet.misis.ru

ISSN 0368-0797 (Print) ISSN 2410-2091 (Online)

Варианты названия:

Известия вузов. Черная металлургия

Izvestiya. Ferrous Metallurgy

Учредители:



Редакционная коллегия:

С. О. Байсанов, д.т.н., профессор, ХМИ им. Ж.Абишева, г. Караганда, Республика Казахстан

В. Д. Белов, д.т.н., профессор, НИТУ МИСИС, г. Москва

А. А. Бродов, к.экон.н., ФГУП «ЦНИИчермет им. И.П. Бардина», г. Москва

Е. П. Волынкина, д.т.н., советник, ОЮЛ «Кузбасская Ассоциация переработчиков отходов», г. Новокузнецк

С. М. Горбатько, д.т.н., профессор, НИТУ МИСИС, г. Москва

К. В. Григорович, академик РАН, д.т.н., ИМЕТ им. А.А. Байкова РАН, г. Москва

В. Е. Громов, д.ф.-м.н., профессор, СибГИУ, г. Новокузнецк

А. Н. Дмитриев, д.т.н., профессор, академик РАЕН, академик АИН РФ, г. Екатеринбург

А. В. Дуб, д.т.н., профессор, ЗАО «Наука и инновации», г. Москва

В. И. Жучков, д.т.н., профессор, ИМЕТ УрО РАН, г. Екатеринбург

Р. Ф. Зингер, д.т.н., профессор, Институт Фридриха-Александра, Германия

М. Зиниград, д.т.н., профессор, Институт Ариэля, Израиль

В. И. Золотухин, д.т.н., профессор, ТулГУ, г. Тула

А. Г. Колмаков, д.т.н., чл.-корр. РАН, ИМЕТ им. А.А. Байкова РАН, г. Москва

В. М. Колокольцев, д.т.н., профессор, МГТУ им. Г.И. Носова, г. Магнитогорск

М. В. Костина, д.т.н., ИМЕТ им. А.А. Байкова РАН, г. Москва

К. Л. Косырев, д.т.н., академик РАЕН, ОАО «Электростальский завод тяжелого машиностроения», г. Москва

Ю. А. Курганова, д.т.н., профессор, МГТУ им. Н.Э. Баумана, г. Москва

Х. Линн, ООО «Линн Хай Терм», Германия

В. И. Лысак, академик РАН, д.т.н., профессор, ВолГТУ, г. Волгоград

В. П. Мешалкин, академик РАН, д.т.н., профессор, РХТУ им. Д.И. Менделеева, г. Москва

В соответствии п. 5 Правил формирования перечня ВАК журнал «Известия вузов. Черная металлургия» входит в перечень ведущих рецензируемых научных журналов и изданий, публикация в которых учитывается при защитах кандидатских и докторских диссертаций как индексируемый в МБД.

Главный редактор:

Леопольд Игоревич Леонтьев, академик РАН, советник, Президиум РАН; д.т.н., профессор, НИТУ «МИСИС»; главный научный сотрудник, Институт металлургии УрО РАН
Россия, 119049, Москва, Ленинский просп., д. 4, стр. 1, Национальный исследовательский технологический университет «МИСИС»

Заместитель главного редактора:

Евгений Валентинович Протопопов, д.т.н., профессор, Сибирский государственный индустриальный университет г. Новокузнецк

Издатель:

Национальный исследовательский технологический университет «МИСИС»

Адреса подразделений редакции:

в Москве

Россия, 119049, Москва, Ленинский просп., д. 4, стр. 1
Национальный исследовательский технологический университет «МИСИС»

Тел.: +7 (495) 638-44-11 E-mail: ferrous@isis.ru

в Новокузнецке

Россия, 654007, Новокузнецк,
Кемеровская обл. – Кузбасс, ул. Кирова, зд. 42
Сибирский государственный индустриальный университет
Тел.: +7 (3843) 74-86-28 E-mail: redjivz@sibsiu.ru

Р. Р. Мулюков, д.ф.м.-н., профессор, чл.-корр. ФГБУН ИПСМ РАН, г. Уфа
С. А. Никулин, д.т.н., профессор, чл.-корр. РАЕН, НИТУ МИСИС, г. Москва
А. Х. Нурумгалиев, д.т.н., профессор, КГИУ, г. Караганда, Республика Казахстан
О. И. Островский, д.т.н., профессор, Университет Нового Южного Уэльса, Сидней, Австралия
Л. Пиетрелли, д.т.н., итальянское национальное агентство по новым технологиям, энергетике и устойчивому экономическому развитию, Рим, Италия
И. Ю. Пышминцев, д.т.н., РосНИТИ, г. Челябинск
А. И. Рудской, академик РАН, д.т.н., профессор, СПбПУ Петра Великого, г. Санкт-Петербург
Б. А. Сивак, к.т.н., профессор, АО АХК «ВНИИМТМАШ», г. Москва
Л. М. Симонян, д.т.н., профессор, НИТУ МИСИС, г. Москва
Л. А. Смирнов, академик РАН, д.т.н., профессор, ОАО «Уральский институт металлов», г. Екатеринбург
С. В. Солодов, к.т.н., НИТУ МИСИС, г. Москва
Н. А. Спирин, д.т.н., профессор, УрФУ, г. Екатеринбург
Г. Танг, Институт перспективных материалов университета Циньхуа, г. Шеньжень, Китай
М. В. Темлянецев, д.т.н., профессор, СибГИУ, г. Новокузнецк
М. Р. Филонов, д.т.н., профессор, НИТУ МИСИС, г. Москва
И. В. Чуманов, д.т.н., профессор, ЮУрГУ, г. Челябинск
О. Ю. Шешуков, д.т.н., профессор УрФУ, г. Екатеринбург
М. О. Шпайдель, д.ест.н., профессор, Швейцарская академия материаловедения, Швейцария
А. Б. Юрьев, д.т.н., ректор, СибГИУ, г. Новокузнецк
В. С. Юсупов, д.т.н., профессор, ИМЕТ им. А.А. Байкова РАН, г. Москва

Индексирование: Scopus, Russian Science Citation Index (RSCI), Research Bible, Chemical Abstracts, OCLC и Google Scholar

Зарегистрирован Федеральной службой по надзору в сфере связи и массовых коммуникаций ПИ № ФС77-35456.



Статьи доступны под лицензией Creative Commons Attribution 4.0 License.

HISTORY OF METALLURGY

- Rudskoi A.I., Kodzhaspirov G.E. History and current state of metallurgy in St. Petersburg 500

METALLURGICAL TECHNOLOGIES

- Ivannikov A.Yu., Yusupov V.S. Recent development in powder metallurgy of high entropy alloys for high-temperature applications. Brief review 509

- Kal'ko A.A., Leont'ev L.I., Volkov E.A. Assessment of the effectiveness of technological measures to extend the campaign of blast furnace No. 5 of PJSC Severstal (2006 – 2024) based on an examination of its working space during a first-category overhaul 520

- Grudinsky P.I., Yurtaeva A.A., Volkov A.I., Dyubanov V.G. A study on processing of blast furnace dust and sludge using reduction roasting and magnetic separation 531

ECOLOGY AND RATIONAL USE OF NATURAL RESOURCES

- Belanov I.P., Shipilova A.M., Mezentseva O.P. Mineralogical and granulometric composition of soils formed on the surface of iron ore tailings dumps 542

MATERIALS SCIENCE

- Em A.Yu., Komolova O.A., Grigorovich K.V., Rumyantseva S.B. Formation of non-metallic inclusions in production of 08Kh18N10T corrosion-resistant steel 549

- Permyakova I.E., Kostina M.V. Deformation and fracture of heat treated ribbon of amorphous Co–Fe–Cr–Si–B alloy during indentation 556

- Gromov V.E., Chapaikin A.S., Bashchenko L.P. Structural-phase states and properties of high-speed surfacing after tempering and electron beam processing 563

- Gostevskaya A.N., Markidonov A.V., Starostenkov M.D., Lubyanoi D.A. Simulation of structural changes in metal under high-intensity external influence 567

ИСТОРИЯ ОТРАСЛИ

- Рудской А.И., Коджаспиров Г.Е. История и современное состояние металлургии в Санкт-Петербурге 500

МЕТАЛЛУРГИЧЕСКИЕ ТЕХНОЛОГИИ

- Иванников А.Ю., Юсупов В.С. Новые достижения в области порошковой металлургии высокоэнтропийных сплавов для высокотемпературных приложений. Краткий обзор 509

- Калько А.А., Леонтьев Л.И., Волков Е.А. Оценка результативности применения технологических мероприятий по продлению кампании доменной печи № 5 ПАО «Северсталь» 2006 – 2024 гг. при исследовании ее рабочего пространства в период проведения капитального ремонта I разряда 520

- Грудинский П.И., Юртаева А.А., Волков А.И., Дюбанов В.Г. Исследование процессов переработки доменных пыли и шлама с использованием восстановительного обжига и магнитной сепарации 531

ЭКОЛОГИЯ И РАЦИОНАЛЬНОЕ ПРИРОДОПОЛЬЗОВАНИЕ

- Беланов И.П., Шпилова А.М., Мезенцева О.П. Минералогический и granulометрический состав почв формирующихся на поверхности железорудных хвостохранилищ 542

МАТЕРИАЛОВЕДЕНИЕ

- Ем А.Ю., Комолова О.А., Григорович К.В., Румянцева С.Б. Формирование неметаллических включений при производстве коррозионностойкой стали 08X18N10T 549

- Пермякова И.Е., Костина М.В. Деформация и разрушение термически обработанных лент аморфного сплава системы Co – Fe – Cr – Si – В при индентировании 556

- Громов В.Е., Чапайкин А.С., Башченко Л.П. Структурно-фазовые состояния и свойства быстрорежущей наплавки после отпуска и электронно-пучковой обработки 563

- Гостевская А.Н., Маркидонов А.В., Старostenков М.Д., Лубяной Д.А. Моделирование структурных изменений в металле при высокоинтенсивном внешнем воздействии 567

**PHYSICO-CHEMICAL BASICS
OF METALLURGICAL PROCESSES**

- Goikhenberg Yu.N., Polukhin D.S.** Effect of silicon and vanadium on corrosion-mechanical properties of high-nitrogen Cr – Mn steels 573
- Tsepelev V.S., Sinitsin N.I., Chikova O.A., Potapov M.G., V'yukhin V.V.** Microheterogeneous structure of liquid cast irons IChKh28N2 and ICh310Kh24M2F4TR 579

**INNOVATIONS IN METALLURGICAL
INDUSTRIAL AND LABORATORY
EQUIPMENT, TECHNOLOGIES
AND MATERIALS**

- Bogdanova N.A., Zhilin S.G.** Influence of compression modes of waxy powders on stress-strain state of compacts used in precision casting 593
- Tkacheva A.V., Abashkin E.E.** Influence of combined thermal effect of electric arc welding with aluminothermic backfill on internal stresses in a steel plate.... 604
- Nikitin A.G., Bazhenov I.A., Kurochkin N.M.** Improving the efficiency of raw material preparation for metallurgical processing 612

**INFORMATION TECHNOLOGIES
AND AUTOMATIC CONTROL
IN FERROUS METALLURGY**

- Belomytsev M.Yu.** Type of generalized mathematical model for describing large hot deformations 616

**ФИЗИКО-ХИМИЧЕСКИЕ ОСНОВЫ
МЕТАЛЛУРГИЧЕСКИХ ПРОЦЕССОВ**

- Гойхенберг Ю.Н., Полухин Д.С.** Влияние кремния и ванадия на коррозионно-механические свойства высокоазотистых Cr – Mn сталей 573
- Цепелев В.С., Синицин Н.И., Чикова О.А., Потопов М.Г., Вьюхин В.В.** Микрогетерогенное строение жидких чугунов ИЧХ28Н2, ИЧ310Х24М2Ф4ТР .. 579

**ИННОВАЦИИ В МЕТАЛЛУРГИЧЕСКОМ
ПРОМЫШЛЕННОМ И ЛАБОРАТОРНОМ
ОБОРУДОВАНИИ, ТЕХНОЛОГИЯХ
И МАТЕРИАЛАХ**

- Богданова Н.А., Жилин С.Г.** Влияние режимов уплотнения воскообразных порошков на напряженно-деформированное состояние прессовок, применяемых в точном литье 593
- Ткачева А.В., Абашкин Е.Е.** Влияние комбинированного теплового воздействия электродуговой сварки с аломотермитной засыпкой на внутренние напряжения в стальной пластине 604
- Никитин А.Г., Баженов И.А., Курочкин Н.М.** Повышение эффективности подготовки сырья для металлургических переделов 612

**ИНФОРМАЦИОННЫЕ ТЕХНОЛОГИИ
И АВТОМАТИЗАЦИЯ
В ЧЕРНОЙ МЕТАЛЛУРГИИ**

- Беломытцев М.Ю.** Вид обобщенной математической модели для описания больших горячих деформаций .. 616



UDC 669

DOI 10.17073/0368-0797-2024-5-500-508



Original article

Оригинальная статья

HISTORY AND CURRENT STATE OF METALLURGY IN ST. PETERSBURG

A. I. Rudskoi, G. E. Kodzhaspirov

■ Peter the Great St. Petersburg Polytechnic University (29 Politekhnicheskaya Str., St. Petersburg 195251, Russian Federation)

✉ gkodzhaspirov@yandex.ru

Abstract. Development of the metallurgical industry in St. Petersburg played an outstanding role in the history of world and domestic science and technology. The founding fathers of domestic metallurgy: D.K. Chernov and his contemporaries had such a strong influence on the development of metal science that metallurgical science in Russia continued to develop successfully throughout the century and achieved impressive results in the 20th century and the beginning of the 21st century both in theoretical and in applied areas. However, the history of metallurgy in St. Petersburg wasn't systematically covered in scientific and technical periodicals in recent years. Publishing this article in the year of the 300th anniversary of the Russian Academy of Sciences, we highlight current issues of history, continuity of traditions and prospects for the development of metallurgy in one of the leading regions of our country.

Keywords: history of metallurgy, steel, alloy, St. Petersburg, industrial enterprises, scientific schools, leading scientists

For citation: Rudskoi A.I., Kodzhaspirov G.E. History and current state of metallurgy in St. Petersburg. *Izvestiya. Ferrous Metallurgy*. 2024;67(5): 500–508. <https://doi.org/10.17073/0368-0797-2024-5-500-508>

ИСТОРИЯ И СОВРЕМЕННОЕ СОСТОЯНИЕ МЕТАЛЛУРГИИ В САНКТ-ПЕТЕРБУРГЕ

А. И. Рудской, Г. Е. Коджаспиров

■ Санкт-Петербургский политехнический университет Петра Великого (Россия, 195251, Санкт-Петербург, ул. Политехническая, 29)

✉ gkodzhaspirov@yandex.ru

Аннотация. Развитие металлургической отрасли в Санкт-Петербурге сыграло выдающуюся роль в истории мировой и отечественной науки и техники. Отцы-основатели отечественной металлургии Д.К. Чернов и его современники оказали столь сильное влияние на развитие науки о металлах, что металлургическая наука в России продолжала успешно развиваться в течение века и достигла в XX в. и начале XXI в. впечатляющих результатов как в теоретической, так и в прикладной областях. Однако история металлургии в Санкт-Петербурге систематически не освещалась в научно-технической периодической печати последних лет. Публикуя данную статью в год 300-летнего юбилея Российской академии наук, мы освещаем актуальные вопросы истории, преемственности традиций и перспектив развития металлургии в одном из ведущих регионов нашей страны.

Ключевые слова: история металлургии, сталь, сплав, Санкт-Петербург, промышленные предприятия, научные школы, ведущие ученые

Для цитирования: Рудской А.И., Коджаспиров Г.Е. История и современное состояние металлургии в Санкт-Петербурге. *Известия вузов. Черная металлургия*. 2024;67(5):500–508. <https://doi.org/10.17073/0368-0797-2024-5-500-508>

HISTORY OF ENTERPRISES IN THE INDUSTRY

One of the first metallurgical enterprises in St. Petersburg and Russia are the Izhora, Kirov (formerly Putilov), and Obukhov plants [1 – 4].

The history of the *Izhora Plants* began in the 18th century with a sawmill that processed timber for shipbuilding. The enterprise was officially established in 1722 by decree of Peter I, the first emperor of Russia. Since then, the Izhora Plants were pioneers in many areas:

the first steamship, the first mine sweepers, and the first tank [3]. It was here that the pride of Russia – the Baltic Fleet – was created. By the beginning of the 21st century, the plant's main focus had become the production of equipment for the nuclear industry and oil and gas refining. The modernization of the enterprise transformed the Izhora Plants into a unique industrial cluster, where equipment is produced for the most complex industries. More than sixty power units of both Russian and foreign nuclear power plants operate on equipment manufactured in Kolpino, and over a hundred high-pressure vessels are in use at oil and gas refineries across the country. Today, the Izhora Plants are capable of producing unique units of any complexity.

The **Kirov Plant** (formerly Putilov), founded in 1801 as an iron foundry for casting shells, became, during Soviet times, the largest plant for tractor and special machinery manufacturing, with almost a full cycle of metallurgical production [2; 3]. In 1868, the plant was purchased from state ownership by engineer and mathematician N.I. Putilov, who quickly organized the rolling of rails, which were of better quality compared to the English and Belgian ones. In 1868, the plant was purchased from the treasury by engineer and mathematician N.I. Putilov, who quickly organized the rolling of rails, which were of better quality compared to English and Belgian ones. The plant produced locomotives, wagons, dredgers, tool steels, and the famous 76-mm regimental gun. Already at that time, Russian engineers were conducting serious scientific research and developing original designs. The chemical and metallographic laboratories played an outstanding role in the creation of new steel grades and in improving technology. Famous metallurgists such as A.A. Rzheshotarsky, N.I. Belyaev, N.T. Gudtsov, and others worked here, developing the theory of steel alloying. There were no automobile factories in Leningrad (St. Petersburg). Tractors “Kirovets” were produced at the Kirov Plant. The plant had and still has a metallurgical production facility (now JSC Metallurgical Works “Petrostal”), including steel production, rolling mills (billet and section), forging and stamping production, thermal treatment workshops, and a well-equipped central factory laboratory with highly qualified personnel (highly skilled engineers, doctors, and candidates of sciences). One of the founders of this laboratory was Academician N.T. Gudtsov, who worked at the Putilov (later Kirov) Plant from 1913 to 1928 as its head. During this period, under his leadership, the structure and properties, as well as the heat treatment regimes, of special structural and tool steels were analyzed [2 – 4]. During the war, N.T. Gudtsov led work on the creation of special steels for the defense industry, and the Kirov Plant carried out work on the creation and production of steels for tanks, which were also manufactured there. In the post-war period, the laboratory became a scientific-production center for mastering steels and

alloys, as well as products made from them, for tanks, military shipbuilding, tractors, and other products. After a prolonged stagnation (in the post-Soviet period), JSC Metallurgical Works “Petrostal” began producing modern steel products and is currently in a development stage, manufacturing carbon and highly alloyed special steels and alloys, including for special purposes.

In 2019 – 2020, technical upgrades were carried out at the enterprise, resulting in the creation of a new metallurgical complex, LLC “NPO Laboratory of Special Steels and Alloys”, capable of producing new steel grades for key industries, namely: the nuclear and defense industries, medicine, shipbuilding and aerospace, instrumentation, special machinery manufacturing, and electrical engineering.

In 2020, to produce higher-quality metallurgical products, the enterprise launched an electro-slag remelting (ESR) facility. Rolling is produced from carbon, alloyed structural, stainless corrosion-resistant, heat-resistant, and tool steels and alloys.

The **Obukhov Plant** was at the forefront of Russian steelmaking, built the first Soviet aircraft engine, and “turned the angel weathervane” on the spire of the Peter and Paul Fortress [5]. In 2020, the enterprise with its 157-year history celebrated a special anniversary – 200 years since the birth of its founder, metallurgist Pavel Obukhov. The Obukhov Plant was established on May 16, 1863, by agreement with the Naval Ministry, but at its origins stood a partnership of three private individuals: metallurgist Pavel Obukhov, industrialist Nikolai Putilov, and merchant Sergey Kudryavtsev. Alexander II allocated part of the land of the former Imperial Alexandrovskaya Manufactory, with residential buildings and structures, for the new production. The main task of the plant was to produce steel for manufacturing artillery guns. The state urgently needed to rearm the army and navy, but replacing obsolete bronze cannons with foreign designs would have been very costly for the treasury. Import substitution was required. The plant was built very quickly. On April 17, 1864, it produced its first 294 poods of steel, and on May 12, in the presence of the emperor, a blank for an eight-foot cannon was cast. The full launch of production took about a year, during which time the partnership had to take a loan from the Naval Ministry to purchase equipment abroad, and until the debt was repaid, the Obukhov Steel and Gun Plant was under the control of this department. Obukhov steel was used to manufacture not only artillery guns but also wheels, tires, and axles for railway cars, armor and parts of steam engines for ships, surgical, drafting, and locksmith tools, as well as barrels and magazine boxes for Berdan rifles. Moreover, Russian steel began to be sold to England and Germany, as it was not inferior in quality to foreign steel but was several times cheaper.

In 1886, the plant was transferred to state ownership with the buyout of shares from the owners. It was a profitable and well-equipped enterprise, consisting of five workshops (crucible, steelmaking, hammering, iron casting, and gun finishing), as well as a forge, laboratory, gas plant, and wood drying facility. Even after transitioning to state ownership, the plant operated on its own funds, allowing it to invest relatively freely in modern equipment, capacity expansion, foreign trips for engineers and technicians, and so on. By 1913, at its 50th anniversary, Obukhov Plant had become one of the largest gun and steelmaking enterprises in Russia and Europe, a major competitor of the German Krupp firm and the British Armstrong. During this period, it produced more than 90 % of the armament of the Russian navy and more than 50 % of army guns, including the legendary gun of the cruiser “Aurora.” By 1914, the plant employed more than 10,000 workers. For its employees, a stone church and residential houses were built, a vocational school and a general school were established, and a library and a hospital with an outpatient clinic were organized. In December 1917, the Obukhov Plant stopped working, and all 12,000 workers were laid off. After 2.5 months of inactivity, the plant received its first large order in the new reality: the production of 1,000 “Holt” system tracked tractors with engines of 40 and 75 horsepower. The first three units were completed in 1919 and sent to the front for transporting large guns.

In 1921, the steel production was revived, and the following year, the plant received a new name – “Bolshevik,” which it bore until 1992. By November 7, 1923, the first Soviet aircraft engine was assembled here. In 1935, the “Sickle and Hammer” emblems were created with inlaid gemstones for the first Kremlin stars – one of which later adorned the spire of the Northern River Terminal in Moscow. In 1937, “Bolshevik” produced the steel frames for the glowing ruby stars.

Between 1929 and 1937, the plant participated in the construction of the Magnitogorsk and Kuznetsk metallurgical complexes, supplying tunnel segments, escalators, and shield tunneling machines for the Moscow Metro.

During World War II, “Bolshevik” produced more than 20,000 armor-piercing and high-explosive shells, 125,000 mines, over 90,000 parts for “Katyusha” rocket launchers, and 11,000 parts for Maxim machine guns. Additionally, 30 artillery batteries were created on railway platforms, and serial production of a 100-mm caliber anti-tank gun was established. Around 6,000 plant employees went to the front. From the factory volunteers, a worker battalion, five partisan units, a fighter battalion, and a people’s militia regiment were formed. Women and teenagers replaced men at the machines and open-hearth furnaces, and veterans returned to the production lines. The work did not stop day or night. Despite all the hard-

ships, in just July and August 1941, as much metal was smelted as during the entire first half of the pre-war year.

In the summer of 1941, part of the workers and technical specialists, along with equipment, were sent to Stalingrad, then to the Urals and Siberia, where they worked at various enterprises in the rear. The damage inflicted on the plant by the war and blockade was immense. The repair of workshops and the restoration of production were completed only by the end of 1948. By this time, the plant had mastered the production of oil pumps for the chemical industry and resumed the production of tunnel segments for the Moscow and later Leningrad metro systems. In 1957, the open-hearth furnaces were automated, making the work of steelmakers easier and more productive.

In the 1960s and 1970s, “Bolshevik” created launch systems for the “Sopka,” “Shtorm,” S-300F “Fort” anti-aircraft and cruise missiles, as well as containers for silo-based intercontinental ballistic missiles. The plant also produced equipment for nuclear reactors at the Leningrad, Ignalina, and Kursk nuclear power plants. In the 1980s, the enterprise continued to produce steel of various grades, cast and forged products, shafts for ships, sucker rod pumps for oil production, components and parts for nuclear power plants, and agricultural machinery.

The plant also manufactured long-range space communication antenna systems with a mirror diameter of up to 70 m, and in 1982, it produced ground equipment for the “Energia-Buran” space system.

In 1992, seventy years after its renaming, the plant once again became the State Obukhov Plant (GOZ). Despite the difficulties experienced by industry after the collapse of the USSR, it continued to operate, striving to preserve its workforce and production capacities. In 1996, the enterprise won several international quality awards: the 10th Anniversary Golden European Award (France) and the 21st International Prize (USA). Additionally, the plant received a German TUV quality certificate. Besides manufacturing traditional machinery products, the enterprise also fulfilled unique orders for St. Petersburg. The State Obukhov Plant chromed the spheres for the Pulkovo Observatory, galvanized the axes of the Rostal Columns, and restored the lost technology for making the bearings of the turning mechanism of the angel on the spire of the Peter and Paul Fortress. In 2002, the plant was incorporated into the Almaz-Antey Air Defense Concern, and in 2003, the Federal State Unitary Enterprise “State Obukhov Plant” was reorganized into the Open Joint-Stock Company “GOZ Obukhov Plant.” In 2004, by decree of the President of the Russian Federation, the plant was included in the list of the 100 most important strategic enterprises of the country. In 2008, a unique defense-industrial technopark was established on the basis of GOZ, uniting seven leading St. Petersburg enterprises of the Almaz-Antey concern.

Today, the Obukhov Plant is one of the leading enterprises in Russia's military-industrial complex. Along with civilian products for the nuclear power industry, shipbuilding, and other sectors, the plant designs, manufactures, and services various weapons systems and military equipment. The plant's traditional customers are the navy, aviation, missile forces, and aerospace forces. Equipment for missile complexes, launch and antenna systems, and damping systems are just part of its product range. The equipment designed and manufactured at the Obukhov Plant is successfully operated in Russia and abroad.

In addition to the aforementioned major enterprises, metallurgy also developed in St. Petersburg (Leningrad) at other plants, including Krasny Vyborzhets (non-ferrous metal production), the Metal Plant, and the Turbine Blade Plant (now part of JSC "Power Machines"), as well as the steel rolling plant. The latter ceased to exist in 2007, but the remaining part of the plant continues to operate under the name LLC "Petersburg Precision Alloys Plant", producing items for the energy machinery industry (manufacturing flat and round rolled products).

HISTORY IN PERSONS

Dmitry Konstantinovich Chernov is rightfully considered the founding father of Russian metallurgy [4; 5]. He graduated from the St. Petersburg Technological Institute in 1858 with a silver medal and began working there. Dmitry Konstantinovich initially worked at the Technological Institute as a lecturer and later as a museum curator and librarian. Three years later, he became actively involved in the creation of the Russian Technical Society, which was inaugurated on May 24, 1866. D.K. Chernov's entire subsequent scientific and public career was closely linked to this society. In 1866, he resigned from the institute and took a position as a technician in the hammer shop of the Obukhov Plant, eventually becoming a metallurgical engineer.

A task was set before the young engineer: to identify and explain the reason for the unsatisfactory quality of some cannons compared to the superior quality of others, cast from the same steel grade under what were thought to be identical conditions at the time. Chernov began his work with great enthusiasm, spending sleepless nights in mechanical and chemical laboratories, staying by the furnaces late into the night, learning from experienced workers how to determine the temperature of red-hot steel forgings by sight. Dmitrii Konstantinovich noticed changes in the structure of fractured surfaces of failed items. He examined the fracture points using a magnifying glass and a microscope and found that their structures were significantly different. He thus established that fine-grained steel could withstand much higher tensile stress. Following this, Chernov set out to discover how steel with a fine-grained structure was formed. Using the method

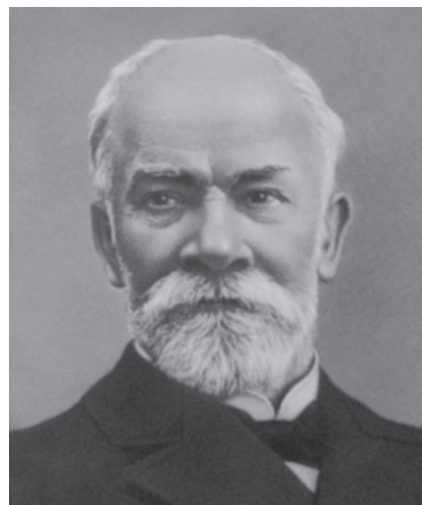


Fig. 1. Dmitrii Konstantinovich Chernov

Рис. 1. Дмитрий Константинович Чернов

of rapid forging with a heavy hammer, the scientist concluded that changes in steel structure occur under the influence of temperature, and that this temperature differs for each steel grade. There were no pyrometers to measure high temperatures at that time, so the engineer learned to determine the temperature by the color of the steel blank. It turned out that if steel is cooled slowly in air, the gradually darkening mass of metal would suddenly heat up, almost as if it had ignited, before darkening again. No one could explain this phenomenon, nor did it occur during rapid cooling. The strange occurrence piqued the researcher's interest. Upon examining two blanks, one that had passed through the "special" point and one that had not, it was found that the first sample did not harden and remained soft. This was a discovery. Dmitrii Konstantinovich continued his research and found that there was yet another special point, corresponding to a different specific temperature. These points became known as "Chernov points" – critical temperatures at which phase changes occur in steel during heating and cooling in its solid state. In this way, "by sight", the herald of a new school of metallurgy, the founder of metallography, was able to confirm the occurrence of phase transformations in steel during its crystallization.

From 1866, Chernov worked as an engineer in the hammer shop of the Obukhov Steel Plant in St. Petersburg, and from 1884, he was employed at the Naval Technical Committee. In 1886, he also became the chief inspector of the Ministry of Railways, responsible for overseeing the execution of orders at metallurgical plants, and from 1889, he served as a professor of metallurgy at the Mikhailov Artillery Academy. Dmitrii Konstantinovich discovered the existence of phase transformations in steel as a result of heating or cooling in its solid state (1866 – 1868), and he established the critical temperatures

(the so-called Chernov points) at which internal transformations occur, determining the structure and properties of steel. In 1879, he presented the theory of the crystallization of steel ingots (dendritic steel crystals are sometimes called Chernov crystals). He thoroughly studied the defects in cast steel and suggested methods to combat them. Chernov substantiated the importance of complete deoxidation of steel during smelting, proposed an original design for a furnace to convert iron ore into steel, and worked on producing high-quality steel gun barrels, steel armor-piercing shells, and other items. Chernov's research greatly contributed to the transformation of metallurgy from a craft into a theoretically grounded scientific discipline.

The creators of the first scientific schools of metallurgists and metallographers in the post-Chernov period were N.S. Kurnakov (1860 – 1941), who later became an academician of the USSR Academy of Sciences and founded a scientific school in the field of physicochemical processes. He chaired the Department of General Chemistry at the Polytechnic Institute from 1902 to 1930. Chernov's students also included A.A. Baikov (1870 – 1946), later an academician of the USSR Academy of Sciences, and A.A. Rzheshotarskii (1847 – 1904). Baikov's students, in turn, were metallurgists such as N.T. Gudtsov and N.V. Ageev (academicians of the USSR Academy of Sciences), B.V. Stark (corresponding member of the USSR Academy of Sciences), and professors M.G. Oknov, M.P. Slavinskii, G.A. Kashchenko, and others. In 1902, A.A. Rzheshotarskii headed the Department of Metallurgy at the Metallurgical Faculty (which had been part of the Polytechnic Institute since its founding in 1899, along with three other faculties: Naval Architecture, Electrical Engineering, and Commerce) (now Peter the Great St. Petersburg Polytechnic University).

A.A. Baikov was invited to work at this institute in 1903 and was immediately sent abroad to prepare for a professorial position. Upon his return in 1904, he was elected associate professor of metallurgy and chemistry. He took on the organization of laboratories and lecturing on general metallurgy and metallography. However, his main achievement was the development of active scientific research.

The industrialization of the young Soviet republic created the conditions for the establishment of new scientific schools. In 1930, at the Metallurgical Faculty of the Polytechnic Institute, which was the main training ground for specialists, two independent departments were formed from the Department of General Metallurgy, headed by A.A. Baikov: the Department of Metallography (non-degree-granting), led by Professor Mikhail Grigorievich Oknov (1930 – 1942), and the Department of Heat Treatment (degree-granting), under the leadership of Professor Nikolai Timofeevich Gudtsov, later an academician of the USSR Academy of Sciences (1930 – 1942). From 1912 to 1928, N.T. Gudtsov worked at the Putilov (later Kirov) Plant as the head of the central factory laboratory, and from 1924, he became an associate professor, and later a professor, at the Metallurgical Faculty of the Leningrad Polytechnic Institute (now Peter the Great St. Petersburg Polytechnic University). In 1926, N.T. Gudtsov, together with prominent scientists of the time, G.V. Kurdyumov (later an academician of the USSR Academy of Sciences, the founder of the Soviet school of metal physicists) and N.Ya. Selyakov, applied X-ray analysis to the study of metals for the first time, making him the founder of the Leningrad (St. Petersburg) school of metallurgists-metallographers-heat treaters. His research on martensite structure, the basics of the theory of the effect of alloy-



Fig. 2. Academician Baikov A.A. with his followers – teachers and students of the Metallurgical Faculty of the Leningrad Polytechnic Institute (now Peter the Great St. Petersburg Polytechnic University), 1939

Рис. 2. Академик Байков А.А. со своими учениками – преподавателями и студентами металлургического факультета Ленинградского политехнического института (ныне Санкт-Петербургский политехнический университет Петра Великого), 1939 г.

ing elements on the structure and properties of steel, and his fundamental works: “*Physical Metallography*”, “*Special Steels*”, and “*Metallography and Heat Treatment of Steel*” – are only some of N.T. Gudtsov’s major contributions.

A separate page should be dedicated to the great scientist Andrey Sergeevich Zav’yalov, whose 100th birthday was celebrated by the scientific community in 2005. A brilliant scientist and organizer, A.S. Zav’yalov made a significant mark on the history of our country and the Leningrad school of metallurgists. Moreover, he nurtured a large number of students, the most prominent of whom was the renowned Igor Vasil’evich Gorynin, academician of the Russian Academy of Sciences, who for many years headed the country’s largest materials science research center – TsNII KM “Prometey” (now part of the Kurchatov Institute). The scientists of this institute made enormous contributions to the development of steels for shipbuilding and nuclear power, titanium, aluminum, and nickel alloys for new technologies, and a wide range of modern functional materials.

Let us provide some historical information, including the current state of this scientific center. The institute was founded in January 1939, based on the armor laboratory of the Izhora Plant. In its early years, the institute was tasked with creating and mastering the production of anti-shell armor for tanks, ships, and aircraft. The armor developed by the institute and put into production was used to protect the globally famous T-34 medium tanks, IS and KV heavy “breakthrough” tanks, self-propelled artillery systems, and the IL-2 attack aircraft.

In 1947, TsNII KM “Prometey” became the leading research institute in the field of metallurgy, metallography, casting technology, hot plastic working, and welding for all structural metallic materials used in military shipbuilding, civil shipbuilding, and the production of various marine equipment. Starting in the late 1940s, the institute carried out large-scale developments to create a series of new high-strength, cold-resistant, weldable hull steels for surface and submarine naval fleets that do not require subsequent heat treatment. These steels were later used to manufacture the hulls of a new generation of civilian fleet vessels (lighter carriers, icebreakers, tankers, gas carriers, marine floating self-elevating and semi-submersible drilling rigs of the “Shelf” type, and unique stationary ice-resistant platforms). A series of Navy submarines and manned and unmanned deep-sea vehicles were built using the high-strength, weldable titanium alloys developed by the institute’s specialists. With the onset of nuclear energy development in 1955, the institute began developing structural materials for nuclear power equipment. From 1981 to 1999, in addition to its traditional areas of focus, the institute also worked on the creation of materials for equipment used in the oil and gas extraction and processing industries, rail trans-

portation, the automotive industry, the agro-industrial complex, medicine, and other sectors.

Today, TsNII KM “Prometey” has a strong scientific, technical, human, and technological capacity, as well as a material and technical base, allowing it to tackle complex tasks in the development of new advanced materials and production technologies. It is headed by a student of Academician I.V. Gorynin, Corresponding Member of the Russian Academy of Sciences A.S. Oryshchenko.

Another major scientific center of St. Petersburg metallurgy is the TsNIIM (Central Research Institute of Materials), whose scientists have made a significant scientific contribution to the creation of new steels and alloys for defense technology. This center began its activity as the Central Scientific and Technical Laboratory of the Military Department (CSTL), which was established in 1914. This laboratory was later transformed into Research Institute 13 and then into TsNIIM. Scientists and specialists at TsNIIM developed high-strength corrosion-resistant weldable steels, titanium and aluminum alloys, and technologies for manufacturing a wide range of parts based on tungsten, molybdenum, ceramics, and heat-protective coatings capable of withstanding gas flow temperatures of 3000 °C and above, as well as exposure to thermal shock and gun steels.

One of the leading research institutes in the field of power engineering in the country is NPO CKTI (I.I. Polzunov Scientific and Development Association on Research and Design of Power Equipment), which celebrated its 90th anniversary several years ago. Throughout the institute’s history, the focus of its scientists and specialists has been on both theoretical work (developing new calculation methods and new power machine schemes) and experimental work, including the creation of new test stands and machines. The institute developed new grades of heat-resistant steels and alloys, new sector-specific federal and industry regulations, and created new testing methods and equipment, conducting systematic research on them. Additionally, experimental work is ongoing, including the examination of the condition of metal parts during their operation in the field of power machine strength.

Along with the giants of Leningrad (St. Petersburg) mechanical engineering and metallurgy, the industry was represented by a series of shipbuilding plants and power engineering plants (turbine manufacturing, compressor manufacturing, diesel engine manufacturing), where the metallurgical field held a significant place. In addition to large factory laboratories, science was developed in a number of industry-specific institutes: besides the aforementioned TsNII KM “Prometey” and TsNIIM (Central Research Institute of Materials), there were also TsKTI (Central Boiler and Turbine Institute), VPTI Elektro (All-Union Design and Engineering Institute of Electrical

Engineering Production Technology), VPTI Energomash (All-Union Design and Technology Institute of Power Engineering Machinery), VNITI (All-Union Scientific Research Institute of Technology), and TsNIITS (Central Institute of Transport Construction) [6–8]. Analyzing the activities of St. Petersburg (Leningrad) metallurgists, it is essential to note the role of the House of Scientific and Technical Propaganda, which for several decades played a significant organizational role in conducting ongoing seminars in the fields of metallurgy of steel and alloys, physics of metals, metallography, and plastic metal processing (chaired by Professors A.S. Zav'yalov, Yu.V. Shakhnazarov, A.M. Parshin, L.I. Vasil'ev, and G.E. Kodzhaspirov).

The seminars were held twice a month, and in addition, annual conferences were organized, attracting scientists and manufacturers from all regions of the former USSR. Unfortunately, during the collapse of the USSR, the House of Scientific and Technical Propaganda ceased to exist.

Traditionally, universities have played and continue to play a special role in the organization of science in our country. Undoubtedly, the main center is the Peter the Great St. Petersburg Polytechnic University (formerly the Polytechnic Institute and Leningrad Polytechnic Institute named after M.I. Kalinin) [4; 9]. The polytechnic school of metallurgists has trained and continues to train highly qualified production and pedagogical specialists not only for the region, but in the past for the entire former Soviet Union, and now for Russia, neighboring countries, and beyond. As mentioned at the beginning of the article, this school was headed by prominent scientists with worldwide recognition. TsNII KM “Prometey” has a special department at SPbPU dedicated to training its personnel.

At the Kalinin Leningrad Polytechnic Institute (now Peter the Great St. Petersburg Polytechnic University),

several departments were dedicated to metallurgy: cast iron and steel, non-ferrous metals, foundry production, metallography and heat treatment, metal forming, physical chemistry, analytical chemistry, and others. These departments were created within the foundational Faculty of Technology and Materials Research (FTMR), formerly known as the Metallurgical and Physical-Metallurgical Faculty. In addition to the aforementioned professors, significant contributions to the development of metallurgical research were made by professors of the Polytechnic: N.A. Menshutkin, N.S. Kurnakov, A.A. Rzheshotarskii, V.E. Grum-Grzhimailo, A.A. Baikov, M.A. Pavlov, F.Yu. Levinson-Lessing, V.A. Kistyakovskii, A.N. Ramm, P.Ya. Ageev, V.S. Smirnov, and others. In addition to the Polytechnic Institute (SPbPU), departments of materials science existed at the Shipbuilding Institute (now St. Petersburg State Marine Technical University, SPbG-MTU) and the Refrigeration Institute (now St. Petersburg State University of Low-Temperature and Food Technologies, SPbGUNIPT), where work was conducted on cold-resistant steels and alloys, among others.

In 2013, the Institute of Metallurgy, Mechanical Engineering, and Transport was established at Peter the Great St. Petersburg Polytechnic University, based on the Faculty of Physical Metallurgy (later the Faculty of Technology and Materials Research) and the Faculty of Mechanical Engineering. Later, it became the Institute of Mechanical Engineering, Materials, and Transport (IMMiT), which now implements programs for modern development in the fields of metallurgy and materials science.

Since 1993, SPbPU has hosted several international conferences, which have become a tradition: “High-Efficiency Technologies in Pre-Form Production” (St. Petersburg, 1993), “Plastic and Heat Treatment of Modern Metallic Materials” (St. Petersburg, 1995), “High Tech-



Fig. 3. Bureau of the Section of Metal Science and Heat Treatment of Leningrad House of Scientific and Technical Propaganda (LHSTP), 1982

Рис. 3. Бюро секции металловедения и термической обработки Ленинградского Дома научно-технической пропаганды (ЛДНТП), 1982 г.

nologies in Modern Materials Science and Engineering” (St. Petersburg, 1997), “Plastic, Heat, and Thermo-mechanical Treatment of Modern Metallic Materials” (St. Petersburg, 1999), “Modern Metallic Materials and Technologies and Their Use in Engineering” (St. Petersburg, 2001, 2006, 2009, 2011, 2013, 2015, 2017), “Modern Achievements in the Theory and Technology of Metal Forming” (SPbPU, 2005, 2007), “Nanotechnologies of Functional Materials” (NFM’2010) (St. Petersburg, SPbPU, 2010, 2012), and “Modern Materials and Advanced Manufacturing Technologies” (SMPPT–2019) (2019, 2021, 2023). Leading scientists and specialists in the fields of materials science, plastic, heat, and thermo-mechanical treatment, powder metallurgy, and in recent years, the promising field of additive technologies, have participated in these conferences. Peter the Great St. Petersburg Polytechnic University is one of the leading research centers in the country in this area.

In conclusion, it should be noted that the high level of the St. Petersburg school of metallurgists, metallographers, and metal physicists remains strong despite difficult times for our science, and our scientists are in demand not only in our country but also abroad. The main scientific contributions of St. Petersburg scientists to metallurgy can be summarized as follows: **D.K. Chernov** – discovery of critical points; **A.A. Baikov** – development of the theory of metallurgical processes and transformations in metals and alloys, creator of one of the first schools of metallographers; **N.T. Gudtsov** – development of the theory of martensite structure and steel alloying, founder of the school of metallographers and heat treaters; **N.V. Ageev** – theory of interatomic bonds and the electronic structure of metals; **M.G. Oknov** – metallography of iron-carbon alloys; **G.A. Kashchenko** – development of metallographic analysis methods; **A.S. Zav’yalov** – development of some aspects of the theory of phase transformations in iron-carbon alloys; **V.I. Vladimirov** – development of the theory of dislocations and disclinations; **V.A. Likhachev** – development of the structural-analytical theory of strength and the design of shape-memory alloys; **A.N. Orlov** – development of the theory of dislocations; **I.V. Gorynin** – development of the theoretical foundations for creating high-strength weldable structural materials for use in extreme conditions, creator and leader of the scientific school of metallographers at TsNII KM “Prometey” (Central Research Institute of Structural Materials “Prometey”); **Yu.P. Solntsev** – development of the scientific foundations for creating cold-resistant materials and methods for assessing resistance to brittle fracture; **A.M. Parshin** – development of the theory of structural recombination of radiation defects during the decomposition of solid solutions (problems of radiation materials science); **Yu.V. Shakhnazarov** – development of the physico-technological foundations for creating martensitic-aging and tool steels [4; 9].



Fig. 4. Participants of the Conference “Modern Metal Materials and Technologies – 2013”

(from left to right: Prof. Kodzhaspirov G.E., Prof. Tsemenko V.N., Academician of the Russian Academy of Sciences Gorynin I.V., Prof. Salishchev G.A., Academician of the Russian Academy of Sciences Rudskoi A.I., Farmakovskii B.V., Prof. Popovich A.A.)

Рис. 4. Участники конференции СММТ-2013

(слева направо: проф. Коджаспиров Г.Е., проф. Цеменко В.Н., академик РАН Горынин И.В., проф. Салищев Г.А., академик РАН Рудской А.И., Фармаковский Б.В., проф. Попович А.А.)

Listing the scientific contributions of each prominent St. Petersburg scientist currently working would take up too much space. Therefore, we will mention only the most well-known scientists to the academic community, as well as those who have led and continue to lead scientific schools: RAS Academician **A.I. Rudskoi** – development of the scientific foundations for structure formation and modeling of steels and a wide range of modern materials during thermomechanical processing and in the field of powder metallurgy; RAS Corresponding Member **A.S. Oryshchenko** – development of the theoretical foundations for creating new heat-resistant and heat-resistant alloys based on Fe–Cr–Ni, technologies for their cast production for high-temperature pyrolysis oil equipment, the creation of corrosion-resistant titanium and aluminum alloys and materials for the hulls of marine nuclear reactors and nuclear power plants, and the creation of an original steel with elements of nanostructuring that increases the power of nuclear reactors by 30 – 40 %; RAS Corresponding Member **V.V. Rybin** – development of the scientific foundations of the physics of advanced plastic deformation of crystals and the structural-kinetic concept of metal fracture; RAS Corresponding Member **Yu.K. Petrenya** – theoretical and technological aspects of the development of alloys for power engineering; Professors, Doctors of Technical and Physical-Mathematical Sciences **A.A. Popovich** – development of mechanochemical synthesis of inorganic compounds, powder metallurgy, and additive technologies; **V.I. Betehtin** – development and advancement of the kinetic approach to the problem of solid body fracture; **E.L. Gyulikhandanov** – theory and technology of chemical-thermal treatment of steels, diffu-

sion processes in metals; **G.E. Kodzhaspirov** – structural transformations in deformed steels and alloys, physico-technological foundations of non-isothermal thermomechanical treatment; **N.G. Kolbasnikov** – mechanisms of deformation and strengthening of low-plastic metals and the creation of the entropic concept of strength and plasticity.

Undoubtedly, not all St. Petersburg metallurgists who contributed to the development of domestic and world metallurgy are mentioned here, and we ask for the understanding of our colleagues who were not included in this list due to the brevity of this presentation.

REFERENCES / СПИСОК ЛИТЕРАТУРЫ

- Zav'yalov S. History of the Izhora Plant. Publishing House Istoriya zavodov; 1934:410. (In Russ.).
Завьялов С. История Ижорского завода. Издательство История заводов; 1934:410.
- Lyubchenko A.A. Role of the Kirov Plant in development of Soviet mechanical engineering and metallurgy. In: *Mechanical Engineering and Metallurgy of the Kirov Plant*. Leningrad: Mashinostroenie; 1967:5–9. (In Russ.).
Любченко А.А. Роль Кировского завода в развитии советского машиностроения и металлургии. В кн.: *Машиностроение и металлургия Кировского завода*. Ленинград: Машиностроение; 1967:5–9.
- Aleksandrov V.P., Dysin B.G. Kirov plant – laboratory of technical progress. In: *Mechanical Engineering and Metallurgy of the Kirov Plant*. Leningrad: Mashinostroenie; 1967:10–13. (In Russ.).
Александров В.П., Дысин Б.Г. Кировский завод-лаборатория технического прогресса. В кн.: *Машиностроение и металлургия Кировского завода*. Ленинград: Машиностроение; 1967:10–13.
- Gyulikhandanov E.L., Kodzhaspirov G.E. History and current state of St. Petersburg physical metallurgy. *Metal Science and Heat Treatment*. 2007;(1):3–8. (In Russ.).
Гюлиханданов Е.Л., Коджаспиров Г.Е. История и современное состояние Санкт-Петербургского металлостроения. *Металловедение и термическая обработка металлов*. 2007;(1):3–8.
- Vinogradova N.A. Obukhov Plant. Essays on the History of 1863–2008. St. Petersburg: Gumanistika; 2010:592. (In Russ.).
Виноградова Н.А. Обуховский завод. Очерки истории 1863–2008. Санкт-Петербург: Издательство Гуманитика; 2010:592.
- Gorynin I.V. Reflections with Optimism. St. Petersburg: Polytechnic University Publishing House; 2014:525. (In Russ.).
Горьнин И.В. Размышления с оптимизмом. Санкт-Петербург: Издательство Политехнического университета; 2014:525.
- Central Research Institute of Materials – 90 Years in Materials Science. Patkin Yu.Yu. ed. Vol. 2. St. Petersburg: Polytechnic University Publishing House; 2004:228. (In Russ.).
ЦНИИ Материалов – 90 лет в материаловедении / под ред. Ю. Ю. Заплаткина. Вып. 2. Санкт-Петербург: Издательство Политехнического университета; 2004:228.
- High-Tech Defense Industry in Action. A Historical Sketch of the Scientific and Technical Activities of the All-Union (All-Russian) Scientific Research Institute of Technology 1947–1997. St. Petersburg: Publishing House “INTEGRAF” JSC “Kirovskii Zavod”; 1997:160. (In Russ.).
Высокие технологии оборонки в действии. Исторический очерк научно-технической деятельности Всесоюзного (Всероссийского) научно-исследовательского технологического института 1947–1997. Санкт-Петербург: Издательство «ИНТЕГРАФ» АО «Кировский завод»; 1997:160.
- St. Petersburg State Polytechnic University: Biographies. St. Petersburg: Gumanistika; 2006:912. (In Russ.).
Санкт-Петербургский государственный политехнический университет: Биографии. СПб: Издательство Гуманитика; 2006:912.

Information about the Authors

Сведения об авторах

Andrei I. Rudskoi, Academician, Dr. Sci. (Eng.), Rector, Peter the Great St. Petersburg Polytechnic University

ORCID: 0000-0001-9517-3905

E-mail: rector@spbstu.ru

Georgii E. Kodzhaspirov, Dr. Sci. (Eng.), Prof. of the Higher School of Physics and Technology of Materials, Peter the Great St. Petersburg Polytechnic University

E-mail: gkodzhaspirov@yandex.ru

Андрей Иванович Рудской, академик, д.т.н., ректор, Санкт-Петербургский политехнический университет Петра Великого

ORCID: 0000-0001-9517-3905

E-mail: rector@spbstu.ru

Георгий Ефимович Коджаспиров, д.т.н., профессор Высшей школы физики и технологий материалов, Санкт-Петербургский политехнический университет Петра Великого

E-mail: gkodzhaspirov@yandex.ru

Received 05.04.2024

Revised 15.04.2024

Accepted 23.08.2024

Поступила в редакцию 05.04.2024

После доработки 15.04.2024

Принята к публикации 23.08.2024



UDC 621.762.4

DOI 10.17073/0368-0797-2024-5-509-519



Review article

Обзорная статья

RECENT DEVELOPMENT IN POWDER METALLURGY OF HIGH-ENTROPY ALLOYS FOR HIGH-TEMPERATURE APPLICATIONS. BRIEF REVIEW

A. Yu. Ivannikov[✉], V. S. Yusupov

Baikov Institute of Metallurgy and Materials Science, Russian Academy of Sciences (49 Leninskii Ave., Moscow 119334, Russian Federation)

✉ aivannikov@imet.ac.ru

Abstract. Powder metallurgy of high-entropy alloys has gained significant attention in modern applications due to its low cost and near-net-shape formability. This overview presents the state-of-the-art research on powder metallurgy of high-entropy alloys for high-temperature applications, covering basic solid state fabricating processes, phase composition, and advanced mechanical properties recently attained. The analysis showed that various methods of production and mixing of powder components, including self-propagating high-temperature synthesis, magnesium reduction, hydrogenation, mechanical alloying, plasma spheroidization, centrifugal plasma sputtering of the bar, and conventional mixing of elemental powders in high-energy mixers are used to produce powder mixtures. The most common consolidation method is spark plasma sintering, which allows obtaining compacts with high speed and preservation of fine structure. Also, for the production of long bars and billets, the extrusion of powder mixtures in shells is used. A key feature of the chemical compositions of billets produced by methods of powder metallurgy are the possibility of obtaining oxide-disperse-strengthened powder compacts, which provides additional hardening at elevated temperatures. The main elements used in the creation of high-entropy alloys for application at elevated temperatures are the refractory metals. Therefore, in order to reduce the density of new alloys, compositions with aluminum, titanium, and refractory oxides are being developed. Finally, this review identifies unresolved and critical issues in the development of approaches to obtaining high-entropy alloys using powder metallurgy methods for their practical implementation in modern industry.

Keywords: powder metallurgy, high-entropy alloys, refractory metals, mechanical alloying, plasma spheroidization, hydrogenation, extrusion, high-temperature application

Acknowledgements: The research was supported by the Russian Science Foundation, grant No. 24-29-00183, <https://rscf.ru/project/24-29-00183/>.

For citation: Ivannikov A.Yu., Yusupov V.S. Recent development in powder metallurgy of high entropy alloys for high-temperature applications. Brief review. *Izvestiya. Ferrous Metallurgy*. 2024;67(5):509-519. <https://doi.org/10.17073/0368-0797-2024-5-509-519>

НОВЫЕ ДОСТИЖЕНИЯ В ОБЛАСТИ ПОРОШКОВОЙ МЕТАЛЛУРГИИ ВЫСОКОЭНТРОПИЙНЫХ СПЛАВОВ ДЛЯ ВЫСОКОТЕМПЕРАТУРНЫХ ПРИЛОЖЕНИЙ. КРАТКИЙ ОБЗОР

А. Ю. Иванников[✉], В. С. Юсупов

Институт металлургии и материаловедения им. А.А. Байкова РАН (Россия, 119991, Москва, Ленинский пр., 49)

✉ aivannikov@imet.ac.ru

Аннотация. Порошковая металлургия высокоэнтروпийных сплавов привлекает значительное внимание благодаря своей высокой технологичности и низкой стоимости. В этом обзоре представлены новейшие исследования в области порошковой металлургии высокоэнтропийных сплавов, разработанных для применения при высоких температурах. Рассматриваются основные процессы получения порошков и компактов из них, химический и фазовый состав, плотность, механические свойства при повышенной температуре, термостабильность. Проведённый анализ показал, что для получения порошковых смесей применяются различные методы производства и смешения порошковых компонентов, включая самораспространяющийся высокотемпературный синтез, магнитохимию, гидрирование, механическое легирование, плазменную сфероидизацию, центробежное распыление прутка плазмой и традиционное смешение элементарных порошков в высокоэнергетических смесителях. Наиболее распространённым способом консолидации является искровое плазменное спекание,

позволяющее получать компакты с высокой скоростью и сохранением тонкой структуры. Также для производства длинномерных прутков и заготовок применяется экструзия порошковых смесей в оболочках. Ключевой особенностью химических составов заготовок, производимых методами порошковой металлургии, является возможность получения дисперсно-упрочненных оксидами порошковых компактов, что обеспечивает дополнительное упрочнение при повышенных температурах. Основными элементами, используемыми при создании высокоэнтропийных сплавов для применения в условиях повышенных температур, являются тугоплавкие металлы. Поэтому для снижения их плотности разрабатываются составы с алюминием, титаном, а также тугоплавкими оксидами. Кроме того, в этом обзоре обозначены нерешенные и критические вопросы разработки подходов к получению высокоэнтропийных сплавов методами порошковой металлургии для практического внедрения их в современную индустрию.

Ключевые слова: порошковая металлургия, высокоэнтропийные сплавы, тугоплавкие металлы, механическое легирование, плазменная сфероидизация, гидрирование, экструдирование, высокотемпературное применение

Благодарности: Исследование выполнено за счет гранта Российского научного фонда № 24-29-00183, <https://rscf.ru/project/24-29-00183/>.

Для цитирования: Иванников А.Ю., Юсупов В.С. Новые достижения в области порошковой металлургии высокоэнтропийных сплавов для высокотемпературных приложений. Краткий обзор. *Известия вузов. Черная металлургия*. 2024;67(5):509–519. <https://doi.org/10.17073/0368-0797-2024-5-509-519>

INTRODUCTION

High-entropy alloys (HEAs) are a new generation of alloys that have been developed since 2004 [1; 2]. Despite intensive research over the past 20 years in the field of high-entropy materials, these alloys have not yet found widespread use in modern industry, although they continue to gain popularity in scientific studies each year [3; 4] due to their high physical, mechanical, and operational properties [5; 6]. High-entropy alloys are resistant to oxidation at high temperatures, which potentially broadens their technological applications, including replacing nickel-based alloys in turbine systems [7; 8]. In their review, O.N. Senkov et al. [9] explore two groups of HEAs for high-temperature applications. The first group includes HEAs based on 3d transition metals such as Co, Cr, Cu, Fe, Mn, Ni, and Ti. These alloys have a yield strength of over 1000 MPa at 600 °C. However, according to the authors, none of the HEAs presented possess properties superior to modern nickel-based heat-resistant alloys. The heat resistance of HEAs quickly decreases at temperatures exceeding ≈ 800 °C, similar to that of nickel-based heat-resistant alloys. Additionally, their ability to withstand high temperatures is limited by their melting points, which are only slightly different from those of commercial nickel-based heat-resistant alloys.

Refractory high-entropy alloys (RHEAs) represent the second group of HEAs, developed by O.N. Senkov and co-authors [10] for high-temperature applications. Since 2010, this category of alloys has attracted the interest of specialists due to their ability to maintain high static strength up to 1600 °C and potentially higher. The first RHEA was created using five refractory components (Mo, Nb, Ta, V, and W), but later alloys were made from elements of Group IV (Ti, Zr, and Hf), Group V (V, Nb, and Ta), and Group VI (Cr, Mo, and W) [10].

Refractory high-entropy alloys show promise for use in structures and products operating at high temperatures (above 1000 °C) and are considered as replacements

for nickel-based heat-resistant alloys. In their recent review, W. Xiong et al. [11] demonstrated that HEAs exhibit excellent mechanical properties over a wide range of temperatures and increased resistance to high-temperature oxidation. Currently, there is a significant increase in research on RHEAs, which is also confirmed by the growing number of reviews on RHEAs developed for applications in nuclear engineering [12; 13].

Traditionally, gas-phase, liquid-phase, and solid-phase methods are used to produce HEAs [3]. Powder metallurgy methods (solid-phase methods) are considered the most rational for obtaining RHEAs for high-temperature applications [14]. Fig. 1 illustrates the process for the production of HEAs, enabling the creation of high-quality billets with geometries that meet consumer requirements. However, the analysis of recent reviews [11 – 13] in the field of HEAs for high-temperature applications indicates a lack of information on solid-phase powder metallurgy processes for HEAs since 2020.

Thus, it becomes relevant to assess the latest developments and trends in the field of HEAs for high-temperature applications. Therefore, this review examines the criteria for selecting chemical elements for the solid-phase powder metallurgy process, as well as consolidation methods, density, phase composition, mechanical properties, and future trends regarding HEAs.

MATERIALS AND METHODS

Using the PRISMA (*Preferred Reporting Items for Systematic Reviews and Meta-Analyses*) criteria [15], both Russian and international databases were analyzed: elibrary.ru, mdpi.com, Springer.com and sciencedirect.com.

The selected studies met the following criteria:

- mechanical properties at elevated temperatures;
- oxidation resistance;
- thermal stability.

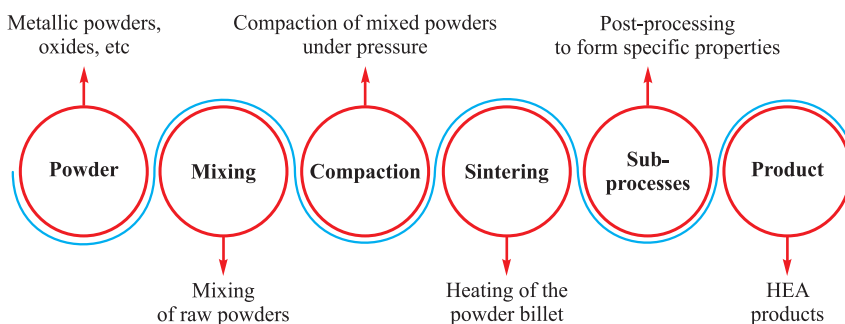


Fig. 1. Flow diagram of powder metallurgy

Рис. 1. Технологическая схема порошковой металлургии

RESULTS AND DISCUSSION

After screening for the specified criteria, thirty-nine studies related to powder metallurgy of high-entropy alloys (HEAs) for high-temperature applications were selected. The Table provides data on the studies that contain results meeting all of the aforementioned criteria.

Chemical composition

Recent studies have examined innovative oxide-dispersion strengthened (ODS) refractory high-entropy alloys (RHEAs). For example, in the study [32], 15 % Al_2O_3 was used to produce lightweight refractory alloys based on TaNbVTi. Zong L. et al. [33] used nanoscale ceramic particles of $m-ZrO_2$ to strengthen the refractory high-entropy alloy NbMoTaW, and in the study [34],

they applied similar reinforcement for the WMoNbTaV alloy. Similarly, nanoscale Y_2O_3 particles were used in the study [35]. A new NbTaTiV ODS RHEA containing 0.35 wt. % Al_2O_3 was investigated in the study [25].

Strengthening HEAs with nanoscale refractory oxides can only be achieved through powder metallurgy methods. The traditional chemical compositions of HEAs, presented in the Table, replicate their compositions obtained earlier using liquid-phase methods [2; 8; 10 – 12]. Therefore, the application of powder metallurgy methods expands the technological capabilities for producing HEAs with the widest range of chemical compositions [36 – 39].

Powder preparation

In the studies [40; 41], the approach of obtaining powder mixtures through simple mixing without additional milling was used. The most common method for producing powder is mechanical alloying in a planetary mill [42].

To expand the raw material base, in the study [43], a powder mixture was synthesized using a blend of titanium hydride and elemental powders. In the same study, Nb hydride powder and Ta hydride powder were used. The release of hydrogen during the decomposition of the hydrides helps to clean the surface of the metal powders from impurities.

For the agglomeration of fine powders, spray drying is applied. In the study [44], after spray drying, the HEA powder granules were processed in a plasma spheroidization unit (Tekna Nano-15). Induction thermal plasma (Fig. 2) was also used in the study [45] for spheroidizing WTaMoNbZr powder, which was originally irregularly shaped and obtained by grinding a hydrogenated ingot. The deoxidation during plasma processing contributed to refining the alloy.

In the study [46], pre-rolled plates with a known grain size were hydrogenated. The authors highlight the economic efficiency of the mechanical milling method and

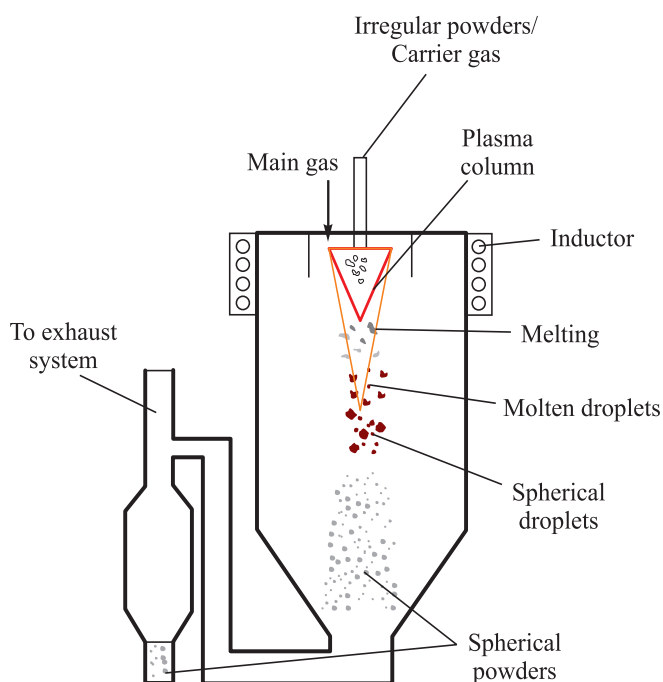


Fig. 2. Schematic diagram of plasma spheroidization system

Рис. 2. Принципиальная схема системы сферондизации плазмы

Information on the reviewed studies

Информация об исследованиях, включенных в обзор

Author, year	Chemical composition	Powder preparation	Mechanical properties at elevated temperature
	Phase composition	Consolidation method	Oxidation resistance/thermal stability
Xiang L. et al., 2020 [16]	TaNbVTiAl _x (x = 0, ..., 1.0)	MA (Mechanical alloying)	Specific strength 88.37 MPa·cm ³ /g, T = 900 °C; specific strength 16.03 MPa·cm ³ /g, T = 1200 °C
	BCC	SPS (Spark plasma sintering)	–
Li H. et al., 2020 [17]	Co ₂₅ Cr ₂₁ Fe ₁₈ Ni ₂₃ Mo ₇ Nb ₃ WC ₂	MA	T = 600 °C, σ _{0.2} = 473 MPa*, σ = 741 MPa*, ε = 10.5 %; T = 900 °C, σ _{0.2} = 142 MPa*, σ = 165 MPa*, ε = 31.0 %
	FCC + Me ₆ C	HP (Hot pressing)	–
Alvaredo-Olmos P. et al., 2021 [18]	Fe _{1.5} Cr ₁ Al _{0.75} Mo _{0.1} Ti _{0.1}	GA (Gas atomization)	T = 400 °C, HV = 6.1 GPa;
	Fe _{1.5} Cr ₁ Al _{0.75} Mo _{0.1} Ti _{0.1} Ni _{0.25}		T = 400 °C, HV = 6.5 GPa
Yang T. et al., 2021 [19]	CoCrFeMnNi	GA	Retention of nanostructure (55 – 160 nm) after heating to 1100 °C
	FCC	HP	–
Zhang R. et al., 2021 [20]	Al _x CrTiMo (x = 0.25, ..., 1.00)	MA	–
	BCC	SPS	Heat resistance at 1000 °C for 7 h
Liu Q. et al., 2021 [21]	MoNbTaTiV	MA	V̇ = 0.5 s ⁻¹ , σ = 400 MPa; V̇ = 0.0005 s ⁻¹ , σ = 30 MPa (T = 1300 °C in vacuum)
	BCC	SPS	–
Peng H. et al., 2022 [22]	NbMoTaWV	MA	T = 1000 °C, σ = 1978 MPa, specific strength 170.51 MPa·cm ³ /g; T = 1200 °C, σ = 1433 MPa, specific strength 123.53 MPa·cm ³ /g
	BCC + Tetrahedral phase	SPS	–
Gao F. et al., 2022 [23]	TiAlV _{0.5} CrMo	MA	–
	BCC + Laves phases	–	Retention of nanostructure at 1200 °C
Ujah C. et al., 2023 [24]	Ti ₂₀ Al ₁₆ V ₁₆ Fe ₁₆ Ni ₁₆ Cr ₁₆	MA	Mechanical properties higher than Ti64 alloy
	FCC + BCC	SPS	–
Zhang X. et al., 2023 [25]	NbTaTiV + 0.35Al ₂ O ₃	MA	σ _{0.2} = 690 MPa (T = 1000 °C)
	BCC + Al ₂ O ₃	HP	–
Kuskov K.V. et al., 2023 [26]	Co ₃₅ Ni ₁₀ Fe ₁₀ Cr ₁₀ Al ₃₅	MA + CBC	σ _{0.2} = 1,120 MPa, T = 600 °C, specific yield strength 167.66 MPa·cm ³ /g
	B2 + BCC + FCC + L1 ₂	SPS	–
Boztemur B. et al., 2023 [27]	WNbMoVTaCrAl	MA	–
	BCC + Ta ₂ VO ₆ + (Nb,Ta)C + W ₂ C _{0.85} + Al ₂ O ₃	SPS	Retention of nanostructure at 1150 °C
Das S. et al., 2023 [28]	AlCoCuFeNi	MA	–
	FCC + BCC	–	Retention of nanostructure at 900 °C
Qin M. et al., 2023 [29]	Ti–Nb–Mo–Ta–W–Ni–Zr	MA	–
	BCC + Secondary phases	SPS	Grain size <150 nm after 5 h annealing at 1300 °C
Gao F. et al., 2023 [30]	TiAlV _{0.5} CrMo	MA	–
	BCC1 + BCC2 + Al ₂ O ₃	SPS	Retention of nanostructure at 1200 °C
Fu A. et al., 2023 [31]	Al–Fe–Co–Cr–Ni	GA	σ _{0.2} = 518 MPa (T = 600 °C)
	FCC + BCC	Hot extrusion (extrusion ratio 7:1, temperature 1150 °C)	–

* Tensile test.

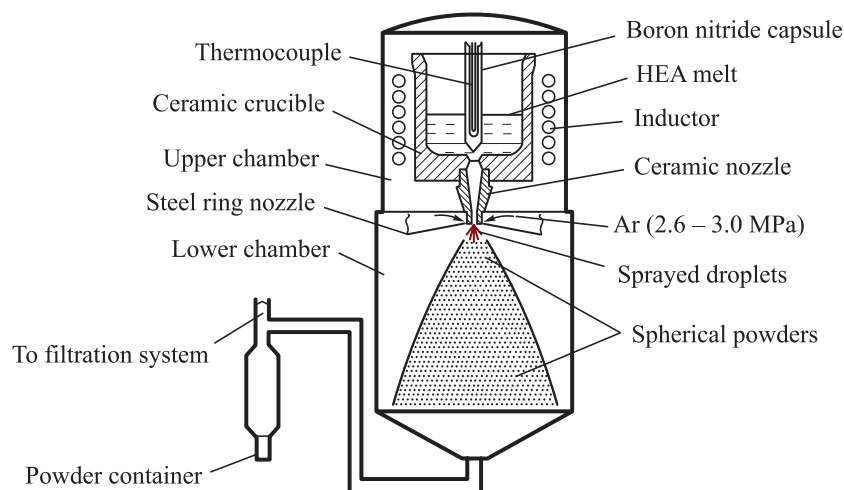


Fig. 3. Scheme of the unit for obtaining spherical powders by spraying the melt with inert gas

Рис. 3. Схема установки получения сферических порошков распылением расплава инертным газом

the clear correlation between the grain size of the plate and the resulting powders, which ranged from 6 to 102 μm .

Gas atomization (Fig. 3) is the primary method used for producing spherical powders. In the study [18], gas atomization was used to produce HEAs from 3d transition elements and refractory elements, while in the study [19], the same method was applied but exclusively for HEAs made from 3d transition elements. These powders have a homogeneous chemical composition and are suitable for various technological processes in powder metallurgy, as well as for additive manufacturing [47]. However, gas-atomized powders contain satellites, which limit their compactness. Therefore, for obtaining powders with a high degree of sphericity, the technology of centrifugal atomization of a rotating electrode is used.

In the study [48], both EIGA (*Electrode Inert Gas Atomization*, Fig. 4, a), and the PREP (*Plasma Rotating Electrode Process*, Fig. 4, b) were used to produce RHEA powders. The results demonstrated that the PREP method produced powders with high sphericity and no satellite particles, although the particle sizes were larger compared to those obtained with EIGA. The average particle sizes were 65.9 μm for PREP and 51.8 μm for EIGA.

In the study [26], self-propagating high-temperature synthesis (SHS) was used to obtain powders from mechanically activated powder, resulting in a change in the material's phase composition. This approach expands the potential for obtaining new properties in known HEA chemical compositions.

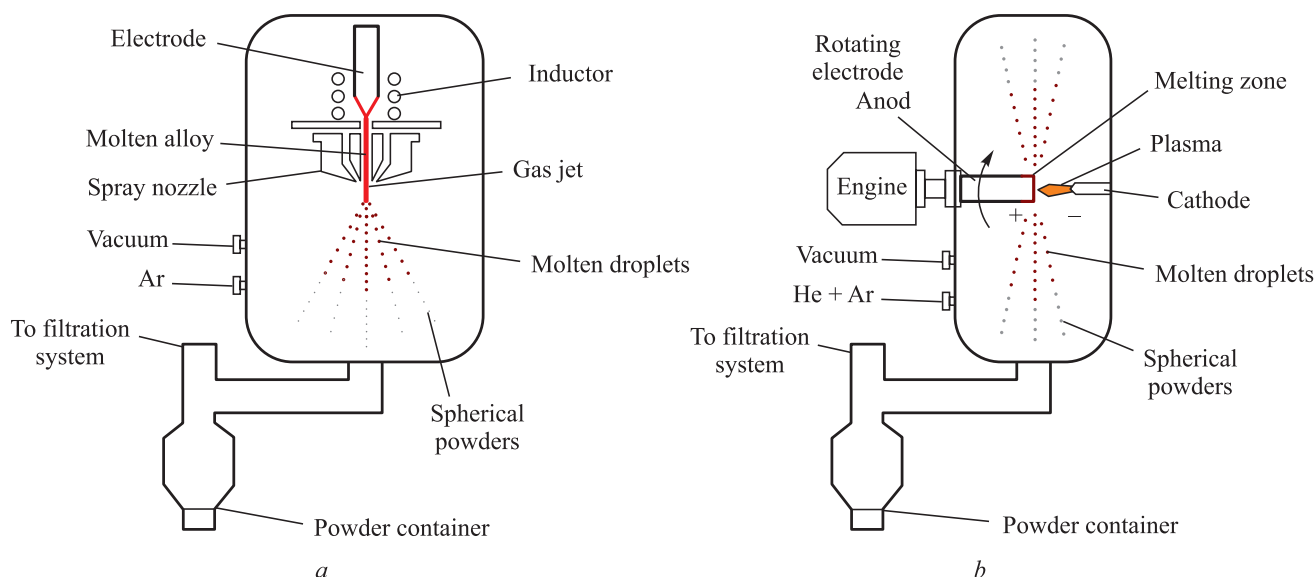


Fig. 4. Schematic diagrams of EIGA (a) and PREP (b) systems

Рис. 4. Принципиальные схемы систем EIGA (a) и PREP (b)

A combination of magnesiothermy and SHS was applied in the study [49]. The authors used a powder mixture of WO_3 , Nb_2O_5 , Ta_2O_3 and MoO_3 in combination with pure magnesium powder for SHS. This approach contributes to the expansion of the raw material base in the production of RHEAs.

The expansion of synthesis methods allows for obtaining powders with various chemical compositions, morphologies, and sizes. This is crucial for the next technological cycle in powder metallurgy, namely consolidation (compaction) processes.

Consolidation process

The most widely used compaction method is spark plasma sintering (SPS). In the studies [50] and [51], the maximum temperature of 1900 °C was achieved under a pressure of 50 MPa. The maximum pressure for SPS, 80 MPa, was applied in the study [52]. A key limiting factor for the pressure is the use of graphite punches in SPS.

The main advantage of the SPS method is the controllable process speed, increased sample density, and the retention of metastable structures due to high cooling rates. However, SPS has limitations in producing complex-shaped and large-sized products.

Sintering by hot pressing (HP) is a widely used technology in powder metallurgy for producing products with minimal residual porosity. The main difference between HP and SPS is in the heating and cooling rates. Additionally, HP is preferable for manufacturing large parts in industry [17; 19].

Cold isostatic pressing (CIP) and pressureless sintering are common methods in powder metallurgy. In the study [53], the maximum sintering temperature using a mixture of H_2 and Ar was 1400 °C. In the study [54], the same sintering atmosphere was used, but the maximum temperature reached 1450 °C. The data obtained on the sintering process can be adapted for high-throughput MIM (*Metal Injection Moulding*) technology [55; 56].

The method of hot extrusion is promising for producing long products with high mechanical properties. In the study [31], spherical powders in a stainless steel container were subjected to hot extrusion at a temperature of 1150 °C (extrusion ratio of 7:1). The production of long bars and wires by hot extrusion can be used both for making rod structures and for additive manufacturing processes, such as thermal spraying or wire arc additive manufacturing.

Among the reviewed studies on HEA powder metallurgy since 2020, no methods for producing billets by metal injection molding or hot isostatic pressing (HIP) were presented [57]. However, these methods enable

the manufacturing of complex-shaped samples with high density and are promising for the production of parts from HEA powders. Thus, in the coming years, these methods are expected to be adapted for producing products for high-temperature applications.

Phase composition

In the reviewed studies (see Table), X-ray diffraction analysis of HEAs based on 3d transition metals primarily revealed a single-phase FCC solid solution, while for compositions based solely on refractory metals, a single-phase BCC solid solution was identified. However, for compositions containing both 3d transition metals and refractory metals, X-ray analysis detected the presence of two phases: FCC and BCC. Additionally, in some cases, the presence of carbide, oxide, sigma, and intermetallic phases was observed, which positively affect the high-temperature properties of the developed alloys.

Density

Density is a key factor for sintered samples, as it allows for assessing the effectiveness of the consolidation method.

Among the analyzed studies, the highest density was achieved for the RHEAs ($\text{W}_{35}\text{Ta}_{35}\text{Mo}_{15}\text{Nb}_{15}$)₉₅Ni₅ (14.55 g/cm³) [58] and equiatomic RHEA NbMoTaWRe (14.36 g/cm³) [49], due to the presence of W, Ta, Nb, Mo, and Re. The lowest density, 5.98 g/cm³, was obtained for the HEA TiAlV_{0.5}CrMo [23]. Overall, chemical compositions containing Al have significantly lower densities. To further reduce the density, oxides are introduced into HEA compositions [32].

The density of powder samples is considered when calculating specific strength, which allows for comparing HEAs with different chemical compositions and densities.

It is important to note that density is also determined by the level of residual porosity, which is highest for pressureless sintering and lowest in the case of HP and SPS.

Mechanical properties at elevated temperatures

Only 20 % of the reviewed studies provide data on the properties of powder HEAs at elevated temperatures.

The authors of the study [16] found that the RHEA TaNbVTiAl_{0.2} exhibits exceptional specific strength both at room temperature (207.11 MPa·cm³/g) and at high temperatures (88.37 MPa·cm³/g at 900 °C and 16.03 MPa·cm³/g at 1200 °C), while maintaining acceptable ductility. Such RHEAs have the potential for use at temperatures exceeding 1200 °C. The high mechanical properties are determined by the homogeneous microstructure and solid solution strengthening.

In the study [17], a comparison of tensile test results at room temperature and at 900 °C showed that deformation increased 5.6 times, and the yield strength decreased fourfold. According to the authors, grain boundary strengthening was the dominant mechanism at elevated temperatures, where carbide particles made a significant contribution to increasing yield strength through dislocation and Orowan strengthening.

In the study [18], nanoindentation showed that increasing the temperature to 400 °C resulted in only a 10 % reduction in hardness.

In the study [21], the hot deformation characteristics of ultrafine-grained RHEA MoNbTaTiV were investigated using isothermal compression tests in the temperature range of 1100 to 1300 °C and strain rates from 0.0005 to 0.5 s⁻¹. It was found that at high temperature and low strain rate, the main deformation mechanism becomes grain boundary sliding, which is somewhat suppressed by grain growth and ultrafine precipitated phases distributed along the grain boundaries.

In the study [22], it was noted that the high strength of the NbMoTaWV alloy at elevated temperatures is primarily due to the presence of a secondary phase, which prevents grain boundary sliding. However, at elevated temperatures, the alloy became less ductile, likely due to the presence of the secondary phase, which leads to crack formation along the grain boundaries. At room temperature, the sintered NbMoTaWV demonstrated higher compressive strength and ductility compared to the corresponding cast HEA. The significant increase in strength is associated with the precipitation of the (Ta, V)O₂ phase and grain boundary strengthening of the BCC matrix.

In the study [25], a new super-strong RHEA NbTaTiV, oxide-dispersion strengthened with 0.35 wt. % Al₂O₃, was produced. The dual-phase material demonstrated a high yield strength (2075 MPa) and compressive ductility (15 %), maintaining high strength across a wide temperature range (25 – 1000 °C). The super-high strength of the dual-phase RHEA was mainly attributed to dispersion strengthening due to the high fraction of submicron Ti-(O, N) particles and solid solution strengthening. The alloy's performance can be significantly improved through oxide strengthening, opening new prospects for developing high-performance RHEAs.

High-temperature tests conducted in all the published studies aimed to evaluate the static strength of materials at elevated temperatures (see Table), but for practical application, an assessment of the reliability of such materials will be required. Therefore, future studies should evaluate fracture toughness, creep resistance, durability, etc.

Oxidation resistance and thermal stability

In 15 % of the reviewed studies, data on thermal stability and/or oxidation resistance were provided.

A key feature of RHEAs is the high-temperature stability of the ultrafine-grained structure, obtained through mechanical alloying followed by SPS. The high recrystallization temperature of RHEAs ensures the retention of the nanostructures formed during the preparation of powder mixtures. Therefore, RHEAs exhibit higher thermal stability compared to HEAs based on 3d elements.

The introduction of active elements Al and Cr into RHEA compositions promotes the formation of oxide films, which enhance heat resistance [20; 30].

CONCLUSIONS AND FUTURE PROSPECTS

This review has examined new and traditional approaches used in the production of high-entropy alloys (HEAs) for high-temperature applications. The primary goal of solid-state methods for producing HEAs from refractory elements is to create cost-effective components with precise geometries and properties that are difficult or impossible to achieve using gas-phase or liquid-phase methods.

Recent research in powder metallurgy shows the use of oxides and hydrides for powder production, significantly expanding the raw material base for HEA metallurgy.

Various approaches are used to produce powder mixtures, including mechanical alloying, SHS (self-propagating high-temperature synthesis), hydride formation, metallothermy, agglomeration, spheroidization, gas atomization, and plasma atomization of a centrifugally rotating electrode.

An analysis of powder sintering methods indicates that the most commonly used method is spark plasma sintering (SPS). However, this method has known limitations regarding the shape and size of products. Therefore, the study of free sintering processes is more important for mass production. In addition, to reduce the porosity of sintered powder samples, hot isostatic pressing (HIP), which is actively used in additive manufacturing for critical products, should be applied.

The production of long bars and wires from HEAs by hot extrusion of powders can be used for making rod structures as well as for additive manufacturing processes, such as thermal spraying or wire arc additive manufacturing.

An analysis of the chemical composition of high-entropy alloys shows that HEAs based on 3d transition elements are suitable for temperatures up to 1000 °C,

while refractory HEAs (RHEAs) are used at higher temperatures. The addition of aluminum is aimed at reducing the density of RHEAs and increasing oxidation resistance.

One of the promising methods for improving strength at high temperatures is oxide dispersion strengthening. However, in some cases, nanoparticles chemically interact with the matrix, altering the chemical composition of the dispersed particles. Therefore, the selection of strengthening nanoscale powders requires prior analysis.

The high thermal stability of RHEAs and the retention of nanoscale grains at temperatures above 1000 °C are determined by the high recrystallisation temperature.

The results of this review confirm that HEAs have potential for use in high-temperature applications. The mechanical properties of sintered RHEA samples are superior to those of samples with similar chemical compositions obtained by liquid-phase methods. However, further research and development are required to improve the oxidation resistance and mechanical properties of powder RHEAs at the desired temperatures.

A key finding from the analysis is the identification of a limited range of methods for evaluating high-temperature properties (such as compressive strength, tensile strength, and nano-hardness). This restricts consumers' ability to fully assess the feasibility of new alloys and production methods for practical applications. Therefore, it is essential to broaden the evaluation approaches to include a wider spectrum of performance characteristics, such as fracture toughness, heat resistance, wear resistance, fatigue strength, and overall durability.

Thus, future research should focus on:

- determining fatigue properties and the durability of powder products to ensure their reliability in real engineering applications;
- manufacturing large parts with complex shapes;
- reducing porosity without significantly increasing cost;
- developing low-temperature deformation methods;
- creating environmentally friendly and highly accurate production technologies.

When planning new research, it is important to focus on scalability, cost-effectiveness, and the practical application of powder synthesis and consolidation methods to enable their broader adoption in real-world engineering projects.

REFERENCES / СПИСОК ЛИТЕРАТУРЫ

1. Yeh J.W., Chen S.K., Lin S.J., Gan J.Y., Chin T.S., Shun T.T., Tsau C.H., Chang S.Y. Nanostructured high-entropy alloys with multiple principal elements: Novel alloy design concepts and outcomes. *Advanced Engineering Materials*. 2004;6(5):299–303. <https://doi.org/10.1002/adem.200300567>
2. Cantor B., Chang I.T.H., Knight P., Vincent A.J.B. Microstructural development in equiatomic multicomponent alloys. *Materials Science and Engineering: A*. 2004;375–377: 213–218. <https://doi.org/10.1016/j.msea.2003.10.257>
3. Murty B.S., Yeh J.W., Ranganathan S., Bhattacharjee P.P. High-Entropy Alloys. London: Elsevier; 2019:388. <https://doi.org/10.1016/C2017-0-03317-7>
4. Jamieson B., Peter K. High-Entropy Materials: Theory, Experiments, and Applications. Switzerland: Springer Cham; 2021:774. <https://doi.org/10.1007/978-3-030-77641-1>
5. Behera A. Advanced Materials. Switzerland: Springer Cham; 2022:748. <https://doi.org/10.1007/978-3-030-80359-9>
6. Liu F., Liaw P.K., Zhang Y. Recent progress with BCC-structured high-entropy alloys. *Metals*. 2022;12(3):501. <https://doi.org/10.3390/met12030501>
7. Patel P., Roy A., Sharifi N., Stoyanov P., Chromik R.R., Moreau C. Tribological performance of high-entropy coatings (HECs): A review. *Materials*. 2022;15(10):3699. <https://doi.org/10.3390/ma15103699>
8. Sonar T., Ivanov M., Trofimov E., Tingaev A., Suleymanova I. An overview of microstructure, mechanical properties and processing of high entropy alloys and its future perspectives in aeroengine applications. *Materials Science for Energy Technologies*. 2024;7:35–60. <https://doi.org/10.1016/j.mset.2023.07.004>
9. Senkov O.N., Miracle D.B., Chaput K.J., Couzinie J.-P. Development and exploration of refractory high entropy alloys – A review. *Journal of Materials Research*. 2018;33: 3092–3128. <https://doi.org/10.1557/jmr.2018.153>
10. Senkov O.N., Wilks G.B., Miracle D.B., Chuang C.P., Liaw P.K. Refractory high-entropy alloys. *Intermetallics*. 2010;18(9):1758–1765. <https://doi.org/10.1016/j.intermet.2010.05.014>
11. Xiong W., Guo A., Zhan S., Liu C., Cao S. Refractory high-entropy alloys: A focused review of preparation methods and properties. *Journal of Materials Science and Technology*. 2023;142:196–215. <https://doi.org/10.1016/j.jmst.2022.08.046>
12. Wang X., Huang H., Shi J., Xu H., Meng D. Recent progress of tungsten-based high-entropy alloys in nuclear fusion. *Tungsten*. 2021;3:143–160. <https://doi.org/10.1007/s42864-021-00092-8>
13. Shi T., Lei P., Yan X., Li J., Zhou Y., Wang Y., Su Z., Dou Y., He X., Yun D., Yang W., Lu C. Current development of bodycentered cubic high-entropy alloys for nuclear applications. *Tungsten*. 2021;3:197–217. <https://doi.org/10.1007/s42864-021-00086-6>
14. Karan, Pachauri P., Kumar A., Maury M. Effect of powder metallurgy on high entropy alloy materials: A review. *Materials Today: Proceedings*. 2021;47(13):4026–4033. <https://doi.org/10.1016/j.matpr.2021.04.529>
15. Page M.J., McKenzie J.E., Bossuyt P.M., Boutron I., Hoffmann T.C., Mulrow C.D., Tetzlaff J.M., Akl E.A., Brennan S.E., Chou R., etc. The PRISMA 2020 statement: An updated guideline for reporting systematic reviews. *BMJ*. 2021;372:n71. <https://doi.org/10.1136/bmj.n71>
16. Xiang L., Guo W., Liu B., Fu A., Li J., Fang Q., Liu Y. Microstructure and mechanical properties of TaNbVTiAl_x refrac-

- tory high-entropy alloys. *Entropy*. 2020;22(3):282. <https://doi.org/10.3390/e22030282>
17. Li H., Lin H., Liang X., He W., Liu B., Liu Y., Wang L. In situ development and high temperature features of CoCrFeNi-M₆C_p high entropy-alloy based hard-metal. *Metals*. 2020;10(3):408. <https://doi.org/10.3390/met10030408>
 18. Alvaredo-Olmos P., Molina-Aldareguía J., Vaz-Romero A., Prieto E., González-Julián J., Monclús M.A. Understanding the links between the composition-processing-properties in new formulations of HEAs sintered by SPS. *Metals*. 2021;11(6):888. <https://doi.org/10.3390/met11060888>
 19. Yang T., Cai B., Shi Y., Wang M., Zhang G. Preparation of nano-structured CoCrFeMnNi high entropy alloy by hot pressing sintering gas atomized powders. *Micron*. 2021;147:103082. <https://doi.org/10.1016/j.micron.2021.103082>
 20. Zhang R., Meng J., Han J., etc. Oxidation resistance properties of refractory high-entropy alloys with varied Al_xCrTiMo content. *Journal of Materials Science*. 2021;56:3551–3561. <https://doi.org/10.1007/s10853-020-05480-y>
 21. Liu Q., Wang G., Liu Y., Sui X., Chen Y., Luo S. Hot deformation behaviors of an ultrafine-grained MoNbTaTiV refractory high-entropy alloy fabricated by powder metallurgy. *Materials Science and Engineering: A*. 2021;809:140922. <https://doi.org/10.1016/j.msea.2021.140922>
 22. Peng H., Kang Z., Long Y., Zhou L. A two-phase ultrafine-grained NbMoTaWV refractory high entropy alloy with prominent compressive properties. *Vacuum*. 2022;199:110930. <https://doi.org/10.1016/j.vacuum.2022.110930>
 23. Gao F., Sun Y., Hu L., Shen J., Liu W., Ba M., Deng C. Microstructural evolution and thermal stability in a nanocrystalline lightweight TiAlV_{0.5}CrMo refractory high-entropy alloy synthesized by mechanical alloying. *Materials Characterization*. 2022;329:133179. <https://doi.org/10.1016/j.matlet.2022.133179>
 24. Ujah C., Popoola A., Popoola O., Afolab A., Uyor U. Mechanical and oxidation characteristics of Ti20-Al16-V16-Fe16-Ni16-Cr16 high-entropy alloy developed via spark plasma sintering for high-temperature/strength applications. *Journal of Materials Engineering and Performance*. 2023;32:18–28. <https://doi.org/10.1007/s11665-022-07066-y>
 25. Zhang X., Li T., Cao Y., Liao T., Xie Z., Fu A., Li J., Fang Q., He Z., Liu B. Oxide dispersion strengthening mediated ultra-high strength at wide temperature range in NbTaTiV refractory high-entropy alloys. *International Journal of Refractory Metals and Hard Materials*. 2023;116:106352. <https://doi.org/10.1016/j.ijrmhm.2023.106352>
 26. Kuskov K.V., Nepapushev A.A., Aydynyan S., Shaysultanov D.G., Stepanov N.D., Nazaretyan K., Kharatyan S., Zakharova E.V., Belov D.S., Moskovskikh D.O. Combustion synthesis and reactive spark plasma sintering of non-equiautomic CoAl-based high entropy intermetallics. *Materials*. 2023;16(4):1490. <https://doi.org/10.3390/ma16041490>
 27. Boztemur B., Bayrak K., Gökçe H., Ayas E., Balcı-Çağiran Ö., Derin B., Ağaoğulları D. Mechanically alloyed and spark plasma sintered WNbMoVTa refractory high entropy alloys: Effects of Cr and Al on the microstructural and mechanical properties. *Journal of Alloys and Compounds*. 2023;965:171415. <http://dx.doi.org/10.1016/j.jallcom.2023.171415>
 28. Das S., Robi P. Processing and characterizations of powder of the AlCoCuFeNi high entropy alloy. *Emergent Materials*. 2023;6:987–997. <https://doi.org/10.1007/s42247-023-00466-3>
 29. Qin M., Shivakumar S., Luo J. Refractory high-entropy nanoalloys with exceptional high-temperature stability and enhanced sinterability. *Journal of Materials Science*. 2023;58:8548–8562. <https://doi.org/10.1007/s10853-023-08535-y>
 30. Gao F., Sun Y., Hu L., Shen J., Liu W., Ba M., Deng C. Microstructure and strengthening mechanisms of novel lightweight TiAlV_{0.5}CrMo refractory high-entropy alloy fabricated by mechanical alloying and spark plasma sintering. *Journal of Alloys and Compounds*. 2023;932:167659. <https://doi.org/10.1016/j.jallcom.2022.167659>
 31. Fu A., Cao Y., Xie Z., Wang J., Liu B. Microstructure and mechanical properties of Al-Fe-Co-Cr-Ni high entropy alloy fabricated via powder extrusion. *Journal of Alloys and Compounds*. 2023;943:169052. <https://doi.org/10.1016/j.jallcom.2023.169052>
 32. Fu A., Cao Y., Liu Y., Xu S. Microstructure and mechanical properties of novel lightweight TaNbVTi-based refractory high entropy alloys. *Materials*. 2022;15(1):355. <https://doi.org/10.3390/ma15010355>
 33. Zong L., Xu L., Luo C., Jiao Z., Li X., Sun W., Wei S. Mechanical properties and strengthening mechanism of the nano-sized m-ZrO₂ ceramic particle reinforced NbMoTaW refractory high-entropy alloy. *International Journal of Refractory Metals and Hard Materials*. 2023;113:106201. <https://doi.org/10.1016/j.ijrmhm.2023.106201>
 34. Zong L., Xu L., Luo C., Li Z., Zhao Y., Xu Z., Zhu C., Wei S. Fabrication of nano-ZrO₂ strengthened WMoNbTaV refractory high-entropy alloy by spark plasma sintering. *Materials Science and Engineering: A*. 2022;843:143113. <https://doi.org/10.1016/j.msea.2022.143113>
 35. Liao T., Cao Y., Guo W., Fang Q., Li J., Liu B. Microstructure and mechanical property of NbTaTiV refractory high-entropy alloy with different Y₂O₃ contents. *Rare Metals*. 2022;41:3504–3514. <https://doi.org/10.1007/s12598-022-02038-6>
 36. Moravcikova-Gouvea L., Moravcik I., Pouchly V., Kovacova Z., Kitzmantel M., Neubauer E., Dlouhy I. Tailoring a refractory high entropy alloy by powder metallurgy process optimization. *Materials*. 2021;14(19):5796. <https://doi.org/10.3390/ma14195796>
 37. Liu Q., Wang G., Sui X., Xu Y., Liu Y., Yang J. Ultra-fine grain Ti_xVNbMoTa refractory high-entropy alloys with superior mechanical properties fabricated by powder metallurgy. *Journal of Alloys and Compounds*. 2021;865:158592. <https://doi.org/10.1016/j.jallcom.2020.158592>
 38. Salemi F., Karimzadeh F., Abbasi M. Evaluation of thermal and mechanical behavior of CuNiCoZnAl high-entropy alloy fabricated using mechanical alloying and spark plasma sintering. *Metallurgical and Materials Transactions A*. 2021;52:1947–1962. <https://doi.org/10.1007/s11661-021-06205-9>
 39. Li Y., Du Z., Fu Y., Sun H., Fan J., Han Y. Microstructures and mechanical properties of novel MoTaVW refractory high-entropy alloys. *Journal of Alloys and Compounds*. 2023;968:172165. <https://doi.org/10.1016/j.jallcom.2023.172165>

40. Wu Y., Liaw P.K., Zhang Y. Preparation of bulk TiZrNbMoV and NbTiAlTaV high-entropy alloys by powder sintering. *Metals*. 2021;11(11):1748. <https://doi.org/10.3390/met11111748>
41. Shkodich N., Sedegov A., Kuskov K., Busurin S., Scheck Y., Vadchenko S., Moskovskikh D. Refractory high-entropy HfTaTiNbZr-based alloys by combined use of ball milling and spark plasma sintering: effect of milling intensity. *Metals*. 2020;10(9):1268. <https://doi.org/10.3390/met10091268>
42. Ivannikov A.Y., Grebennikov I.K., Klychevskikh Y.A., Mikhailova A.V., Sergienko K.V., Kaplan M.A., Lysenkov A.S., Sevostyanov M.A. Fabrication, microstructure, and physico-mechanical properties of Fe–Cr–Ni–Mo–W high-entropy alloys from elemental powders. *Metals*. 2022;12(10):1764. <https://doi.org/10.3390/met12101764>
43. Sharma B., Nagano K., Saxena K.K., Fujiwara H., Ameyama K. Application of hydride process in achieving equimolar TiNbZrHfTa BCC refractory high entropy alloy. *Crystals*. 2020;10(11):1020. <https://doi.org/10.3390/cryst10111020>
44. Chen Y., Liu P., Dong Z., Liu H., Wang J., Guo X., Xia Y., Wang Q. Sintering, microstructure, and mechanical properties of TiTa NbZrHf high-entropy alloys prepared by cold isostatic pressing and pressure-less sintering of hydrides. *Materials*. 2023;16:1759. <https://doi.org/10.3390/ma16051759>
45. Liu B., Duan H., Li L., Zhou C., He J., Wu H. Microstructure and mechanical properties of ultra-hard spherical refractory high-entropy alloy powders fabricated by plasma spheroidization. *Powder Technology*. 2021;382:550–555. <https://doi.org/10.1016/j.powtec.2021.01.021>
46. Xia M., Chen Y., Chen K., Tong Y., Liang X., Shen B. Synthesis of WTaMoNbZr refractory high-entropy alloy powder by plasma spheroidization process for additive manufacturing. *Journal of Alloys and Compounds*. 2022;917:165501. <https://doi.org/10.1016/j.jallcom.2022.165501>
47. Wang H., Niu Z., Chen C., Chen H., Zhu X., Zhou F., Zhang X., Liu X., Wu Y., Jiang S. Powder production of an equimolar NbTaTiZr high-entropy alloy via hydrogen embrittlement. *Materials Characterization*. 2022;193:112265. <https://doi.org/10.1016/j.matchar.2022.112265>
48. Kolmakov A.G., Ivannikov A.Yu., Kaplan M.A., Kirsankin A.A., Sevost'yanov M.A. Corrosion-resistant steels in additive manufacturing. *Izvestiya. Ferrous Metallurgy*. 2021;64(9):619–650. (In Russ.). <https://doi.org/10.17073/0368-0797-2021-9-619-650>
Колмаков А.Г., Иванников А.Ю., Каплан М.А., Кирсанкин А.А., Севостьянов М.А. Коррозионностойкие стали в аддитивном производстве. *Известия вузов. Черная металлургия*. 2021;64(9):619–650. <https://doi.org/10.17073/0368-0797-2021-9-619-650>
49. Gao S., Fu A., Xie Z., Liao T., Cao Y., Liu B. Preparation and microstructure of high-activity spherical TaNbTiZr refractory high-entropy alloy powders. *Materials*. 2023;16(2):791. <https://doi.org/10.3390/ma16020791>
50. Moser M., Dine S., Vrel D., Perrière L., Pirès-Brazuna R., Couque H., Bernard F. Elaboration and characterization of WMoTaNb high entropy alloy prepared by powder metallurgy processes. *Materials*. 2022;15(15):5416. <https://doi.org/10.3390/ma15155416>
51. Gu T., Wang L.M., Hu Q., Liang X., Fu D., Chen Y., Zhao X., Sheng Y. Effect of mechanical alloying and sintering behavior on the microstructure and properties of NbMoTaWRE refractory high entropy alloy. *Metals and Materials International*. 2022;28:2571–2582. <https://doi.org/10.1007/s12540-021-01165-6>
52. Liu J., Zhao X., Zhang S., Sheng Y., Hu Q. Microstructure and mechanical properties of MoNbTaW refractory high-entropy alloy prepared by spark plasma sintering. *Journal of Materials Research*. 2023;38:484–496. <https://doi.org/10.1557/s43578-022-00833-6>
53. Maharana S., Prasad D., Seetharaman S., Sabat M. Effect of sintering parameters on phase evolution, microstructural development and mechanical behavior of Ni₄₆Al₁₂Co₁₈Cr₈Fe₁₂Mo₄ high entropy alloy synthesized via mechanical alloying and spark plasma sintering. *Materials Science and Engineering: A*. 2023;886:145695. <https://doi.org/10.1016/j.msea.2023.145695>
54. Chen C., Chang C., Chen H. Investigation of Cr content, second phase, and sintering temperature on characteristics of WMoVTiCr refractory high entropy alloys. *International Journal of Refractory Metals and Hard Materials*. 2023;110:106034. <https://doi.org/10.1016/j.ijrmhm.2022.106034>
55. Zhang Y., Bian T., Shen X., Wang Z., Ye S., Feng S., Yu K., Ding C., Yu P. Sintering mechanism and microstructure evolution of a CoCrFeNiMn high entropy alloy fabricated by metal injection molding. *Journal of Alloys and Compounds*. 2021;868:158711. <https://doi.org/10.1016/j.jallcom.2021.158711>
56. Anwer Z., Umer M., Adeel F., Hafeez M., Yaqoob K., Luo X., Ahmad I. Microstructure and mechanical properties of hot isostatic pressed tungsten heavy alloy with FeNiCoCrMn high entropy alloy binder. *Journal of Materials Research and Technology*. 2023;22:2897–2909. <https://doi.org/10.1016/j.jmrt.2022.12.078>
57. Tang Z., Senkov O., Parish C., Zhang C., Zhang F., Santodonato L., Wang G., Zhao G., Yang F., Liaw P. Tensile ductility of an AlCoCrFeNi multi-phase high-entropy alloy through hot isostatic pressing (HIP) and homogenization. *Materials Science and Engineering: A*. 2015;647:229–240. <https://doi.org/10.1016/j.msea.2015.08.078>
58. Duan B., Yu Y., Liu X., Wang D., Wu Z. A novel non-equiatomic (W₃₅Ta₃₅Mo₁₅Nb₁₅)₉₅Ni₅ refractory high entropy alloy with high density fabricated by powder metallurgical process. *Metals*. 2020;10(11):1436. <https://doi.org/10.3390/met10111436>

Information about the Authors

Сведения об авторах

Aleksandr Yu. Ivannikov, Cand. Sci. (Eng.), Senior Researcher of the Laboratory of Plastic Deformation of Metals, Baikov Institute of Metallurgy and Materials Science, Russian Academy of Sciences

ORCID: 0000-0003-1113-391X

E-mail: aivannikov@imet.ac.ru

Александр Юрьевич Иванников, к.т.н., старший научный сотрудник лаборатории пластической деформации металлов, Институт металлургии и материаловедения им. А.А. Байкова РАН

ORCID: 0000-0003-1113-391X

E-mail: aivannikov@imet.ac.ru

Vladimir S. Yusupov, Dr. Sci. (Eng.), Chief Researcher, Head of the Laboratory of Plastic Deformation of Metals, Baikov Institute of Metallurgy and Materials Science, Russian Academy of Sciences

ORCID: 0000-0002-0640-2217

E-mail: vsyusupov@mail.ru

Владимир Сабитович Юсупов, д.т.н., главный научный сотрудник, заведующий лабораторией пластической деформации металлов, Институт металлургии и материаловедения им. А.А. Байкова РАН

ORCID: 0000-0002-0640-2217

E-mail: vsyusupov@mail.ru

Contribution of the Authors

Вклад авторов

A. Yu. Ivannikov – writing the text, search and analysis of literature.

V. S. Yusupov – scientific guidance, article analysis.

А. Ю. Иванников – подготовка текста статьи, поиск и анализ литературы.

В. С. Юсупов – научное руководство, анализ статьи.

Received 28.06.2024

Revised 11.09.2024

Accepted 23.09.2024

Поступила в редакцию 28.06.2024

После доработки 11.09.2024

Принята к публикации 23.09.2024



UDC 669.1

DOI 10.17073/0368-0797-2024-5-520-530



Original article

Оригинальная статья

ASSESSMENT OF THE EFFECTIVENESS OF TECHNOLOGICAL MEASURES TO EXTEND THE CAMPAIGN OF BLAST FURNACE NO. 5 OF PJSC SEVERSTAL (2006 – 2024) BASED ON AN EXAMINATION OF ITS WORKING SPACE DURING A FIRST-CATEGORY OVERHAUL

A. A. Kal'ko¹, L. I. Leont'ev^{2,3}, E. A. Volkov¹¹ PJSC Severstal, Cherepovets Steel Mill (30 Mira Str., Cherepovets, Vologda Region 162608, Russian Federation)² I.P. Bardin Central Research Institute of Ferrous Metallurgy (23/9 Radio Str., Moscow 105005, Russian Federation)³ Scientific Council on Metallurgy and Metal Science of Russian Academy of Sciences (Department of Chemistry and Material Sciences) (32a Leninskii Ave., Moscow 119991, Russian Federation)

✉ aakalko@severstal.com

Abstract. The paper presents the findings from the study of the working space of blast furnace No. 5 of PJSC Severstal during its first-category overhaul in 2024 lasting 17.46 years, which significantly exceeded the standard service life. The effectiveness of technological measures taken to extend the furnace's campaign from 2006 to 2024, aimed at protecting the refractory lining in critical areas such as the hearth, lower shaft, and the upper bosh, was evaluated. The residual thickness of the refractory lining in the shaft, hearth, and metal receiver is analyzed, and maps showing the actual thickness of the lining across different sections are generated. The measured maximum wear of the shaft refractory lining is 344 mm (37.4 % of the original value); the measured maximum wear of carbon blocks in the area of cesspool openings – 313 mm (23.4 % of the original block size). In the upper part of the hearth, the minimum residual thickness of refractories with an Al_2O_3 content of 43 % is 220 mm or 31.9 % of the initial value. The paper also discusses safe remote measurement methods, including 3D laser scanning of the furnace shaft during the removal of residual charge materials. It highlights the advantages of ground-based laser scanners in capturing dense, high-quality 3D geometric data. Additionally, the paper describes the experience of remotely measuring the residual thickness of carbon blocks around the raking openings. Comparisons are made between the actual residual thickness of the refractory lining in the hearth, bottom carbon blocks, and high-alumina refractories of the tuyere zone, and the results obtained using ultrasonic echo-sounding technology (AU-E) during the furnace's operation. The paper also includes a description of the stress wave propagation technology, which utilizes data analysis in the time and frequency domains to determine lining thickness and detect anomalies. The results of the current and previous blast furnace campaigns are compared in terms of pig iron production, the number of cooling system failures, and refractory wear across the entire working space of the furnace. The total production of pig iron in the 2006 – 2024 campaign, related to the furnace area, amounted to 420.0 thousand tons/m² and exceeded the figure for the previous campaign by 1.90 times.

Keywords: blast furnace, 3D scanning, residual lining thickness, hearth erosion, campaign duration, PJSC Severstal, hearth, shaft, totterman, hearth washing, skull formation, specific natural gas consumption, solid fuel consumption per ton of pig iron, ultrasonic echo sounding, iron ore materials, coke, CSR indicator

For citation: Kal'ko A.A., Leont'ev L.I., Volkov E.A. Assessment of the effectiveness of technological measures to extend the campaign of blast furnace No. 5 of PJSC Severstal (2006 – 2024) based on an examination of its working space during a first-category overhaul. *Izvestiya. Ferrous Metallurgy*. 2024;67(5):520–530. <https://doi.org/10.17073/0368-0797-2024-5-520-530>

ОЦЕНКА РЕЗУЛЬТАТИВНОСТИ ПРИМЕНЕНИЯ ТЕХНОЛОГИЧЕСКИХ МЕРОПРИЯТИЙ ПО ПРОДЛЕНИЮ КАМПАНИИ ДОМЕННОЙ ПЕЧИ № 5 ПАО «СЕВЕРСТАЛЬ» 2006 – 2024 ГГ. ПРИ ИССЛЕДОВАНИИ ЕЕ РАБОЧЕГО ПРОСТРАНСТВА В ПЕРИОД ПРОВЕДЕНИЯ КАПИТАЛЬНОГО РЕМОНТА I РАЗРЯДА

А. А. Калько¹, Л. И. Леонтьев^{2,3}, Е. А. Волков¹

¹ ПАО «Северсталь» Череповецкий металлургический комбинат (Россия, 162608, Вологодская область, Череповец, ул. Мира, 30)

² Центральный научно-исследовательский институт черной металлургии им. И.П. Бардина (Россия, 105005, Москва, ул. Радио, 23/9)

³ Президиум РАН (Россия, 119991, Москва, Ленинский пр., 32а)

✉ aakalko@severstal.com

Аннотация. В работе представлен опыт изучения рабочего пространства доменной печи № 5 ПАО «Северсталь» по результатам кампании 2006 – 2024 гг. продолжительностью 17,46 лет, существенно превысившей нормативные сроки эксплуатации. Выполнена оценка результативности технологических мероприятий по продлению кампании доменной печи, применявшихся для защиты огнеупорной футеровки в критических зонах горна, нижней части шахты и верха заплечиков. Авторы провели анализ остаточной толщины огнеупорной футеровки шахты, горна и металлоприемника доменной печи, сформировали карты фактического разгара огнеупорной футеровки по различным сечениям. Измеренный максимальный износ огнеупорной футеровки шахты составил 344 мм или 37,4 % первоначальной величины, измеренный максимальный разгар углеродистых блоков в районе выгребных проемов – 313 мм или 23,4 % первоначального размера блока. В верхней части горна минимальная остаточная толщина огнеупоров с содержанием $Al_2O_3 = 43\%$ составила 220 мм или 31,9 % исходной величины. Представлены способы безопасного дистанционного измерения фактического профиля шахты доменной печи с помощью лазерного 3D сканирования в процессе выгребки остатков шихтовых материалов. Время выполнения 3D сканирования в рабочем пространстве печи составило 50 мин. В работе проведен сравнительный анализ фактической остаточной толщины футеровки в районе углеродистых блоков горна и лещади и высокоглиноземистых огнеупоров фурменной зоны с результатами оценок с использованием технологии ультразвукового зондирования эхо-методом (AU-E), выполнявшихся в период работы доменной печи. Приведено описание технологии распространения волн напряжения с использованием анализа данных в временном и частотном домене для определения толщины футеровки или для обнаружения аномалий. Авторы провели сравнение результатов предыдущей и текущей кампаний доменной печи по объему произведенного чугуна, количеству вышедших из строя элементов системы охлаждения, износу огнеупоров по всему рабочему пространству доменной печи. Суммарное производство чугуна в кампании 2006 – 2024 гг., отнесенное к площади горна, составило 420,0 тыс. т/м² и превысило показатель предыдущей кампании в 1,90 раза.

Ключевые слова: доменная печь, 3D сканирование, остаточная толщина футеровки, разгар горна, продолжительность кампании, ПАО «Северсталь», горн, шахта, тотерман, промывка горна, гарнисажеобразование, удельный расход природного газа, расход твердого топлива на тонну чугуна, ультразвуковое зондирование эхо-методом, железорудные материалы, кокс, показатель CSR

Для цитирования: Калько А.А., Леонтьев Л.И., Волков Е.А. Оценка результативности применения технологических мероприятий по продлению кампании доменной печи № 5 ПАО «Северсталь» 2006 – 2024 гг. при исследовании ее рабочего пространства в период проведения капитального ремонта I разряда. *Известия вузов. Черная металлургия.* 2024;67(5):520–530.
<https://doi.org/10.17073/03688-0797-2024-5-520-530>

INTRODUCTION

The extension of a blast furnace (BF) campaign, defined as the period between first-category overhauls, allows for a reduction in the cost of pig iron production. To increase the length of the inter-repair period, both technical and technological measures are developed. The effectiveness of these measures is generally evaluated based on the results of the completed campaign, taking into account its duration and the volume of pig iron produced during the inter-repair period. The end of the campaign is primarily determined by reaching the minimum permissible residual thickness of the refractory lining. Many researchers [1 – 4] have noted that the achievement of a long, safe, and accident-free opera-

tion of the blast furnace largely depends on the durability of the hearth and the bottom. While the residual thickness of the shaft lining can be measured periodically during brief furnace shutdowns when the charge level is lowered, direct measurements of the refractory thicknesses in the hearth and bottom during the campaign are extremely difficult, and wear assessment can only be performed using non-destructive testing methods [5]. This makes the information about the actual condition of the refractories in the working space of the furnace, obtained during a shutdown for re-lining, usually during a first-category overhaul, particularly valuable. Such information not only allows for the evaluation of the adequacy of non-destructive testing methods and the calculation models used during the campaign to assess the lining thickness,

but also helps identify critical areas requiring protection and adjustments to the smelting technology in the future.

This paper presents the experience of studying the working space of blast furnace No. 5 of PJSC Severstal during its first-category overhaul in 2024. The furnace operated in its campaign from October 20, 2006, to April 2, 2024, for a total of 17.46 years (referred to as the current campaign hereinafter), significantly exceeding the standard service life typical for blast furnaces of similar design. During the campaign, over 75 million tons of pig iron were produced, surpassing the cumulative pig iron output of the first two campaigns. These results were achieved on a blast furnace of “classic” design, without any major capital-intensive changes to the refractory lining of the shaft and hearth, but through the development of new methods for managing, controlling, and adjusting the pig iron smelting technology [6].

PREREQUISITES FOR THE RESEARCH

Based on the results of the study of the working space of blast furnace No. 5, which was blown out at the end of the previous campaign (1995 – 2006), certain zones requiring protection and adjustments to the smelting technology for the current campaign (2006 – 2024) were identified. These were the hearth, the lower shaft, and the upper bosh, as the zones were found to have low residual refractory thickness and little to no protective skull.

In the current campaign, a set of measures was implemented, including regular hearth washing to remove coke debris and flux residues, maintaining a stable self-renewing skull in the lower shaft, and ensuring effective distribution of different types of solid fuel across the furnace’s cross-section, as described in detail in [6]. The need to assess the effectiveness of these measures formed the basis for launching a program to study the working space of blast furnace No. 5 during its 2024 overhaul. It should be noted that blast furnace No. 5 accounts for up to 40 % of the total pig iron production at PJSC Severstal, imposing strict time constraints on the repair schedule and the duration of any studies aimed at extending this timeframe. Based on this premise, it was decided to minimize human presence during measurements in the working space of the furnace and to maximize the use of modern remote measurement methods with laser scanners.

MEASUREMENT OF ACTUAL LINING WEAR IN THE SHAFT OF BF NO. 5 USING THE LEICA RTC360 SCANNER

Ground-based laser scanners (GLS) are instruments capable of quickly capturing dense, high-quality 3D geometric data of the surrounding environment. They have become standard tools in numerous applications, such as as-built modeling, environmental and geological sciences, forensic analysis, and engineering. Photogrammetry and

geodesy, being engineering disciplines with the highest accuracy requirements, have recently driven significant improvements in this measurement technology, making it competitive even for the most complex measurement tasks [7].

The scanning was performed on April 12, 2024, during the furnace raking process, using the Leica RTC360 scanner. Measurements were taken from the throat platform at three points and from the cesspool area at the casthouse level. The results of the scan yielded a point cloud consisting of 117.5 million points. The points were processed using Leica TruView software. Due to the limitations of direct visibility to all sections of the furnace’s inner surface, some areas were partially not covered by the scan. The overall view of the measured point cloud, representing the inner surface of the blast furnace and the location of the scanning stations, is shown in Fig. 1. Measurements of the actual internal diameters of the furnace at various levels were taken at heights of +43,900 mm, +41,350 mm, +40,500 mm, +39,500 mm, +38,500 mm, +37,500 mm, +36,500 mm, +35,500 mm, +34,500 mm,

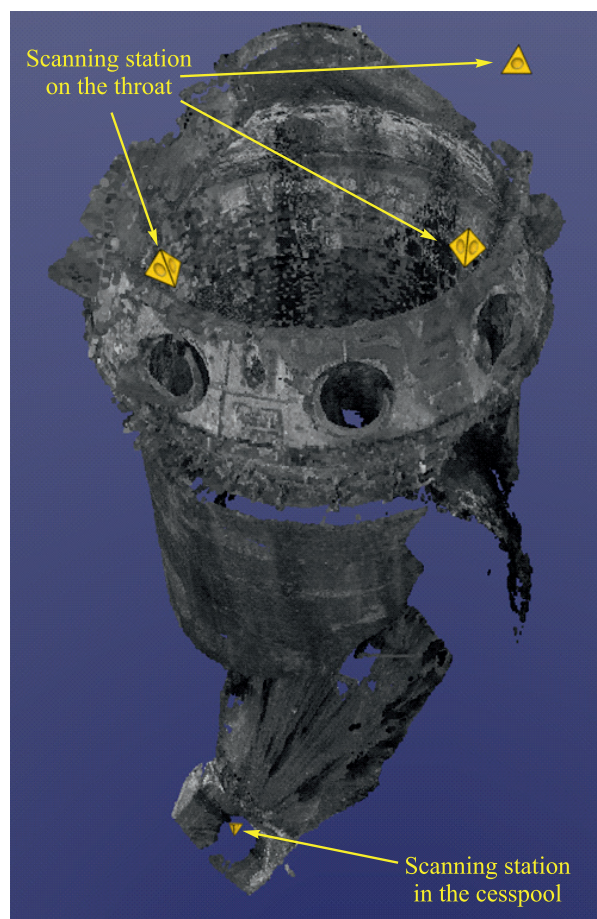


Fig. 1. General view of the scanning results of the internal space of blast furnace No. 5, showing the location of the scanning stations

Рис. 1. Общий вид результатов сканирования внутреннего пространства ДП № 5 с указанием расположения станций сканирования

Table 1. Actual wear of the refractory lining in the shaft of blast furnace No. 5 by sections of diametrically opposite iron tapholes

Таблица 1. Фактический износ огнеупорной футеровки шахты ДП № 5 по сечениям диаметрально противоположных леток

Height, mm	Design diameter, mm	Measurements across the diametrically opposite tapholes, mm				
		iron tapholes 1 – 3	iron tapholes 2 – 4	average residual diameter at the height	deviation of residual diameter (actual vs. design)	refractory lining wear
+43,900	11,200	11,163	11,102	11,133	-68	-34
+43,000	11,200	11,278	11,252	11,265	65	32
+42,000	11,200	11,284	11,283	11,283	83	42
+41,350	11,239	11,790	12,065	11,928	689	344
+40,500	11,460	11,937	11,950	11,944	484	242
+40,000	11,590	11,975	11,996	11,986	396	198
+39,500	11,720	12,061	12,125	12,093	373	187
+39,000	11,850	12,300	12,338	12,319	469	235
+38,500	11,979	12,363	12,308	12,336	356	178
+38,000	12,109	12,529	12,548	12,539	429	215
+37,500	12,239	12,654	12,539	12,597	357	179
+37,000	12,369	12,620	12,700	12,660	291	146
+36,500	12,499	12,751	12,749	12,750	251	125
+36,000	12,629	12,902	12,896	12,899	270	135
+35,500	12,759	12,939	13,042	12,991	232	116
+35,000	12,889	13,225	13,172	13,198	310	155
+34,500	13,019	13,200	13,325	13,263	244	122
+34,000	13,149	13,331	13,333	13,332	183	92
+33,500	13,278	13,503	13,392	13,448	169	85
+33,000	13,408	13,640	13,628	13,634	226	113
+32,500	13,538	13,663	13,748	13,706	167	84
+32,000	13,668	13,897	13,889	13,893	225	112

+33,500 mm, and +32,500 mm. Horizontal sections of the scanning areas at the corresponding heights were used to determine these diameters. An example of a diameter measurement at +43,900 mm, with reference to the location of the tap holes, is shown in Fig. 2.

Additionally, orthogonal projections of the scanning results were constructed with a 1 m step and an initial offset of 0.5 m from the aforementioned height levels (from +43,000 mm to +32,000 mm inclusive), which made it possible to create a map of the actual wear of the refractory lining in the shaft of blast furnace No. 5, as shown in Table 1.

The negative value of the lining wear at the height of +43,900 mm is explained by the shift in the position of the throat armour segments as a result of prolonged operation. The graphical representation of the variations in the lining wear value depending on the height of the blast furnace shaft is shown in Fig. 3.

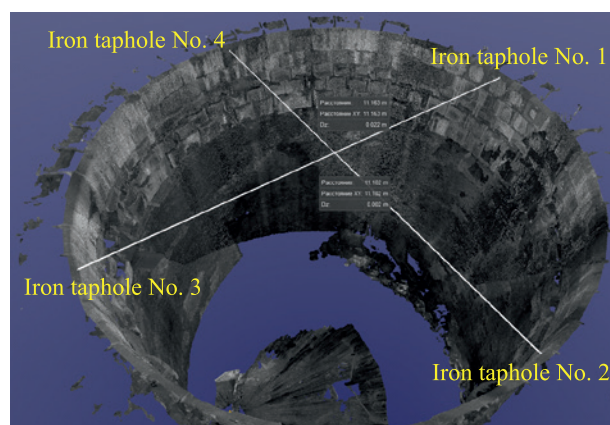


Fig. 2. Example of measuring the diameter of the internal space of blast furnace No. 5 at +43,900 mm (throat armour) with reference to the location of iron tapholes

Рис. 2. Пример измерения диаметра внутреннего пространства ДП № 5 на отметке +43 900 мм (колошниковая защита) с привязкой к расположению чугунных леток

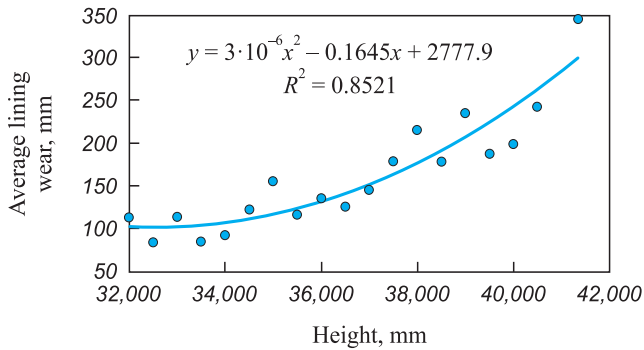


Fig. 3. Variations in the actual wear of the refractory lining (uncooled section) based on the height of blast furnace shaft No. 5, according to the results of the 2006 – 2024 campaign

Рис. 3. Изменение фактической величины износа огнеупорной футеровки (неохлаждаемая часть) в зависимости от высотной отметки шахты ДП № 5 по результатам кампании 2006 – 2024 гг.

Thus, the maximum wear of the refractory lining in the upper uncooled section of the shaft of blast furnace No. 5 during the 2006 – 2024 campaign was observed in the upper rows of refractories, directly beneath the throat armour segments, and amounted to 242–344 mm, or 37.4 % of the original lining thickness. At deeper levels, up to 10 m below the charge level, the lining wear did not exceed 100 – 150 mm, or 11 – 16 % of the original thickness. During the previous campaign of the furnace (1996 – 2006), a significant reduction in the thickness of the shaft lining was recorded – the upper rows had a residual thickness of 270 – 300 mm, and the wear of the uncooled section of the shaft reached 67 %, which was 1.8 times greater than in the current campaign.

The condition of the cooled section of the shaft of blast furnace No. 5 based on the results of the current campaign is shown in Fig. 4. The dashed line (A – B) indicates the boundary of the uncooled section of the shaft, below which is located the combined cooling system consisting of alternating rows of plate and horizontal coolers. The broken line (C – D – E – F ... – K) represents the vertically hidden rows of shaft coolers under the lining, with the segments C – D, E – F, etc., corresponding to the space occupied by the rows of plate coolers. From Fig. 4, it can be seen that the lining in the cooled section was preserved up to a height of four to six rows of plate coolers. Intensive wear of the shaft was recorded below the third row from the top of the cooled section of the plate coolers or below the level of +30,500 mm. The wear ranges from 340 mm (according to the design, from the original lining to the nose part of the horizontal cooler of the shaft) to 510 mm (wear based on the results of the 3D scan) in the areas of the plate coolers.

It is worth noting the relatively satisfactory condition of the blast furnace shaft cooling system elements during the current campaign. The top four rows of plate coolers and up to eight upper rows of horizontal coolers

remain protected by refractory lining. The coolers located below have largely retained their operability. In total, during the current campaign, 146 plate coolers, 262 horizontal shaft coolers, and 1 bosh cooler were damaged, accounting for 23.2, 45.2, and 0.01 % of the total number of coolers of these types, respectively. In the previous campaign (1995 – 2006), 9 plate coolers, 221 horizontal coolers, and 25 bosh coolers were damaged, or 1.4, 38.1, and 20.8 % of the total number of these coolers, respectively. Pig iron production at blast furnace No. 5 amounted to 75.18 million tons in the current campaign and 39.48 million tons in the previous campaign, while the total number of damaged elements of the cooling system above the tuyeres was 409 and 255 units, respectively. Thus, 183.8 thousand tons of pig iron were produced per damaged cooling element in the bosh and shaft system during the current campaign, which is 19 % higher than the previous campaign’s figure of 154.8 thousand tons of pig iron per damaged element.

A comparison of the results of the previous and current campaigns suggests the high effectiveness of the measures applied to protect the refractory lining and the cooling elements of the bosh and shaft, which included:

- the use of a previously developed method to ensure the self-renewal of the protective skull in the shaft [8], which involves the cyclical loading of charge materials, including a skull-forming mixture consisting of iron ore and sinter. This mixture generates primary slag melt in the amount of 20 – 25 %, with an iron oxide content in this melt of no more than 15 %;

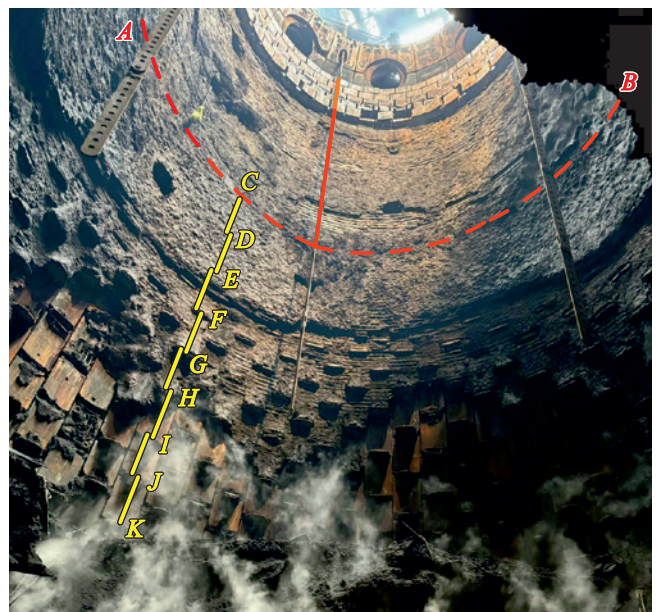


Fig. 4. Condition of the refractory lining in the cooled section of blast furnace shaft No. 5, based on the results of the 2006 – 2024 campaign

Рис. 4. Состояние огнеупорной футеровки в шахте ДП № 5 по результатам кампании 2006 – 2024 гг., охлаждаемая часть

– the development and application of methods during the current campaign for the effective distribution of various types of solid fuel across the furnace’s cross-section, and a material distribution system that includes a predetermined distribution of ore load across the furnace’s cross-section. This also involves the cyclic use of axial, pre-washing, and washing batches to ensure the central operation of the furnace under variable charge and gas-blowing conditions [6].

It is important to note that the study of the condition of the refractory lining in the shaft of blast furnace No. 5 was conducted within very tight time frames. The total scanning time at four stations was 50 min, which allowed the repair work on the furnace to proceed without delay.

MEASUREMENT OF REFRACTORY LINING THICKNESS IN THE TUYERE ZONE AND HEARTH OF BF NO. 5

The measurement of refractory lining thickness in the hearth and bottom areas was carried out during the raking out of residual charge materials from the working space of blast furnace No. 5. To prevent people from entering the danger zone, a remote measurement method was used, capturing photographic images of refractory lining elements and scaling the linear dimensions of these elements against known dimensions of the furnace struc-

ture that remain unchanged during operation (such as the thickness of the shell, plate coolers in the hearth, and bottom, etc.). This method not only allows for safe measurements but also significantly reduces the time required for the study, as the photographic documentation occurs quickly during technological pauses in the raking process, and the mathematical processing of the results can be done at any convenient time. In this study, the procedure for comparing the dimensions of objects by measuring the lengths of lines recorded in the photographs was performed using the digital tool Visio. The known linear dimension used for scaling was the thickness of the hearth cooling stave, which is 160 mm.

The raking of residual charge materials was performed through two cesspools installed in the furnace shell at the level of the tuyere zone (upper) and bottom (lower). A map showing the location of the cesspools in the horizontal section of the hearth of blast furnace No. 5, with reference to the main structural elements, is presented in Fig. 5.

The tuyeres are positioned around the circumference at intervals of $360/40 = 9^\circ$. The right side of the lower cesspool, where the residual thickness of the carbon blocks was measured, is located 17.15° to the left of the axis of iron taphole No. 4, corresponding to the area between tuyeres 32 and 33 ($9/2 + 9 = 13.5^\circ$ and $9/2 + 9 + 9 = 22.5^\circ$,

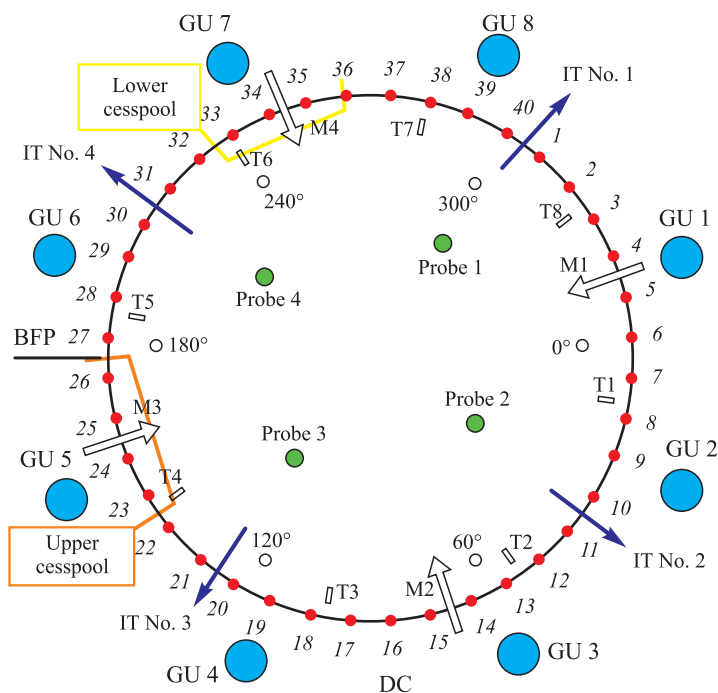


Fig. 5. Map showing the location of cesspools in the horizontal section of the hearth of blast furnace No. 5: BFP – blast furnace pipeline; DC – dust collector; GU 1, GU 2, ...GU 8 – projection of the gas uptakes locations; T1, T2, ... T16 – projection of the of thermocouple locations for measuring peripheral gas temperatures; IT No. 1, IT No. 2, ... IT No. 4 – location of the iron tapholes

Рис. 5. Карта расположения выгребных проемов в горизонтальном сечении горна ДП № 5: BFP – конвейер доменный; DC – расположение пылеуловителя; GU 1, GU 2, ...GU 8 – проекции расположения газоотводов; T1, T2, ...T16 – проекции расположения термомпар измерения температуры периферийных газов; IT No. 1, IT No. 2, ...IT No. 4 – расположение чугунных леток

respectively). The left side of the lower cesspool, where the residual thickness of the carbon blocks was measured, is located $31.7 + 17.15 = 48.85^\circ$ to the left of the axis of iron taphole No. 4, corresponding to the area of tuyere 36 ($9/2 + 9 \cdot 5 = 49.5^\circ$).

The right side of the upper cesspool is located 18.15° to the left of the axis of iron taphole No. 3, which corresponds to the area between tuyeres 22 and 23 ($9/2 + 9 = 13.5^\circ$ and $9/2 + 9 + 9 = 22.5^\circ$, respectively). The left side of the upper cesspool is located $35.7 + 18.15 = 53.85^\circ$ to the left of the axis of iron taphole No. 3, which corresponds to the area between tuyeres 26 and 27 ($9/2 + 9 \cdot 5 = 49.5^\circ$ and $9/2 + 9 \cdot 6 = 58.5^\circ$, respectively).

An example of using the Visio tool to measure the residual thickness of carbon refractory blocks in the right side of the lower cesspool (between tuyeres 32 and 33) is shown in Fig. 6. In this example, considering the scale, the actual residual size of the block is calculated as

$$89.8888 \cdot 160 / 7.4677 = 1926 \text{ mm},$$

where 89.8888 is the size of the block in the photograph, mm, 160 is the design thickness of the cast iron stove, mm, and 7.4677 is the thickness of the cooler in the photograph, mm.

The results of the calculation of the residual thickness of the carbon block correspond well with the control measurement taken during a technological pause in the raking process. The same method was used to assess the residual thickness of the refractories along the height of both the lower and upper cesspools.

The measurements performed made it possible to create a map of the actual erosion of the carbon blocks in the area of the lower cesspool between tuyeres 32 and 36, which is presented in Table 2.

Using the same method as for measuring the actual wear of the carbon blocks in the area of the lower cess-



Fig. 6. Example of using the Visio tool to determine the residual linear size of a carbon refractory block (segment A – B) by scaling the known thickness of a cast iron stove (segment C – D)

Рис. 6. Пример применения инструмента Visio для определения остаточного линейного размера углеродистого огнеупорного блока (отрезок A – B) способом масштабирования известной толщины горнового холодильника (отрезок C – D)

pool, the residual thickness of the refractory lining in the hearth was measured near the upper cesspool. This allowed the formation of actual erosion lines of the bottom and hearth lining of blast furnace No. 5 along vertical sections in the areas of tuyeres 22, 26, and 32, 36, respectively. A graphical representation of these lines, compared with the results of ultrasonic echo-sounding (AU-E), is shown in Fig. 7.

The AU-E method is a technology that uses stress wave propagation and data analysis in both the time and frequency domains to determine lining thickness or detect anomalies, such as cracks, voids, or metal penetration into the lining [9 – 11]. During the measurements,

Table 2. Actual wear of the carbon refractory blocks in the hearth of blast furnace No. 5 in the lower cesspool area between tuyeres 32 and 36

Таблица 2. Фактический износ углеродистых огнеупорных блоков горна ДП № 5 в районе нижнего выгребного проема между воздушными фурмами 32 и 36

Original block length (per design), mm	Block to the left of the cesspool (area of tuyere 36)		Block to the right of the cesspool (area of tuyere 32)		Average value across the width of the cesspool	
	residual thickness (at the bottom edge of the block), mm	erosion, mm	residual thickness (at the top edge of the block), mm	erosion, mm	residual thickness, mm	erosion, mm
1500	1267	233	1353	147	1310	190
1650	1337	313	1383	267	1360	290
1800	1521	279	1627	173	1574	226
1950	1870	80	1926	24	1898	52

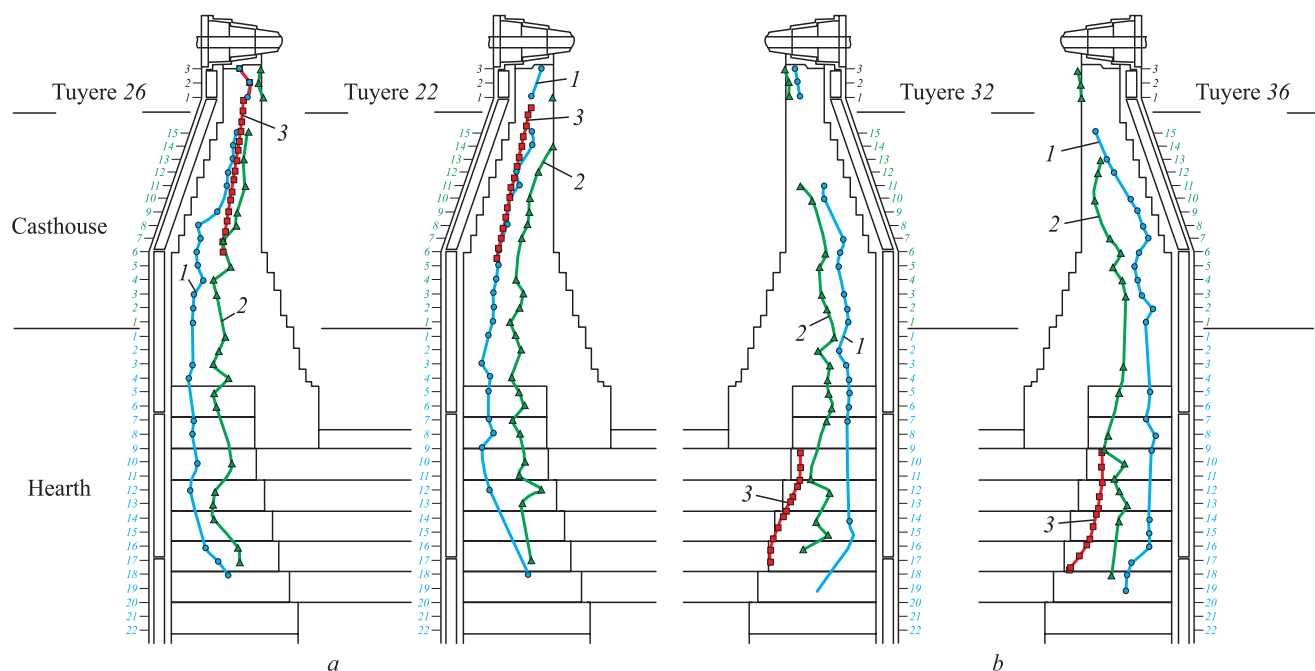


Fig. 7. Graphical representation of the actual erosion of the refractory lining in the hearth and bottom areas, compared with the ultrasonic echo-sounding data (AU-E) in the regions of the upper (a) and lower (b) cesspools:

- 1 – thickness of the residual lining detected by the echo method (AU-E);
- 2 – thickness of the modified lining/skull detected by the echo method (AU-E);
- 3 – actual erosion line of the refractory lining, discovered during major repairs

Рис. 7. Графическое изображение линий фактического разгара огнеупорной футеровки горна и лещади в сравнении с данными ультразвукового зондирования методом АУ-Е в районах верхнего (а) и нижнего (б) выгребных проемов:

- 1 – толщина обнаруженной методом АУ-Е остаточной футеровки;
- 2 – толщина обнаруженной методом АУ-Е измененной футеровки/гарнисажа;
- 3 – фактическая линия разгара огнеупорной футеровки, обнаруженная при проведении капитального ремонта

a mechanical impact on the surface of the structure (using a hammer or an impact-mechanical source) generates a stress impulse, which propagates through the lining layers. The wave is partially reflected due to changes in the properties of the lining layer, but the primary wave energy propagates through the continuous layers until it fully dissipates. Compression waves reach the sensors/receivers, and the signals are analyzed to provide a qualitative assessment of the lining. Factors such as density, temperature gradient, geometry, and elasticity properties affect the wave speed. A sudden change in density and/or elasticity properties of the material leads to partial or full wave reflection. Thus, signals are reflected by interfaces, such as the lining-metal melt boundary or the interfaces between refractory blocks. Additionally, stress-free zones, such as cracks and voids, also result in partial or full reflection of the signals. It should be noted that during the AU-E ultrasonic sounding performed by HATCH specialists, several significant reservations were made, specifically:

- the AU-E method can only detect cracks that run parallel to the furnace shell (i.e., perpendicular to the signal direction from the impact). Any cracks or delaminations parallel to the signal direction (i.e., toward the furnace center) cannot be detected;

- “stable lining” refers to unchanged lining that is in almost the same condition as when it was manufactured, whereas “modified lining” has likely undergone significant changes or cracking.

Comparing the actual erosion lines shown in Fig. 7 with the results of ultrasonic echo-sounding (AU-E), the following conclusions can be drawn:

- in the upper part of the hearth, lined with refractory brick containing 43 % Al_2O_3 , the echo-sounding method shows satisfactory accuracy. Actual measurements of the minimum residual lining thickness range from 220 to 330 mm (excluding skull), which corresponds to the results of the ultrasonic sounding;

- in the lower part of the hearth and the bottom, lined with carbon blocks, the HATCH specialists’ measurements showed extremely low values of residual lining thickness (an average value around the circumference and height of the hearth was 540 mm, or 21 % of the original thickness, with a minimum value of 240 mm, or 10 % of the original thickness). Even considering the reservations and the “modified lining with skull” line presented in the reports, the actual residual thickness of the carbon blocks, measured during the repair, exceeded 80 %, meaning it was significantly higher.

The data in Table 2 and Fig. 7 allow for an assessment of the effectiveness of the measures taken during the current campaign of blast furnace No. 5 to ensure the preservation of the refractory lining in the hearth and bottom. It is known that the factors determining the wear of refractory linings include:

- abrasive action of liquid iron flows;
- chemical impact of iron and slag;
- infiltration and thermomechanical stress in the lining [12 – 14]. It is widely recognized that the service life of the hearth lining is largely determined by the quality of the coke being charged, and that there are currently no wear-resistant hearth designs [15].

In the current campaign, measures were developed and consistently implemented to prevent the development of abrasive action by liquid iron flows in the peripheral (near-wall) zone, ensuring the intensive filtration of molten products through the totterman and good gas permeability in the furnace’s central zone. Under real blast furnace operating conditions, due to fluctuations in the coke’s hot strength (CSR), water entering the hearth from defective elements of the cooling system, and the introduction of localized masses of high-melting-point components in the blast furnace charge, the porosity of the totterman can significantly decrease. Continuous monitoring of the permeability of the furnace’s central zone was organized through totterman probing. To clean the hearth from high-

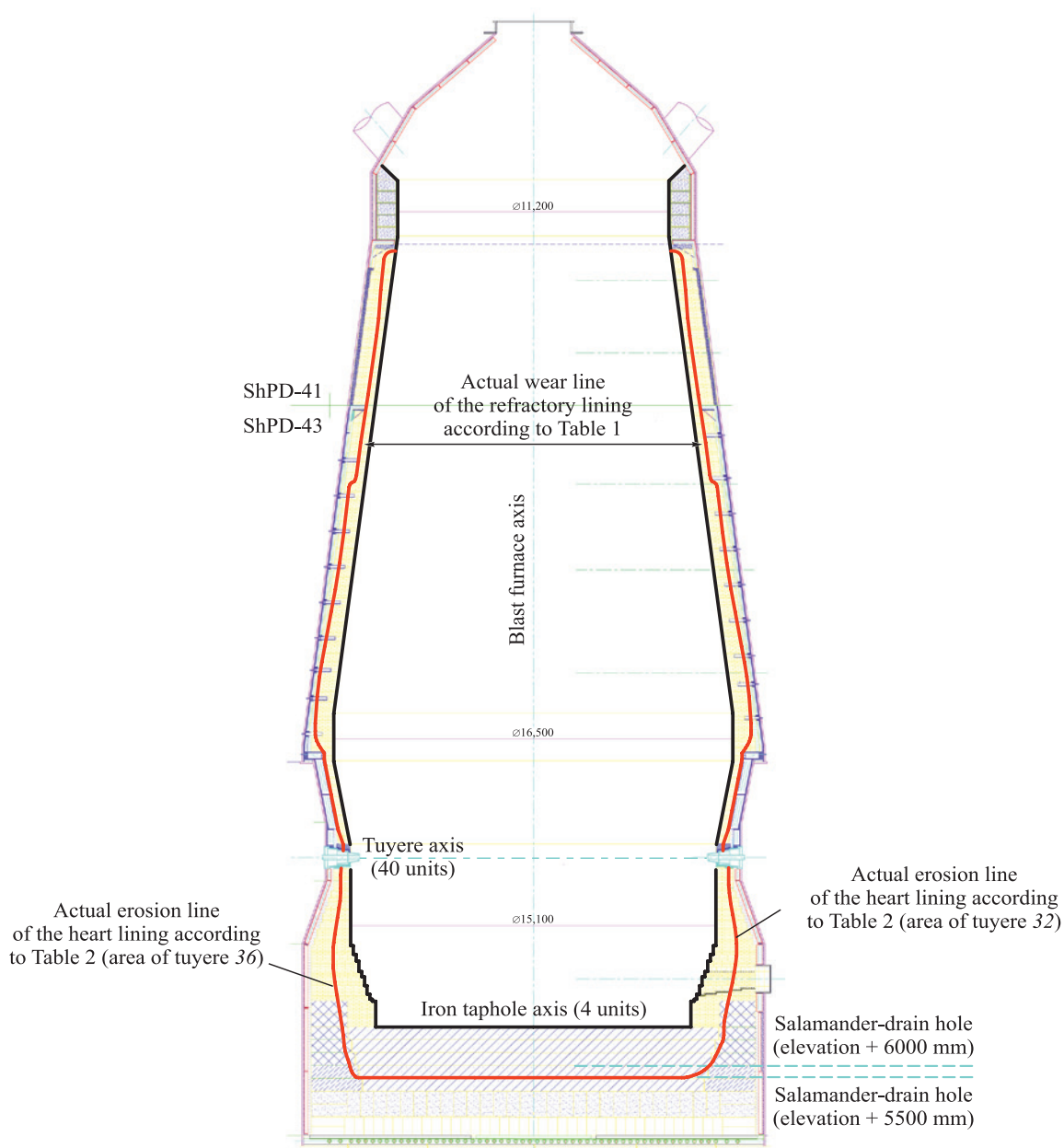


Fig. 8. Map of the actual erosion of the refractory lining of blast furnace No. 5 at the end of the 2006 – 2024 campaign

Рис. 8. Карта фактического разгара футеровки ДП № 5 по завершению кампании 2006 – 2024 гг.

melting-point flux residues and small coke fractions, comprehensive washing of the hearth volume was introduced. To reduce the chemical erosion of the carbon blocks in the hearth and bottom due to the non-equilibrium chemical composition of the molten iron, a method for controlling the technological process was developed by monitoring the ratio of actual carbon content in the iron (A_c) to the saturation content (S_c) through the regulation of natural gas injection into the furnace.

Comparing the results of the previous campaign of blast furnace No. 5 (by the end of 2006, the refractory thickness around the iron tapholes did not exceed 200 – 250 mm, and the carbon peripheral blocks in the upper bottom area, located directly below the tapholes, were deformed with cracks and chips in some places) with the data in Table 2, we can conclude that the measures taken during the current campaign significantly improved the durability of the carbon lining in the hearth and bottom.

As a numerical assessment of the effectiveness of the measures to extend the campaign of blast furnace No. 5, the total pig iron production per hearth area in the current campaign reached 420.0 thousand tons/m², exceeding the previous campaign's figure of 220.6 thousand tons/m² by 1.90 times, or by 90.4 %.

At the same time, the results of the studies on the residual thickness of the lining indicate that the tuyere zone requires the development of additional protective measures for the next furnace campaign.

MAP OF THE ACTUAL EROSION OF THE REFRACTORY LINING IN BF NO. 5

Based on the results of the study of the working space of blast furnace No. 5, a comprehensive map of the actual erosion of the lining during the 2006 – 2024 campaign was created, as shown in Fig. 8.

CONCLUSIONS

As a result of comprehensive studies conducted during the first-category overhaul of blast furnace No. 5, the effectiveness of the measures developed and implemented during the current campaign to protect the refractory lining of the shaft, hearth, and metal receiver of the furnace was confirmed. These measures extended the furnace's service life by 1.75 times and ensured its highly efficient operation throughout the 2006 – 2024 campaign.

Using remote measurement techniques, including 3D laser scanning, the actual erosion profile of the refractory lining of blast furnace No. 5 was determined, and areas of increased erosion with reduced residual thickness along the height of the furnace were identified.

The analysis of the actual residual thickness of the refractory lining in the hearth of blast furnace

No. 5 demonstrated satisfactory accuracy of the AU-E ultrasonic sounding method in the area of the alumina refractory lining of the tuyere zone, but insufficient accuracy when measuring the carbon blocks.

REFERENCES / СПИСОК ЛИТЕРАТУРЫ

1. Kurunov I.F., Loginov V.N., Tikhonov D.N. Methods of extending a blast-furnace campaign. *Metallurgist*. 2006;50: 605–613. <https://doi.org/10.1007/s11015-006-0131-5>
Курунов И.Ф., Логинов В.Н., Тихонов Д.Н. Методы продления кампании доменной печи. *Металлург*. 2006;(12): 34–39.
2. Vinogradov E., Karimov M., Dmitriev A., etc. Blast furnace campaign extension at CherMK, Severstal. In: *AISTech 2018 Proceedings – Iron and Steel Technology Conference and Exposition*. 2018:551–560.
3. Mozhareno N.M., Kanaev V.V., Panchokha G.V. Influence of smelting technology on metal receiver lining of blast furnace. *Metallurgicheskaya i gornorudnaya promyshlennost'*. 2003;(5):5–8. (In Russ.).
Можаренко Н.М., Канаев В.В., Панчоха Г.В. Влияние технологии плавки на футеровку металлоприемника доменных печей. *Металлургическая и горнорудная промышленность*. 2003;(5):5–8.
4. The influence of blast furnace productivity on the duration of its campaign. *Novosti chernoï metallurgii za rubezhom*. 2005;(1):21–24. (In Russ.).
Влияние производительности доменной печи на продолжительность ее кампании. *Новости черной металлургии за рубежом*. 2005;(1):21–24.
5. Shul'te M., Klima R., Ringel' D., Foss M. Monitoring the wear of the blast furnace hearth using heat flow sensors. *Chernye metally*. 1998;(4):17–22. (In Russ.).
Шульте М., Клима Р., Рингель Д., Фосс М. Контроль износа горна доменной печи с помощью датчиков теплового потока. *Черные металлы*. 1998;(4):17–22.
6. Kal'ko A.A., Vinogradov E.N., Kal'ko O.A., Kal'ko A.A. Development and implementation of technological measures to extend the campaign of blast furnace No. 5 of PJSC Severstal. *Izvestiya. Ferrous Metallurgy*. 2024;67(3): 260–269. <https://doi.org/10.17073/0368-0797-2024-3-260-269>
Калько А.А., Виноградов Е.Н., Калько О.А., Калько А.А. Разработка и внедрение технологических мероприятий по продлению кампании доменной печи № 5 ПАО «Северсталь». *Известия вузов. Черная металлургия*. 2024;67(3):260–269.
<https://doi.org/10.17073/0368-0797-2024-3-260-269>
7. Medic M.Sc.T. Efficient calibration strategies for panoramic terrestrial laser scanners. Dissertation Zur Erlangung des akademischen Grades Doktor der Ingenieurwissenschaften (Dr.–Ing.). Bonn: Institut für Geodäsie und Geoinformation der Universität Bonn; 2021.
8. Loginov V.N., Sukhanov M.Yu., Gurkin M.A., Vasil'ev L.E., Karimov M.M., Bol'shakov V.I., Nesterov A.S., Mozhareno N.M., Yakushev V.S. Method for creating a protective skull in a blast furnace shaft. Patent RF no. 2251575. МПК C21B 5/00. *Byulleten' izobretenii*. 2005;(13). (In Russ.).

- Пат. 2251575 RU. Способ создания защитного гарнисажа в шахте доменной печи / Логинов В.Н., Суханов М.Ю., Гуркин М.А., Васильев Л.Е., Каримов М.М., Большаков В.И., Нестеров А.С., Можаренко Н.М., Якушев В.С.; заявлено 21.04.2004; опубликовано 10.05.2005. Бюллетень № 13.
9. Gebiski P., Sadri A., Ying W. Development of the system for furnace integrity monitoring based on real-time continuous acoustic emission data acquisition and analysis. In: *Conf. of Metallurgists (COM), October 2–5, 2011, Montreal, Canada*, 2011.
 10. Vinogradov E., Kalko A., Chikinov S., Ivashov A., Balahonov D., Gurkin M., Karunova E., Gordon Y., Sadri A., Buser J. Development of strategy for sustaining, enhancement and cost reduction at Severstal's primary end. In: *Proceedings of the Iron & Steel Technology Conference. Association for Iron and Steel Technology*; 2020:178–186.
 11. Vinogradov E., Karimov M., Dmitriev A. Careful control of refractory lining conditions to ensures prolonged campaign of blast furnace. In: *7th ECIC Proceedings, Linz, Austria*, 2016.
 12. Kaplun L.I., Malygin A.V., Onorin O.P., Parkhachev A.V. Construction and Design of Blast Furnaces: Tutorial. Ekaterinburg: URFU; 2016:217. (In Russ.).
Кaplун Л.И., Мaлыгин А.В., Онорин О.П., Пархачев А.В. Устройствo и проектирoвание доменных печей: Учебное пособие. Екатеринбург: УрФУ; 2016:217.
 13. Bliznyukov A.S., Feshchenko S.A., Kurunov I.F., etc. Study of the blast furnace hearth lining. Message 1. *Ferrous Metallurgy. Bulletin of Scientific, Technical and Economic Information*. 2010;(9):31–36. (In Russ.).
Близнюков А.С., Фещенко С.А., Курунов И.Ф. и др. Исследование футеровки горна доменной печи. Сообщение 1. *Черная металлургия. Бюллетень научно-технической и экономической информации*. 2010;(9):31–36.
 14. Bol'shakov V.I., Gladkov N.A., Murav'eva I.G., etc. The structure of the lower part of the charge column and the role of its elements in the organization of smelting processes. In: *Proceedings of IFM. Fundamental and Applied Problems of Ferrous Metallurgy*. 2004;(8):112–119. (In Russ.).
Большаков В.И., Гладков Н.А., Муравьева И.Г. и др. Структура нижней части столба шихты и роль ее элементов в организации процессов плавки. В сборнике научных трудов ИЧМ: *Фундаментальные и прикладные проблемы черной металлургии*. 2004;(8):12–119.
 15. Koval'ski V., Lyungen Kh.B., Shtrikker K.P. Durability of blast furnaces: Current level, development and company development measures. *Chernye metally*. 1999;(9):26–35. (In Russ.).
Ковальски В., Люнген Х.Б., Штриккер К.П. Стойкость доменных печей: современный уровень, развитие и мероприятия по развитию компании. *Черные металлы*. 1999;(9):26–35.

Information about the Authors

Сведения об авторах

Andrei A. Kal'ko, Head of Technological Development Center Upstream, PJSC Severstal, Cherepovets Steel Mill
E-mail: aakalko@severstal.com

Leopol'd I. Leont'ev, Academician, Adviser, Russian Academy of Sciences; Advisor to the General Director, I.P. Bardin Central Research Institute of Ferrous Metallurgy
ORCID: 0000-0002-4343-914X
E-mail: leo@presidium.ras.ru

Evgenii A. Volkov, Leading Expert of Technological Development Center Upstream, PJSC Severstal, Cherepovets Steel Mill
E-mail: eavolkov@severstal.com

Андрей Александрович Калько, руководитель Центра технологического развития Upstream, ПАО «Северсталь» Череповецкий металлургический комбинат
E-mail: aakalko@severstal.com

Леопольд Игоревич Леонтьев, академик, советник, Президиум РАН; советник генерального директора, Центральный научно-исследовательский институт черной металлургии им. И.П. Бардина
ORCID: 0000-0002-4343-914X
E-mail: leo@presidium.ras.ru

Евгений Александрович Волков, ведущий эксперт Центра технологического развития Upstream, ПАО «Северсталь» Череповецкий металлургический комбинат
E-mail: eavolkov@severstal.com

Contribution of the Authors

Вклад авторов

A. A. Kal'ko – analysis of the results of measuring residual thickness of blast furnace lining, identification of problem areas, analysis of effectiveness of measures to increase the durability of blast furnace hearth lining and organization of an effective structure of the charge column in blast furnace.

L. I. Leont'ev – setting the research task, analysis of results, drawing conclusions on the work.

E. A. Volkov – analysis of the results of measuring residual thickness of blast furnace lining, conducting comparative calculations of lining residual thicknesses by various methods.

А. А. Калько – анализ результатов измерений остаточных толщин футеровки доменной печи, определение проблемных зон, анализ эффективности мероприятий для повышения стойкости футеровки горна доменной печи и организации эффективной структуры столба шихты в доменной печи.

Л. И. Леонтьев – постановка задачи исследования, анализ результатов, формирование выводов по работе.

Е. А. Волков – анализ результатов измерений остаточных толщин футеровки доменной печи, сравнительные расчеты остаточных толщин футеровки различными методами.

Received 26.08.2024
Revised 28.09.2024
Accepted 30.09.2024

Поступила в редакцию 26.08.2024
После доработки 28.09.2024
Принята к публикации 30.09.2024



UDC 669.054.83

DOI 10.17073/0368-0797-2024-5-531-541



Original article

Оригинальная статья

A STUDY ON PROCESSING OF BLAST FURNACE DUST AND SLUDGE USING REDUCTION ROASTING AND MAGNETIC SEPARATION

P. I. Grudinsky¹, A. A. Yurtaeva¹, A. I. Volkov², V. G. Dyubanov¹

¹ Baikov Institute of Metallurgy and Materials Science, Russian Academy of Sciences (49 Leninskii Ave., Moscow 119334, Russian Federation)

² I.P. Bardin Central Research Institute of Ferrous Metallurgy (23/9 Radio Str., Moscow 105005, Russian Federation)

✉ pgrudinskiy@imet.ac.ru

Abstract. Blast furnace dust and sludge are by-products of ironmaking that contain high levels of iron and carbon, along with zinc. The increased zinc content complicates their recycling in the sintering and blast furnace processes, leading to their accumulation in waste dumps. This study investigates different treatment methods for recovering valuable elements from blast furnace dust (BFD) and blast furnace sludge (BFS) through reduction roasting and magnetic separation. Thermodynamic calculations and laboratory experiments were conducted to evaluate three approaches: magnetic separation without the roasting, as well as roasting stages to reduce iron to magnetite at 800 °C or metallic iron at 1200 °C, respectively. Direct magnetic separation without roasting and with the preliminary roasting at 800 °C resulted in magnetic concentrates of 49 – 63 % Fe from the BFD and BFS samples, but with elevated zinc content. The best results were achieved using reduction roasting at 1200 °C for 120 min, followed by grinding the samples to –0.054 mm and magnetic separation with a magnetic field of 0.1 T. As a result, the metallized magnetic concentrate containing 73.8 % Fe and 0.048 % Zn was obtained from the BFS sample (initially containing 39.5 % Fe and 0.31 % Zn), while a concentrate containing 80 % Fe and 0.019 % Zn was produced from the BFD sample (initially containing 44.6 % Fe and 0.31 % Zn). The iron recovery into the concentrates for the BFS and BFD samples was 92.8 and 89.7 %, respectively. The proposed approach can produce valuable materials for ferrous and non-ferrous metallurgy from these by-products, increase the efficiency of sintering and blast furnace processes, and reduce waste accumulation.

Keywords: blast furnace dust, blast furnace sludge, processing, reduction roasting, magnetic separation, carbothermic reduction, iron, zinc

Acknowledgements: The work was performed according to a state assignment No. 075-00320-24-00.

For citation: Grudinsky P.I., Yurtaeva A.A., Volkov A.I., Dyubanov V.G. A study on processing of blast furnace dust and sludge using reduction roasting and magnetic separation. *Izvestiya. Ferrous Metallurgy*. 2024;67(5):531–541. <https://doi.org/10.17073/0368-0797-2024-5-531-541>

ИССЛЕДОВАНИЕ ПРОЦЕССОВ ПЕРЕРАБОТКИ ДОМЕННЫХ ПЫЛИ И ШЛАМА С ИСПОЛЬЗОВАНИЕМ ВОССТАНОВИТЕЛЬНОГО ОБЖИГА И МАГНИТНОЙ СЕПАРАЦИИ

П. И. Грудинский¹, А. А. Юртаева¹, А. И. Волков², В. Г. Дюбанов¹

¹ Институт металлургии и материаловедения им. А.А. Байкова РАН (Россия, 119334, Москва, Ленинский пр. 49)

² Центральный научно-исследовательский институт черной металлургии им. И.П. Бардина (Россия, 105005, Москва, ул. Радио, 23/9)

✉ pgrudinskiy@imet.ac.ru

Аннотация. Пыли и шламы доменного производства – техногенные материалы с высоким содержанием железа и углерода, в которых присутствует также цинк. Повышенное содержание цинка препятствует их рециклингу в аглодоменном переделе и приводит к накоплению этих материалов в отвалах. В настоящей работе исследованы различные варианты переработки образцов доменной пыли (ДП) и доменного шлама (ДШ) с извлечением ценных элементов на основе восстановительного обжига и магнитной сепарации. С помощью термодинамических расчетов и лабораторных экспериментов изучены три варианта реализации этого способа: магнитная сепарация без предварительного обжига, а также со стадиями обжига с восстановлением железа до магнетита при 800 °C и металлического железа при 1200 °C соответственно. Способы прямой магнитной сепарации без обжига и с предварительным обжигом при 800 °C позволяют получить из образцов ДП и ДШ магнитные концентраты с 49 – 63 % Fe, но содержание цинка в них остается повышенным. Лучшие результаты были получены с использованием восстановительного обжига при 1200 °C продолжительностью 120 мин, последующего размола образцов до –0,054 мм и магнитной сепарации при индукции магнитного поля 0,1 Тл. В результате из ДШ, содержащего 39,5 % Fe и 0,31 % Zn,

получен металлизированный магнитный концентрат с содержанием 73,8 % Fe и 0,048 % Zn, а из ДП, содержащей 44,6 % Fe и 0,31 % Zn – металлизированный магнитный концентрат с содержанием 80 % Fe и 0,019 % Zn. Степень извлечения железа в концентрат для ДШ и ДП составила 92,8 и 89,7 % соответственно. Предложенный подход позволяет получать ценные материалы для черной и цветной металлургии из техногенного сырья, увеличить эффективность аглодоменного передела и избежать накопления отходов.

Ключевые слова: доменная пыль, доменный шлам, переработка, восстановительный обжиг, магнитная сепарация, карботермическое восстановление, железо, цинк

Благодарности: Работа выполнена по государственному заданию № 075-00320-24-00.

Для цитирования: Грудинский П.И., Юртаева А.А., Волков А.И., Дюбанов В.Г. Исследование процессов переработки доменных пыли и шлама с использованием восстановительного обжига и магнитной сепарации. *Известия вузов. Черная металлургия.* 2024;67(5):531–541. <https://doi.org/10.17073/0368-0797-2024-5-531-541>

INTRODUCTION

Dust and sludge generated in blast furnace ironmaking are by-products with high iron content collected in dry and wet gas cleaning systems, respectively. The production of such dust and sludge ranges from 5.5 to 40 kg/t of hot pig iron [1]. The conventional method for their recycling is sintering followed by blast furnace processing. However, the recycling through the sintering and blast furnace route becomes complicated when zinc content in these materials increases causing technological difficulties in the blast furnace smelting process [2]. When the dust or sludge contains >0.05 % Zn, the recycling in the sintering process becomes complicated; if the zinc content exceeds 0.3 – 0.5 % Zn, the recycling is nearly impossible [3]. In such cases, dust and sludge are dumped in landfills and classified as IV class hazardous waste leading to adverse environmental impacts near disposal sites.

Several studies have suggested that blast furnace dust and sludge can be recycled in the production of cement [4], ceramics [5], and road construction [6; 7]; however, these studies do not address the recycling of dust and sludge with high zinc content. Additionally, it is possible to use such dust and sludge as adsorbents [8; 9], catalysts [10; 11], and for coagulant production [12], but these applications can only utilize a small portion of the accumulated and generated waste. Various approaches have been explored for processing blast furnace dust and sludge [13] including the recovery of iron, carbon, zinc, and other valuable elements by hydrometallurgical, pyrometallurgical, and beneficiating methods. Hydrometallurgical processes using various solvents are often multistage [14], have low selectivity for separating zinc and iron [15], and make it impossible to recycle iron-containing residues rendering them inefficient for zinc contents <10 % [13]. Beneficiating methods for processing blast furnace dust and sludge include gravity concentration [16], air classification [17], flotation [18], magnetic separation [19], and their various combinations [20; 21]. These methods allow for selective separation of carbon and iron but struggle to segregate zinc into a separate product. In contrast, pyrometallurgical methods based on zinc

reduction and evaporation enable selective separation of zinc from iron, with the carbon content in the dust and sludge serving as a reducing agent [22]. Therefore, combining pyrometallurgical and beneficiating methods is a promising approach for the comprehensive recovery of valuable elements from blast furnace dust and sludge.

In this study, we explore a method for processing blast furnace dust and sludge based on carbothermic reduction roasting and magnetic separation, which has shown high efficiency for other materials containing zinc and iron [23; 24]. Based on thermodynamic calculations and laboratory experiments, we identified the characteristics of three variations of this method: without roasting, with roasting to reduce iron to magnetite, and with roasting to reduce iron to its metallic form. Based on the research results, the prospects and directions for recycling of magnetic separation products were assessed.

MATERIALS AND METHODS

Samples of blast furnace sludge (BFS) and blast furnace dust (BFD) were obtained from PJSC NLMK (Lipetsk, Russia). Chemical analysis of the samples was carried out using a PANalytical AXIOS^{mAX} Advanced X-ray fluorescence spectrometer (Netherlands). The iron content in the samples was determined by redox titration according to GOST 32517-1-2013. Carbon and sulfur contents were measured using a LECO CS-400 analyzer (USA).

Mineralogical analysis of the initial samples was carried out with a DRON-3 diffractometer (Russia) using CuK_α radiation, while the magnetic separation products were analyzed with a Difrey diffractometer (Russia) using CrK_α radiation. X-ray diffraction (XRD) patterns were interpreted using the Match 3.15 software (Germany) [25].

Quantitative determination of divalent and metallic iron in the samples was conducted via redox titration, following the methods outlined in GOST 23581.3–79 and 26482–90, respectively. The proportion of ferric iron was calculated as the difference between Fe_{tot} and the sum of Fe_{met} and Fe^{2+} .

Thermodynamic calculations of the equilibrium states of iron and zinc compounds at the temperatures of the reduction roasting were performed using the Equilibrium composition module of the HSC Chemistry 9.9 software (Finland) [26]. The calculations were conducted in the temperature range of 300 – 1400 °C, under atmospheric pressure, with an inert atmosphere for 100 kg of blast furnace sludge (BFS) or blast furnace dust (BFD).

Laboratory experiments with BFS and BFD were carried out using three approaches: magnetic separation of the samples without the preliminary roasting, magnetizing roasting at 800 °C followed by magnetic separation, and metallizing roasting at 1200 °C followed by magnetic separation.

Magnetic separation of the samples ground to the required particle size was performed using an XCGS-50 wet tubular magnetic separator (China) with a magnetic field of 0.1 T. The separation process was conducted for the samples with coarse (–1 mm) and fine (–0.054 mm) grinding. A 10 g sample was placed in the separator, processed in tap water, and the resulting slurry was filtered using vacuum filtration with a suction flask and funnel. The separation products were then dried at 100 °C for 120 min. If needed, the products were further ground for additional analyses.

The magnetizing roasting of 50 g samples of BFS and BFD at 800 °C was carried out in a muffle furnace for 30 min. The samples were placed in corundum crucibles, inverted, and then positioned inside a larger corundum crucible. The roasting duration was selected based on literature data [27 – 29] indicating that full reduction of iron to magnetite in similar materials occurs within 30 min. After the roasting, the samples were removed from the furnace, quenched in water to prevent secondary oxidation of magnetite, filtered using a vacuum pump and suction flask, and dried at 100 °C for 120 min. The samples were subsequently ground and sieved to the required particle size.

The magnetizing metallizing roasting was conducted in a muffle furnace at 1200 °C for 120 min in a nitrogen atmosphere. Samples weighting 50 g were placed into corundum crucibles on a graphite layer with the +2.5 mm fraction, followed by another graphite layer on top. The temperature and roasting duration were selected with an excess margin to ensure complete iron metallization and zinc removal, based on literature data [30], where iron reduction and only trace zinc content from a similar blast furnace dust sample were achieved at 1200 °C for 100 min. The samples were heated to 1200 °C at a rate of 5 °C/min, held at this temperature for 120 min, and then cooled down to 200 °C over 900 min along with the furnace. The entire heating, holding, and cooling process was carried out in a nitrogen atmosphere ($\geq 99.6\%$ N₂ and $\leq 0.4\%$ O₂) to prevent secondary oxidation of iron. Two experiments were conducted with the BFS and BFD

samples: one without any additives and the other with a 15 % excess of carbon. High-purity graphite was used as a carbon-containing reducing agent. After roasting, the samples were ground and sieve to the required size for subsequent magnetic separation.

The efficiency of roasting and magnetic separation processes was calculated using the following formulas:

$$\gamma_c = \frac{m_c}{m_0} 100 \% ; \quad (1)$$

$$\gamma_t = \frac{m_t}{m_0} 100 \% ; \quad (2)$$

$$\varepsilon_c = \frac{m_c \% \text{Fe}_c}{m_0 \% \text{Fe}_0} 100 \% ; \quad (3)$$

$$\varepsilon_t = \frac{m_t \% \text{Fe}_t}{m_0 \% \text{Fe}_0} 100 \% ; \quad (4)$$

$$\mu_0 = \frac{\% \text{Fe}_{0(\text{met})}}{\% \text{Fe}_0} 100 \% ; \quad (5)$$

$$\mu_c = \frac{\% \text{Fe}_{c(\text{met})}}{\% \text{Fe}_c} 100 \% ; \quad (6)$$

$$\xi_{\text{Zn}} = \left(1 - \frac{m_r \% \text{Zn}_r}{m_w \% \text{Zn}_w} \right) 100 \% , \quad (7)$$

where γ_c and γ_t is yield of magnetic and non-magnetic fractions, respectively, %; m_0 is initial mass of the samples for magnetic separation, g; m_c and m_t mass of magnetic and non-magnetic fractions obtained after magnetic separation, g; ε_c and ε_t is iron recovery in the magnetic and non-magnetic fractions, respectively, %; % Fe₀ is total iron content in the initial samples for magnetic separation, wt. %; % Fe_c and % Fe_t is total iron content in the magnetic and non-magnetic fractions, respectively, wt. %; μ_0 and μ_c is iron metallization degree in the initial samples for magnetic separation and magnetic fraction, respectively, %; % Fe_{0(met)} and % Fe_{c(met)} is metallic iron content in the initial samples for magnetic separation and magnetic fraction, respectively, %; ξ_{Zn} is zinc removal degree during roasting, %; % Zn_r and % Zn_w is zinc content in the roasted and initial samples, respectively, wt. %; m_r and m_w is mass the roasted and initial samples, respectively, g.

Zinc content in the samples was analyzed using an inductively coupled plasma atomic emission spectrometer (ICP-AES) Vista Pro (Australia). The zinc content in the form of ZnO was determined according to the procedure outlined in [31], which involved sample leaching in an aqueous solution of NH₄Cl + NH₄OH. A 0.5 g sample was placed in a conical flask containing 50 ml of the solution prepared by dissolving 22 g of NH₄Cl in a mixture of 80 ml of NH₄OH (density 0.9 g/cm³) and 120 ml of water. The solution and sample were stirred on a magnetic agita-

tor at 50 – 60 °C for 120 min, then filtered. The zinc content in the filtrates was then analyzed using the ICP-AES device.

RESULTS AND DISCUSSION

Table 1 presents the elemental composition of the BFS and BFD samples, while Fig. 1 shows the XRD patterns of the samples with the identified phases marked.

The main components of the BFS and BFD samples are iron and carbon. The iron content in BFD is higher than in BFS, whereas the carbon content is lower. The level of phosphorus and sulfur, which are the main harmful impurities in iron and steel metallurgy, along with other undesirable impurities such as arsenic and copper, are within acceptable limits for the recycling in sintering and blast furnace processes. However, the elevated zinc content, as shown in the data, poses a significant challenge for the recycling these wastes in iron and steel metallurgy.

As indicated by the XRD patterns, the primary minerals of both samples are hematite and magnetite, which are the main components of iron ore raw materials used in blast furnace operations. Metallic iron and wustite are present in significantly smaller quantities. Carbon in the samples is predominantly in the form of graphite, which originates from coke and enters the gas cleaning waste, along with a small amount of calcite. The high graphite content in the samples is advantageous for the reduction roasting process. It should be noted that an amorphous ring is present in both XRD patterns, likely due to the presence of blast furnace slag particles in the wastes. The BFS sample contains small amounts of hydrate minerals, such as ettringite and gypsum, which were likely formed during the wet gas cleaning process.

The analysis of iron form distribution in BFS and BFD revealed that the majority of iron in both the samples is in the trivalent form (Fe^{3+}), accounting for 90.9 % in BFS and 89.1 % BFD. Divalent iron (Fe^{2+}) constitutes 6.1 and 7.7 % of the iron in BFS and BFD, respectively, while metallic iron (Fe_{met}) accounts for 3.0 and 3.2 %, respectively. Therefore, the distribution of iron forms in BFS and BFD is quantitatively similar.

The composition of the BFS and BFD used for thermodynamic calculation based on the results of chemi-

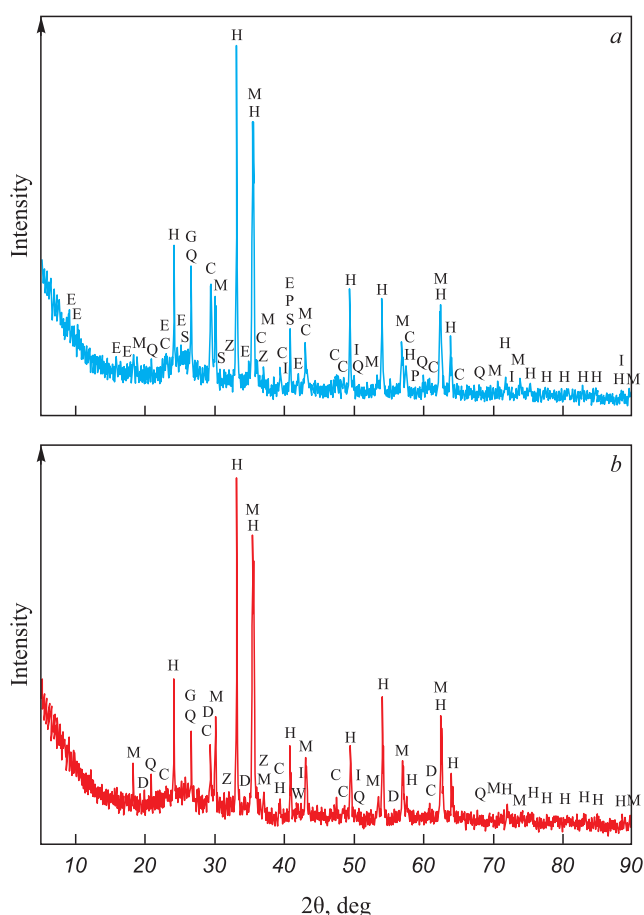


Fig 1. XRD patterns of BFS (a) and BFD (b):

H – hematite ($\alpha-Fe_2O_3$); M – magnetite (Fe_3O_4); C – calcite ($CaCO_3$); G – graphite (C); Q – quartz (SiO_2); I – iron ($\alpha-Fe$); W – wustite (FeO); E – ettringite ($Ca_6Al_2(SO_4)_3(OH)_{12} \cdot 26H_2O$); D – diopside ($CaMgSi_2O_6$); P – periclase (MgO); Z – zincite (ZnO); S – gypsum ($CaSO_4 \cdot 2H_2O$)

Рис. 1. Дифрактограммы ДШ (a) и ДП (b):

H – гематит ($\alpha-Fe_2O_3$); M – магнетит (Fe_3O_4); C – кальцит ($CaCO_3$); G – графит (C); Q – кварц (SiO_2); I – железо ($\alpha-Fe$); W – вюстит (FeO); E – этtringит ($Ca_6Al_2(SO_4)_3(OH)_{12} \cdot 26H_2O$); D – диопсид ($CaMgSi_2O_6$); P – периклаз (MgO); Z – цинкит (ZnO); S – гипс ($CaSO_4 \cdot 2H_2O$)

cal and mineralogical analyses and was adopted as follows, wt. %:

– BFS: 44.27 Fe_2O_3 ; 9.94 Fe_3O_4 ; 1.20 Fe; 21.43 C; 0.29 ZnO; 1.15 MgO; 6.11 SiO_2 ; 0.93 $CaSO_4$; 13.12 $CaCO_3$; 0.60 Al_2O_3 ; 0.26 $ZnFe_2O_4$; 0.21 $Ca(OH)_2$; 0.16 $Al_2(SO_4)_3$;

– BFD: 46.86 Fe_2O_3 ; 14.32 Fe_3O_4 ; 1.42 Fe; 14.97 C; 0.07 ZnO; 1.01 MgO; 5.75 SiO_2 ; 1.67 $CaMgSi_2O_6$; 11.91 $CaCO_3$; 0.81 $CaSO_4$; 1.11 Al_2O_3 .

Table 1. Chemical composition of the BFS and BFD samples, wt. %

Таблица 1. Химический состав образцов ДШ и ДП, мас. %

Waste	Fe	Zn	Al	Ca	Si	Mg	K	Mn	Cr	Cu	Ti	P	Pb	As	S	C
BFS	39.5	0.31	0.75	5.61	2.86	0.69	0.01	0.19	0.02	0.011	0.066	0.049	0.198	0.02	0.24	23.0
BFD	44.6	0.06	0.59	5.29	3.12	0.80	0.05	0.21	0.02	–	0.048	0.048	–	0.01	0.17	16.4

Fig. 2 illustrates the equilibrium amounts of iron and zinc compounds, as well as graphite in the system based on BFS and BFD at temperatures ranging from 300 to 1400 °C.

According to the data obtained, the reduction of iron to metal and the evaporation of metallic zinc are thermodynamically probable at temperatures above 700 °C. It should be noted that the amount of carbon in both samples is sufficient for the reduction of iron and zinc, although the BFD system contains a small amount of iron sulfide (Fig. 2, c). In the BFS system, the carbon content is more than sufficient, as evidenced by the presence of 7 – 10 kg of excess graphite at temperatures above 700 °C.

Literature data suggest that, contrary to thermodynamic calculations, favorable kinetic conditions for the carbothermic reduction of iron to metal only occur at temperatures above 1000 °C [32]. At temperatures of 700 – 900 °C, the magnetizing roasting with the carbothermic reduction of iron to Fe₃O₄ is possible [29]. These findings were taken into account in the experiments.

Table 2 lists the results of the analysis of the roasted samples obtained from BFS and BFD.

As shown in Table 2, the iron content in the samples after the roasting at 800 °C increases slightly. The con-

tent of metallic iron decreases due to its oxidation during the roasting. The degree of zinc removal in these samples is negligible, with only a slight change in the ZnO content.

After the roasting at 1200 °C, the iron content increases further, with most of the iron transforming into a metallic form. The iron content in the samples with an excess of carbon is lower than in the samples without the carbon addition, due to the presence of residual unreacted graphite. The degree of iron metallization in the samples ranges from 84 to 96 %. It is worth noting that the addition of carbon decreases the degree of iron metallization in the BFS sample, while it increases it in the BFD sample. The degree of zinc removal during the roasting is approximately 93 % for the BFS sample and 54 – 68 % for the BFD sample. The residual zinc content in the roasted samples is in the range of 0.02 – 0.04 % indicating that these roasted samples could potentially be used as part of the sinter burden without subsequent magnetic separation. Furthermore, the reduction roasting process can yield an additional valuable by-product: a sublimate with a high zinc content.

Table 3 shows the characteristics of the magnetic separation process for BFS and BFD samples, along with the analysis results of the products.

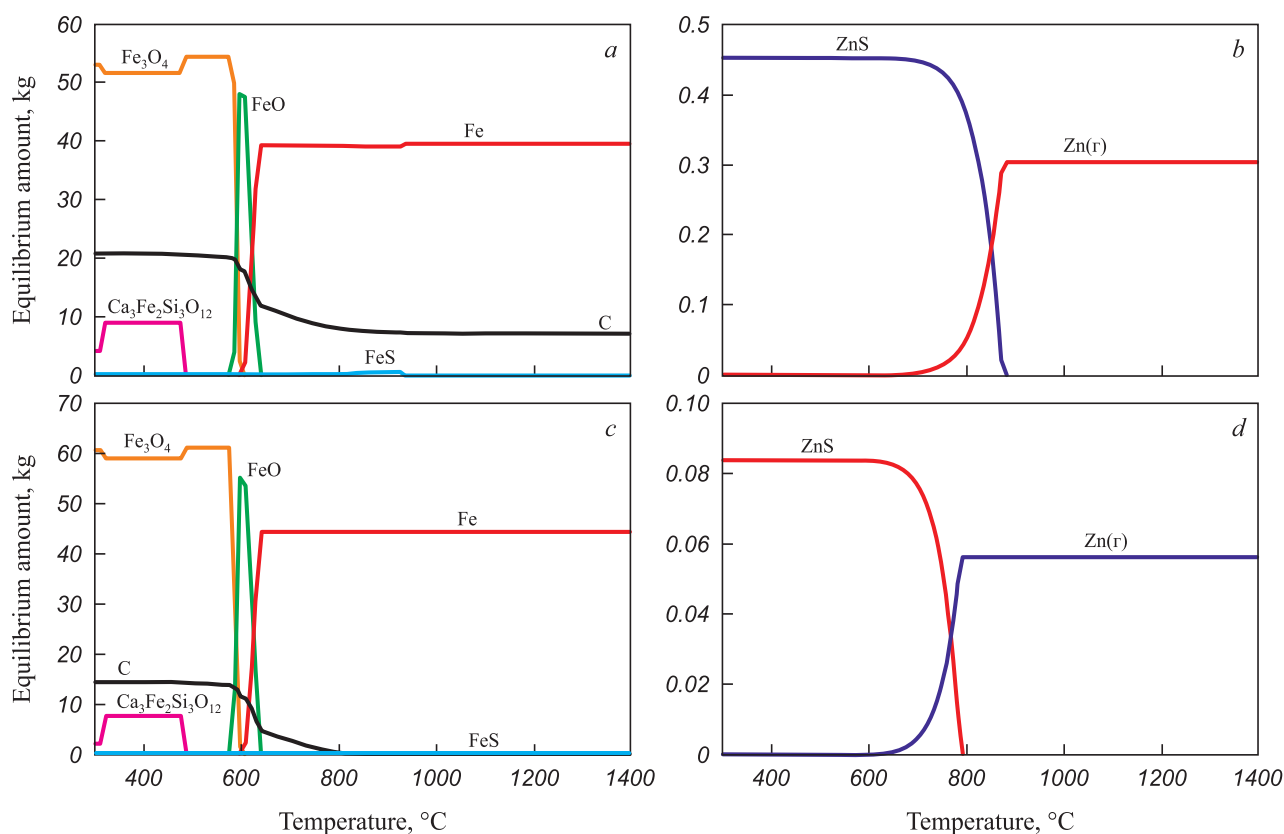


Fig. 2. Equilibrium amounts of graphite and iron compounds (a, c), as well as zinc compounds (b, d) in the BFS (a, b) and BFD (c, d) at 300 – 1400 °C

Рис. 2. Равновесные количества графита и соединений железа (a, c), а также соединений цинка (b, d) в ДШ (a, b) и ДП (c, d) при 300 – 1400 °C

Table 2. Chemical composition of the BFS and BFD samples and the products of their roasting at 800 and 1200 °C, along with the zinc removal degree

Таблица 2. Химический состав ДШ и ДП и продуктов их обжига при 800 и 1200 °C, а также степень удаления из них цинка

Initial sample	Roasting conditions	Content, wt. %			Zn removal degree (ξ_{Zn}), %	Fe metallization degree (μ_0), %
		Fe _{tot}	Zn _{tot}	Zn _{ZnO}		
BFS	No roasting	39.48	0.310	0.230	–	3.03
	800 °C, 30 min	41.16	0.320	0.210	1.0	2.03
	1200 °C, 120 min	59.18	0.030	n/d	93.2	90.4
	1200 °C, 120 min, + 15 % C	49.26	0.023	n/d	93.5	88.4
BFD	No roasting	44.56	0.060	0.055	–	3.19
	800 °C, 30 min	45.97	0.062	0.060	0.5	1.21
	1200 °C, 120 min	63.92	0.039	n/d	54.3	84.5
	1200 °C, 120 min, + 15 % C	58.02	0.023	n/d	68.2	96.2

Note: n/d – no data.

Table 3. Yield, recovery degree and content of Fe and Zn in magnetic and non-magnetic fractions obtained from BFS and BFD using magnetic separation, as well as roasting at 800 and 1200 °C followed by magnetic separation

Таблица 3. Выход, степень извлечения и содержание Fe и Zn в магнитной и немагнитных фракциях, полученных из ДШ и ДП магнитным, а также обжиг-магнитным методами с обжигом при 800 и 1200 °C

Waste	Roasting conditions	Magnetic separation conditions	Fraction yield (γ), %		Fe recovery degree in the fraction (ε), %		Content in the fraction, wt. %			Fe metallization degree in magnetic fraction (μ_c), %
			magn.	non-magn.	magn.	non-magn.	magn.		non-magn.	
							Fe _{tot}	Zn	Fe _{tot}	
BFS	No roasting	0.1 T, –1 mm	35.30	58.90	45.7	50.30	51.1	0.260	33.70	9.34
		0.1 T, –0.054 mm	33.40	62.80	52.7	45.50	62.3	0.210	28.60	8.42
	800 °C, 30 min	0.1 T, –1 mm	79.50	17.90	97.3	2.05	51.4	0.390	4.73	9.62
		0.1 T, –0.054 mm	63.80	32.30	94.6	3.45	61.0	0.430	4.40	8.25
	1200 °C, 120 min	0.1 T, –1 mm	84.20	14.00	90.8	1.91	63.8	n/d	8.04	94.60
		0.1 T, –0.054 mm	74.40	22.50	92.8	4.00	73.8	0.048	10.50	88.90
	1200 °C, 120 min, + 15 % C	0.1 T, –1 mm	85.20	13.60	90.0	3.68	52.0	n/d	13.30	89.50
		0.1 T, –0.054 mm	63.30	36.20	84.2	8.69	65.6	0.048	11.80	88.70
BFD	No roasting	0.1 T, –1 mm	62.00	38.70	68.3	26.20	49.1	0.120	30.20	9.80
		0.1 T, –0.054 mm	45.60	50.80	63.4	35.00	63.0	0.070	28.60	8.08
	800 °C, 30 min	0.1 T, –1 mm	80.00	21.50	92.1	1.73	52.9	0.080	3.70	9.01
		0.1 T, –0.054 mm	71.20	22.80	92.6	5.74	61.0	0.100	11.60	7.97
	1200 °C, 120 min	0.1 T, –1 mm	91.40	8.86	97.2	2.18	68.7	n/d	15.80	89.00
		0.1 T, –0.054 mm	77.80	18.90	93.5	4.93	76.9	0.066	16.60	89.40
	1200 °C, 120 min, + 15 % C	0.1 T, –1 mm	85.80	13.50	96.8	2.16	65.5	n/d	9.31	93.10
		0.1 T, –0.054 mm	65.00	31.50	89.7	7.85	80.0	0.019	14.50	92.30

Note: n/d – no data.

As indicated by the data, after all types of roasting, fine grinding (-0.054 mm) leads to a significantly higher iron content in the magnetic concentrates compared to coarse grinding (-1 mm). On average, across all experiments, the iron content in the magnetic concentrates obtained after fine grinding is 11.2 % higher, and this trend is consistent for both BFS and BFD samples. However, it is important to note that due to the high cost associated with fine grinding equipment, fine grinding operations and the required significant investment for grinding [33], fine grinding does not always improve the overall efficiency of processing flowsheets. Therefore, specific technical and economic conditions of an enterprise should be considered when selecting process parameters.

Magnetic separation without preliminary roasting yielded magnetic concentrates with an iron content of 49 – 62 %, which differs insignificantly from the concentrates produced with roasting. However, the yield of the concentrates and the degree of iron recovery were relatively low, and the iron content in the non-magnetic tailings remained substantially higher. This is primarily due to the high hematite content in the initial samples. In this case, most of the zinc passed into the tailings, although the zinc content in the magnetic concentrates was only slightly lower than in the original BFS and BFD samples. These findings align with those of [19], where it was found that increasing the magnetic field strength to 0.3 T during direct magnetic separation of blast furnace sludge could improve iron recovery to 78 %. However, the study did not address the issue of increased zinc content in the magnetic separation products.

The preliminary roasting of the BFS and BFD samples at 800 °C followed by magnetic separation produced magnetic concentrates with an iron content of 51 – 61 % and an iron recovery degree of 92 – 97 %. These results differ from those of other studies, where magnetizing roasting of blast furnace dust at 600 – 800 °C with sawdust [34] and charcoal [35] was followed by magnetic separation, resulting in an iron recovery degree of approximately 85 %, which is lower than the values obtained in this study. Furthermore, those studies demonstrated that the use of sawdust or charcoal additives during the roasting enabled the transformation of a significant portion of zinc into ZnO resulting in concentrates with reduced zinc content (0.15 – 0.19 %) after magnetic separation. In contrast, despite achieving higher magnetic separation indicators in this study, no significant zinc transformation to ZnO occurred during the roasting (see Table 2). It should be noted that the most of the zinc passed into the magnetic concentrates, with the increased zinc content (0.39 – 0.43 % in the BFS sample) complicating the use of the obtained concentrates in sintering and blast furnace processes.

Thus, our study has shown that direct magnetic separation of the BFS and BFD samples, as well as the roas-

ting-magnetic approach with carbothermic reduction at 800 °C, does not eliminate the elevated zinc content, which remains the primary challenge in processing blast furnace dust and sludge.

The metallizing roasting of the BFS and BFD samples at 1200 °C followed by magnetic separation produced magnetic concentrates with an iron content of 52 – 80 % and an iron metallization degree of 88.7 – 94.6 %, while the iron recovery in the concentrates reached 84.2 – 97.2 %. The zinc content in the concentrate obtained from the BFD sample with carbon addition was lower than in the sample without it. The zinc content of 0.048 % in the concentrates obtained from the BFS sample is below the limit for sinter product (0.05 %) allowing them to be used without issue in sintering processes.

The addition of carbon to the BFS sample did not improve the iron recovery or metallization degree in the concentrate; in fact, it slightly reduced the iron content due to the presence of excess unreacted carbon, consistent with the thermodynamic calculations (Fig. 2, *a*). In contrast, BFD processing using the roasting-magnetic method with carbon addition, followed by grinding to a particle size of -0.054 mm, resulted in an increase in both the iron content and metallization degree in the concentrate. This is likely due to the insufficient initial carbon amount in BFD to fully reduce the iron, as suggested by the absence of residual graphite in the equilibrium state after iron reduction, in contrast to the BFS case (Fig. 2, *c*). The iron content in the tailings ranged from 8.0 to 16.6 % with an iron recovery degree in the tailings of 1.9 – 8.7 % indicates the efficiency of iron extraction from blast furnace waste using the roasting and magnetic separation process.

Based on laboratory experiments, the optimal conditions for BFS and BFD processing were identified as follows: roasting at 1200 °C for 120 min, grinding the roasted samples to -0.054 mm, magnetic separation at a field strength of 0.1 T. The best magnetic separation results were observed for BFS without carbon addition and for BFD with 15 % carbon addition. Table 4 presents the chemical composition of these magnetic concentrates, while Fig. 3 illustrates their XRD patterns.

From the results obtained, it is evident that, in addition to metallic iron, the magnetic concentrates contain a considerable amount of silicates such as akermanite, gehlenite, merwinite, and anorthite, which formed during the roasting from the initial BFS and BFD components. A small amount of iron carbide was also present. The primary phase in the tailings is graphite. The concentrates and tailings also contain minor amounts of iron oxides, such as magnetite, maghemite, and hematite, which were likely formed during sample cooling due to secondary oxidation caused by the presence of oxygen impurities in the inert gas. The mineralogical composition of the

Table 4. Chemical composition of magnetic concentrates obtained from BFS and BFD using reduction roasting and magnetic separation (roasting at 1200 °C, 120 min; grinding to –0.054 mm; magnetic separation at 0.1 T), wt. %

Таблица 4. Химический состав магнитных концентратов, полученных из ДШ и ДП путем восстановительного обжига и магнитной сепарации (обжиг 1200 °C, 120 мин; размол –0,054 мм; магнитная сепарация при 0,1 Тл), мас. %

Initial sample	Content, wt. %						
	Fe	Zn	Al	Ca	Si	Mg	P
BFS	73.8	0.048	0.72	6.29	2.93	0.96	0.060
BFD + 15 % C	80.0	0.019	0.31	3.47	1.99	0.63	0.036

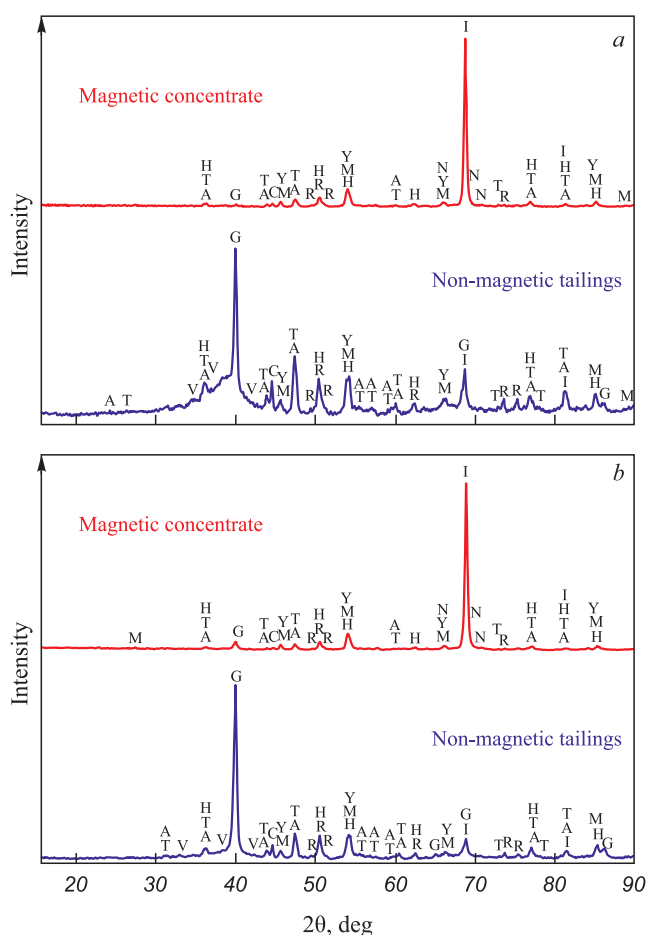


Fig. 3. XRD patterns of magnetic concentrate and non-magnetic tailings obtained from BFS (a) and BFD with 15 % C (b) by roasting–magnetic method (roasting at 1200 °C, 120 min; grinding to –0.054 mm; magnetic separation at 0.1 T):
 I – (α-Fe); H – hematite (α-Fe₂O₃); Y – maghemite (γ-Fe₂O₃); M – magnetite (Fe₃O₄); G – graphite (C); A – okermanite (Ca₂MgSi₂O₇); T – gehlenite (Ca₂Al₂SiO₇); R – merwinite (Ca₃MgSi₂O₈); V – anorthite (CaAl₂Si₂O₈); C – calcite (CaCO₃); N – cementite (Fe₃C)

Рис. 3. Дифрактограммы магнитного концентрата и немагнитных хвостов, полученных из ДШ (a) и ДП с присадкой 15 % C (b) обжиг-магнитным методом (обжиг 1200 °C, 120 мин; размол –0,054 мм; магнитная сепарация при 0,1 Тл):
 I – (α-Fe); H – гематит (α-Fe₂O₃); Y – маггемит (γ-Fe₂O₃); M – магнетит (Fe₃O₄); G – графит (C); A – окерманит (Ca₂MgSi₂O₇); T – геленит (Ca₂Al₂SiO₇); R – мервинит (Ca₃MgSi₂O₈); V – анортит (CaAl₂Si₂O₈); C – кальцит (CaCO₃); N – цементит (Fe₃C)

concentrate and tailings obtained from the BFS and BFD samples shows only slight differences.

After the roasting and magnetic separation under the conditions above, the magnetic concentrate with low zinc content can be recycled as part of the sinter burden. The zinc-containing sublimate obtained during the reduction roasting can be considered as a raw material for zinc production, while the non-magnetic tailings obtained during magnetic separation can be used as a raw material in the production of construction materials. Another option is to bypass the magnetic separation stage after the reduction roasting of BFS and BFD, which would avoid the costly grinding of the roasted product and allow the direct recycling in sinter production. However, this would result in the introduction of gangue into the blast furnace charge. A significant advantage of the obtained concentrates is the high reduced iron content, which accelerates the agglomeration process. The use of such concentrates in sinter production reduces the consumption of coke and lime, enables waste recycling, and decreases the need for natural iron-containing raw materials.

It is also worth noting that the metallized concentrates could potentially be used as a charge for electric arc furnace smelting. However, the concentrates do not currently meet the requirements of existing enterprises [36], which include % Fe_{tot} ≥ 88, % Fe_{met} ≥ 79, iron metallization degree ≥ 90 %, % P ≤ 0.015, % Si ≤ 0.5. In order to evaluate the feasibility of using these concentrates in steelmaking, further industrial testing is needed, along with possible adjustments to metallized raw material requirements for EAF smelting and improvements in the roasting and magnetic separation processes for blast furnace dust and sludge.

CONCLUSIONS

The study has shown that the optimal solution for processing BFS and BFD samples is preliminary magnetizing roasting at 1200 °C for 120 min, followed by grinding to –0.054 mm and magnetic separation with a magnetic field of 0.1 T. This process resulted in a dezinced concentrate from BFS with an iron content

of 73.8 %, an iron metallization degree of 88.9 %, and an iron recovery degree of 92.8 %. For BFD, the addition of 15 % carbon produced a dezincing magnetic concentrate with an iron content of 80 %, an iron metallization degree of 92.3 %, and an iron recovery degree of 89.7 %.

REFERENCES / СПИСОК ЛИТЕРАТУРЫ

1. Omran M., Fabritius T., Paananen T. Effect of blast furnace sludge (BFS) characteristics on suitable recycling process determining. *Journal of Minerals and Materials Characterization and Engineering*. 2017;5(4):185–197. <https://doi.org/10.4236/jmmce.2017.54016>
2. Jiao K.X., Zhang J.L., Liu Z.J., Chen C.L., Liu F. Circulation and accumulation of harmful elements in blast furnace and their impact on the fuel consumption. *Ironmaking and Steelmaking*. 2017;44(5):344–350. <https://doi.org/10.1080/03019233.2016.1210913>
3. Letimin V.N., Nasyrov T.M., Makarova I.V. Evaluation of pyrometallurgical methods for dezincification of dust and sludge from steelmaking workshops. *Teoriya i tekhnologiya metallurgicheskogo proizvodstva*. 2013;(1(13)):67–70. (In Russ.).
Летимин В.Н., Насыров Т.М., Макарова И.В. Оценка пирометаллургических способов обесцинкования пыли и шламов сталеплавильных цехов. *Теория и технология металлургического производства*. 2013;(1(13)):67–70.
4. Vaidya R., Kumar Ghosh S., Parlikar U.V. Blast furnace flue dust co-processing in cement kiln – A pilot study. *Waste Management and Research*. 2019;37(3):261–267. <https://doi.org/10.1177/0734242X18816791>
5. Francis A.A. Crystallization kinetics of magnetic glass-ceramics prepared by the processing of waste materials. *Materials Research Bulletin*. 2006;41(6):1146–1154. <https://doi.org/10.1016/j.materresbull.2005.11.002>
6. López-Díaz A., Ochoa-Díaz R., Grimaldo-León G.E. Use of BOF slag and blast furnace dust in asphalt concrete: An alternative for the construction of pavements. *DYNA (Colombia)*. 2018;85(204):24–30. <https://doi.org/10.15446/dyna.v85n206.70404>
7. Díaz R.O., Rojas A.P., León G.G. Use of blast furnace dust in the production of asphalt concrete for pavements, performance and environmental contribution. *Journal of Sustainable Architecture and Civil Engineering*. 2023;32(1):224–232. <https://doi.org/10.5755/j01.sace.32.1.32300>
8. Xie B., Geng N., Yu Q., He D., Wang F., Liu T., Gao J., Ning P., Song X., Jia L. Removal of SO₂ from flue gas using blast furnace dust as an adsorbent. *Environmental Science and Pollution Research*. 2022;29:15642–15653. <https://doi.org/10.1007/s11356-021-16842-7>
9. Carrillo Pedroza F.R., Soria Aguilar M. de J., Sánchez Castillo M.A., Martínez Luévanos A., Picazo Rodríguez N.G. Adsorption of chromium from steel plating wastewater using blast furnace dust. *Revista Internacional de Contaminación Ambiental*. 2017;33(4):591–603. <https://doi.org/10.20937/RICA.2017.33.04.04>
10. Liu S., Zhou W., Niu S., Han K., Wang Y., Lu C, Li Y., Wang J. Insight into blast furnace dust for selective catalytic reduction of NO_x: An experimental and DFT study. *Fuel*. 2023;344:128006. <https://doi.org/10.1016/j.fuel.2023.128006>
11. Mu Y., Liang X., Wu M., Li C., Xia T., Chen K., Li X. Utilizing blast-furnace dust as a novel persulfate catalyst for the efficient removal of petroleum contaminants from soil. *Journal of Cleaner Production*. 2024;434:140112. <https://doi.org/10.1016/j.jclepro.2023.140112>
12. Zhang Y., Li S., Wang X., Li X. Coagulation performance and mechanism of polyaluminum ferric chloride (PAFC) coagulant synthesized using blast furnace dust. *Separation and Purification Technology*. 2015;154:345–350. <https://doi.org/10.1016/j.seppur.2015.09.075>
13. Xiao X., Zhang S., Sher F., Chen J., Xin Y., You Z., Wen L., Hu M., Qui G. A Review on recycling and reutilization of blast furnace dust as a secondary resource. *Journal of Sustainable Metallurgy*. 2021;7:340–357. <https://doi.org/10.1007/s40831-021-00377-9>
14. Zeydabadi B.A., Mowla D., Shariat M.H., Kalajahi J.F. Zinc recovery from blast furnace flue dust. *Hydrometallurgy*. 1997;47(1):113–125. [https://doi.org/10.1016/S0304-386X\(97\)00039-X](https://doi.org/10.1016/S0304-386X(97)00039-X)
15. Soria-Aguilar M.D.J., Davila-Pulido G.I., Carrillo-Pedroza F.R., Gonzalez-Ibarra A.A., Picazo-Rodriguez N., Lopez-Saucedo F.D.J., Ramos-Cano, J. Oxidative leaching of zinc and alkalis from iron blast furnace sludge. *Metals (Basel)*. 2019;9(9):1015. <https://doi.org/10.3390/met9091015>
16. Zhang J.X., Niu F.S., Li L., Xie J. Beneficiability study of the blast furnace dust from Tangshan iron and steel company. *Advanced Materials Research*. 2013;712–715:420–423. <https://doi.org/10.4028/www.scientific.net/AMR.712-715.420>
17. Lanzerstorfer C. Air classification of blast furnace dust catcher dust for zinc load reduction at the sinter plant. *International Journal of Environmental Science and Technology*. 2016;13:755–760. <https://doi.org/10.1007/s13762-015-0903-1>
18. Tripathy S.K., Jaiswal S., Rama Murthy Y., Nag S. Separation analysis of flotation to recover the carbon values from blast furnace gas cleaning plant sludge. *Metallurgical Research & Technology*. 2016;113(3):303. <https://doi.org/10.1051/metal/2016011>
19. Jena M.K., Mahanta J., Mahapatra M.M., Baliarsingh M., Mishra S. Recovery of iron values from blast furnace gas cleaning process sludge by medium intensity magnetic separation method. In: *Recent Advances in Mechanical Engineering. Lecture Notes in Mechanical Engineering*. Pradhan P., Patanayak B., Das H.C., Mahanta P. eds. Singapore: Springer; 2023:449–454. https://doi.org/10.1007/978-981-16-9057-0_48
20. Das B., Prakash S., Reddy P.S.R., Biswal S.K., Misra V.N. Effective utilization of blast furnace flue dust of integrated steel plants. *The European Journal of Mineral Processing and Environmental Protection*. 2002;2(2):61–68.
21. Yehia A., El-Rahiem F.H. Recovery and utilization of iron and carbon values from blast furnace flue dust. *Mineral Processing and Extractive Metallurgy*. 2005;114(4):207–211. <https://doi.org/10.1179/037195505X28519>
22. Deng X., Huang R., Lv X., Yang J., Yang J. Separation and recovery of metallic zinc and iron concentrate from blast furnace dust by vacuum carbothermal reduction. *Process Safety and Environmental Protection*. 2022;162:746–751. <https://doi.org/10.1016/j.psep.2022.04.050>
23. Luo L., Zhang X., Wang H., Zheng B., Wei C. Comparing strategies for iron enrichment from Zn- and Pb-bearing refractory iron ore using reduction roasting-magnetic separation. *Powder Technology*. 2021;393:333–341. <https://doi.org/10.1016/j.powtec.2021.07.085>

24. Xu X., Guo Z., Zhu D., Pan J., Yang C., Li S. Application of coal-based direct reduction-magnetic separation process for recycling of high-iron-content non-ferrous metallurgical wastes: Challenges and opportunities. *Process Safety and Environmental Protection*. 2024;183:59–76. <https://doi.org/10.1016/j.psep.2023.12.057>
25. Putz H., Brandenburg K. Match! – Phase identification from powder diffraction, version 3.15, Crystal Impact, Bonn 2023. Available at URL: <https://www.crystalimpact.de/match> (Accessed 12.09.2024).
26. Roine A. HSC Chemistry® software, version 9.9, Outotec, Pori, Finland 2019. Available at URL: <https://www.outotec.com/HSC> (Accessed 12.09.2024).
27. Sun Y., Zhu X., Han Y., Li Y. Green magnetization roasting technology for refractory iron ore using siderite as a reductant. *Journal of Cleaner Production*. 2019;206:40–50. <https://doi.org/10.1016/j.jclepro.2018.09.113>
28. Li C., Sun H., Bai J., Li L. Innovative methodology for comprehensive utilization of iron ore tailings. Part I. The recovery of iron from iron ore tailings using magnetic separation after magnetizing roasting. *Journal of Hazardous Materials*. 2010;174(1-3):71–77. <https://doi.org/10.1016/j.jhazmat.2009.09.018>
29. Zhao Q., Xue J., Chen W. A Novel self-magnetizing roasting process for recovering Fe from low-grade pyrite cinder and blast furnace sludge. *Transactions of the Indian Institute of Metals*. 2019;72:2547–2556. <https://doi.org/10.1007/s12666-019-01724-x>
30. Chen B., Yi X., Zhan W., Gao L., He Z., Zhang J. Pyrometallurgical recovery of zinc and valuable metals from hazardous blast furnace dust via self-reduction roasting: Phase transformations and morphological evolution. *Materials Today Sustainability*. 2023;24:100590. <https://doi.org/10.1016/j.mtsust.2023.100590>
31. Filippova N.A. Phase Analysis of Ores and Products of their Processing. Moscow: Khimiya; 1975:111. (In Russ.). Филиппова Н.А. Фазовый анализ руд и продуктов их переработки. Москва: Химия; 1975:111.
32. Roy S.K., Nayak D., Rath S.S. A review on the enrichment of iron values of low-grade Iron ore resources using reduction roasting-magnetic separation. *Powder Technology*. 2020;367:796–808. <https://doi.org/10.1016/j.powtec.2020.04.047>
33. Yagupov A.V., Zamytskii V.S., Klykov Yu.G., Zamytskii O.V. Increasing the efficiency of ore processing. *Gornyi informatsionno-analiticheskii byulleten'*. 1997;(2):163–165. (In Russ.). Ягупов А.В., Замыцкий В.С., Клыков Ю.Г., Замыцкий О.В. Повышение эффективности переработки руд. *Горный информационно-аналитический бюллетень*. 1997;(2):163–165.
34. Wang B., Feng Y., Li H., Ju J., Yang Y. Separation of iron and zinc values from blast furnace dust adopting reduction roasting-magnetic separation method by sawdust pyrolysis. *Mining, Metallurgy & Exploration*. 2023;40:1357–1368. <https://doi.org/10.1007/s42461-023-00803-4>
35. Ju J., Feng Y., Li H., Zhang Q. Study of recycling blast furnace dust by magnetization roasting with straw charcoal as reductant. *Physicochemical Problems of Mineral Processing*. 2022;58(3):149265. <https://doi.org/10.37190/ppmp/149265>
36. Medenkov S.A. Promising use of metallized pellets in electrometallurgy. In: *Materials of the 66th Sci. Conf. Science of SUSU. Sections of Technical Sciences*. Chelyabinsk: SUSU; 2014:1404–1410. (In Russ.). Мединков С.А. Перспективное использование металлизированных окатышей в электрометаллургии. В кн.: *Материалы 66-й научной конференции Наука ЮУрГУ. Секции технических наук*. Челябинск: ИД ЮУрГУ; 2014:1404–1410.

Information about the Authors

Сведения об авторах

Pavel I. Grudinsky, Junior Researcher of the Bardin Laboratory of Metallurgy of Complex Ores, Baikov Institute of Metallurgy and Materials Science, Russian Academy of Sciences

ORCID: 0000-0002-7358-150X

E-mail: pgrudinskiy@imet.ac.ru

Anfisa A. Yurtaeva, Senior Laboratory Research Assistant of the Bardin Laboratory of Metallurgy of Complex Ores, Baikov Institute of Metallurgy and Materials Science, Russian Academy of Sciences

ORCID: 0009-0005-4449-2208

E-mail: anfisayurtaeva@mail.ru

Anton I. Volkov, Cand. Sci. (Chem.), Director of N.P. Lyakishev Scientific Center of Complex Processing of Raw Materials, I.P. Bardin Central Research Institute of Ferrous Metallurgy

ORCID: 0000-0003-1777-3889

E-mail: rhenium@list.ru

Valerii G. Dyubanov, Cand. Sci. (Eng.), Leading Researcher of the Bardin Laboratory of Metallurgy of Complex Ores, Baikov Institute of Metallurgy and Materials Science, Russian Academy of Sciences

ORCID: 0009-0001-5830-7799

E-mail: vdyubanov@imet.ac.ru

Павел Иванович Грудинский, младший научный сотрудник лаборатории проблем металлургии комплексных руд им. академика И.П. Бардина, Институт металлургии и материаловедения им. А.А. Байкова РАН

ORCID: 0000-0002-7358-150X

E-mail: pgrudinskiy@imet.ac.ru

Анфиса Александровна Юртаева, старший лаборант-исследователь лаборатории проблем металлургии комплексных руд им. академика И.П. Бардина, Институт металлургии и материаловедения им. А.А. Байкова РАН

ORCID: 0009-0005-4449-2208

E-mail: anfisayurtaeva@mail.ru

Антон Иванович Волков, к.х.н., директор Научного центра комплексной переработки сырья им. Н.П. Лякишева, Центральный научно-исследовательский институт черной металлургии им. И.П. Бардина

ORCID: 0000-0003-1777-3889

E-mail: rhenium@list.ru

Валерий Григорьевич Дюбанов, к.т.н., ведущий научный сотрудник лаборатории проблем металлургии комплексных руд им. академика И.П. Бардина, Институт металлургии и материаловедения им. А.А. Байкова РАН

ORCID: 0009-0001-5830-7799

E-mail: vdyubanov@imet.ac.ru

Contribution of the Authors

Вклад авторов

P. I. Grudinsky – conceptualization, writing the text, conducting thermodynamic calculations and laboratory experiments, titrimetric iron analysis, processing and analysis of the results.

A. A. Yurtaeva – conducting laboratory experiments, titrimetric iron analysis, editing the text.

A. I. Volkov – X-ray fluorescence analysis, editing the text.

V. G. Dyubanov – scientific guidance, editing the text.

П. И. Грудинский – разработка концепции работы, написание текста статьи, выполнение термодинамических расчетов и лабораторных экспериментов, титриметрическое определение железа, обработка и анализ результатов.

А. А. Юртаева – выполнение лабораторных экспериментов, титриметрическое определение железа, редактирование текста статьи.

А. И. Волков – рентгенофлуоресцентный анализ, редактирование текста статьи.

В. Г. Дюбанов – научное руководство, редактирование текста статьи.

Received 07.03.2024

Revised 21.03.2023

Accepted 23.08.2024

Поступила в редакцию 07.03.2024

После доработки 21.03.2023

Принята к публикации 23.08.2024



UDC 669.046:504.054

DOI 10.17073/0368-0797-2024-5-542-548



Original article

Оригинальная статья

MINERALOGICAL AND GRANULOMETRIC COMPOSITION OF SOILS FORMED ON THE SURFACE OF IRON ORE TAILINGS DUMPS

I. P. Belanov¹, A. M. Shipilova², O. P. Mezentseva²

¹ Institute of Soil Science and Agrochemistry, Siberian Branch of the Russian Academy of Sciences (8/2 Akademika Lavrent'eva Ave., Novosibirsk 630099, Russian Federation)

² Siberian State Industrial University (42 Kirova Str., Novokuznetsk, Kemerovo Region – Kuzbass 654007, Russian Federation)

✉ asya_nk77@mail.ru

Abstract. Hydraulic dumps for storing waste from primary and secondary iron ore processing (tailings dumps) were selected as objects for research. In the course of the study, data on the mineralogical composition of soil-forming rock samples of technogenic landscapes were obtained. This indicator is one of the main factors of soil formation when considering lithology at a lower hierarchical level. The mineralogical composition influences the content and ratio of nutrients and toxicants in soils, ion exchange processes, soil resistance to degradation and overall soil fertility. The mineralogical composition is the matrix of soil formation and regulates the transformation, migration and accumulation of matter, energy and information of the external environment and anthropogenic impact in the soil. The hydraulic filling method of waste storage has an impact on the spatial distribution of material in tailings dumps. First of all, a contrasting addition in terms of granulometric composition is distinguished due to the deposition of particles in aqueous conditions under the influence of a gravitational field. The deposition rate depends on the mass, size, shape and density of the particle substance, viscosity and density of the medium, as well as on acceleration, gravity and centrifugal forces acting on the particles. Despite a significant amount of research on the effect of mineralogical composition on soil development, this problem was not sufficiently studied. This determines the absence of generally accepted indicators of the development rate of soils formed on a man-made mineral substrate and the accumulation degree of biophilic elements in such soils.

Keywords: mineralogical composition, soil-forming rocks, tailings dump, soils of man-made landscapes, granulometric composition

For citation: Belanov I.P., Shipilova A.M., Mezentseva O.P. Mineralogical and granulometric composition of soils formed on the surface of iron ore tailings dumps. *Izvestiya. Ferrous Metallurgy*. 2024;67(5):542–548. <https://doi.org/10.17073/0368-0797-2024-5-542-548>

МИНЕРАЛОГИЧЕСКИЙ И ГРАНУЛОМЕТРИЧЕСКИЙ СОСТАВЫ ПОЧВ, ФОРМИРУЮЩИХСЯ НА ПОВЕРХНОСТИ ЖЕЛЕЗОРУДНЫХ ХВОСТОХРАНИЛИЩ

И. П. Беланов¹, А. М. Шипилова², О. П. Мезенцева²

¹ Институт почвоведения и агрохимии Сибирского отделения РАН (Россия, 630099, Новосибирск, пр. Академика Лаврентьева, 8/2)

² Сибирский государственный индустриальный университет (Россия, 654007, Кемеровская обл. – Кузбасс, Новокузнецк, ул. Кирова, 42)

✉ asya_nk77@mail.ru

Аннотация. Объектом исследования являются гидроотвалы складирования отходов первичного и вторичного обогащений железной руды (хвостохранилища). В ходе исследования получены данные минералогического состава образцов почвообразующей породы техногенных ландшафтов. Рассматриваемый показатель является одним из основных факторов почвообразования при изучении литологии на более низком иерархическом уровне. Минералогический состав оказывает влияние на содержание и соотношение в почвах элементов питания и токсикантов, процессы ионного обмена, устойчивость почв к деградации и общее плодородие почв. Он является матрицей формирования почв и регулирует трансформацию, миграцию и аккумуляцию в почве веществ, энергии и информации внешней среды и антропогенного воздействия. Гидроналивной способ складирования отходов оказывает влияние на пространственное распределение материала в хвостохранилищах. Прежде всего выделяется контрастное сложение по гранулометрическому составу из-за осаждения частиц в водных условиях под действием гравитационного поля. Скорость осаждения зависит от массы, размера, формы и плотности вещества частиц, вязкости и плотности среды, а также от ускорения, силы тяжести и действующих на частицы центробежных сил. Несмотря

на значительное количество исследований по влиянию минералогического состава на развитие почв, данная проблема изучена недостаточно. Это определяет отсутствие общепринятых показателей скорости развития почв, формирующихся на техногенном минеральном субстрате, и степени накопления в таких почвах биофильных элементов.

Ключевые слова: минералогический состав, почвообразующие породы, хвостохранилище, почвы техногенных ландшафтов, гранулометрический состав

Для цитирования: Беланов И.П., Шипилова А.М., Мезенцева О.П. Минералогический и гранулометрический составы почв, формирующихся на поверхности железорудных хвостохранилищ. *Известия вузов. Черная металлургия.* 2024;67(5):542–548.

<https://doi.org/10.17073/0368-0797-2024-5-542-548>

INTRODUCTION

Kuzbass is one of Russia's most industrially developed regions. High concentration of industrial enterprises, combined with the unsustainable use of natural resources, has led to the creation of man-made landscapes on land that was once fertile. In the southern part of Kemerovo Region – Kuzbass, the EVRAZ United West-Siberian Metallurgical Plant (EVRAZ ZSMK) is located, a full-cycle facility that produces rolled metal for the construction, railway, and other industries. The raw material used is iron ore, which is processed at the Abagur beneficiation and sintering plant (formerly the Mundybash beneficiation plant). The ore processing generates waste (enrichment tailings) that is stored in hydraulic dumps. As a result, man-made landscapes have emerged in the region, where young soils are now beginning to form on their surfaces.

The mineralogical composition of soils is a key factor that directly influences their physical and chemical properties, as well as the processes occurring within them. It serves as a matrix for the development of soil properties, regulating the transformation, migration, and accumulation of matter, energy, and environmental information. Unlike other factors such as climate, topography, and vegetation, which determine the mechanisms and pace of soil formation, the mineral substrate provides the material foundation from which the soil profile develops [1; 2].

Studying the mineralogical composition not only aids in understanding soil properties but also in grasping the genesis of newly forming man-made soils, as it sets the stage for the direction and intensity of soil-forming processes (humus accumulation, internal weathering, illimerization, podzolization, gleying, brunification, and more). Therefore, determining and accounting for mineralogical composition is essential when classifying soils [1; 3; 4].

The main aim of this work is to investigate the mineralogical and granulometric composition of rocks from primary and secondary iron ore enrichment tailings, where the formation of young soils (embryozems) is currently underway.

OBJECTS AND METHODS OF RESEARCH

The objects of the study were the hydraulic dumps of the Mundybash beneficiation plant (primary

(N53°13'28.90" E86°16'04.01") and the Abagur beneficiation and sintering plant (secondary) (N53°42'11.95" E87°14'12.50").

The Mundybash beneficiation plant was built between 1931 and 1935 to enrich iron ore from the nearby Telbes mine of the Kuznetsk Metallurgical Plant. The plant operated until April 2015, after which it ceased its activities. The hydraulic dump has presumably been out of operation since 2000.

The Abagur beneficiation and sintering plant processes primary concentrates and produces secondary concentrate. The plant's product is supplied to EVRAZ ZSMK. The production capacity of units 1 and 2 is 3.560 million tons of industrial products per year and 2.780 million tons of concentrate (from the mines of Gornaya Shoria and Abakanskoye Mine). The production capacity of unit 3 is 2.858 million tons of industrial products per year and 1.960 million tons of concentrate (from the Teiskoe mine and 10 % from the Gornaya Shoria mines). The studied hydraulic dump has been out of operation since 2001.

At each of the studied iron ore hydraulic dumps, four concentric zones were identified, differing in the degree of material dispersion (the mouth, main, near-core, and core zones). The upper part of the sedimentation basin (mouth zone) is characterized by a light mechanical composition and high drainage capacity. The main zone, formed by particles of medium dispersion, occupies most of the tailings area. The near-core and core zones, which are thixotropic or water-covered, form the accumulative center of the drainage basin. In each zone, samples were taken from a 0 – 40 cm layer, as this layer potentially acts as the accumulation zone for 90 % of root mass.

The mineralogical and petrographic compositions of samples from different sedimentation zones of the tailings were studied using an MBS-10 stereoscopic microscope (magnification 8 – 16) in reflected light. The study included the examination of external (macroscopic) characteristics and physical properties. In some cases, simple microchemical drop reactions and powder reactions were applied [5; 6].

Granulometric composition, as one of the important indicators of soil that affects many aspects of soil existence and functioning, was analyzed using the Kachinsky pyrophosphate method of sample preparation. The analy-

sis focused on fractions of physical sand and physical clay with sizes greater than 0.01 mm (up to 1 mm) and less than 0.01 mm.

RESEARCH RESULTS

The hydraulic filling method of storing ore enrichment waste influences the spatial distribution of material in the hydraulic dumps. A contrasting structure in terms of granulometric composition is primarily distinguished due to particle sedimentation in aqueous conditions under the influence of the gravitational field. The rate of sedimentation depends on the mass, size, shape, and density of the particle substance, the viscosity and density of the medium, as well as acceleration, gravitational force, and centrifugal forces acting on the particles.

All sedimentation zones exhibit spatial heterogeneity in granulometric composition: an increase in the clay content and a decrease in sand fractions are observed from the mouth zone to the core zone (see Table). All samples consisted of fine earth, with no particles larger than 1 mm. The redistribution of clay fractions in the sedimentation zones at all research sites follows a similar pattern, with the relative quantities in each zone forming the following sequence: fine silt (about 50 %) – medium silt (about 30 %) – clay (about 20 %). The redistribution of fractions within the physical sand group across all studied sites is heterogeneous and depended on the type of disintegrated rock.

The mouth zone, located at the outer perimeter of the hydraulic dumps, is characterized by a sandy (Mundy-

bash beneficiation plant) or sandy loam (Abagur sintering plant) granulometric composition. In this zone, soil formation is slow across all observation sites, so the soil cover mainly consists of initial embryozems. The vegetation cover is either absent or represented by isolated specimens of ruderal vegetation from the xerophytic ecogroup. In the physical sand fraction of the Mundybash plant hydraulic dump, just under 50 % of the particles are fine sand, while the remainder is equally divided between coarse-medium sand and coarse dust. A similar pattern of sand fraction distribution is observed in the hydraulic dump of the Abagur sintering plant. In general, it is worth noting that the highest degree of deflation and erosion processes is observed in this zone on the surface of the hydraulic dumps.

The mineralogical composition includes both primary and secondary minerals. The mineral composition of the Mundybash plant hydraulic dump is characterized by the presence of magnetite fragments less than 0.5 mm (about 10 %), and occasionally up to 1.5 mm; isolated inclusions of molybdenite; numerous calcite crystals, including marble fragments ranging in size from 1.5 to 2.0 mm and smaller; serpentine fragments (1.5 to 2.0 mm) about 10 – 15 %; isolated talc flakes; pyroxenes less than 5 %; and rare quartz. For the Abagur sintering plant, the mineral composition includes magnetite dust (about 5 – 10 %); isolated occurrences of iron slag and chalcopyrite; isolated pyrite; calcite crystals, and a dominance of marble fragments; quartz around 10 %; muscovite about 20 %; pyroxenes around 1 – 3 %; and rare occurrences of amphibole and gypsum (selenite).

Granulometric composition of sludge from tailings dumps

Гранулометрический состав шламов хвостохранилищ

Sedimentation zone	Predominant soil type	Particle size distribution, %, diameter, mm							
		1.00 – 0.25	0.25 – 0.05	0.05 – 0.01	0.01 – 0.005	0.005 – 0.001	0.001 – 0.0001	Physical clay (<0.01 mm)	Physical sand (<0.01 mm)
Hydraulic dump of the Mundybash Beneficiation Plant									
IV	E. initial	23.31	42.35	24.77	3.41	4.63	1.52	9.6	90.4
III	E. organo-accumulative	0.42	6.60	65.52	10.15	13.32	3.99	27.5	72.5
III	E. turf	3.94	19.67	36.42	14.55	20.20	5.21	40.0	60.0
I	E. coarse-humus-accumulative gley	0.49	0	43.04	21.10	28.03	7.34	56.5	43.5
Hydraulic dump of the Abagur Sintering Plant									
IV	E. initial	22.67	33.41	19.61	8.96	12.44	2.91	24.3	75.7
III	E. organo-accumulative	28.91	16.40	26.03	9.11	14.23	5.32	28.7	71.3
III	E. organo-accumulative gley	4.10	0	25.54	28.42	34.65	7.30	70.4	29.6
I	E. organo-accumulative gley	0.96	0	26.05	27.35	36.94	8.71	73.0	27.0

Note. E. – Embryozem; I – Core Zone; II – Near-core Zone; III – Main Zone; IV – Mouth Zone.

The presence of secondary minerals, such as goethite and hematite, is characteristic of the sedimentation zone of the tailings, although they occur infrequently.

Based on observations, organo-accumulative embryozems have formed in the main sedimentation zone of the two hydraulic dumps [7; 8]. The surface is covered with ruderal vegetation from the xerophytic ecogroup, with a total projected coverage not exceeding 2 – 5 %. The total physical sand content in this zone ranges from 71 to 90 %, and the granulometric composition of the hydraulic dumps corresponds to light loam. Nevertheless, the redistribution of sand fractions differs across each site: at the Mundybash beneficiation plant tailings dump, the predominant fraction is 0.05 – 0.01 mm (approximately 90 %), while at the Abagur sintering plant, it is 1.00 – 0.25 mm (about 39 %) and 0.05 – 0.01 mm (about 36 %). Erosion processes are evident on the surface, with rills 15 to 40 cm deep and clear signs of deflation processes.

The mineralogical composition of the Mundybash beneficiation plant zone consists of fragments smaller than 0.5 mm (about 10 %) of magnetite and iron slag, with a dominance of calcite crystals and marble fragments less than 0.5 mm (occasionally 1.0 – 1.5 mm); serpentine fragments less than 0.5 mm (rarely 1.0 – 1.5 mm) make up about 5 %; isolated flakes of talc and quartz; pyroxene fragments 1.0 – 1.5 mm and smaller (about 1 – 5 %). Goethite presents as a secondary mineral, albeit rarely. The mineralogical composition in the main zone of the tailings dump is identical to that of the mouth zone, although the fragments are smaller (less than 0.5 – 1.0 mm). In the dust fraction: magnetite (about 5 – 10 %), with calcite, quartz, and muscovite dominating; pyroxenes are present, and secondary minerals are absent.

The near-core zone serves as a distinct transitional boundary marked by the predominance or significant increase of physical clay in the granulometric composition. This increase is due to the specific conditions of hydraulic filling in the hydraulic dump and the sedimentation of rock particles, as well as the influx of fine dust fractions resulting from erosion processes during rainfall. The shift in granulometric composition from medium loam to medium clay (see Table) leads to the formation of turf and organo-accumulative or organo-accumulative gleyic embryozems (with traces of iron oxides due to seasonal waterlogging) on the surface of the hydraulic dumps. As a result, differences are observed in the ecogroups of ruderal vegetation that have formed. In the main zone, mesoxerophytic or xeromesophytic groups dominate, with a projected coverage of up to 10 %, and on the Mundybash plant hydraulic dump, up to 50 %.

The mineralogical composition of the beneficiation plant tailings dump consists of particles smaller than

0.5 mm of iron slag and magnetite (about 10 %); fragments of coal and slag; calcite crystals and marble fragments measuring 1.0 – 0.5 mm and smaller (about 3 %); isolated quartz and talc flakes; and numerous fragments of modern vegetation. Secondary minerals are absent. The mineralogical composition of the near-core zone of the sintering plant tailings dump is identical to that of the mouth zone but has some distinct features: mineral fragments are smaller (less than 0.5 – 1.0 mm); magnetite dust content is about 5 – 10 %; quartz and calcite dominate; pyrite content is around 0.5 %; secondary minerals are absent.

In each of the studied sites, the core zone is the final accumulation zone for clay particles. In the analyzed samples, the physical clay content ranges from 56 to 73 %. While the proportion of fractions within the physical clay remains relatively stable, a redistribution in favor of finer particles can be assumed. The physical sand fraction lacks coarse-medium and fine sand (1.00 – 0.05 mm), with the entire portion consisting of coarse dust (0.05 – 0.01 mm). The heavy granulometric composition hinders filtration and leads to prolonged stagnation of meltwater and rainwater. Currently, two types of gleyic embryozems have been identified on the surface of the core zone (see Table). The difference in embryozem formation across sites is due to the duration of the post-technogenic period, the lithogenic properties of the rocks, and the productivity of the plant communities [9; 10]. The resulting phytocenoses belong to the xeromesophytic/mesophytic ecogroup, with occasional hygrophytes (such as bulrush, sedge, and others). However, during drought periods (when moisture is deficient), these plants either die or remain in a suppressed state.

The mineralogical composition of the core zone of the primary beneficiation tailings dump consists of iron slag and magnetite particles smaller than 0.01 mm (about 1 – 3 %); indeterminate mineral particles smaller than 0.01 mm; as well as modern plant fragments (about 15 %). Secondary minerals are absent. The mineralogical composition of the near-core zone of the tailings dump formed during secondary beneficiation is characterized by the same composition as the previous dominant zones in the relief. However, it has some distinguishing features: a predominance of mineral fragments smaller than 0.5 – 1.0 mm, the presence of magnetite dust (about 5 – 10 %), and a dominance of calcite and quartz. Secondary minerals are absent, as in the previous two sedimentation zones.

RESULTS AND DISCUSSION

Despite the considerable number of studies on the influence of mineralogical composition on the development of soils formed on the surfaces of iron ore tailings

dumps, this issue remains insufficiently studied [11 – 14]. This explains the lack of generally accepted indicators for the rate of soil development on man-made mineral substrates and the accumulation of biophilic elements in such soils.

The most common primary minerals dominating the large fractions of natural soils are quartz, calcite, and micas. It is important to note that this set of minerals serves as an indicator of favorable soil formation processes on the surfaces of man-made landscapes [15 – 17]. The physical properties of soils depend on these primary minerals, which already act as a reserve source of ash elements for plant nutrition. As they undergo transformation, secondary minerals are formed (simple salt minerals, oxide and hydroxide minerals, and clay minerals). Simple salt minerals (calcite, magnesite, dolomite, gypsum, and others) determine the qualitative and quantitative composition of soil salinization. Oxide and hydroxide minerals, due to their large surface area, absorb significant amounts of phosphorus, making it less available to plants. Clay minerals (montmorillonite, kaolinite) and hydromicas, which dominate the fine-dispersed fractions, together with humic acids, improve the water-physical properties of soils, act as sources of mineral nutrients for plants, and determine the soil's absorptive capacity [8].

Calcite is a key indicator of pedogenic transformations in the soils of man-made landscapes [18; 19]. The presence of carbonates throughout the profile clearly reflects the transformation of the original substrate during the soil formation process. The highest calcite concentrations are observed in the mouth, main, and near-core zones of the Mundybash tailings dump. The quantity and variety of calcite forms reflect the intensity of soil formation processes and the transformation of the original substrate. Calcite content is determined, on one hand, by more favorable hydrological conditions (flushing water mode), and on the other hand, by the likely extended duration of soil formation in areas subject to periodic flooding in the core zone.

The presence of secondary minerals (goethite), which form as a result of pyroxene oxidation and hematite dehydration (in the mouth and main zones of the tailings dumps), indicates the intensity and speed of weathering processes. It can be assumed that nearly all iron-containing minerals, upon alteration due to water and humic acid exposure, are transformed into limonite. Additionally, the weathering of iron oxides (magnetite, hematite, goethite), which are found in the mineral composition of the studied tailings dumps, may lead to the release of iron into pore water and its precipitation as ferrihydrite [20 – 22], as well as the formation of iron hydroxide in water and its precipitation in aquifers. Ferrihydrite is further transformed into hematite, with goethite also possibly forming. The type of final mineral depends on the physical and chemical factors influencing the func-

tioning of the hydraulic dumps from iron ore beneficiation waste (temperature, pH levels, Fe(III) concentration in solution, and the nature and quantity of accompanying anions). Hematite content reaches a maximum in a slightly alkaline environment and a minimum in moderately acidic conditions. Increasing temperature and decreasing moisture accelerate ferrihydrite transformation and increase the hematite-to-goethite ratio [22]. When in contact with water containing sulfides, iron hydrosulfide forms, which can adsorb onto the surface of mineral grains and transform into iron oxides. In more complex processes, iron oxide FeO_2 may also be involved.

The mineral skeleton of the soil, which primarily consists of quartz, calcite, and primary and secondary iron minerals, serves as the foundation within which the majority of chemical, physicochemical, and biochemical processes essential to soil formation occur on the surface of the studied tailings dumps. Soil formation, as a form of biological weathering, leads to transformations in the granulometric composition, while periodic water infiltration results in the redistribution and change of fraction ratios. For example, winter infiltration in gray forest soils leads to the averaging of fractions to 0.01 mm and increases the mobility of silt, which enhances the transformation of soil-forming rocks [23].

A more intensive soil formation process is currently observed on the mineral substrate surface of the Mundybash beneficiation plant hydraulic dump. Over a pragmatically acceptable time period, coarse-humus-accumulative and turf embryozems have formed there. This is due to the more balanced granulometric composition of the rocks, consisting of no more than 60 % physical clay, which does not impede the seasonal infiltration of the root layer and allows for the filtration of excess moisture into the lower horizons. When the physical clay content exceeds 60 % in both the near-core and core zones of the Abagur sintering plant hydraulic dump, an aquiclude forms almost at the surface of the mineral layer (within the 10 – 30 cm layer), leading to water stagnation, especially during the spring and autumn periods. This phenomenon slows the soil formation processes on the surface of the tailings dumps. As a result, only organo-accumulative embryozems have formed over an extended period in these areas, indicating an unsatisfactory soil-ecological condition under stagnant water modes.

CONCLUSIONS

Mineral transformations are dynamic in the soils of man-made landscapes formed from the waste of primary and secondary beneficiation of ferrous metal ores. The mineral component of the soil-forming rock from primary beneficiation waste is primarily composed of magnetite, calcite, quartz, and talc flakes, and it under-

goes minimal changes between sedimentation zones. In the secondary beneficiation tailings dump, the mineral component is more homogeneous across zones, consisting mainly of muscovite, quartz, calcite, and magnetite dust. The formation of secondary minerals (goethite and hematite) is characteristic of the main and mouth sedimentation zones of both tailings dumps. It is assumed that hematite forms through the dehydration of iron hydroxides. Hematite develops via a ferrihydrite phase, a process typical of soils (especially in humid regions), and under certain hydrothermal conditions, goethite may also form.

Even with a favorable mineralogical composition of the soil-forming rock, the soil formation process is slowed due to the granulometric properties of iron ore tailings dumps. When the physical clay content in the rock exceeds 60 %, only organo-accumulative embryozems form within a pragmatically acceptable time frame (no less than 20 years).

REFERENCES / СПИСОК ЛИТЕРАТУРЫ

- Sokolov I.A. Theoretical Problem of Genetic Soil Science. Novosibirsk: Nauka; 2004:288. (In Russ.).
Соколов И.А. Теоретическая проблема генетического почвоведения. Новосибирск: Наука; 2004:288.
- Friedland V.M. Basic Principles and Elements of Basic Soils Classification and Program for its Creation. Moscow: Soil. V.V. Dokuchaev Institute; 1982:150.
Фридланд В.М. Основные принципы и элементы базовой классификации почв и программа работ по ее созданию. Москва: Почв. ин-т им. В.В. Докучаева; 1982:150.
- Vassilev S.V., Vassileva C.G. Mineralogy of combustion wastes from coal-fired power station. *Fuel Processing Technology*. 1996;47(3):261–280.
[https://doi.org/10.1016/0378-3820\(96\)01016-8](https://doi.org/10.1016/0378-3820(96)01016-8)
- Dolinskii V.A. Factories for Iron Ore Dressing. Novokuznetsk: SibGIU; 2007:144. (In Russ.).
Долинский В.А. Фабрики для обогащения железных руд. Новокузнецк: ИЦ СибГИУ; 2007:144.
- Sazonov A.M. Optical Determination of Rock-Forming Minerals. Krasnoyarsk: SFU. 2017:100. (In Russ.).
Сазонов А.М. Оптическое определение породообразующих минералов. Красноярск: СФУ; 2017:100.
- Gromoglasov A.A., Kopylov A.F., Pilschikov A.P. Water Preparation: Processes and Devices. Moscow: Energoatomizdat; 1990:99.
- Titlyanova A.A., Kosykh N.P., Mironycheva-Tokareva N.P., Romanova I.P. Underground Plant Organs in Grass Ecosystems. Novosibirsk: Nauka; 1996:125. (In Russ.).
Подземные органы растений в травяных экосистемах / А.А. Титлянова, Н.П. Косых, Н.П. Миронычева-Токарева, И.П. Романова. Новосибирск: Наука; 1996:125.
- Skryabina O.A. Mineralogical Composition of Soils and Soil-Forming Rocks. Perm: Permskaya GSKhA; 2010:120. (In Russ.).
Скрябина О.А. Минералогический состав почв и почвообразующих пород. Пермь: ФГОУ ВПО «Пермская ГСХА»; 2010:120.
- Androkhonov V.A., Kulyapina V.D., Kurachev V.M. Soils of Man-Made Landscapes: Genesis and Evolution. Novosibirsk: Izd-vo SB RAS; 2004:50–51. (In Russ.).
Андроханов В.А., Куляпина В.Д., Курачев В.М. Почвы техногенных ландшафтов: генезис и эволюция. Новосибирск: Изд-во СО РАН; 2004:50–51.
- Carras J.N., Day S.J., Saghafi A., Williams D.J. Greenhouse gas emissions from low-temperature oxidation and spontaneous combustion at open-cut coal mines in Australia. *International Journal of Coal Geology*. 2009;78(2):161–168.
<http://dx.doi.org/10.1016/j.coal.2008.12.001>
- Deng Y., Flury M., Harsh J.B., Felmy A.R., Qafoku O. Cancrinite and sodalite formation in the presence of cesium, potassium, magnesium, calcium and strontium in Hanford tank waste simulants. *Applied Geochemistry*. 2006; 21(12):2049–2063.
<http://dx.doi.org/10.1016/j.apgeochem.2006.06.019>
- Ram L.C., Tripathi P.S.M., Mishra S.P. Mossbauer spectroscopic studies on the transformations of iron-bearing minerals during combustion of coals: Correlation with fouling and slagging. *Fuel Processing Technology*. 1995;42(1):47–60.
[https://doi.org/10.1016/0378-3820\(94\)00111-6](https://doi.org/10.1016/0378-3820(94)00111-6)
- Reed S.J.B. Electron Microscope Analysis and Scanning Electron Microscopy in Geology. Cambridge University Press; 2005:206.
- Manakov Yu.A. The disturbed lands of Kuzbass. The way to solve the problem is the reclamation fund. *Промышленная экология*. 2008;(4):29–34. (In Russ.).
Манаков Ю.А. Нарушенные земли Кузбасса. Путь решения проблемы – фонд рекультивации. *Промышленная экология*. 2008;(4):29–34.
- Novoselov A.A. Indicators of soil formation on technogenic substrates of ash dumps. *Rossiiskii zhurnal prikladnoi ekologii*. 2019;(3(19)):46–50. (In Russ.).
Новоселов А.А. Индикаторы почвообразования на техногенных субстратах золоотвалов. *Российский журнал прикладной экологии*. 2019;(3(19)):46–50.
- Querol X., Izquierdo M., Monfort E., Alvarez E., Font O., Moreno T., Alastuey A., Zhuang X., Lud W., Wang Y. Environmental characterization of burnt coal gangue banks at Yangquan, Shanxi Province, China. *International Journal of Coal Geology*. 2008;75(2):93–104.
<https://doi.org/10.1016/j.coal.2008.04.003>
- Finkelman R.B. Potential health impacts of burning coal beds and waste banks. *International Journal of Coal Geology*. 2004;59(1-2):19–24.
<https://doi.org/10.1016/j.coal.2003.11.002>
- Uzarowicz Ł., Skiba S. Technogenic soils developed on mine spoils containing iron sulphides: Mineral transformations as an indicator of pedogenesis. *Geoderma*. 2011;163(1-2):95–108.
<http://dx.doi.org/10.1016/j.geoderma.2011.04.008>
- Uzarowicz Ł., Skiba S., Leue M., Zagórski Z., Gąsiński A. Technogenic soils (Technosols) developed from fly ash and bottom ash from thermal power stations combusting bituminous coal and lignite. Part II. Mineral transformations and soil evolution. *Catena*. 2018;62(1):255–259.
<http://dx.doi.org/10.1016/j.catena.2017.11.005>
- Warren C.J., Dudas M.J. Formation of secondary minerals in artificially weathered fly ash. *Journal of Environmental Quality*. 1985;14(3):405–410.
<https://doi.org/10.2134/JEQ1985.00472425001400030019X>

21. Zevenbergen C., Bradley J.P., Van Reeuwijk L.P., Shyam A.K., Hjelmar O., Comans R.N.J. Clay formation and metal fixation during weathering of coal fly ash. *Environmental Monitoring and Assessment*. 1999;33(19):3405–3409. <http://dx.doi.org/10.1021/es9900151>
22. Vodyanitskii Yu.N. Iron Compounds and Their Role in Soil Protection. Moscow: Pochv. in-t im. V.V. Dokuchaeva; 2010:155. (In Russ.).
23. Дюкарев А.Г. Landscape-Dynamic Aspects of Taiga Soil Formation in Western Siberia. Tomsk: Izd-vo Nauchno-tekhnicheskoi literatury; 2005:283. (In Russ.).
- Дюкарев А.Г. Ландшафтно-динамические аспекты таежного почвообразования в Западной Сибири. Томск: Изд-во Научно-технической литературы; 2005:283.

Information about the Authors

Сведения об авторах

Ivan P. Belanov, *Cand. Sci. (Biological)*, Senior Researcher of the Laboratory of Soil Reclamation, Institute of Soil Science and Agrochemistry, Siberian Branch of the Russian Academy of Sciences
E-mail: bel_ivan@rambler.ru

Asya M. Shipilova, *Cand. Sci. (Agricultural)*, Assist. Prof. of the Chair of Geology, Geodesy and Life Safety, Siberian State Industrial University
E-mail: asya_nk77@mail.ru

Ol'ga P. Mezentseva, *Cand. Sci. (Geol.-Mineralogical)*, Assist. Prof. of the Chair of Geology, Geodesy and Life Safety, Siberian State Industrial University
E-mail: mesentsevaop@yandex.ru

Иван Петрович Беланов, к.б.н., старший научный сотрудник Лаборатории рекультивации почв, Институт почвоведения и агрохимии Сибирского отделения РАН
E-mail: bel_ivan@rambler.ru

Ася Максимовна Шипилова, к.с.-х.н., доцент кафедры геологии, геодезии и безопасности жизнедеятельности, Сибирский государственный индустриальный университет
E-mail: asya_nk77@mail.ru

Ольга Петровна Мезенцева, к.г.-м.н., доцент кафедры геологии, геодезии и безопасности жизнедеятельности, Сибирский государственный индустриальный университет
E-mail: mesentsevaop@yandex.ru

Contribution of the Authors

Вклад авторов

I. P. Belanov – sampling, writing the text.
A. M. Shipilova – sample processing and analysis.
O. P. Mezentseva – sample processing and analysis.

И. П. Беланов – отбор проб, написание статьи.
А. М. Шипилова – обработка и анализ проб.
О. П. Мезенцева – обработка и анализ проб.

Received 30.10.2023
 Revised 01.07.2024
 Accepted 21.08.2024

Поступила в редакцию 30.10.2023
 После доработки 01.07.2024
 Принята к публикации 21.08.2024



UDC 669.18

DOI 10.17073/0368-0797-2024-5-549-555



Original article

Оригинальная статья

FORMATION OF NON-METALLIC INCLUSIONS IN PRODUCTION OF 08KH18N10T CORROSION-RESISTANT STEEL

A. Yu. Em¹, O. A. Komolova^{1,2}, K. V. Grigorovich^{1,2}, S. B. Romyantseva¹

¹ Baikov Institute of Metallurgy and Materials Science, Russian Academy of Sciences (49 Leninskii Ave., Moscow 119991, Russian Federation)

² National University of Science and Technology “MISIS” (4 Leninskii Ave., Moscow 119049, Russian Federation)

✉ tony.yem1994@gmail.com

Abstract. Corrosion-resistant steels are in demand in the modern world due to their high performance properties and a wide range of applications. Such areas of application include kitchenware, furniture, medical equipment, nuclear reactors, spacecraft, etc. Oxygen in steel, especially in corrosion-resistant steel, is one of the most harmful elements. Oxide inclusions disrupt the homogeneity of the metal, negatively affect the ductility, fracture toughness, fatigue strength and corrosion resistance of steel. In corrosion-resistant steels, non-metallic inclusions (NI) lead to the formation of defects in cold-rolled sheets. Aluminate inclusions also lead to clogging of steel-casting equipment. An analysis of the production technology of corrosion-resistant steel 08Kh18N10T was carried out in order to determine the causes of NI formation that affect the pourability of steel and its quality. The studies determined the content of total oxygen and nitrogen, as well as oxygen bound in various non-metallic inclusions at the stages of ladle processing and continuous steel casting. It was shown that after the introduction of titanium wire into the melt, the total nitrogen content decreases due to the formation and subsequent removal of titanium nitrides. At the same time, the content of titanium oxides in the melt increases. It was shown that the causes of clogging of steel-pouring nozzles during continuous casting are complex non-metallic inclusions based on titanium oxides, which were deposited on the inner surface of the pouring nozzle-doser. Recommendations were made to adjust the technology of steel melting in EAF and ladle processing. Based on the results of electron microscopic analysis, it was established that mixing of refining liquid-mobile slag in ladle steel processing units contributed to the assimilation of non-metallic inclusions by slag and a decrease in their sizes in the metal. After the implementation of the corrective recommendations, clogging of steel-pouring nozzles during continuous casting was not observed.

Keywords: corrosion-resistant steel, fractional gas analysis, non-metallic oxide inclusions, steel quality

For citation: Em A.Yu., Komolova O.A., Grigorovich K.V., Romyantseva S.B. Formation of non-metallic inclusions in production of 08Kh18N10T corrosion-resistant steel. *Izvestiya. Ferrous Metallurgy*. 2024;67(5):549–555. <https://doi.org/10.17073/0368-0797-2024-5-549-555>

ФОРМИРОВАНИЕ НЕМЕТАЛЛИЧЕСКИХ ВКЛЮЧЕНИЙ ПРИ ПРОИЗВОДСТВЕ КОРРОЗИОННОСТОЙКОЙ СТАЛИ 08X18N10T

А. Ю. Ем¹, О. А. Комолова^{1,2}, К. В. Григорович^{1,2}, С. Б. Румянцева¹

¹ Институт металлургии и материаловедения им. А.А. Байкова РАН (Россия, 119991, Москва, Ленинский пр., 49)

² Национальный исследовательский технологический университет «МИСИС» (Россия, 119049, Москва, Ленинский пр., 4)

✉ tony.yem1994@gmail.com

Аннотация. Коррозионностойкие стали востребованы в современном мире из-за их высоких эксплуатационных свойств и широкого спектра применения. К таким областям применения относятся кухонная утварь, мебель, медицинское оборудование, ядерные реакторы, космические аппараты и т. д. Кислород в стали, особенно в коррозионностойкой, является одним из самых вредных элементов. Оксидные включения нарушают однородность металла, отрицательно влияют на пластичность, вязкость разрушения, усталостную прочность и коррозионную стойкость стали. В коррозионностойких сталях неметаллические включения (НВ) приводят к образованию дефектов в холоднокатаном листе. Включения алюминатов также приводят к засорению сталеразливочного оборудования. В работе выполнен анализ технологии производства коррозионностойкой стали 08X8N10T с целью определения причин образования НВ, влияющих на разливаемость стали и ее качество. В ходе исследований определено содержание общего кислорода и азота, а также кислорода, связанного в различные НВ на стадиях ковшевой обработки и непрерывной разливки стали. После введения в расплав титановой проволоки общее содержание азота снижается за счет образования и последующего удаления нитридов титана. При этом увеличивается содержание оксидов титана в расплаве. Показано, что причинами засорения сталеразливочных стаканов при непрерывной разливке являются комплексные НВ на основе оксидов титана, которые осаждались на внутренней поверхности разливного стакана-дозатора. В работе даны рекомендации по корректировке технологии выплавки стали в ДСП и ковшевой обработки. По результатам электронно-микроскопического анализа установ-

лено, что перемешивание рафинирующего жидкоподвижного шлака в агрегатах ковшевой обработки стали способствовало ассимиляции НВ шлаком и уменьшению их размеров в металле. После внедрения корректирующих рекомендаций засорения сталеразливочных стаканов при непрерывной разливке не наблюдалось.

Ключевые слова: коррозионностойкая сталь, фракционный газовый анализ, оксидные неметаллические включения, качество стали

Для цитирования: Ем А.Ю., Комолова О.А., Григорович К.В., Румянцева С.Б. Формирование неметаллических включений при производстве коррозионностойкой стали 08X18N10T. *Известия вузов. Черная металлургия.* 2024;67(5):549–555.
<https://doi.org/10.17073/0368-0797-2024-5-549-555>

INTRODUCTION

In 2023, the total global steel production amounted to 1.489 billion tons, with corrosion-resistant steel accounting for around 60 million tons. Corrosion-resistant steels play a key role in industry due to their high performance characteristics and wide range of applications [1 – 3].

Between 2015 and 2019, the production of corrosion-resistant steel continuously increased. The decrease in production in 2020 was due to the coronavirus pandemic during the first half of 2020, as many countries imposed lockdowns. However, following the recovery of the global economy in 2021, global production of corrosion-resistant steel increased by 11.6 % compared to 2020, not only reaching the record levels of 52.2 million tons in 2019, but also surpassing them to reach 56.8 million tons per year [4].

Corrosion-resistant steel production in Russia steadily increased from 2015 to 2023, reaching 278.2 thousand tons per year. At the same time, the consumption of corrosion-resistant steel in Russia exceeded domestic production by almost 2.5 times. Increasing the volume of corrosion-resistant steel production in Russia is, therefore, a highly relevant issue [4].

When smelting 08Kh18N10T corrosion-resistant steel, producers face problems such as clogging of the pouring nozzle dispensers, low yield, and surface defects [5 – 8]. The oxygen content in steel, particularly in corrosion-resistant grades, is one of the key indicators of the final product's quality [9 – 11]. Dissolved oxygen in the metal reacts with deoxidizers, forming non-metallic inclusions (NMI). These NMIs compromise the integrity of the metal, adversely affecting ductility, toughness, fatigue strength, and corrosion resistance [12 – 14]. In corrosion-resistant steels, NMIs lead to the formation of defects such as “rub marks” in cold-rolled sheets, while Al_2O_3 inclusions contribute to the clogging of steel casting equipment during casting [15 – 17].

Deep surface defects in steel are caused by high levels of NMIs, such as oxides of chromium, manganese, silicon, aluminum, titanium, and titanium nitrides. In studies [11 – 12], the authors state that deep surface defects occur due to the entry of coarse slag crusts from the mold into the metal. The cause of the formation of these coarse slag-metal crusts is oxides and nitrides of titanium, which

form as a result of the interaction of dissolved oxygen and nitrogen in the metal with titanium, a common alloying element [18].

This study analyzes the smelting, ladle processing, and casting technology of 08Kh18N10T corrosion-resistant steel to identify factors negatively impacting steel quality and NMI formation.

MATERIALS AND METHODS

To identify the causes of contamination of 08Kh18N10T corrosion-resistant steel by various NMIs, an analysis was performed using data from industrial heats' passports and production records, and samples of metal were taken throughout the entire ladle processing chain for examination. The monitoring of changes in the content of the main types of oxide NMIs in metal samples selected at all stages of ladle processing, casting, and from continuously cast billets (CCB) was carried out using the method of fractional gas analysis (FGA). The study was conducted using a LECO TC600 gas analyzer with the original OxSeP Pro software. Fractional gas analysis is a modification of the method of reduction melting of the test sample in a graphite crucible in a stream of carrier gas at a specified linear heating rate [19 – 21].

To determine the morphology and chemical composition of the main types of NMIs found in the collected metal samples, a Jeol JXA-iSP100 EPMA scanning electron microscope with X-ray microanalysis was used, equipped with energy- and wavelength-dispersive spectrometers.

RESULTS AND DISCUSSION

During the study, metal samples taken throughout the entire production process were analyzed for two heats of 08Kh18N10T corrosion-resistant steel:

- heat 1: before the changes to the steel production technological parameters;
- heat 2: after the corrective actions were implemented.

Fig. 1 shows the results of determining the total oxygen and nitrogen content (right ordinate axis) as well as the oxygen content in various types of oxide NMIs (left ordinate axis) in the collected metal samples.

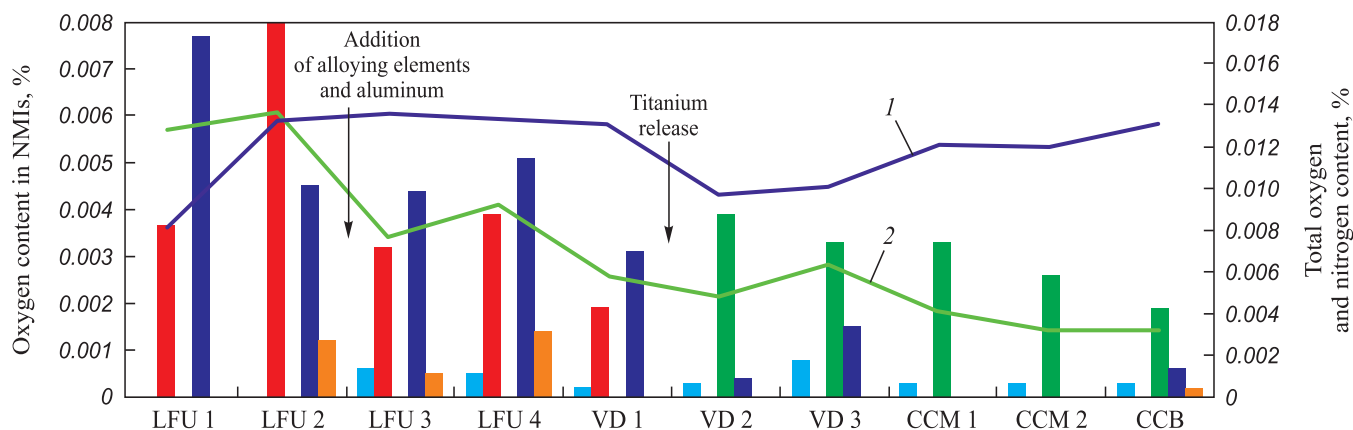


Fig. 1. FGA results of the metal samples of heat 1:

■ – chromium oxides; ■ – silicates; ■ – titanium oxides; ■ – aluminates; ■ – spinels; 1 – total N; 2 – total O

Рис. 1. Результаты ФГА проб металла плавки 1:

■ – оксиды хрома; ■ – силикаты; ■ – оксиды титана; ■ – алюминаты; ■ – шпинели; 1 – общий N; 2 – общий O

During the casting process of heat 1, clogging of the pouring nozzles was observed. The FGA analysis of samples taken from the buildup on the pouring nozzle (Fig. 2) revealed high levels of total oxygen and nitrogen, as well as calcium aluminosilicates, spinels, and titanium oxides modified with calcium and magnesium.

At the technological stage of ladle-furnace unit (LFU) 4 – vacuum degasser (VD) 2 of heat 1, a decrease in the total oxygen and nitrogen content in the melt and an increase in the titanium oxide content were observed. In sample VD 3 of heat 1, chromium oxides, titanium oxides, and aluminates were detected.

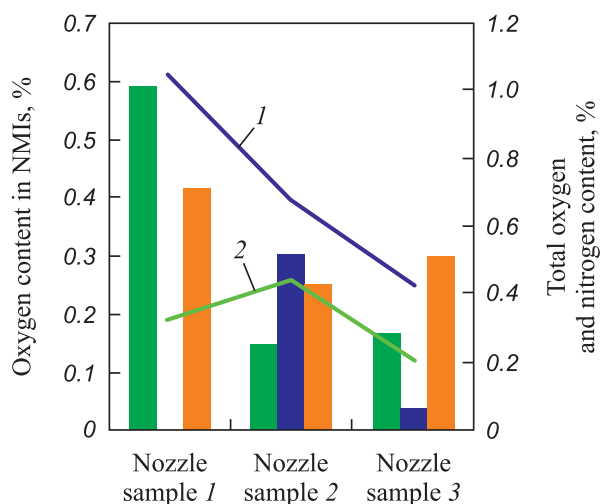


Fig. 2. FGA results of metal samples taken from the clogging in pouring nozzle:

■ – titanium oxides; ■ – aluminates; ■ – spinels; 1 – total O; 2 – total N

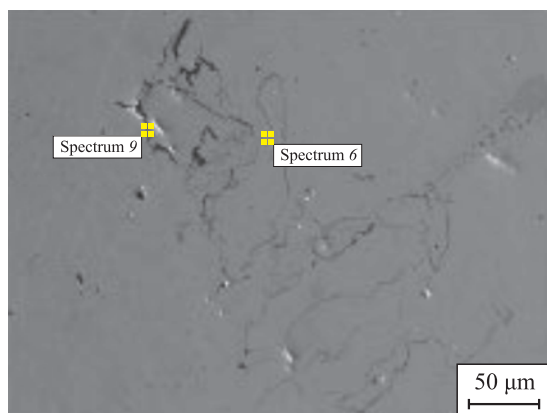
Рис. 2. Результаты ФГА образцов проб металла, отобранных от нароста в сталеразливочном стакане: ■ – оксиды титана; ■ – алюминаты; ■ – шпинели; 1 – общий O; 2 – общий N

In metal samples taken from the tundish of the continuous casting machine (CCM) 1 for heat 1, titanium oxides were mainly detected. It should be noted that the nitrogen content in the sample taken from the continuous casting unit (CCU) 1 for heat 1 increased by 20 ppm compared to the nitrogen content in the metal sample taken from the vacuum degasser (sample VD 3 of heat 1). At the same time, the total oxygen content decreased from 60 ppm (sample VD 3 of heat 1) to 30 – 40 ppm (sample CCU 1 of heat 1). The increase in nitrogen content in sample CCU 1 can be explained by the influence of secondary oxidation of the metal during casting. During secondary oxidation, the melt interacts with atmospheric air. The solubility limit of oxygen in aluminum-deoxidized steel does not exceed 0.0005 %, with the remaining oxygen present in oxide inclusions, which are partially removed into the slag during casting. The solubility limit of nitrogen in the molten metal at this temperature is determined by the concentration of alloying elements and is significantly higher than its actual concentration. This leads to an increase in the dissolved and total nitrogen content in the molten metal during secondary oxidation.

The results of the metal sample studies under an electron microscope confirm the results of the FGA. At the casting stage, oxide films larger than 400 μm were detected in metal samples from heat 1 (Fig. 3).

Fig. 4 shows the results of metallographic studies of the chemical composition of samples taken from the clogging in the inner surface of the pouring nozzle. The study revealed:

- a high content of titanium oxides modified with calcium;
- the presence of conglomerates of calcium, silicon, aluminum, and titanium oxides;



Name	Chemical composition, %					
	O	Al	Si	Ca	Ti	Cr
Spectrum 6	44.88	3.52	9.10	1.33	34.70	6.47
Spectrum 9	37.78	0.59	–	–	52.59	9.04
Average	41.33	2.05	9.10	1.33	43.64	7.76
Standard deviation	3.55	1.46	–	–	8.95	1.28

Fig. 3. Complex oxide NMI in selected metal samples

Рис. 3. Комплексное оксидное НВ в отобранных пробах металла

- particles of undissolved ferrochrome and titanium nitrides;
- chromium oxides modified with titanium, silicon, and aluminum;
- calcium aluminosilicates, spinels, and titanium oxides modified with calcium and magnesium.

It is likely that film conglomerates of NMIs, such as titanium oxides, titanium oxides with calcium and aluminum, as well as titanium nitrides, precipitating from the melt onto the walls of the pouring nozzle, formed a framework on which metal buildup accumulated, thus hindering the casting process. The high contamination of the metal with titanium oxides and nitrides indicates that the deoxidation technology currently used at the plant is not optimal. The significant increase in nitrogen content in the melt during casting, the presence of oxide films

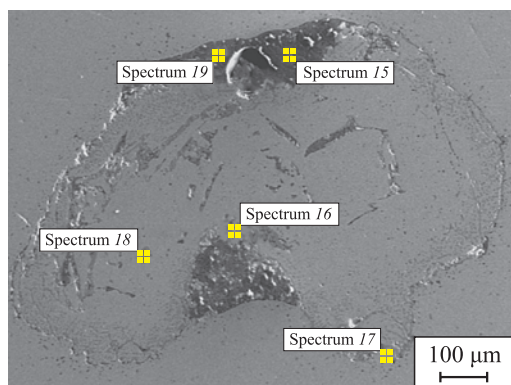
and stringer inclusions of titanium oxides in the melt, and the large amount of titanium nitrides in the finished metal may suggest the influence of secondary oxidation processes during casting.

During the study, recommendations were made to adjust the ladle processing technology, specifically: transferring the nickel alloying operation from the LFU to the EAF, introducing a refining fluid slag, and performing soft inert gas blowing of the melt for at least 15 min after the addition of SiCa. The plant conducted experimental heat 2, incorporating the provided recommendations. Metal samples were selected during the experimental heat. The results of determining the total oxygen and nitrogen content and the oxygen contained in various types of oxide NMIs in metal samples taken throughout the entire steel production process are shown in Fig. 5.

According to Fig. 5, it can be seen that in sample VD 1 of heat 2, the primary type of NMI was aluminates. In sample VD 2, after the addition of titanium powder wire and silicon-calcium, a decrease in the aluminate content was observed, while the content of chromium, manganese, titanium oxides, and silicates increased. In samples VD 3 and CCM, there was an increase in the total oxygen and nitrogen content, which may indicate the occurrence of secondary oxidation of the metal. In samples from continuously cast billets (CCB), the primary type of NMIs were titanium oxides, with small amounts of aluminates, silicates, and spinels also present.

The analysis of the selected samples under an electron microscope confirmed the FGA results for the main groups of oxide NMIs. One of the results of element mapping of NMIs in the metal sample using micro-X-ray spectral analysis is shown in Fig. 6.

Transferring the nickel alloying operation from the LFU to the EAF allowed the ladle processing time to be reduced by approximately one hour. The reduction in metal processing time in the LFU led to a decrease in the operating time of the electric arcs, which are a significant source of nitrogen entry into the metal melt. This



Name	Chemical composition, %							
	O	Al	Si	Ca	Ti	Cr	Mn	Bcero
Spectrum 15	45.82	2.02	25.63	0.74	7.53	18.26	–	100,00
Spectrum 16	43.20	1.32	5.32	0.41	2.86	46.12	–	100,00
Spectrum 17	38.94	0.52	0.79	–	4.65	54.79	–	100,00
Spectrum 18	34.89	0.42	–	–	6.83	38.97	18.89	100,00
Spectrum 19	48.32	1.54	19.11	5.34	6.79	18.12	–	100,00
Average	42.24	1.16	12.71	2.16	5.73	35.25	18.89	–
Standard deviation	4.81	0.61	10.06	2.25	1.73	18.80	–	–

Fig. 4. Complex NMI in metal samples taken from the clogging on pouring nozzle surface

Рис. 4. Комплексное оксидное НВ в отобранных пробах металла от нароста на поверхности разливочного стакана

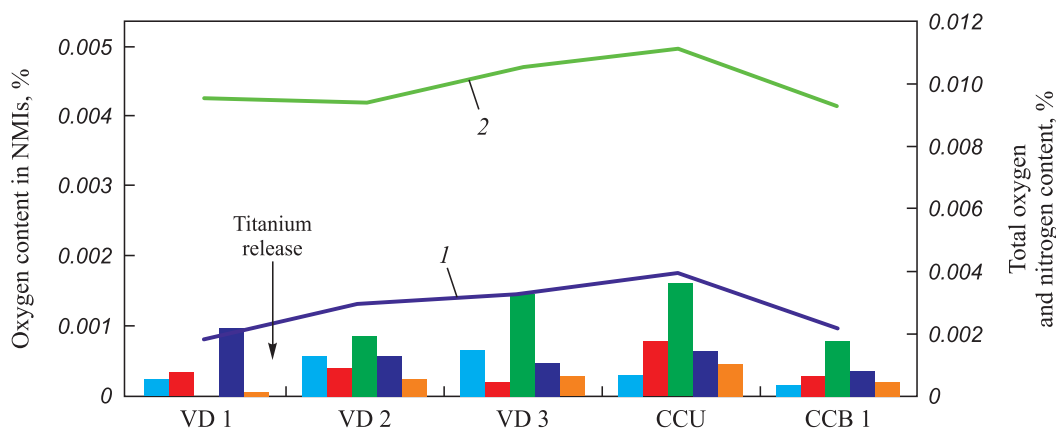


Fig. 5. FGA results of the metal samples of heat 2:

■ – chromium and manganese oxides; ■ – silicates + manganese; ■ – titanium oxides; ■ – aluminates; ■ – spinels; 1 – total O; 2 – total N

Рис. 5. Результаты ФГА проб металла плавки 2:

■ – оксиды хрома и марганца; ■ – силикаты + марганец; ■ – оксиды титана; ■ – алюминаты; ■ – шпинели; 1 – общий O; 2 – общий N

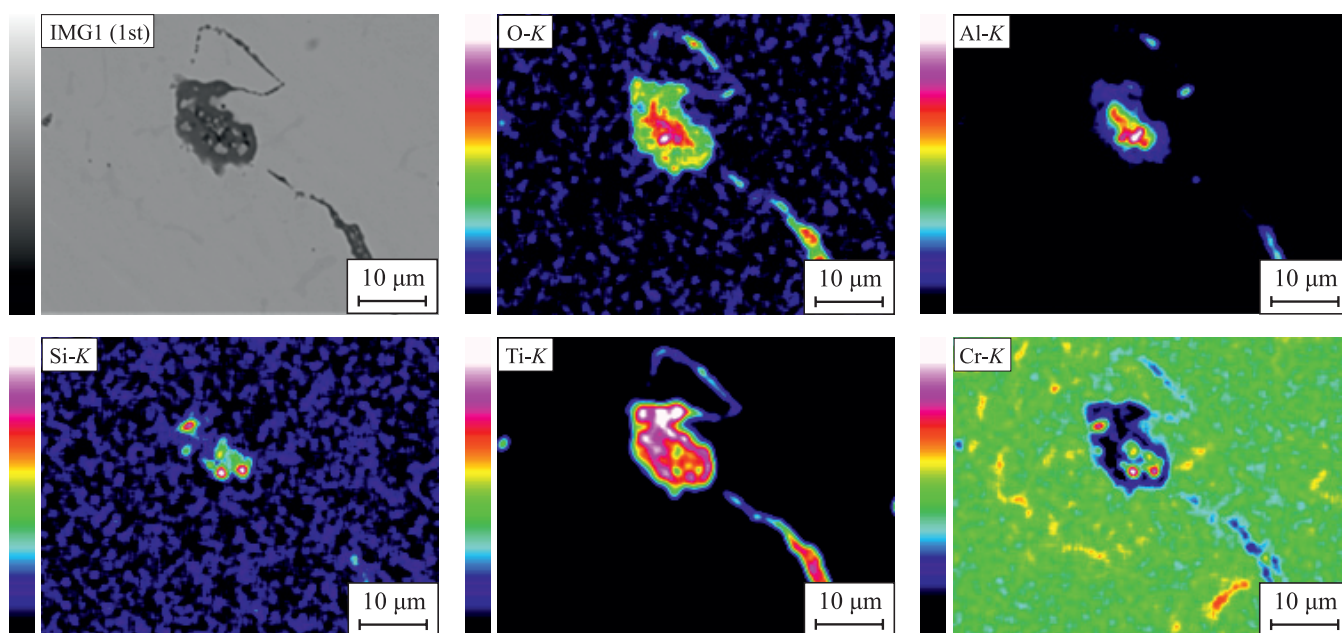


Fig. 6. Complex oxide NMI in selected metal sample

Рис. 6. Комплексное оксидное НВ в металле

also reduced the wear of the lining and minimized contamination of the melt by the products of lining degradation. Based on the results of electron microscope studies, it was determined that the introduction of fluid refining slag led to the removal of NMIs and a reduction in their size – the inclusions became smaller (heat 2). No clogging of the pouring nozzles was observed in the experimental heat after the corrective actions were implemented.

CONCLUSIONS

An analysis of the production technology of 08Kh18N10T corrosion-resistant steel was performed to determine the causes of NMI formation that affect

the pourability and quality of the metal. During the study, the total oxygen and nitrogen content, as well as the oxygen contained in various types of oxide NMIs at the stages of ladle processing and casting, were determined. The results of the electron microscope analysis confirmed the FGA findings, specifically the predominance of NMIs that are detrimental to corrosion-resistant steels: titanium oxides and nitrides, as well as aluminates. It was shown that after the addition of titanium wire, the total nitrogen content decreased due to the formation of titanium nitrides, which were subsequently removed into the slag. At the same time, an increase in titanium oxide content was observed. It was demonstrated that the cause of clogging of the casting equipment is the formation of complex

NMIs based on titanium oxide, which “stick” to the surface of the pouring nozzle during steel casting.

Recommendations were made to adjust the ladle processing technology. Based on the results of electron microscope studies, it was determined that the induction of fluid refining slag contributed to the assimilation of NMIs and their size reduction (heat 2). After the implementation of corrective measures, no clogging of the casting equipment was observed.

REFERENCES / СПИСОК ЛИТЕРАТУРЫ

- Beddoes J., Parr J.G. Introduction to Stainless Steels. 3rd ed. Materials Park, OH, USA: ASM International; 1999:315.
- Novak C.J., Peckner D., Bernstein I.M. Handbook of Stainless Steels. New York: McGraw-Hill; 1977:1120.
- Lakshmi A.A., Rao Ch.S., Gangadhar J., Srinivasu Ch., Singh S.K. Review of processing maps and development of qualitative processing maps. *Materials Today: Proceedings*. 2017;4(2):946–956. <https://doi.org/10.1016/j.matpr.2017.01.106>
- Volkova A.V. Market of Stainless Steel Products – 2021. HSE University; 2021:76. (In Russ.).
Волкова А.В. Рынок нержавеющей металлопродукции – 2021. Высшая школа экономики; 2021:76.
- Tokovoy O.K., Shaburov D.V. Study of “cake” defect in continuously cast austenitic stainless steel 18Cr-10Ni-1Ti. Report 1. *Izvestiya. Ferrous Metallurgy*. 2013;56(7):19–22. (In Russ.). <https://doi.org/10.17073/0368-0797-2013-7-19-22>
Токовой О.К., Шабуров Д.В. Исследование дефекта «корж» в непрерывнолитой нержавеющей аустенитной стали X18H10T. Сообщение 1. *Известия вузов. Черная металлургия*. 2013;56(7):19–22. <https://doi.org/10.17073/0368-0797-2013-7-19-22>
- Surgaeva E.V., Elanskii G.N., Galkin M.P., Yachmeneva N.A. Investigation of slag-metal crust formed in the mold during continuous casting of 08Kh17T steel. *Elektrometallurgiya*. 2002;(5):22–25. (In Russ.).
Сургаева Е.В., Еланский Г.Н., Галкин М.П., Ячменева Н.А. Исследование шлакометаллической корочки, образующейся в кристаллизаторе при непрерывной разливке стали 08X17T. *Электrometallurgiya*. 2002;(5):22–25.
- Surgaeva E.V., Galkin M.P., Elanskii G.N. The work of slag-forming mixture in CCM mold during casting of corrosion-resistant titanium-containing steels. In: *Transactions of the 7th Congress of Steelmakers*. 2002:524–529. (In Russ.).
Сургаева Е.В., Галкин М.П., Еланский Г.Н. Работа шлакообразующей смеси в кристаллизаторе при разливке на УНРС коррозионностойких титаносодержащих сталей. *Труды седьмого конгресса сталеплавателей*. 2002:524–529.
- Elanskii G.N., Paderin S.N., Surgaeva E.V. The causes of captivity and slag-metal crusts during casting of titanium-containing corrosion-resistant steels. *Stal’*. 2005;(9):17–19. (In Russ.).
Еланский Г.Н., Падерин С.Н., Сургаева Е.В. Причины возникновения пленок и шлакометаллических корочек при разливке титаносодержащих коррозионностойких сталей. *Сталь*. 2005;(9):17–19.
- Sowa L., Bokota A. Numerical model of thermal and flow phenomena the process growing of the CC slab. *Archives of Metallurgy and Materials*. 2011;56(2):359–366. <https://doi.org/10.2478/v10172-011-0038-4>
- Wegrzyn T., Miroslawski J., Silva A.P., Pinto D.G., Miros M. Oxide inclusions in steel welds of car body. *Materials Science Forum*. 2010;636–637:585–591. <https://doi.org/10.4028/www.scientific.net/MSF.636-637.585>
- Hashimoto K., Fujimatsu T., Tsunekage N., Hiraoka K., Kida K., Costa Santos E. Study of rolling contact fatigue of bearing steels in relation to various oxide inclusions. *Materials & Design*. 2011;32(3):1605–1611. <https://doi.org/10.1016/j.matdes.2010.08.052>
- Zhang L., Thomas B.G. State of the art in the control of inclusions during steel ingot casting. *Metallurgical and Materials Transactions B*. 2006;37(5):733–761. <https://doi.org/10.1007/s11663-006-0057-0>
- Zhang L. Indirect methods of detecting and evaluating inclusions in steel – A review. *Journal of Iron and Steel Research International*. 2006;13(4):1–8. [https://doi.org/10.1016/s1006-706x\(06\)60067-8](https://doi.org/10.1016/s1006-706x(06)60067-8)
- Zhang L. Nucleation, growth, transport, and entrapment of inclusions during steel casting. *JOM*. 2013;65(9):1138–1144. <https://doi.org/10.1007/s11837-013-0688-y>
- Gao Y., Sorimachi K. Formation of clogging materials in an immersed nozzle during continuous casting of titanium stabilized stainless steel. *ISIJ International*. 1993;33(2):291–297. <https://doi.org/10.2355/isijinternational.33.291>
- Sasai K., Mizukami Y. Mechanism of alumina adhesion to continuous caster nozzle with reoxidation of molten steel. *ISIJ International*. 2001;41(11):1331–1339. <https://doi.org/10.2355/isijinternational.41.1331>
- Long M., Zhang L., Zuo X., Chen D. Kinetic modeling on nozzle clogging during steel billet continuous casting. *ISIJ International*. 2010;50(5):712–720. <https://doi.org/10.2355/isijinternational.50.712>
- Lozovskii E.P., Ushakov S.N., Yurechko D.V. Causes of formation of a “captivity” defect due to non-metallic inclusions in slabs on rolled products. *Stal’*. 2009;(10):26–28. (In Russ.).
Лозовский Е.П., Ушаков С.Н., Юречко Д.В. Изучение причин образования дефекта «плена» из-за неметаллических включений в слябах на прокате. *Сталь*. 2009;(10):26–28.
- Grigorovich K.V., Krasovskii P.V., Isakov S.A., Gorokhov A.A., Krylov A.S. Processing and interpretation of the results of fractional gas analysis. *Zavodskaya laboratoriya. Diagnostika materialov*. 2002;68(9):3–9. (In Russ.).
Григорович К.В., Красовский П.В., Исаков С.А., Горюхов А.А., Крылов А.С. Обработка и интерпретация результатов фракционного газового анализа. *Заводская лаборатория. Диагностика материалов*. 2002;68(9):3–9.
- Grigorovich K., Komolova O., Terebikina D. Analysis and optimization of ladle treatment technology of steels processing. *Journal of Chemical Technology and Metallurgy*. 2015;50(6):574–580.
- Shibaev S.S., Krasovskii P.V., Grigorovich K.V. Determination of oxygen concentrations in stainless steels by the method of reducing melting. *Zavodskaya laboratoriya. Diagnostika materialov*. 2006;72(6):10–16. (In Russ.).
Шибяев С.С., Красовский П.В., Григорович К.В. Определение форм нахождения кислорода в нержавеющей сталях методом восстановительного плавления. *Заводская лаборатория. Диагностика материалов*. 2006;72(6):10–16.

Information about the Authors

Сведения об авторах

Anton Yu. Em, Junior Researcher of the Laboratory of Materials Diagnostics, Baikov Institute of Metallurgy and Materials Science, Russian Academy of Sciences

ORCID: 0000-0002-9743-5996

E-mail: tony.yem1994@gmail.com

Ol'ga A. Komolova, Cand. Sci. (Eng.), Senior Researcher of the Laboratory of Materials Diagnostics, Baikov Institute of Metallurgy and Materials Science, Russian Academy of Sciences; *Assist. Prof. of the Chair of Metallurgy of Steel, New Production Technologies and Metal Protection*, National University of Science and Technology "MISIS"

ORCID: 0000-0001-9517-8263

E-mail: o.a.komolova@gmail.com

Konstantin V. Grigorovich, Academician, Dr. Sci. (Eng.), Head of the Laboratory of Materials Diagnostics, Baikov Institute of Metallurgy and Materials Science, Russian Academy of Sciences; *Prof. of the Chair of Metallurgy of Steel, New Production Technologies and Metal Protection*, National University of Science and Technology "MISIS"

ORCID: 0000-0002-5669-4262

E-mail: grigorov@imet.ac.ru

Sof'ya B. Rumyantseva, Cand. Sci. (Eng.), Research Associate of the Laboratory of Materials Diagnostics, Baikov Institute of Metallurgy and Materials Science, Russian Academy of Sciences

E-mail: sbvarlamova@gmail.com

Антон Юрьевич Ем, младший научный сотрудник лаборатории диагностики материалов, Институт металлургии и материаловедения им. А.А. Байкова РАН

ORCID: 0000-0002-9743-5996

E-mail: tony.yem1994@gmail.com

Ольга Александровна Комолова, к.т.н., старший научный сотрудник лаборатории диагностики материалов, Институт металлургии и материаловедения им. А.А. Байкова РАН; *доцент кафедры металлургии стали, новых производственных технологий и защиты металлов*, Национальный исследовательский технологический университет «МИСИС»

ORCID: 0000-0001-9517-8263

E-mail: o.a.komolova@gmail.com

Константин Всеволодович Григорович, академик РАН, д.т.н., *заведующий лабораторией диагностики материалов*, Институт металлургии и материаловедения им. А.А. Байкова РАН; *профессор кафедры металлургии стали, новых производственных технологий и защиты металлов*, Национальный исследовательский технологический университет «МИСИС»

ORCID: 0000-0002-5669-4262

E-mail: grigorov@imet.ac.ru

Софья Борисовна Румянцева, к.т.н., научный сотрудник лаборатории диагностики материалов, Институт металлургии и материаловедения им. А.А. Байкова РАН

E-mail: sbvarlamova@gmail.com

Contribution of the Authors

Вклад авторов

A. Yu. Em – metal sampling, analysis of melting certificates for corrosion-resistant steel production, gas analysis.

O. A. Komolova – problem statement, thermodynamic calculations.

K. V. Grigorovich – formation of results and conclusions.

S. B. Rumyantseva – conducting a microrentgenospectral analysis.

А. Ю. Ем – отбор проб металла, анализ паспортов плавок производства коррозионностойкой стали, проведение газового анализа.

О. А. Комолова – постановка задачи, проведение термодинамических расчетов.

К. В. Григорович – формирование результатов и выводов.

С. Б. Румянцева – проведение микрорентгеноспектрального анализа.

Received 17.07.2024

Revised 22.08.2024

Accepted 26.08.2024

Поступила в редакцию 17.07.2024

После доработки 22.08.2024

Принята к публикации 26.08.2024



UDC 539.213.27:539.24:620.186.4

DOI 10.17073/0368-0797-2024-5-556-562



Original article

Оригинальная статья

DEFORMATION AND FRACTURE OF HEAT TREATED RIBBON OF AMORPHOUS Co – Fe – Cr – Si – B ALLOY DURING INDENTATION

I. E. Permyakova , M. V. Kostina

Baikov Institute of Metallurgy and Materials Science, Russian Academy of Sciences (49 Leninskii Ave., Moscow 119334, Russian Federation)

inga_perm@mail.ru

Abstract. Indentation is an attractive method for studying the deformation behavior of amorphous alloys for a number of reasons: not being specific to the sample size, these tests are easy to perform and do not lead to macrofracture; plastic deformation in the material is locally limited, which facilitates the study of plastic flow in the zones surrounding and located under the indenter; direct comparison of indentation results with responses, for example, to bending or tension further makes the indentation method an effective “probe” for understanding the physics of plastic deformation and fracture of amorphous alloys. The morphology of microprints of melt-quenched ribbon of $\text{Co}_{70.5}\text{Fe}_{0.5}\text{Cr}_4\text{Si}_7\text{B}_{18}$ amorphous alloys subjected to heat treatment in a wide range of temperatures was studied after indentation on an elastic substrate. Structural-phase transformations were controlled by X-ray structural analysis and differential scanning calorimetry. We discovered characteristic modifications in the patterns of their deformation and fracture during the transition from amorphous to crystalline state. Three temperature ranges with characteristic deformation zones on the surface of the studied samples were established. At $T_{\text{room}} < T_f$, amorphous alloy demonstrates unique plasticity. The shear bands appear around the imprint only at the maximum load on the indenter. $T_f \leq T_{\text{an}} \leq T_{\text{sb}}$ is a transitional interval, since cracks do not form at lower temperatures, and there are no shear bands at higher temperatures. The alloy is in an amorphous but brittle state, so radial and ring cracks, as well as spalls, are observed. The interval $T_{\text{sb}} < T_{\text{an}} \leq T_{\text{cryst}}$ corresponds to the final transformation of the alloy into a crystalline state; symmetrical patterns of fracture are formed, consisting of square crack networks. It is possible to give an approximate express assessment of the structural state of amorphous alloys based on an “atlas” of local loading zones (presence/absence of shear bands, cracks, their relative position) compiled taking into account the corresponding temperature intervals under different loads.

Keywords: amorphous alloy, crack, shear band, indentation, imprint, structural state, embrittlement, deformation, fracture, heat treatment

For citation: Permyakova I.E., Kostina M.V. Deformation and fracture of heat treated ribbon of amorphous Co–Fe–Cr–Si–B alloy during indentation. *Izvestiya. Ferrous Metallurgy*. 2024;67(5):556–562. <https://doi.org/10.17073/0368-0797-2024-5-556-562>

ДЕФОРМАЦИЯ И РАЗРУШЕНИЕ ТЕРМИЧЕСКИ ОБРАБОТАННЫХ ЛЕНТ АМОРФНОГО СПЛАВА СИСТЕМЫ Co – Fe – Cr – Si – B ПРИ ИНДЕНТИРОВАНИИ

И. Е. Пермякова , М. В. Костина

Институт металлургии и материаловедения им. А.А. Байкова РАН (Россия, 119334, Москва, Ленинский пр., д. 49)

inga_perm@mail.ru

Аннотация. Индентирование является привлекательным методом для изучения деформационного поведения аморфных сплавов по ряду причин: не будучи специфичными к размеру образца, эти испытания просты в выполнении и не приводят к макроразрушению; пластическая деформация в материале ограничена локально, что облегчает изучение пластического течения в зонах окружающих и находящихся под индентором; прямое сравнение результатов индентирования с откликами, например, на изгиб или растяжение дополнительно делает метод индентирования эффективным «зондом» для понимания физики пластической деформации и разрушения аморфных сплавов. В настоящей работе представлены результаты исследований морфологии микроотпечатков после индентирования на эластичной подложке лент быстрозакаленных аморфных сплавов $\text{Co}_{70.5}\text{Fe}_{0.5}\text{Cr}_4\text{Si}_7\text{B}_{18}$, подвергнутых термической обработке в широком диапазоне температур. Структурно-фазовые превращения контролировались проведением рентгеноструктурного анализа и дифференциально-сканирующей калориметрией. Обнаружены характерные видоизменения картин их деформации и разрушения при переходе из аморфного в кристаллическое состояние. Установлены три температурных интервала с характерными зонами деформирования на поверхности исследуемых образцов. При $T_{\text{комн}} < T_f$ аморфный сплав демонстрирует уникальную пластичность, при максимальной нагрузке на индентор появляются только полосы сдвига вокруг отпечатка. Интервал $T_f \leq T_{\text{ан}} \leq T_{\text{сб}}$ – переходный, так как при более низких температурах не образуются трещины, а при более высоких нет полос сдвига. Сплав находится в аморфном, но охрупченном состоянии, поэтому наблюдаются ради-

альные и кольцевые трещины, а также отколы. Интервал $T_{sb} < T_{an} \leq T_{cryst}$ соответствует окончательной трансформации сплава в кристаллическое состояние, формируются симметричные картины разрушения, состоящие из квадратных сеток трещин. Таким образом, на основании составленного с учетом соответствующих температурных интервалов «атласа» зон локального нагружения (наличие/отсутствие полос сдвига, трещин, их взаимное расположение) при разных нагрузках возможно дать приближенную экспресс-оценку структурного состояния аморфных сплавов.

Ключевые слова: аморфный сплав, трещина, полоса сдвига, индентирование, отпечаток, структурное состояние, охрупчивание, деформация, разрушение, термическая обработка

Для цитирования: Пермякова И.Е., Костина М.В. Деформация и разрушение термически обработанных лент аморфного сплава системы Co – Fe – Cr – Si – B при индентировании. *Известия вузов. Черная металлургия.* 2024;67(5):556–562.
<https://doi.org/10.17073/0368-0797-2024-5-556-562>

INTRODUCTION

The process of amorphization, achieved by ultrapid melt-quenching, allows for the production of homogeneous multicomponent amorphous alloys (AA). By varying the conditions of melt-quenching, it is possible to significantly expand the range of mutual solubility of elements, enabling a broader variation of AA properties compared to crystalline materials [1 – 4]. If heat treatment is also applied, a wide range of intermediate states can be obtained – from “purely” amorphous to amorphous-nanocrystalline and fully crystalline – enabling the creation of unique and diverse amorphous systems (metastable forms of binary, ternary, and multicomponent alloys) [5 – 7]. By adjusting the composition and applying controlled heating, it is possible to achieve useful and predefined physical properties, expanding the application of AA in engineering and industry as structural and functional materials [8 – 11]. The excellent magnetic properties of AA are complemented by other valuable characteristics such as high strength, hardness, electrical resistivity, corrosion resistance, and satisfactory plasticity. However, when applied in practice, issues such as thermal stability, embrittlement, and spontaneous crystallization at elevated temperatures are of particular concern [12 – 14]. To evaluate the structural-phase state of AA, a comprehensive set of research methods is used (e.g., transmission electron microscopy (TEM), X-ray structural analysis, differential thermal analysis, etc.). Some of these methods require multi-stage sample preparation and involve lengthy and labor-intensive phase identification processes. Moreover, when AA has been processed at temperatures below crystallization and remains in an amorphous state, there are significant challenges in studying the amorphous structure. Even high-resolution TEM and EXAFS-spectroscopy (Extended X-Ray Absorption Fine Structure) cannot definitively provide information about atomic arrangements and positional changes during relaxation. Studying structure-sensitive property responses (mechanical, electrical, chemical, magnetic) allows the analysis of structural relaxation processes [15 – 17].

Currently, the micro- and nanoindentation is an informative method for investigating the mechanical charac-

teristics of melt-quenched amorphous alloys (hardness, Young’s modulus, fracture toughness) [18 – 22]. This method is also valuable for understanding the micro-mechanisms of their deformation, as it allows for the visualization of the deformation pattern and the assessment of the extent and shape of deformation zones in correlation with the structural state of the amorphous alloys. Indentation testing is an excellent tool for such studies, especially when only a small amount of material is required. Deformation during indentation is essentially stable, at least macroscopically, since the contact area between the indenter and the deformed material increases during indentation to accommodate any applied load. However, local loading of amorphous alloys has several specific features related to their unique geometry – small thickness of amorphous alloys ribbons and the qualitative difference between the contact side (adjacent to the quenching drum during production) and the free side of the ribbon [23]. Moreover, plastic flow in amorphous alloys under high stresses and low temperatures occurs non-uniformly, localizing in shear bands along planes of maximum shear [24; 25]. The formation of these shear bands is associated with localized atomic rearrangements correlated with regions of excess free volume [26 – 28]. Shear bands are crucial for the deformation behavior of amorphous alloys, and controlling them is equivalent to managing the plasticity and fracture of the material.

The aim of this work is to study the mechanical behavior of heat-treated thin melt-quenched amorphous alloy ribbons during microindentation, specifically to reveal the patterns of deformation zone modification and surface microfracture of amorphous alloys around the imprints formed by the Vickers pyramid, as the annealing temperature increases.

MATERIALS AND METHODS

The object of the study was an amorphous alloy $\text{Co}_{70.5}\text{Fe}_{0.5}\text{Cr}_4\text{Si}_7\text{B}_{18}$ (at. %), produced by melt-spinning process in the form of a ribbon with a thickness of 30 μm and a width of 20 mm. Alloy samples measuring 15×20 mm were subjected to vacuum annealing in the temperature range of $T_{an} = 538 – 823$ K for 10 min. Afterward, they

were fixed using an elastic substrate – “Moment” glue (20.52.10.190 ОКПД 2 / GOST 22345-77) with a thickness of approximately 1.0 – 1.5 mm on a steel plate. As a result, a composite blank was formed (Fig. 1, a).

Indentation was performed on the free side of the amorphous alloy ribbons across a wide range of loads (0.3 – 2.0 N) using a PMT-3M microhardness tester (LOMO). It is important to note that local loading on a hard substrate (for example, putty) presents a fundamentally unavoidable difficulty: cracks may initially form in the substrate and subsequently initiate the failure of the coating, i.e., the amorphous alloy.

The macroscopic plasticity behavior of the amorphous alloys was assessed by the *U*-method (by bending deformation). For this, the sample was placed between two flat parallel plates, and as the plates moved closer together at a constant speed, the distance *d* at which the bent sample fractured was determined (Fig. 1, b). The plasticity measure ε_f was taken as the ratio

$$\varepsilon_f = \frac{h}{d - h},$$

where *h* is the thickness of the ribbon.

The ductile-to-brittle transition temperature T_f was calculated as the average temperature between T_1 and T_2 , where T_1 – is the highest annealing temperature at which $\varepsilon_f = 1$, and T_2 is the lowest recorded temperature at which a sharp decrease in plasticity occurs ($\varepsilon_f \rightarrow 0$).

The crystallization temperature was assessed using differential scanning calorimetry on a DSC 8271 analyzer (Rigaku). The transition from the amorphous to crystal-

line state during heat treatment was monitored through X-ray structural analysis using the ULTIMA IV multifunctional diffractometer (Rigaku).

RESULTS AND DISCUSSION

The experiment revealed that during the indentation of the $\text{Co}_{70.5}\text{Fe}_{0.5}\text{Cr}_4\text{Si}_7\text{B}_{18}$, amorphous alloys, as they transition from the amorphous to the crystalline state during annealing, there is a significant evolution in the micro-patterns of their deformation and fracture. Fig. 2 illustrates the variety of morphological modifications on the surface of the amorphous alloy following indentation with different loads.

As the alloy is heated, distinct patterns in the formation of deformation zones become apparent. In the temperature range $T_{\text{room}} < 613$ K, typical indenter imprints are observed at low loads, while at higher loads, the imprint is surrounded by shear bands (Fig. 2, a, b). Shear bands represent a phenomenon of plastic instability, where large shear deformations are localized within a relatively narrow band during material deformation. In the temperature range of $613 \text{ K} \leq T_{\text{an}} \leq 748$ K, straight radial cracks appear in the area of local loading on the amorphous alloy (Fig. 2, c). Some of these cracks may intersect with ring cracks (Fig. 2, d). Despite the embrittlement, plastic deformation of the amorphous alloy remains possible (with occasional shear bands) up to $T_{\text{an}} = 748$ K. Finally, in the heating range of $748 \text{ K} < T_{\text{an}} \leq 803$ K, the imprints predominantly form a network of cracks oriented parallel to the faces of the indenter pyramid (Fig. 2, e). Additionally, ring cracks may form further away from the indentation zone (Fig. 2, f).

After indentation at the maximum load of $P = 2$ N, the annealing temperature T_{cr} , at which the first cracks formed and propagated in the amorphous alloy samples with a probability of no less than 0.5, was determined to be $T_{\text{cr}} = 628$ K [29]. The T_{cr} established on the elastic substrate effectively represents the ductile-to-brittle transition temperature of the amorphous alloy, closely matching the independent test data from *U*-bend testing of amorphous ribbons: $T_f = 613$ K (Fig. 3).

Subsequent attention was focused on calorimetric and structural studies to clarify the temperature ranges of phase transitions that the AA $\text{Co}_{70.5}\text{Fe}_{0.5}\text{Cr}_4\text{Si}_7\text{B}_{18}$ amorphous alloy undergoes. According to DSC data, the crystallization temperature of the studied amorphous alloy is $T_{\text{crys}} = 803$ K (Fig. 4).

According to structural studies, the formation of the first nanocrystals in the amorphous matrix, corresponding to α -Co with an HCP lattice ($a = b = 2.514$ Å, $c = 4.105$ Å), occurs after annealing above 688 K [30]. As the temperature increases, an intensification of crystallization processes and an increase in the volumetric frac-

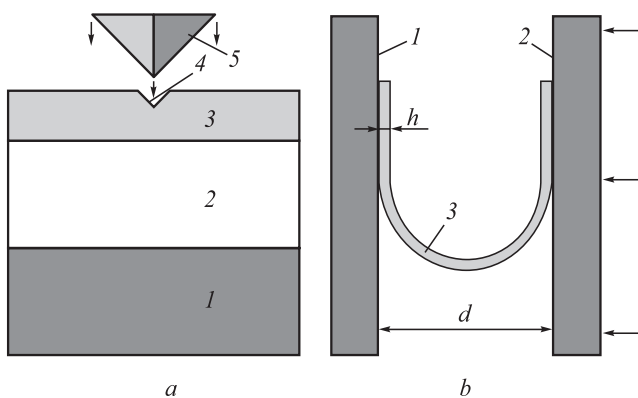


Fig. 1. Scheme of mechanical tests of ribbon of amorphous alloys: a – microindentation (1 – steel base, 2 – substrate, 3 – sample of amorphous alloy, 4 – imprint, 5 – Vickers pyramid); b – *U*-method (1 and 2 – fixed and movable plates, 3 – sample of amorphous alloy)

Рис. 1. Схема механических испытаний лент АС:

a – микроиндентирование (1 – стальная основа, 2 – подложка, 3 – образец АС, 4 – отпечаток, 5 – пирамида Виккерса); b – *U*-метод (1 и 2 – неподвижная и подвижная пластины, 3 – образец АС)

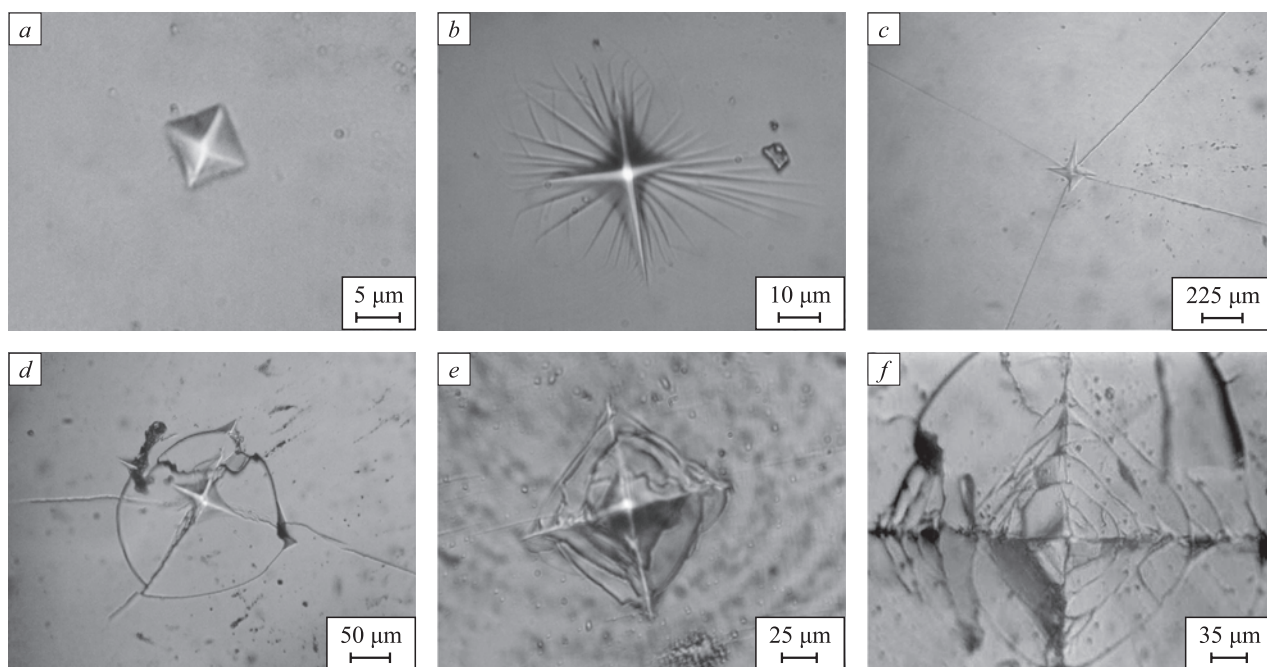


Fig. 2. Atlas of deformation and fracture patterns of annealed $\text{Co}_{70.5}\text{Fe}_{0.5}\text{Cr}_4\text{Si}_7\text{B}_{18}$ amorphous alloy during indentation on an elastic substrate: $a - T_{an} = 573 \text{ K}, P = 0.5 \text{ H}$; $b - T_{an} = 573 \text{ K}, P = 1.5 \text{ H}$; $c - T_{an} = 673 \text{ K}, P = 1.2 \text{ H}$; $d - T_{an} = 728 \text{ K}, P = 1.0 \text{ H}$; $e - T_{an} = 773 \text{ K}, P = 1.1 \text{ H}$; $f - T_{an} = 800 \text{ K}, P = 1.3 \text{ H}$

Рис. 2. Атлас картин деформации и разрушения отожженных АС $\text{Co}_{70.5}\text{Fe}_{0.5}\text{Cr}_4\text{Si}_7\text{B}_{18}$ при индентировании на эластичной подложке: $a - T_{an} = 573 \text{ K}, P = 0,5 \text{ H}$; $b - T_{an} = 573 \text{ K}, P = 1,5 \text{ H}$; $c - T_{an} = 673 \text{ K}, P = 1,2 \text{ H}$; $d - T_{an} = 728 \text{ K}, P = 1,0 \text{ H}$; $e - T_{an} = 773 \text{ K}, P = 1,1 \text{ H}$; $f - T_{an} = 800 \text{ K}, P = 1,3 \text{ H}$

tion of crystalline phases are observed. Along with $\alpha\text{-Co}$, the $\beta\text{-Co}$ phase with an FCC lattice ($a = b = c = 3.554 \text{ \AA}$), appears, as well as Co_2Si , Co_4B , Co_3B , Co_2B (Fig. 5).

By comparing the morphological atlas of the surface of the annealed Co-Fe-Cr-Si-B amorphous alloy after indentation (Fig. 2) with the results of its structural changes (Figs. 4, 5), three temperature ranges can be distinguished. The transition from one range to another

results in changes in the characteristic deformation and fracture patterns, which are a consequence of ongoing structural relaxation processes and subsequent crystallization [31].

- At $T_{\text{room}} < T_f$, the amorphous alloy demonstrates its unique plasticity, where even the maximum load on the indenter can only cause highly localized plastic deformation in the form of shear bands around the imprint.

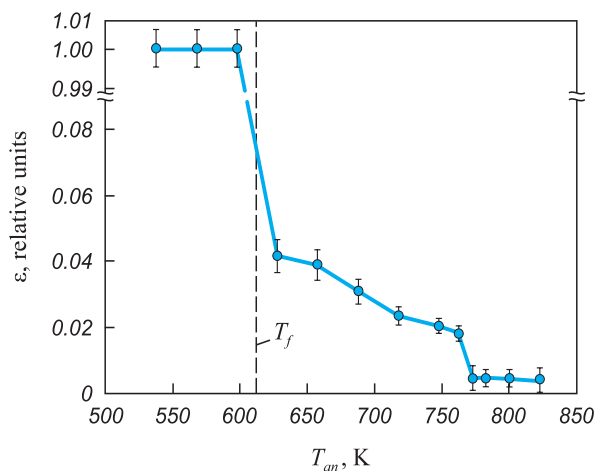


Fig. 3. Plasticity behavior of $\text{Co}_{70.5}\text{Fe}_{0.5}\text{Cr}_4\text{Si}_7\text{B}_{18}$ amorphous alloy during heat treatment

Рис. 3. Поведение пластичности АС $\text{Co}_{70.5}\text{Fe}_{0.5}\text{Cr}_4\text{Si}_7\text{B}_{18}$ при термической обработке

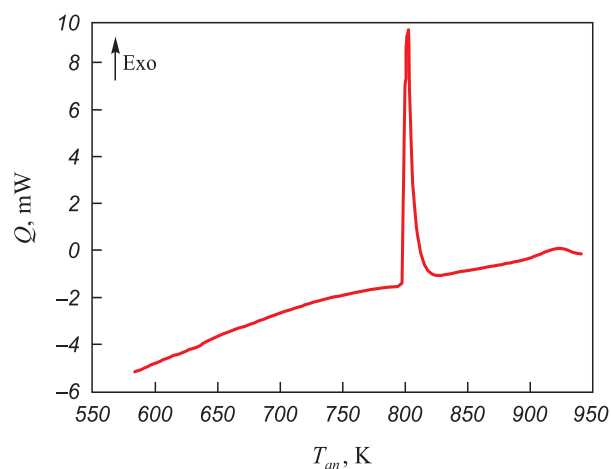


Fig. 4. DSC curve of $\text{Co}_{70.5}\text{Fe}_{0.5}\text{Cr}_4\text{Si}_7\text{B}_{18}$ amorphous alloy during heating at a rate of $20 \text{ }^\circ\text{C}/\text{min}$

Рис. 4. Кривая ДСК АС $\text{Co}_{70.5}\text{Fe}_{0.5}\text{Cr}_4\text{Si}_7\text{B}_{18}$ при нагреве со скоростью $20 \text{ }^\circ\text{C}/\text{мин}$

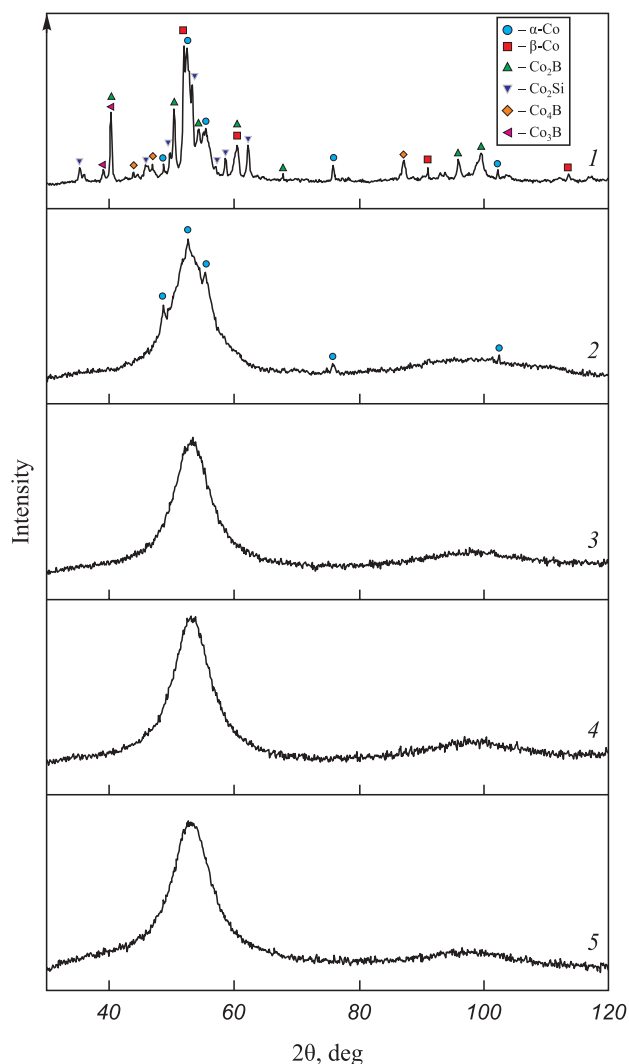


Fig. 5. X-ray spectra of $\text{Co}_{70.5}\text{Fe}_{0.5}\text{Cr}_4\text{Si}_7\text{B}_{18}$ amorphous alloy after annealing (CoK_α -radiation):

823 K (1); 763 K (2); 723 K (3); 623 K (4); without annealing (5)

Рис. 5. Рентгеновские спектры АС $\text{Co}_{70.5}\text{Fe}_{0.5}\text{Cr}_4\text{Si}_7\text{B}_{18}$ после отжига (CoK_α -излучение) при температуре:

823 К (1); 763 К (2); 723 К (3); 623 К (4); без отжига (5)

• The temperature range $T_f \leq T_{an} \leq T_{sb}$ is transitional, as no cracks form at lower temperatures (for $\text{Co}_{70.5}\text{Fe}_{0.5}\text{Cr}_4\text{Si}_7\text{B}_{18}$, the temper brittleness temperature is $T_f = 613$ K), and at higher temperatures, shear bands are absent (the temperature of complete disappearance of shear bands for $\text{Co}_{70.5}\text{Fe}_{0.5}\text{Cr}_4\text{Si}_7\text{B}_{18}$ is $T_{sb} = 748$ K). In this temperature range, the amorphous alloy is still in an amorphous but embrittled state due to the ductile-to-brittle transition phenomenon. Therefore, large radial and ring cracks, as well as spalls, are observed.

• The range $T_{sb} < T_{an} \leq T_{cryst}$ corresponds to the final transformation of the amorphous alloy into a crystalline state (for $\text{Co}_{70.5}\text{Fe}_{0.5}\text{Cr}_4\text{Si}_7\text{B}_{18}$ $T_{cryst} = 803$ K). A distinctive feature of this range is the formation of relatively symmetrical fracture patterns consisting of square crack networks nested within each other.

CONCLUSIONS

Using the example of melt-quenched amorphous alloy ribbons of the Co–Fe–Cr–Si–B system, it was demonstrated that indentation on an elastic substrate with different loads enables an approximate express assessment of the structural state of the amorphous alloy. This is due to the fact that the deformation and fracture zones formed under the indenter (presence/absence of shear bands, cracks, their mutual arrangement) are highly structure-sensitive and exhibit characteristic features in specific annealing temperature ranges.

Overall, indentation testing is an attractive method for studying the deformation behavior of amorphous alloys for the following reasons. First, these tests are easy to perform and do not lead to macrofracture, as they are not specific to the sample size. Second, plastic deformation in the material is locally confined, facilitating the study of plastic flow in the zones surrounding and located under the indenter. Moreover, direct comparison of indentation results with responses, such as to bending or tension, further makes the indentation method an effective “probe” for understanding the physics of plastic deformation and fracture in amorphous alloys.

REFERENCES / СПИСОК ЛИТЕРАТУРЫ

1. Amorphous and Nanocrystalline Materials: Preparation, Properties, and Applications. Inoue A., Hashimoto K. eds. Berlin, Heidelberg, Germany: Springer; 2001:206. <https://doi.org/10.1007/978-3-662-04426-1>
2. Chen H.S. Glass temperature, formation and stability of Fe, Co, Ni, Pd and Pt based glasses. *Materials Science and Engineering*. 1976;23(2–3):151–154. [https://doi.org/10.1016/0025-5416\(76\)90185-3](https://doi.org/10.1016/0025-5416(76)90185-3)
3. Inoue A. Stabilization of metallic supercooled liquid and bulk amorphous alloys. *Acta Materialia*. 2000;48(1):279–306. [https://doi.org/10.1016/S1359-6454\(99\)00300-6](https://doi.org/10.1016/S1359-6454(99)00300-6)
4. Louzguine-Luzgin D.V. Structural changes in metallic glass-forming liquids on cooling and subsequent vitrification in relationship with their properties. *Materials*. 2022;15(20):7285. <https://doi.org/10.3390/ma15207285>
5. Li F.C., Liu T., Zhang J.Y., Shuang S., Wang Q., Wang A.D., Wang J.G., Yang Y. Amorphous-nanocrystalline alloys: Fabrication, properties, and applications. *Materials Today Advances*. 2019;4:100027. <https://doi.org/10.1016/j.mtadv.2019.100027>
6. Glezer A.M., Permyakova I.E. Melt-Quenched Nanocrystals. Boca Raton, FL, USA: CRC Press, Taylor & Francis Group; 2013:369. <https://doi.org/10.1201/b15028>
7. Halim Q., Mohamed N.A.N., Rejab M.R.M., Naim W.N.W.A., Ma Q. Metallic glass properties, processing method and development perspective: A review. *The International Journal of Advanced Manufacturing Technology*. 2021;112(5–6): 1231–1258. <https://doi.org/10.1007/s00170-020-06515-z>
8. Abrosimova G.E., Matveev D.V., Aronin A.S. Nanocrystal formation in homogeneous and heterogeneous amorphous phases. *Physics-Uspekhi*. 2022;65:227–244. (In Russ.). <https://doi.org/10.3367/UFNe.2021.04.038974>

- Абросимова Г.Е., Матвеев Д.В., Аронин А.С. Формирование наноструктур в гомогенной и гетерогенной аморфной фазе. *Успехи физических наук*. 2022;192(3):247–266. <https://doi.org/10.3367/UFNr.2021.04.038974>
9. Permyakova I., Glezer A. Mechanical behavior of Fe- and Co-based amorphous alloys after thermal action. *Metals*. 2022;12(2):297. <https://doi.org/10.3390/met12020297>
 10. McHenry M.E., Willard M.A., Laughlin D.E. Amorphous and nanocrystalline materials for application as soft magnet. *Progress in Materials Science*. 1999;44(4):291–433. [https://doi.org/10.1016/S0079-6425\(99\)00002-X](https://doi.org/10.1016/S0079-6425(99)00002-X)
 11. Gheiratmand T., Madaah Hosseini H.R. Finemet nanocrystalline soft magnetic alloy: Investigation of glass forming ability, crystallization mechanism, production techniques, magnetic softness and the effect of replacing the main constituents by other elements. *Journal of Magnetism and Magnetic Materials*. 2016;408(19):177–192. <https://doi.org/10.1016/j.jmmm.2016.02.057>
 12. Glezer A.M., Potekaev A.I., Cheretaeva A.O. Thermal and Time Stability of Amorphous Alloys. Boca Raton, FL, USA: CRC Press, Taylor & Francis Group; 2017:180. <https://doi.org/10.1201/9781315158112>
 13. Schuh C.A., Hufnagel T.C., Ramamurty U. Mechanical behavior of amorphous alloys. *Acta Materialia*. 2007;55(12):4067–4109. <https://doi.org/10.1016/j.actamat.2007.01.052>
 14. Trexler M.M., Thadhani N.N. Mechanical properties of bulk metallic glasses. *Progress in Materials Science*. 2010;55(8):759–839. <https://doi.org/10.1016/j.pmatsci.2010.04.002>
 15. Khonik V., Kobelev N. Metallic glasses: A new approach to the understanding of the defect structure and physical properties. *Metals*. 2019;9(5):605. <https://doi.org/10.3390/met9050605>
 16. Alekhin V.P., Khonik V.A. Structure and Physical Regularities of Deformation of Amorphous Alloys. Moscow: Metallurgy; 1992:248. (In Russ.).
Алехин В.П., Хоник В.А. Структура и физические закономерности деформации аморфных сплавов. Москва: Металлургия; 1992:248.
 17. Kekalo I.B. Structural Relaxation Processes and Physical Properties of Amorphous Alloys. Moscow: MISiS; 2016;2:834. (In Russ.).
Кекало И.Б. Процессы структурной релаксации и физические свойства аморфных сплавов. Москва: Издательский дом МИСиС; 2016;2:834.
 18. Burgess T., Ferry M. Nanoindentation of metallic glasses. *Materials Today*. 2009;12(1–2):24–32. [https://doi.org/10.1016/S1369-7021\(09\)70039-2](https://doi.org/10.1016/S1369-7021(09)70039-2)
 19. Golovin Yu.I., Ivogin V.I., Khonik V.A., Kitagawa K., Tyurin A.I. Serrated plastic flow during nanoindentation of a bulk metallic glass. *Scripta Materialia*. 2001;45(8):947–952. [https://doi.org/10.1016/S1359-6462\(01\)01116-2](https://doi.org/10.1016/S1359-6462(01)01116-2)
 20. Jain A., Prabhu Y., Gunderov D., Ubyivovk E.V., Bhatt J. Study of micro indentation assisted deformation on HPT processed $Zr_{62}Cu_{22}Al_{10}Fe_5Dy_1$ bulk metallic glass. *Journal of Non-Crystalline Solids*. 2021;566(12):120877. <https://doi.org/10.1016/j.jnoncrysol.2021.120877>
 21. Jana S., Ramamurty U., Chattopadhyay K., Kawamura Y. Subsurface deformation during Vickers indentation of bulk metallic glasses. *Materials Science and Engineering: A*. 2004;375–377:1191–1195. <https://doi.org/10.1016/j.msea.2003.10.068>
 22. Schuh C.A., Nieh T.G. A survey of instrumented indentation studies on metallic glasses. *Journal of Materials Research*. 2004;19(1):46–57. <https://doi.org/10.1557/jmr.2004.19.1.46>
 23. Glezer A.M., Permyakova I.E. Modern concepts of methods for studying mechanical properties of metallic glasses (REVIEW). *Deformatsiya i razrushenie materialov*. 2006;(3):2–11. (In Russ.).
Глезер А.М., Пермякова И.Е. Современные представления о методах исследования механических свойств металлических стекол (ОБЗОР). *Деформация и разрушение материалов*. 2006;(3):2–11.
 24. Greer A.L., Cheng Y.Q., Ma E. Shear bands in metallic glasses. *Materials Science and Engineering: R: Reports*. 2013;74(4):71–132. <https://doi.org/10.1016/j.mser.2013.04.001>
 25. Axinte E.M., Wang Y., Tabacaru L.L., Radwan N. Shear banding in metallic glasses: major weakness or potential advantage? *Recent Patents on Materials Science*. 2016;9(1):2–19. <https://doi.org/10.2174/1874464809666160407212236>
 26. Wilde G., Rösner H. Nanocrystallization in a shear band: An *in situ* investigation. *Applied Physics Letters*. 2011;98(25):251904. <https://doi.org/10.1063/1.3602315>
 27. Jiang M.Q., Wilde G., Dai L.H. Shear band dilatation in amorphous alloys. *Scripta Materialia*. 2017;127:54–57. <https://doi.org/10.1016/j.scriptamat.2016.08.038>
 28. Bhowmick R., Raghavan R., Chattopadhyay K., Ramamurty U. Plastic flow softening in a bulk metallic glass. *Acta Materialia*. 2006;54(16):4221–4228. <https://doi.org/10.1016/j.actamat.2006.05.011>
 29. Feodorov V., Permyakova I., Ushakov I. Evolution of mechanical characteristics of a metallic glass Co–Fe–Cr–Si at annealing. *Proceedings of SPIE (The International Society for Optical Engineering)*. 2005;5831:143–147. <https://doi.org/10.1117/12.619685>
 30. Permyakova I.E., Glezer A.M., Savchenko E.S., Shchetinin I.V. Effect of external actions on magnetic properties and corrosion resistance of $Co_{70.5}Fe_{0.5}Cr_4Si_7B_{18}$ amorphous alloy. *Bulletin of the Russian Academy of Sciences: Physics*. 2017;81(11):1310–1316. (In Russ.). <https://doi.org/10.3103/S1062873817110144>
Пермякова И.Е., Глезер А.М., Савченко Е.С., Щетинин И.В. Влияние внешних воздействий на магнитные свойства и коррозионную стойкость аморфного сплава $Co_{70.5}Fe_{0.5}Cr_4Si_7B_{18}$. *Известия Российской академии наук. Серия физическая*. 2017;81(11):1458–1465. <https://doi.org/10.7868/S0367676517110059>
 31. Permyakova I.E. Evolution of the structure, properties of amorphous alloys and amorphous-nanocrystalline composite materials under external influences: Dr. Tech. Sci. Diss. Moscow: Baikov Institute of Metallurgy and Materials Science; 2023:267.
Пермякова И.Е. Эволюция структуры, свойства аморфных сплавов и аморфно-нанокристаллических композитных материалов при внешних воздействиях: Диссертация ... доктора физико-математических наук. Москва: ИМЕТ РАН; 2023:267.

Information about the Authors

Сведения об авторах

Inga E. Permyakova, Dr. Sci. (Phys.-Math.), Senior Researcher of the Laboratory “Physicochemistry and Mechanics of Metallic Materials”, Baikov Institute of Metallurgy and Materials Science, Russian Academy of Sciences

ORCID: 0000-0002-1163-3888

E-mail: inga_perm@mail.ru

Mariya V. Kostina, Dr. Sci. (Eng.), Assist. Prof., Senior Researcher, Head of the Laboratory “Physicochemistry and Mechanics of Metallic Materials”, Baikov Institute of Metallurgy and Materials Science, Russian Academy of Sciences

ORCID: 0000-0002-2136-5792

E-mail: mvkst@yandex.ru

Инга Евгеньевна Пермякова, д.ф.-м.н., ведущий научный сотрудник лаборатории физикохимии и механики металлических материалов, Институт металлургии и материаловедения им. А.А. Байкова РАН

ORCID: 0000-0002-1163-3888

E-mail: inga_perm@mail.ru

Мария Владимировна Костина, д.т.н., доцент, ведущий научный сотрудник, заведующий лабораторией физикохимии и механики металлических материалов, Институт металлургии и материаловедения им. А.А. Байкова РАН

ORCID: 0000-0002-2136-5792

E-mail: mvkst@yandex.ru

Contribution of the Authors

Вклад авторов

I. E. Permyakova – researching, writing the text, processing the experimental results.

M. V. Kostina – finalization of the text, correction of conclusions.

И. Е. Пермякова – проведение исследований, подготовка текста статьи, обработка экспериментальных результатов.

М. В. Костина – доработка текста, корректировка выводов.

Received 11.08.2024

Revised 14.08.2024

Accepted 22.08.2024

Поступила в редакцию 11.08.2024

После доработки 14.08.2024

Принята к публикации 22.08.2024



UDC 621.791.92:621.727:620.178

DOI 10.17073/0368-0797-2024-5-563-566



Short Report

Краткое сообщение

STRUCTURAL-PHASE STATES AND PROPERTIES OF HIGH-SPEED SURFACING AFTER TEMPERING AND ELECTRON BEAM PROCESSING

V. E. Gromov , A. S. Chapaikin, L. P. Bashchenko

Siberian State Industrial University (42 Kirova Str., Novokuznetsk, Kemerovo Region – Kuzbass 654007, Russian Federation)

 gromov@physics.sibsiu.ru

Abstract. In this work, the authors used the methods of modern physical materials science to investigate the structure, defective substructure, phase composition, tribological and mechanical properties of the surfacing subjected to high-temperature tempering at 580 °C and subsequent electron beam processing. The deposited layers up to 10 mm thick are formed by plasma surfacing with PP-18YU powder wire in a nitrogen medium. According to the phase composition, the deposited layers consist of α -Fe and carbides of Me_6C composition. After tempering, the polycrystalline structure of the deposited layer contains grains of 7.0 – 22.5 μ m in size with layers of the second phase along the boundaries and at the joints of grains with composition V_4C_3 , Cr_7C_3 , Fe_3C , $Cr_{23}C_6$, WC_{1-x} . Electron beam processing forms a thin surface layer (30 – 50 μ m) with grains of cellular (columnar) structure of high-speed crystallization of submicron (100 – 250 nm) size. Particles of the second phase of the nanoscale range of globular and faceted shapes were detected in the volume of grains and along the boundaries.

Keywords: high-speed steel, structure, phase composition, electron microscopy, mechanical and tribological properties

Acknowledgements: The work was supported by the Russian Science Foundation, grant No. 23-19-00186, <https://rscf.ru/project/23-19-00186/>. Authors express their gratitude to Dr. Sci. (Phys.-Math.), Prof. I.Y. Litovchenko for his assistance in conducting electron microscopic studies and Dr. Sci. (Eng.), Assist. Prof. N.N. Malushin for the samples provided.

For citation: Gromov V.E., Chapaikin A.S., Bashchenko L.P. Structural-phase states and properties of high-speed surfacing after tempering and electron beam processing. *Izvestiya. Ferrous Metallurgy*. 2024;67(5):563–566. <https://doi.org/10.17073/0368-0797-2024-5-563-566>

СТРУКТУРНО-ФАЗОВЫЕ СОСТОЯНИЯ И СВОЙСТВА БЫСТРОРЕЖУЩЕЙ НАПЛАВКИ ПОСЛЕ ОТПУСКА И ЭЛЕКТРОННО-ПУЧКОВОЙ ОБРАБОТКИ

В. Е. Громов , А. С. Чапайкин, Л. П. Бащенко

Сибирский государственный индустриальный университет (Россия, 654007, Кемеровская обл. – Кузбасс, Новокузнецк, ул. Кирова, 42)

 gromov@physics.sibsiu.ru

Аннотация. В работе авторы методами современного физического материаловедения исследовали структуру, дефектную субструктуру, фазовый состав, трибологические и механические свойства наплавки, подвергнутой высокотемпературному отпуску при 580 °C и последующей электронно-пучковой обработке. Наплавленные слои толщиной до 10 мм формируются плазменной наплавкой порошковой проволокой ПП-18Ю в среде азота. По фазовому составу наплавленные слои состоят из α -Fe и карбидов состава Me_6C . После отпуска поликристаллическая структура наплавленного слоя содержит зерна размером 7,0 – 22,5 мкм с прослойками второй фазы по границам и в стыках зерен составов V_4C_3 , Cr_7C_3 , Fe_3C , $Cr_{23}C_6$, WC_{1-x} . Электронно-пучковая обработка формирует тонкий поверхностный слой (30 – 50 мкм) с зернами ячеистой (зеренной) структуры высокоскоростной кристаллизации субмикронного (100 – 250 нм) размера. В объеме зерен и по границам выявлены частицы второй фазы наноразмерного диапазона глобулярной и ограненной форм.

Ключевые слова: быстрорежущая сталь, структура, фазовый состав, электронная микроскопия, механические и трибологические свойства

Благодарности: Работа выполнена при поддержке гранта Российского научного фонда № 23-19-00186, <https://rscf.ru/project/23-19-00186/>.

Выражаем признательность д.ф.-м.н. профессору И.Ю. Литовченко за помощь в проведении электронно-микроскопических исследований и д.т.н. доценту Н.Н. Малущину за предоставленные образцы.

Для цитирования: Громов В.Е., Чапайкин А.С., Бащенко Л.П. Структурно-фазовые состояния и свойства быстрорежущей наплавки после отпуска и электронно-пучковой обработки. *Известия вузов. Черная металлургия.* 2024;67(5):563–566.
<https://doi.org/10.17073/0368-0797-2024-5-563-566>

INTRODUCTION

In the mining, metallurgical, and construction industries, surfacing is applied to protect products from various types of wear, corrosion, and static and dynamic loads, ensuring high functional properties [1; 2].

Recently, scientific research and practical developments in plasma surfacing with high hardness materials (R18, R6M5, R2M9, and others) using nitrogen as an alloying element have been actively advancing [1]. When selecting a surfacing material that meets operational conditions, it is crucial to thoroughly investigate the structure, phase composition, mechanical, and tribological properties, as well as their evolution during subsequent heat treatment [3].

It is important to note that surface layers play a significant role, and the formation of microdefects in these layers can lead to macro-failure. In this regard, developing highly effective methods for forming surface layers with high performance characteristics on working surfaces becomes relevant. This problem can be addressed by traditional strengthening methods (chemical-thermal, mechanical, physical, etc.) [3]; however, in some cases, these methods do not ensure good adhesion to the substrate. From this perspective, electron beam processing (EBP) is an effective method, significantly enhancing the mechanical properties of the entire material by optimizing the structural-phase states of surface layers [4]. The application of EBP is considerably more effective than traditional material processing methods.

The aim of this study is to investigate the structural-phase states and properties of surfacing formed in a nitrogen-rich protective and alloying environment from high-speed steel R18Yu during subsequent high-temperature tempering and EBP.

MATERIALS AND METHOD

The material used for the study consisted of 30KhGSA steel samples with a deposited layer of R18Yu steel. The deposited layer was applied using plasma surfacing in a nitrogen environment, with the use of non-current-carrying powder wire PP-R18Yu. The chemical composition of R18Yu steel (wt. %): C 0.87; Cr 4.41; W 17.00; Mo 0.10; V 1.50; Ti 0.35; Al 1.15; N 0.06; the balance is iron. During plasma surfacing, the consumption of the shielding gas (nitrogen) Q_{shield} was 20 – 22 l/min, and the consumption of the plasma-forming gas (argon) Q_{plasma} was 6 – 8 l/min. The methodology of plasma surfacing and the justification for the chosen mode are detailed in previous works [1; 2]. The studies were

conducted after surfacing, high-temperature tempering at a heating temperature of 580 °C (holding time 1 h, with four tempering cycles), and EBP. The irradiation was carried out with an electron beam energy density of 30 J/cm². The pulse duration was 50 μs, the number of irradiation pulses was 5, and the pulse repetition frequency was 0.3 s⁻¹.

The investigation of the structure, defect substructure, phase, and elemental composition was performed using scanning electron microscopy (KYKY-EM 6900) and transmission electron microscopy (JEM-2100 JEOL) [5 – 7]. Microhardness was measured by the Vickers method (HVS-1000 device) with a load of 1 N on the indenter, and tribological properties were evaluated using a Pin on Disc and Oscillating Tribotester.

RESULTS AND DISCUSSION

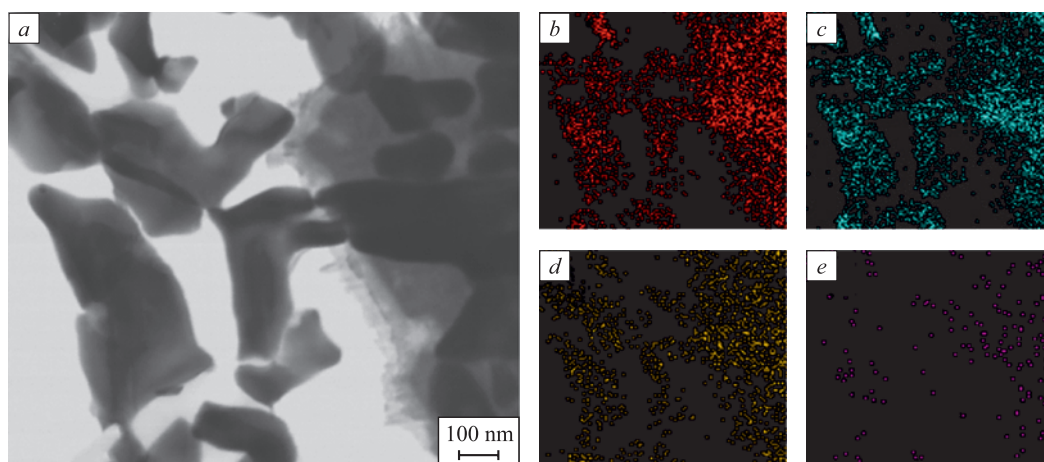
Plasma surfacing forms a layer in which the main phases are α-Fe and Me₆C carbides, which create a carbide network and serve as the primary strengthening phase. During the formation of the deposited layer, nanosized particles of the carbide phase form within the grains. The values of microhardness H_{μ} , wear rate V , and friction coefficient k are provided in the Table.

After high-temperature tempering, the grain size ranges from 7.0 to 22.5 μm. The results of the elemental composition study, conducted by mapping the frame mesh of the deposited layer, indicate that the mesh grains are enriched with tungsten, iron, and chromium atoms (see the Figure). Analysis of micro-electron diffraction patterns shows that the frame is composed of complex carbides Fe₃W₃C (Fe₂W₄C). The carbide phase grain sizes range from 80 to 350 nm. Mapping of the solid solution grains based on α-Fe shows the presence of tungsten, chromium, vanadium, iron, and carbon atoms, suggesting the presence of nanosized particles of complex carbide phases. These particles are round or faceted in shape, with sizes ranging from 10 to 18 nm.

Microhardness and tribological parameters of the deposited layer

Микротвердость и трибологические параметры наплавленного слоя

State	H_{μ} , GPa	$V \cdot 10^6$, mm ³ /(N·m)	k
Deposition	4.7	8.9	0.70
Deposition + tempering	5.3	9.9	0.65
Deposition + tempering + EBP	5.3	3.3	0.58



Electron microscopic image of a frame mesh section of the deposited layer:

a – light field; *b* – *e* – images of the foil section obtained in characteristic *X*-ray radiation of atoms W (*b*), Fe (*c*), Cr (*d*), C (*e*)

Электронно-микроскопическое изображение участка каркасной сетки наплавленного слоя:

a – светлое поле; *b* – *e* – изображения данного участка фольги, полученные в характеристическом рентгеновском излучении атомов W (*b*), Fe (*c*), Cr (*d*), C (*e*)

Analysis of the corresponding micro-electron diffraction patterns shows that the globular particles, randomly distributed within the α -Fe grains, are carbides of compositions V_4C_3 or Cr_7C_3 . The faceted particles are carbides of compositions $Cr_{23}C_6$ ($Me_{23}C_6$), Fe_3C or WC_{1-x} .

After tempering, the microhardness increases by 13 %, reaching 5.3 GPa, the wear rate increases by 12.3 %, and the friction coefficient decreases by 7 % (see Table).

Electron beam processing (EBP) of the tempered deposited layer forms a thin (30 – 50 μ m) surface layer with a cellular (grain) structure of high-speed crystallization with submicron grain sizes (100 – 250 nm). Particles of the second phase, with transverse sizes of 10 – 15 nm, are located along the crystallization cell boundaries. In some cases, particles of faceted or globular shape, up to 45 nm in size, are detected at the boundaries and within the cells. Second-phase particles are also observed within the cells, with particle sizes ranging from 5 to 10 nm. Analysis of the micro-electron diffraction patterns indicates that these are complex carbides Me_6C , $Me_{23}C_6$, Me_3C , and Me_7C_3 (where *Me* represents chromium, iron, and tungsten). EBP results in a multiple (threefold or more) increase in the material's wear resistance, a reduction in the friction coefficient, while maintaining the same microhardness.

CONCLUSIONS

Using modern physical materials science methods, the structure, elemental and phase composition, defect substructure, and mechanical and tribological properties of the deposited layer of R18Yu high-speed steel in a nitrogen-based protective-alloying environment, subjected to high-temperature tempering and additional irradiation by a pulsed electron beam in the mode of high-speed melting of the thin surface layer, were studied.

REFERENCES / СПИСОК ЛИТЕРАТУРЫ

- Malushin N.N., Gromov V.E., Romanov D.A., Bashchenko L.P. Hardening of Heat-Resistant Alloys by Plasma in a Nitrogen Environment. Novokuznetsk: Poligrafist; 2022:232. (In Russ.).
Упрочнение теплостойких сплавов плазмой в среде азота / Н.Н. Малущин, В.Е. Громов, Д.А. Романов, Л.П. Башченко. Новокузнецк: Полиграфист; 2022:232.
- Raikov S.V., Kormyshev V.E., Gromov V.E., Ivanov Yu.F., Konovalov S.V. Wear-Resistant Surfacing on Steel: Structure, Phase Composition and Properties: Monograph. Novokuznetsk: SibSIU; 2017:318. (In Russ.).
Износостойкие накладки на сталь: структура, фазовый состав и свойства: монография / С.В. Райков, В.Е. Кормышев, В.Е. Громов, Ю.Ф. Иванов, С.В. Коновалов. Новокузнецк: ИЦ СибГИУ; 2017:318.
- Chaus A.S., Murgas M., Latyshev I.V., Tot R. Heat treatment of cast carburising high-speed steel alloyed with Ti, Nb and V. *Metal Science and Heat treatment*. 2001;43:220–223. <http://doi.org/10.1023/A:1012317911735>
- Evolution of Surface Layer Structure of Steel Subjected to Electron-Ion-Plasma Processing. Koval' N.N., Ivanov Yu.F. eds. Tomsk: Izd-vo NTL; 2016:304. (In Russ.).
Эволюция структуры поверхностного слоя стали, подвергнутой электронно-ионно-плазменным методам обработки / Под общ. ред. Н.Н. Коваля и Ю.Ф. Иванова. Томск: Изд-во НТЛ; 2016:304.
- Egerton F.R. *Physical Principles of Electron Microscopy*. Basel: Springer International Publishing; 2016:196.
- Kumar C.S.S.R. *Transmission Electron Microscopy. Characterization of Nanomaterials*. New York: Springer; 2014:717. <http://doi.org/10.1007/978-3-642-38934-4>
- Carter C.B., Williams D.B. *Transmission Electron Microscopy*. Berlin: Springer International Publishing; 2016:518. <http://doi.org/10.1017/S1431927618000296>

Information about the Authors

Сведения об авторах

Viktor E. Gromov, Dr. Sci. (Phys.-Math.), Prof., Head of the Chair of Science named after V.M. Finkel', Siberian State Industrial University

ORCID: 0000-0002-5147-5343

E-mail: gromov@physics.sibsiu.ru

Aleksandr S. Chapaikin, Postgraduate of the Chair of Science named after V.M. Finkel', Siberian State Industrial University

E-mail: thapajkin.as@yandex.ru

Lyudmila P. Bashchenko, Cand. Sci. (Eng.), Assist. Prof. of the Chair "Thermal Power and Ecology", Siberian State Industrial University

ORCID: 0000-0003-1878-909X

E-mail: luda.baschenko@gmail.com

Виктор Евгеньевич Громов, д.ф.-м.н., профессор, заведующий кафедрой естественнонаучных дисциплин им. профессора В.М. Финкеля, Сибирский государственный индустриальный университет

ORCID: 0000-0002-5147-5343

E-mail: gromov@physics.sibsiu.ru

Александр Сергеевич Чапайкин, аспирант кафедры естественнонаучных дисциплин им. профессора В.М. Финкеля, Сибирский государственный индустриальный университет

E-mail: thapajkin.as@yandex.ru

Людмила Петровна Бащенко, к.т.н., доцент кафедры теплоэнергетики и экологии, Сибирский государственный индустриальный университет

ORCID: 0000-0003-1878-909X

E-mail: luda.baschenko@gmail.com

Contribution of the Authors

Вклад авторов

V. E. Gromov – work conceptualization, scientific guidance, writing the text.

A. S. Chapaikin – literary review, conducting mechanical tests, preparing samples for TEM.

L. P. Baschenko – discussion of the results, editing the text.

В. Е. Громов – концепция работы, научное руководство, написание текста.

А. С. Чапайкин – обзор литературы, проведение механических испытаний, подготовка образцов для ПЭМ.

Л. П. Бащенко – обсуждение результатов, редактирование текста.

Received 12.10.2023

Revised 20.05.2024

Accepted 21.08.2024

Поступила в редакцию 12.10.2023

После доработки 20.05.2024

Принята к публикации 21.08.2024



UDC 538.911

DOI 10.17073/0368-0797-2024-5-567-572



Original article

Оригинальная статья

SIMULATION OF STRUCTURAL CHANGES IN METAL UNDER HIGH-INTENSITY EXTERNAL INFLUENCE

A. N. Gostevskaya¹, A. V. Markidonov^{1, 2},
M. D. Starostenkov³, D. A. Lubyanoi⁴

¹ Siberian State Industrial University (42 Kirova Str., Novokuznetsk, Kemerovo Region – Kuzbass 654007, Russian Federation)

² Kuzbass Humanitarian Pedagogical Institute of Kemerovo State University (23 Tsiolkovskogo Str., Novokuznetsk, Kemerovo Region – Kuzbass 654041, Russian Federation)

³ Polzunov Altai State Technical University (46 Lenina Ave., Barnaul, Altai Territory 656038, Russian Federation)

⁴ Prokopyevsk Branch of the Kuzbass State Technical University named after T.F. Gorbachev (32 Nogradskaya Str., Prokopyevsk, Kemerovo Region – Kuzbass 653039, Russian Federation)

✉ lokon1296@mail.ru

Abstract. Today, researchers and industry are faced with the task of improving the physical and mechanical properties of various metal products. To strengthen the structures, there are various technologies for processing the material surface by high-temperature exposure. At the same time, the use of laser technologies is of great interest. High-speed local laser heating of the material surface followed by rapid cooling with heat removal into the volume depth, as well as the absence of mechanical action, allows us to obtain unique nonequilibrium structures with a wide range of properties. Obviously, the development of these technologies requires deep fundamental research. In this work, the molecular dynamics method revealed the features of structural changes in the surface layers of an iron crystal under high-temperature exposure. The choice of such a method is due to the fact that the phenomena under consideration are difficult to study through real experiments and direct observations. Conditions of the computer experiment were set in such a way that after the melting point is reached, a phase transition occurs in the simulated system, during which particles are separated from the surface of the liquid phase. As a result of the study, the threshold temperature of particle ejection was estimated and the mechanisms of particle cluster formation were investigated. When heated, the number of clusters increases, and when cooled, it decreases, but at the same time their sizes increase, which indicates the implementation of the condensation mechanism of ablation products. Additionally, the influence of external pressure on the simulated particle system was studied. It is shown that as the pressure increases, the number of clusters decreases.

Keywords: crystal, model, temperature, surface, ablation, cluster

Acknowledgements: The study was conducted within the framework of the state assignment of the Ministry of Science and Higher Education of the Russian Federation No. 075-00087-2401.

For citation: Gostevskaya A.N., Markidonov A.V., Starostenkov M.D., Lubyanoi D.A. Simulation of structural changes in metal under high-intensity external influence. *Izvestiya. Ferrous Metallurgy*. 2024;67(5):567-572. <https://doi.org/10.17073/0368-0797-2024-5-567-572>

МОДЕЛИРОВАНИЕ СТРУКТУРНЫХ ИЗМЕНЕНИЙ В МЕТАЛЛЕ ПРИ ВЫСОКОИНТЕНСИВНОМ ВНЕШНЕМ ВОЗДЕЙСТВИИ

А. Н. Гостевская¹✉, А. В. Маркидонов^{1, 2},
М. Д. Старостенков³, Д. А. Лубяной⁴

¹ Сибирский государственный индустриальный университет (Россия, 654007, Кемеровская обл. – Кузбасс, Новокузнецк, ул. Кирова, 42)

² Кузбасский гуманитарно-педагогический институт Кемеровского государственного университета (Россия, 654041, Кемеровская обл. – Кузбасс, Новокузнецк, ул. Циолковского, 23)

³ Алтайский государственный технический университет имени И.И. Ползунова (Россия, 656038, Алтайский край, Барнаул, пр. Ленина, 46)

⁴ Филиал Кузбасского государственного технического университета имени Т.Ф. Горбачева в г. Прокопьевске (Россия, 653039, Кемеровская обл. – Кузбасс, Прокопьевск, ул. Ноградская, 32)

✉ lokon1296@mail.ru

Аннотация. На сегодняшний день перед исследователями и промышленностью стоит задача улучшения физико-механических свойств различных металлических изделий. Для упрочнения конструкций существуют различные технологии обработки поверхности материала путем высокотемпературного воздействия. Большой интерес при этом вызывает применение лазерных технологий. Высокоскоростной локальный лазерный нагрев поверхности материала с последующим быстрым охлаждением путем отвода тепла в глубь объема, а также отсутствие механического воздействия позволяют получить уникальные неравновесные структуры с широким набором свойств. Очевидно, что развитие этих технологий требует глубоких фундаментальных исследований. В настоящей работе методом молекулярной динамики выявлялись особенности структурных изменений поверхностных слоев кристалла железа при высокотемпературном воздействии. Выбор такого метода обусловлен тем, что рассматриваемые явления затруднительно изучать путем реальных экспериментов и прямых наблюдений. Условия компьютерного эксперимента были заданы таким образом, чтобы после прохождения точки температуры плавления в моделируемой системе происходил фазовый переход, при котором осуществляется отрыв частиц от поверхности жидкой фазы. В результате проведенного исследования выполнена оценка пороговой температуры эжектирования частиц и проведено исследование механизмов образования кластеров частиц. При нагреве происходит увеличение количества кластеров, а при охлаждении – его уменьшение, но при этом размеры кластеров увеличиваются, что свидетельствует о реализации механизма конденсации продуктов абляции. Дополнительно проведено исследование влияния внешнего давления на моделируемую систему частиц. Показано, что при увеличении давления количество кластеров уменьшается.

Ключевые слова: кристалл, модель, температура, поверхность, абляция, кластер

Благодарности: Исследование проводилось в рамках государственного задания Министерства науки и высшего образования Российской Федерации № 075-00087-2401.

Для цитирования: Гостевская А.Н., Маркидонов А.В., Старостенков М.Д., Лубяной Д.А. Моделирование структурных изменений в металле при высокоинтенсивном внешнем воздействии. *Известия вузов. Черная металлургия.* 2024;67(5):567–572.

<https://doi.org/10.17073/0368-0797-2024-5-567-572>

INTRODUCTION

Under the influence of high temperatures, the structure of the material undergoes changes. Studying the effect of high temperatures on structural changes in metals in the field of condensed matter mechanics poses numerous challenges related to the fundamental properties and structural transformations of materials. It is worth noting that there has been growing interest in methods for producing nanoparticles through material ablation under high-temperature exposure. Irradiation with ultrashort laser pulses is of practical interest [1; 2], and both experimental and theoretical studies have been devoted to this topic [3 – 5]. Currently, theoretical methods are available that are based on the construction of thermal models [6] and the analysis of energy balance scattering during laser emission [7]. These methods allow us to evaluate the effect of laser irradiation on surface structure modifications. It should be noted that phenomena characteristic of laser irradiation of materials,

such as ablation and desorption, have been studied using molecular dynamics simulations [8; 9]. Applied to solids, molecular dynamics can reveal the differences between desorption and ablation, predict the distribution of clusters in samples [10 – 12], the distribution of particles by radial and axial velocities, and explain the dependence of ablation on laser properties [13 – 15], such as energy density and pulse duration [16; 17]. It is known that for many materials, the ablation process is accompanied by the formation of particle clusters. Mechanisms for their formation include condensation of the ejected particle cloud, phase explosion, hydrodynamic spraying, and photomechanical effects [18; 19]. As part of this study, the mechanisms of particle cluster formation were investigated.

RESEARCH METHODOLOGY

To conduct the numerical experiment, the molecular dynamics method was chosen, which allows for the simu-

lation of various statistical ensembles of particles, as well as the comparison of obtained results in real time.

The implementation of the molecular dynamics simulation largely depends on the interatomic potential. For the potential calculation, the “embedded atom” model was used, based on the theory of calculating the electronic structure of many-particle systems in physics.

During the calculation of the particle system modeled in the study, metal cells (BCC lattices) with a lattice parameter of $a_0 = 2.855 \text{ \AA}$, were constructed and translated along the x , y , and z axes. The resulting simulation cell imitated an iron crystal and contained 30,000 particles. The infinite extent of the crystal was achieved using periodic boundary conditions, and to create the surface along the y -axis, free boundary conditions were applied.

During the simulation, the computational cell was divided into regions, each assigned a specific temperature decreasing with distance from the surface. Using the semi-infinite solid body model, an analytically exact solution to the thermal problem can be obtained through integral transformations [20]. In this case, if the source intensity is constant, the temperature distribution in the depth of the sample during the heating stage is determined as a function of the coordinates using the formula:

$$T(y, t) = \frac{2Aq}{\lambda} \sqrt{at} \operatorname{ierfc}\left(\frac{y}{2\sqrt{at}}\right), \quad (1)$$

where $A = 0.68$ is the absorptivity; $q = 3.5 \div 6.5 \text{ MW/cm}^2$ is the energy density; $\lambda = 80 \text{ W/(m}\cdot\text{K)}$ is the thermal conductivity coefficient; $a = 2.621 \cdot 10^{-5} \text{ m}^2/\text{s}$ is the thermal diffusivity; $\tau = 10 \cdot 10^{-12} \text{ s}$ is the exposure duration.

The function $\operatorname{ierfc}(x)$ is the integral of the complementary error function:

$$\operatorname{ierfc}(x) = \int_x^\infty \operatorname{erfc}(x) dx. \quad (2)$$

After the laser exposure ceases, the cooling stage begins, and the temperature distribution is determined by the following formula:

$$T(y, t) = \frac{2Aq}{\lambda} \left[\sqrt{at} \operatorname{ierfc}\left(\frac{y}{2\sqrt{at}}\right) - \sqrt{a(t-\tau)} \operatorname{ierfc}\left(\frac{y}{2\sqrt{a(t-\tau)}}\right) \right]. \quad (3)$$

RESULTS AND DISCUSSION

To identify clusters, the particle system was divided into separate groups based on a distance criterion, which was set to be twice the value of the lattice parameter. A cluster is defined as a group of particles where each particle is located at a distance no greater than the cut-

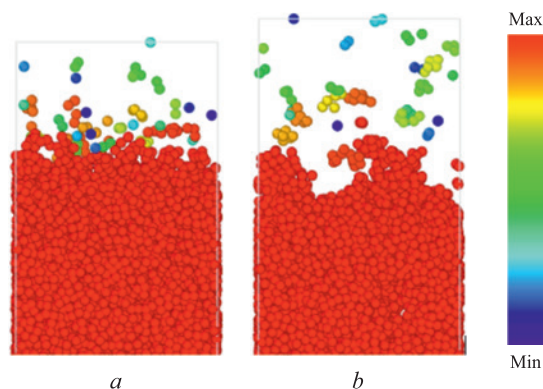


Fig. 1. Visualization of identified clusters after 10 (a) and 18 ps (b) of model time ($q = 5 \text{ MW/cm}^2$; color visualization matches sizes of clusters)

Рис. 1. Визуализация идентифицируемых кластеров через 10 (a) и 18 пс (b) модельного времени ($q = 5 \text{ МВт/см}^2$; цветовая визуализация соответствует размерам кластеров)

off radius from one or more particles of the same group. Once the particle clusters are identified, they are colored according to their size. The color gradient changes from violet to red as the number of particles in the cluster increases.

The conducted research demonstrated that during the heating process, an increasing number of clusters are gradually identified, which are generally represented by individual particles (Fig. 1, a). During the cooling process, the number of identified clusters decreases while their size increases, meaning that previously ejected particles start to group together (Fig. 1, b). The condensation mechanism of ablation products is realized in the considered model.

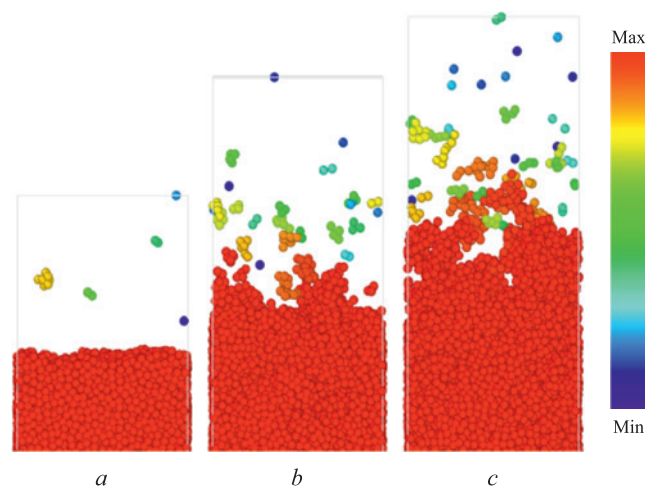


Fig. 2. Visualization of identified clusters after 20 ps of model time at a laser radiation energy density of 3.5; 5.0 and 6.5 MW/cm^2 (a – c) (color visualization matches sizes of clusters)

Рис. 2. Визуализация идентифицируемых кластеров через 20 пс модельного времени при плотности энергии лазерного излучения 3,5; 5,0 и 6,5 МВт/см^2 (a – c) (цветовая визуализация соответствует размерам кластеров)

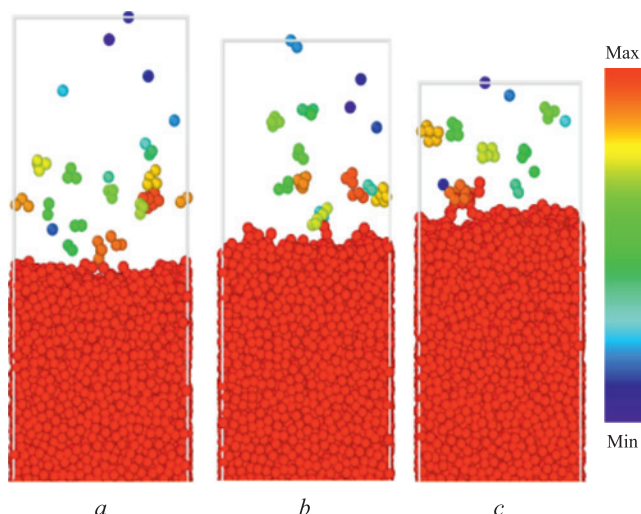


Fig. 3. Visualization of identified clusters after 20 ps of model time at pressures of 1, 2 and 3 GPa (a – c) ($q = 5 \text{ MW/cm}^2$; color visualization matches sizes of clusters)

Рис. 3. Визуализация идентифицируемых кластеров через 20 пс модельного времени при давлении 1, 2 и 3 ГПа (a – c) ($q = 5 \text{ МВт/см}^2$; цветовая визуализация соответствует размерам кластеров)

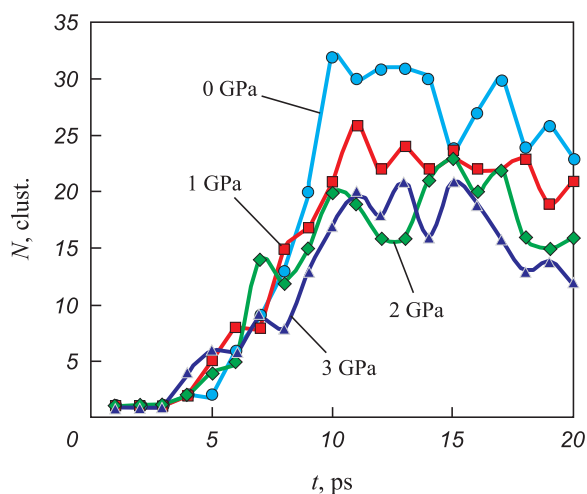


Fig. 4. Change in the number of clusters during simulation at different pressures ($q = 5 \text{ MW/cm}^2$)

Рис. 4. Изменение количества кластеров при моделировании при различном давлении ($q = 5 \text{ МВт/см}^2$)

Identified clusters at different laser radiation densities are shown in Fig. 2. A higher laser energy density contributes to the formation of more clusters (for $q = 3.5, 5.0,$ and 6.5 MW/cm^2 , the number of clusters is 6, 23, and 38, respectively).

A study of the effect of system pressure on the number of forming clusters was also conducted. The barostat algorithm used in the simulation ensures that the system’s volume becomes a variable quantity, adjusting to maintain constant pressure [20]. Clusters formed under different pressure levels are shown in Fig. 3.

The number of clusters decreases with increasing pressure. The change in their number during the simulation process is shown in Fig. 4.

CONCLUSIONS

As a result of the conducted research, a model was developed using the molecular dynamics method, which made it possible to study the laser ablation process occurring under the influence of short pulses with low energy density. A study of the formation of particle clusters during ablation was conducted. A numerical dependence of the number of formed clusters on the pressure applied to them was established.

REFERENCES / СПИСОК ЛИТЕРАТУРЫ

- Gostevskaya A.N. Effect of ultra-short high power laser pulses on a solid body. In: *Current Issues of Physical Metallurgy of Steels and Alloys. Abstracts of the XXVI Ural School of Metallurgists-Thermists*. Ekaterinburg, 2022:259–261. (In Russ.).
Гостевская А.Н. Воздействие ультракоротких сверхмощных лазерных импульсов на твердое тело. В кн.: *Актуальные проблемы физического металловедения сталей и сплавов. Сб. тезисов докладов XXVI Уральской школы металловедов-термистов*. Екатеринбург, 2022:259–261.
- Mazhukin V.I., Mazhukin A.V., Demin M.M., Shapranov A.V. Nonequilibrium effects accompanying the action of pulsed laser radiation on metals. *Journal of Optical Technology*. 2011;78(8):491–497. <https://doi.org/10.1364/JOT.78.000491>
Мажукин В.И., Мажукин А.В., Демин М.М., Шапранов А.В. Эффекты неравновесности при воздействии импульсного лазерного излучения на металлы. *Оптический журнал*. 2011;78(8):29–37.
- Zhigilei L.V., Kodali P.B.S., Garrison B.J. Molecular dynamics model for laser ablation and desorption of organic solids. *The Journal of Physical Chemistry B*. 1997;101(11):2028–2037. <https://doi.org/10.1021/jp9634013>
- Tabetah M., Matei A., Constantinescu C. The minimum amount of “matrix” needed for matrix-assisted pulsed laser deposition of biomolecules. *The Journal of Physical Chemistry B*. 2014;118(46):13290–13299. <http://dx.doi.org/10.1021/jp508284n>
- Bauerle D. *Laser Processing and Chemistry*. Luxembourg: Springer Science Business Media; 2011:851.
- Gostevskaya A.N., Markidonov A.V. Changes in the internal structure of metals when exposed to laser pulses. In: *Innovative Technologies in Materials Science and Mechanical Engineering. Materials of the 5th All-Russian Sci. and Pract. Conf. with Int. Participation*. Perm: Publ. of the Perm National Research Polytechnic University; 2021:60–63. (In Russ.).

Гостевская А.Н., Маркидонов А.В. Изменение внутреннего строения металлов при воздействии лазерных импульсов. В кн.: *Инновационные технологии в материаловедении и машиностроении. Материалы 5-й Всероссийской научно-практической конференции с международным участием*. Пермь: Изд-во Пермского нац. исслед. политехн. ун-та; 2021:60–63.

7. Gostevskaya A.N., Markidonov A.V., Kovalenko V.V. Molecular dynamic modeling of laser ablation. In: *Promising Materials and Technologies: Proceedings of the Int. Symp., Minsk, August 23–27, 2021*. Rubanik V.V. ed. Minsk: Belarusian State Institute of Standardization and Certification; 2021:21. (In Russ.).
Гостевская А.Н., Маркидонов А.В., Коваленко В.В. Молекулярно-динамическое моделирование лазерной абляции. В кн.: *Перспективные материалы и технологии: материалы международного симпозиума, Минск, 23–27 августа 2021 г.* / Под. ред. В.В. Рубаника. Минск: Белорусский государственный институт стандартизации и сертификации; 2021:21.
8. Willis D.A., Grosu V. The effect of melting-induced volumetric expansion on initiation of laser-induced forward transfer. *Applied Surface Science*. 2007;253(10):4759–4763.
<https://doi.org/10.1016/j.apsusc.2006.10.046>
9. Fardel R., Nagel M., Nuesch F. Energy balance in a laser-induced forward transfer process studied by shadowgraphy. *Journal of Physical Chemistry C*. 2009;113(27):11628–11633.
<http://dx.doi.org/10.1021/jp901340s>
10. Zhigilei L., Yingling Ya., Itina T., Schoolcraft T., Garrison B. Molecular dynamics simulations of matrix-assisted laser desorption-connections to experiment. *International Journal of Mass Spectrometry*. 2003;226(1):85–106.
[https://doi.org/10.1016/S1387-3806\(02\)00962-4](https://doi.org/10.1016/S1387-3806(02)00962-4)
11. Anisimov S.I., Luk'yanchuk B.S. Selected problems of laser ablation theory. *Physics – Uspekhi*. 2007;45(3):293. (In Russ.). <https://doi.org/10.1070/pu2002v045n03abeh000966>
Анисимов С.И., Лукьянчук Б.С. Избранные задачи теории лазерной абляции. *Успехи физических наук*. 2007; 45(3):293. <https://doi.org/10.3367/ufnr.0172.200203b.0301>
12. Zavyalova M.A. Surface modification of quartz glass by picosecond laser pulses. *Computer Optics*. 2016;40(6): 863–870. (In Russ.).
<https://doi.org/10.18287/2412-6179-2016-40-6-863-870>
Завьялова М.А. Поверхностная модификация кварцевого стекла импульсами пикосекундного лазера. *Компьютерная оптика*. 2016;40(6):863–870.
<https://doi.org/10.18287/2412-6179-2016-40-6-863-870>
13. Kuznetsov P.M., Fedorov V.A. Formation of crater relief under laser radiation on Fe – Si alloy surface. *Vestnik TGU*. 2010;15(6):1790–1793. (In Russ.).
Кузнецов П.М., Федоров В.А. Формирование рельефа кратера при воздействии лазерного излучения на поверхность сплава Fe – Si. *Вестник ТГУ*. 2010;15(6): 1790–1793.
14. Yavtushenko T.O., Kadochnikov A.S., Novikov S.G., Berintsev A.V., Stolyarov D.A. Experimental research of metal surface structuring via high power femtosecond laser pulses. *Izvestiya Samarskogo nauchnogo tsentra Rossiiskoi akademii nauk*. 2013;15(4-5):1033–1037. (In Russ.).
Явтушенко Т.О., Кадочников А.С., Новиков С.Г., Беринцев А.В., Столяров Д.А. Экспериментальное исследование процесса структурирования поверхности металла фемтосекундными лазерными импульсами высокой мощности. *Известия Самарского научного центра Российской академии наук*. 2013;15(4-5):1033–1037.
<https://doi.org/10.1051/mateconf/201816703011>
15. Kuo J.-K., Huang P.-H., Chien S.-K., Huang K.-Y., Chen K.-T. Molecular dynamics simulations of crater formation induced by laser ablation on the surface of α -Fe substrate. *MATEC Web of Conferences*. 2018;167:03011.
<https://doi.org/10.1051/mateconf/201816703011>
16. Gong X.-F., Yang G.-X., Li P., Wang Y., Ning X.-J. Molecular dynamics simulation of pulsed laser ablation. *International Journal of Modern Physics B*. 2011;25(4):543–550.
<http://dx.doi.org/10.1142/S0217979211058122>
17. Cheng C., Wu A.Q., Xu X. Molecular dynamics simulation of ultrafast laser ablation of fused silica. *Journal of Physics: Conference Series*. 2007;59:100–104.
<http://dx.doi.org/10.1088/1742-6596/59/1/022>
18. Rykalkin N.N., Uglov A.A., Zuev I.V., Kokora A.N. Laser and Electron Beam Processing of Materials: Reference Book. Moscow: Mashinostroenie; 1985:496. (In Russ.).
Рыкалкин Н.Н., Углов А.А., Зуев И.В., Кокора А.Н. Лазерная и электронно-лучевая обработка материалов. Москва: Машиностроение; 1985:496.
19. Zhigilei L.V., Levegl' E., Ivanov D.S., Lin Zh., Volkov A.N. Modeling of Short-Pulse Laser Ablation by Molecular Dynamics: Mechanisms of Material Ejection and Formation of Nanoparticles. Novosibirsk: IT SB RAS; 2009:147–220.
Жигилей Л.В., Левегль Э., Иванов Д.С., Лин Ж., Волков А.Н. Моделирование короткоимпульсной лазерной абляции методом молекулярной динамики: механизмы эжекции материала и формирования наночастиц. Новосибирск: ИТ СО РАН. 2009:147–220.
20. Andersen H.C. Molecular dynamics simulations at constant pressure and/or temperature. *The Journal of Chemical Physics*. 1980;72(4):2384–2393.
<https://doi.org/10.1063/1.439486>

Information about the Authors

Сведения об авторах

Anastasia N. Gostevskaya, Postgraduate of Chair of Science named after V.M. Finkel', Siberian State Industrial University
ORCID: 0000-0002-7328-5444
E-mail: lokon1296@mail.ru

Artem V. Markidonov, Dr. Sci. (Phys.-Math.), Assist. Prof. of the Chair of Science named after V.M. Finkel', Siberian State Industrial University; Head of the Chair of Informatics and Computer Engineering named after V.C. Butorin, Kuzbass Humanitarian Pedagogical Institute of Kemerovo State University
ORCID: 0000-0002-4566-528X
E-mail: markidonov_artem@mail.ru

Анастасия Николаевна Гостевская, аспирант кафедры естественнонаучных дисциплин им. профессора В.М. Финкеля, Сибирский государственный индустриальный университет
ORCID: 0000-0002-7328-5444
E-mail: lokon1296@mail.ru

Артем Владимирович Маркидонов, д.ф.-м.н., доцент кафедры естественнонаучных дисциплин имени В.М. Финкеля, Сибирский государственный индустриальный университет; заведующий кафедрой информатики и вычислительной техники им. В.К. Буторина, Кузбасский гуманитарно-педагогический институт Кемеровского государственного университета
ORCID: 0000-0002-4566-528X
E-mail: markidonov_artem@mail.ru

Mikhail D. Starostenkov, Dr. Sci. (Phys.-Math.), Prof., Head of the Chair of Physics, Polzunov Altai State Technical University

ORCID: 0000-0002-6326-7613

E-mail: genphys@mail.ru

Dmitrii A. Lubyanoi, Cand. Sci. (Eng.), Assist. Prof. of the Chair of Technology and Integrated Mechanization of Mining, Prokopyevsk Branch of the Kuzbass State Technical University named after T.F. Gorbachev

ORCID: 0000-0001-9773-3558

E-mail: lubjanoy@yandex.ru

Михаил Дмитриевич Старостенков, д.ф.-м.н., профессор, заведующий кафедрой физики, Алтайский государственный технический университет им. И.И. Ползунова

ORCID: 0000-0002-6326-7613

E-mail: genphys@mail.ru

Дмитрий Анатольевич Лубяной, к.т.н., доцент кафедры технологии и комплексной механизации горных работ, Филиал Кузбасского государственного технического университета им. Т.Ф. Горбачева в г. Прокопьевск

ORCID: 0000-0001-9773-3558

E-mail: lubjanoy@yandex.ru

Contribution of the Authors

Вклад авторов

A. N. Gostevskaya – formulation and implementation of computational results, literature review, writing the text.

A. V. Markidonov – building a computer model, writing a program code, visualizing and analyzing the simulation results.

M. D. Starostenkov – formulation of the research concept, discussion of the results.

D. A. Lubyanoi – discussion of the results.

А. Н. Гостевская – постановка и проведение вычислительных экспериментов, обзор литературы, написание текста статьи.

А. В. Маркидонов – построение компьютерной модели, написание программного кода, визуализация и анализ результатов моделирования.

М. Д. Старостенков – формулирование концепции исследования, обсуждение результатов.

Д. А. Лубяной – обсуждение результатов.

Received 27.10.2023

Revised 30.03.2024

Accepted 21.08.2024

Поступила в редакцию 27.10.2023

После доработки 28.03.2024

Принята к публикации 21.08.2024



UDC 669:620.19+669.15-194.56

DOI 10.17073/0368-0797-2024-5-573-578



Original article

Оригинальная статья

EFFECT OF SILICON AND VANADIUM ON CORROSION-MECHANICAL PROPERTIES OF HIGH-NITROGEN Cr – Mn STEELS

Yu. N. Goikhenberg¹, D. S. Polukhin² ¹ South Ural State University (76 Lenina Ave., Chelyabinsk 454080, Russian Federation)² LLC “Scientific and Technical Centre KONAR” (8 Eniseiskaya Str., Chelyabinsk 455030, Russian Federation)

poluhin.dmitriy@konar.ru

Abstract. The authors studied the phase composition, crystal lattice parameters, mechanical properties and stress corrosion resistance of high-nitrogen austenitic and austenitic-ferritic Cr–Mn steels after homogenizing treatment, aging and cold plastic deformation. It was established that alloying of Cr–Mn steels with silicon and vanadium can lead to the formation of different amounts of ferromagnetic δ -ferrite and, from its low content, to significant hardening due to the grain-boundary effect. The presence of δ -ferrite has a hardening effect both after homogenizing treatment and during cold plastic deformation. In vanadium-alloyed Cr–Mn steels, even after austenitization treatment at 1250 °C, a finer grain of austenite of 8–9 numbers is retained than those of steels alloyed with silicon, having after quenching from a lower temperature (1150–1170 °C) larger grain of 6–7 numbers. Formation of even small amounts of δ -ferrite leads to a decrease in corrosion cracking resistance of high-nitrogen chromium-manganese steels. At the same time, corrosion resistance of high-nitrogen steels with δ -ferrite is significantly lower than that of austenitic steels containing 0.4 % nitrogen and more single-phase Cr–Mn. Aging causes significant hardening of high-nitrogen, alloyed with both silicon and vanadium, Cr–Mn steels with δ -ferrite and is accompanied by a loss of ferromagnetism with a significant decrease in toughness and ductility. Disappearance of ferromagnetism seems to be due to the fact that δ -ferrite disintegrates into a σ -phase and a paramagnetic nitrogen-containing austenite. Microstructural and X-ray diffraction studies indicate that the aging of steel with δ -ferrite proceeds by a continuous mechanism, accompanied by a monotonous decrease in the lattice parameter of austenite due to the release of nitrides from it. Aging of two-phase steels, leading to the disappearance of δ -ferrite and ferromagnetism, caused a catastrophic decrease in corrosion cracking resistance.

Keywords: high-nitrogen Cr – Mn steels, δ -ferrite, microstructure, mechanical properties, stress corrosion resistance

For citation: Goikhenberg Yu.N., Polukhin D.S. Effect of silicon and vanadium on corrosion-mechanical properties of high-nitrogen Cr – Mn steels. *Izvestiya. Ferrous Metallurgy*. 2024;67(5):573–578. <https://doi.org/10.17073/0368-0797-2024-5-573-578>

ВЛИЯНИЕ КРЕМНИЯ И ВАНАДИЯ НА КОРРОЗИОННО-МЕХАНИЧЕСКИЕ СВОЙСТВА ВЫСОКОАЗОТИСТЫХ Cr – Mn СТАЛЕЙ

Ю. Н. Гойхенберг¹, Д. С. Полухин² ¹ Южно-Уральский государственный университет (Россия, 454080, Челябинск, пр. Ленина, 76)² ООО «Научно-технический центр Конар» (Россия, 454010, Челябинск, Енисейская ул., 8)

poluhin.dmitriy@konar.ru

Аннотация. Исследованы фазовый состав, параметры кристаллической решетки, механические свойства и коррозионная стойкость под напряжением высокоазотистых аустенитных и аустенито-ферритных Cr–Mn сталей после гомогенизирующей обработки, старения и холодной пластической деформации. Установлено, что легирование Cr–Mn сталей кремнием и ванадием может приводить к образованию разных количеств ферромагнитного δ -феррита и уже с малых его содержаний к существенному упрочнению, обусловленному зернограничным эффектом. Присутствие δ -феррита оказывает упрочняющий эффект как после гомогенизирующей обработки, так и при холодной пластической деформации. В легированных ванадием Cr–Mn сталях даже после аустенитизирующей обработки при 1250 °C сохраняется более мелкое зерно аустенита 8–9 номера, чем у сталей, легированных кремнием, имеющих после закалки от более низкой температуры (1150–1170 °C) большее по размеру зерно 6–7 балла. Образование даже небольших количеств δ -феррита приводит к снижению сопротивления коррозионному растрескиванию высокоазотистых хромомарганцевых сталей. При этом сопротивление коррозионному растрескиванию высокоазотистых сталей с δ -ферритом оказывается значительно ниже, чем у содержащих 0,4 % азота

и более однофазных Cr–Mn аустенитных сталей. Старение вызывает существенное упрочнение высокоазотистых, легированных как кремнием, так и ванадием, Cr–Mn сталей с δ-ферритом и сопровождается потерей ферромагнетизма при значительном уменьшении ударной вязкости и пластичности. Исчезновение ферромагнетизма, по-видимому, обусловлено тем, что происходит распад δ-феррита на σ-фазу и парамагнитный азотсодержащий аустенит. Микроструктурные и рентгеноструктурные исследования свидетельствуют о том, что старение стали с δ-ферритом протекает по непрерывному механизму, сопровождающемуся монотонным снижением параметра решетки аустенита в связи с выделением из него нитридов. Старение двухфазных сталей, приводящее к исчезновению δ-феррита и ферромагнетизма, вызвало катастрофическое снижение стойкости против коррозионного растрескивания.

Ключевые слова: высокоазотистые Cr – Mn стали, δ-феррит, микроструктура, механические свойства, коррозионная стойкость под напряжением

Для цитирования: Гойхенберг Ю.Н., Полухин Д.С. Влияние кремния и ванадия на коррозионно-механические свойства высокоазотистых Cr – Mn сталей. *Известия вузов. Черная металлургия.* 2024;67(5):573–578. <https://doi.org/10.17073/0368-0797-2024-5-573-578>

INTRODUCTION

When assessing the prospects, sequence of adoption, and results of carbon-free technologies in metallurgy, it has been noted [1] that nitrogen could serve as an alternative to carbon as a strengthening element in steel, providing greater strengthening than carbon in traditional steels [2; 3]. Corrosion-resistant high-nitrogen steels have been developed, containing at least 12 wt. % chromium, which exhibit high static and cyclic strength, wear resistance, and enhanced capability for plastic deformation while maintaining good ductility and impact toughness [4; 5]. It is known that austenitic Cr–Ni and Cr–Mn steels, as well as corrosion-resistant martensitic and austenitic-martensitic steels, have low resistance to stress corrosion cracking (SCC) [6]. Higher long-term corrosion resistance is observed in ferritic and austenitic-ferritic steels. Austenitic high-nitrogen Cr – Mn steels, which are also highly resistant to hydrogen embrittlement and possess high corrosion fatigue strength, have demonstrated resistance to SCC in various environments [7 – 10].

The studies [10; 11] examined the influence of silicon on the fine structure and wear resistance of high-nitrogen Cr–Mn steels under dry sliding friction. It was established that alloying with silicon improves resistance to adhesive wear while maintaining low friction coefficients ($f = 0.25 – 0.33$). The effect of silicon on the tribological properties of these steels is associated with the activation of planar dislocation slip. Additionally, in [10], it is noted that metastable austenitic Cr–Mn steels, alloyed

with 0.15 – 0.25 wt. % nitrogen, exhibit increased resistance to cavitation-erosion damage [12] and abrasive wear [13], which is largely explained by the formation of deformation-induced α-martensite under contact loading. The high resistance of Nitronic 60 steel to adhesive wear is attributed by the authors [14; 15] to the low stacking fault energy of austenite, the steel’s ability for intensive strain hardening, and the formation of oxide films on the friction surface that prevent galling.

It is of interest to evaluate the SCC resistance of nitrogen-containing Cr–Mn steels with an austenitic-ferritic structure. The aim of this study is to investigate the influence of certain ferrite-forming elements (such as silicon and vanadium) on the corrosion-mechanical properties of Cr–Mn steels.

MATERIALS AND METHODS

The steels were melted under normal conditions at atmospheric pressure in a 60-kg induction furnace. The chemical composition of the studied steels is shown in Table 1. The sulfur and phosphorus content in all the melted steels did not exceed 0.01 and 0.04 wt. %, respectively. The ingots of nitrogen-containing steels were homogenized at 1150 °C for 8 – 15 h and forged into bars with a cross-section of 20×20 mm². From these, standard fivefold tensile test specimens with a working diameter of 5 mm and standard specimens with a 10×10 mm² cross-section and a U-shaped notch were prepared for impact toughness testing.

Table 1. Chemical composition of high-nitrogen Cr – Mn steels and content of δ-ferrite in them

Таблица 1. Химический состав высокоазотистых Cr – Mn сталей и содержание в них δ-феррита

Steel grade	Element content, wt. %						Amount of δ-ferrite, %
	N	Si	V	Cr	Mn	C	
10Kh16G17S4A0.3	0.28	4.50	0.09	16.0	17.1	0.11	3
12Kh19G19S2A0.5	0.50	2.37	0.13	19.3	19.4	0.13	0
10Kh19G20S4A0.5	0.52	4.30	0.18	19.6	20.3	0.10	32
07Kh18G19FA0.4	0.42	0.49	1.04	17.5	18.9	0.07	5
07Kh19G18FA0.7	0.73	0.35	1.07	18.8	18.0	0.07	0

The ultimate tensile strength and yield strength of the steels were determined with an error margin of ±5 MPa, and the elongation was measured with an accuracy of 0.1 %. SCC (stress corrosion cracking) tests were conducted using a specially developed method [16] in a 20 % aqueous sodium chloride solution in distilled water at room temperature and at stresses ranging from 0.80 to 0.95 of the yield strength.

The microstructure was studied using an Axio Observer.D1m optical microscope. Magnetic measurements were performed on an α-phase meter, which records the content of δ-ferrite.

X-ray diffraction studies were conducted on a DRON-4-07 diffractometer using iron radiation. Qualitative and quantitative phase analysis was performed using the Rietveld method [17], following the optimization of interference maxima. The accuracy of the quantitative phase analysis was ±5 %. Precision measurements of the austenite lattice parameter were carried out using the final interference lines 311_{α1} and 222_{α1}, recorded in discrete mode with a step of 0.02° [18; 19].

RESULTS AND DISCUSSION

X-ray diffraction and magnetometric phase analysis indicate that Cr–Mn steels 12Kh19G19S2A0.5 and 07Kh19G18FA0.7 are in the austenitic state (Table 1). In steels with lower nitrogen content, a small amount (3 – 5 %) of the ferromagnetic δ-ferrite phase is additionally present, while in steel with 4 % silicon, the δ-ferrite content reaches 32 %. Dispersed grains of δ-ferrite of various shapes and sizes are mainly located along the boundaries of austenite grains (Fig. 1).

Steels alloyed with silicon, after homogenizing treatment at 1150 – 1170 °C, exhibited the same austenite grain size, corresponding to 6 – 7 numbers. In vanadium-alloyed steels, even after austenitizing treatment at 1250 °C, a finer austenite grain size of 8 – 9 numbers was retained.

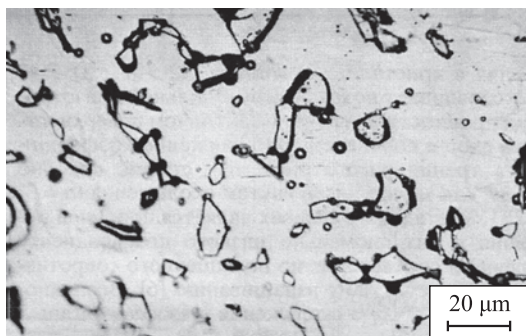


Fig. 1. Microstructure of quenched from 1100 °C 10Kh19G20S4A0.5 steel with δ-ferrite

Рис. 1. Микроструктура закаленной от 1100 °C стали 10X19Г20С4А0,5 с δ-ферритом

The mechanical properties of the steels after homogenizing treatment are shown in Table 2. For comparison, the lower part of the table provides the mechanical properties of similar Cr–Mn austenitic steels with a similar nitrogen concentration but not alloyed with silicon or vanadium. It can be seen that at equal nitrogen concentrations, steels containing δ-ferrite have higher strength properties and lower values of elongation and impact toughness compared to austenitic steels not alloyed with silicon or vanadium, which promote the formation of ferrite.

High-nitrogen Cr–Mn steels containing δ-ferrite, like similar austenitic steels, are significantly hardened during cold plastic deformation while maintaining good ductility. The hardening degree (Δσ/Δε) of steels with different nitrogen and silicon concentrations, as well as the critical degree of cold deformation (e_{cr}) required to achieve a yield strength of 1200 N/mm² in some critical components (e.g., retaining rings of powerful turbogenerators), are shown in Table 3.

In terms of these parameters, austenitic-ferritic steels containing 0.3 – 0.5 % nitrogen and 4 % silicon were found to be comparable to steels not alloyed with silicon but containing a higher nitrogen content. At the same time, alloying austenitic steel 12Kh19G19S2A0.5 with 2 % silicon had virtually no effect on the hardening degree or the critical deformation degree e_{cr}. These parameters were similar to those of steel 08Kh18G18A0.5. Thus, it can be inferred that the presence of δ-ferrite has a hardening effect (grain-boundary hardening), both after homogenizing treatment and during cold plastic deformation.

At the same time, even the formation of small amounts of δ-ferrite reduces the stress corrosion cracking (SCC) resistance of high-nitrogen Cr–Mn steels. For instance, while the formation of 3 % δ-ferrite in steel 10Kh16G17S4A0.3 did not significantly affect

Table 2. Mechanical properties of high-nitrogen steels after homogenizing treatment

Таблица 2. Механические свойства высокоазотистых сталей после гомогенизирующей обработки

Steel grade	σ _{0.2} , N/mm ²	σ _u , N/mm ²	δ, %	Ψ, %	KCU, J/cm ²
10Kh16G17S4A0.3	465	908	66	63	287
12Kh19G19S2A0.5	522	924	65	72	–
10Kh19G20S4A0.5	590	982	52	61	–
07Kh18G19FA0.4	530	890	46	63	122
07Kh19G18FA0.7	720	1100	43	62	181
05Kh14G20A0.3	350	720	68	74	–
08Kh18G18A0.5	530	910	67	73	360
08Kh19G19A0.7	570	990	63	72	300

Table 3. Hardening degree ($\Delta\sigma/\Delta\epsilon$) during cold plastic deformation by 15, 30, 40 % and critical deformation degree (e_{cr}) for different Cr – Mn steels

Таблица 3. Степень упрочнения ($\Delta\sigma/\Delta\epsilon$) при холодной пластической деформации на 15, 30, 40 % и критическая степень деформации (e_{cr}) для разных Cr – Mn сталей

Steel grade	$\Delta\sigma/\Delta\epsilon$ for various degrees of deformation, %			e_{cr} , %	SCC test duration, h
	15	30	40		
10Kh16G17S4A0.3	56.0	36.2	30.5	37	450 – 500 √
12Kh19G19S2A0.5	56.0	37.0	31.2	36	3000 ^
10Kh19G20S4A0.5	65.4	41.6	34.2	27	300 – 2000 √
05Kh14G20A0.3	42.0	29.0	24.7	50	430 – 550 √
08Kh18G18A0.5	55.0	36.7	31.0	36	5000 ^
08Kh19G19A0.7	66.0	42.0	34.7	26	5300 ^

Note: √ – samples failed during SCC testing; ^ – samples were withdrawn from testing without signs of SCC.

SCC resistance compared to the similar silicon-free austenitic steel 05Kh14G20N4A0.3, which has low resistance, the presence of 32 % δ -ferrite in steel 10Kh19G20S4A0.5 drastically reduced its SCC resistance compared to the austenitic steel 08Kh18G18A0.5, which is not susceptible to SCC [20 – 22] (Table 3). In the case of silicon alloying while retaining the austenitic structure (steel 12Kh19G19S2A0.5), no reduction in SCC resistance is observed. Similarly, the presence of δ -ferrite affects vanadium-alloyed steels. For example, the two-phase steel 07Kh18G19FA0.4 is prone to SCC within 250 – 750 h under stresses of 1050 – 1150 N/mm², while austenitic steel 07Kh19G18FA0.7, subjected to the same stress levels, was removed from testing after 5000 h without any signs of SCC.

Aging causes significant hardening of high-nitrogen Cr–Mn steels alloyed with both silicon and vanadium,

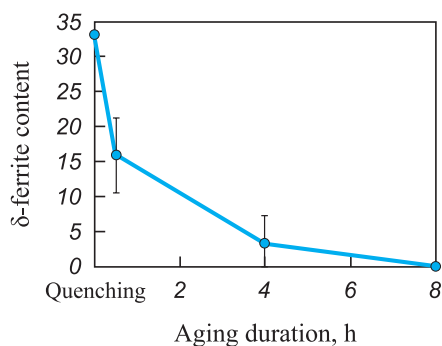


Fig. 2. Change in the content of δ -ferrite in 10Kh19G20S4A0.5 steel depending on duration of aging at 700 °C

Рис. 2. Изменение содержания δ -феррита в стали 10X19Г20С4А0,5 в зависимости от продолжительности старения при 700 °С

converting them into a non-magnetic state. For example, the yield strength of the vanadium-containing high-nitrogen steel 07Kh18G19FA0.4 with 5 % δ -ferrite increases by 290 N/mm² after 16 h at 650 °C, whereas in the austenitic steel 07Kh19G18FA0.7, it increases by only 190 N/mm² compared to homogenizing treatment, with a significant decrease in impact toughness and ductility in both steels. The negative effect of vanadium and silicon on ductility and impact toughness is also noted in aging carbon-containing austenitic steels [23]. It is worth noting that in the high-nitrogen steel alloyed with silicon and containing 32 % δ -ferrite, hardness increases to 35 – 37 HRC after 2 – 4 h at 700 °C, comparable to the hardness of highly tempered alloy steels with 0.4 % carbon.

It should be noted that after aging, steels with δ -ferrite become non-magnetic, apparently due to its decomposition (according to the phase diagram) into the σ -phase and paramagnetic nitrogen-containing austenite. In this case, the content of δ -ferrite decreases monotonically with increasing aging time (Fig. 2). Microstructural and X-ray diffraction studies (Fig. 3) indicate that the aging of steel with δ -ferrite proceeds by a continuous mechanism, accompanied by a gradual decrease in the austenite lattice parameter due to the precipitation of nitrides. At the same time, in high-nitrogen Cr–Mn austenitic steels containing more than 0.3 % nitrogen and not alloyed with silicon, the intermittent decomposition of austenite becomes significantly more pronounced during aging [24].

Aging of two-phase steels, leading to the disappearance of δ -ferrite, resulted in a catastrophic decrease in SCC resistance. Aged samples experienced stress corrosion cracking under the selected test conditions within 10 – 70 h.

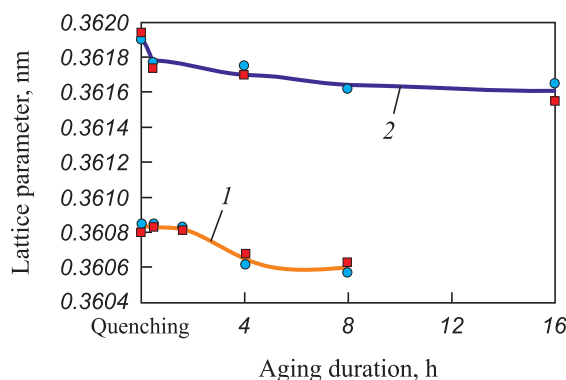


Fig. 3. Dependence of austenite lattice parameter of steels 10Kh16G17S4A0.3 (1) and 10Kh19G20S4A0.5 (2) on duration of aging at 700 °C: ● – calculation by line 311_{a1}; ■ – calculation by line 222_{a1}

Рис. 3. Зависимость параметра решетки аустенита сталей 10X16Г17С4А0,3 (1) и 10X19Г20С4А0,5 (2) от продолжительности старения при 700 °С: ● – расчет по линии 311_{a1}; ■ – расчет по линии 222_{a1}

CONCLUSIONS

Alloying high-nitrogen Cr–Mn steels with silicon or vanadium leads to the formation of δ -ferrite and significant hardening, both after homogenizing treatment and during cold plastic deformation, which is due to the grain-boundary effect.

In vanadium-alloyed Cr–Mn steels, even after austenitizing treatment at 1250 °C, a finer austenite grain size (8 – 9 numbers) is retained compared to silicon-alloyed steels, which exhibit a coarser grain size (6 – 7 numbers) after quenching at 1150 – 1170 °C.

The formation of even small amounts (3 – 5 %) of δ -ferrite in high-nitrogen Cr–Mn austenitic steels, along with hardening, leads to a reduction in stress corrosion cracking resistance.

Aging is accompanied by a further reduction in stress corrosion resistance, the disappearance of magnetism, and significant hardening of high-nitrogen Cr–Mn steels containing δ -ferrite, likely due to its decomposition into the σ -phase and nitrogen-containing paramagnetic austenite, as well as the precipitation of nitrides.

REFERENCES / СПИСОК ЛИТЕРАТУРЫ

- Roshchin V.E., Roshchin A.V., Kuznetsov Yu.S., Goikhenberg Yu.N. Technological and materials science aspects of the transition in ferrous metallurgy to carbon-free processes. *Chernye metally*. 2021;(11):10–17. (In Russ.). <https://doi.org/10.17580/chm.2021.11.02>
Рошин В.Е., Рошин А.В., Кузнецов Ю.С., Гойхенберг Ю.Н. Технологические и материаловедческие аспекты перехода в черной металлургии на безуглеродные процессы. *Черные металлы*. 2021;(11):10–17. <https://doi.org/10.17580/chm.2021.11.02>
- Rashev Ts.V. High Nitrogen Steels. Metallurgy under Pressure: Monograph. Sofia: Bulg. Acad. Sci. “Prof. Marin Drinov”; 1995:268. (In Russ.).
Рашев Ц.В. Высокоазотистые стали. Металлургия под давлением. София: Издательство Болгарской АН «Проф. Марин Дринов»; 1995:268.
- Vannykh O.A., Blinov V.M., Kostina M.V. Nitrogen as an alloying element in iron-based alloys. Phase and structural transformations in steels. In: *Phase and Structural Transformations in Steels: Collection of Sci. Papers. Vol. 3*. Urtsev V.N. ed. Magnitogorsk; 2003:576. (In Russ.).
Банная О.А., Блинов В.М., Костина М.В. Азот как легирующий элемент в сплавах на основе железа. В сборнике научных трудов: *Фазовые и структурные превращения в сталях. Выпуск 3*. Под ред. В.Н. Урцева. Магнитогорск; 2003:576.
- Kostina M.V., Rigina L.G. Nitrogen-containing steels and methods of their production. *Izvestiya. Ferrous Metallurgy*. 2020;63(8):606–622. (In Russ.). <https://doi.org/10.17073/0368-0797-2020-8-606-622>
Костина М.В., Ригина Л.Г. Азотсодержащие стали и способы их производства. *Известия вузов. Черная металлургия*. 2020;63(8):606–622. <https://doi.org/10.17073/0368-0797-2020-8-606-622>
- Singhal L.K. Characteristics, distinctive advantages & wide ranging applications of chrome-manganese stainless steels. *Advanced Materials Research*. 2013;794:103–116. <https://doi.org/10.4028/www.scientific.net/amr.794.103>
- Goldstein M.I., Grachev S.V., Veksler Yu.G. Special Steels. Moscow: Metallurgiya; 1985:270–271. (In Russ.).
Гольдштейн М.И., Грачев С.В., Векслер Ю.Г. Специальные стали. Москва: Металлургия; 1985:270–271.
- Stein G. Generator-Kappenringe aus nichtmagnetisierbaren Stählen ihre mechanisch-technologischen Werkstoffkennwerte und ihr Widerstand gegen Korrosion. *VGB Kraftwerkstechnik*. 1985;65(11):1069–1074. (In Germ.).
- Speidel M.O. Nichtmagnetisierbare Stähle für Generator-Kappenringe, ihr Widerstand gegen Korrosionsermüdung. *VGB Kraftwerkstechnik*. 1981;61(12):1048–1053. (In Germ.).
- Goikhenberg Yu.N., Zhuravlev L.G., Mirzaev D.A., Zhuravleva V.V., Silina E.P., Vnukov V.Yu. Investigation of corrosion cracking, structure and properties of Cr–Mn hardened austenitic steels with nitrogen. *Fizika metallov i metallove-denie*. 1988;65(6):1131–1137. (In Russ.).
Гойхенберг Ю.Н., Журавлев Л.Г., Мирзаев Д.А., Журавлева В.В., Силина Е.П., Внук В.Ю. Исследование коррозионного растрескивания, структуры и свойств упрочненных Cr–Mn аустенитных сталей с азотом. *Физика металлов и металловедение*. 1988;65(6):1131–1137.
- Korshunov L.G., Goikhenberg Yu.N., Chernenko N.L. Effect of silicon on the structure, tribological behavior, and mechanical properties of nitrogen-containing chromium-manganese austenitic steels. *Physics of Metals and Metallography*. 2003;96(5):535–544.
Коршунов Л.Г., Гойхенберг Ю.Н., Черненко Н.Л. Влияние кремния на структуру, трибологические и механические свойства азотсодержащих хромомарганцевых аустенитных сталей. *Физика металлов и металловедение*. 2003;96(5):100–110.
- Korshunov L.G., Goikhenberg Yu.N., Chernenko N.L. Microstructure, tribological and mechanical properties of nitrogen-containing stainless austenitic steels based on chromium manganese. In: *Phase and Structural Transformations in Steels: Collection of Sci. Papers. Vol. 3*. Urtsev V.N. ed. Magnitogorsk; 2003:576.
Коршунов Л.Г., Гойхенберг Ю.Н., Черненко Н.Л. Микроструктура, трибологические и механические свойства азотсодержащих нержавеющей аустенитных сталей на хромомарганцевой основе. В сборнике научных трудов: *Фазовые и структурные превращения в сталях. Выпуск 3*. Под ред. В.Н. Урцева. Магнитогорск; 2003:215–242.
- Bogachev I.N. Cavitation Destruction and Cavitation-Resistant Alloys. Moscow: Metallurgiya; 1972:189.
Богачев И.Н. Кавитационное разрушение и кавитационно-стойкие сплавы. Москва: Металлургия; 1972:189.
- Lenel U.R., Knott B.R. Structure and properties of corrosion and wear resistant Cr–Mn–N steels. *Metallurgical Transactions A*. 1987;18:847–855. <https://doi.org/10.1007/BF02646926>
- Schumacher W.J. Stainless steel alternative to cobalt wear alloys. *Chemical Engineering*. 1981;88(19):149–152.

15. Ohriner R.K., Wada T., Whelan E.P., Ocken H. The chemistry and structure of wear-resistant, iron-base hardfacing alloys. *Metallurgical and Materials Transactions A*. 1991;22(5): 983–991. <https://doi.org/10.1007/BF02661091>
16. Zhuravlev L.G., Zhuravleva V.V., Goikhenberg Yu.N., Mirzaev D.A. Methodology of accelerated testing of plastic deformed metals for corrosion cracking. *Zavodskaya laboratoriya*. 1992;58(3):44–46.
Журавлев Л.Г., Журавлева В.В., Гойхенберг Ю.Н., Мирзаев Д.А. Методика ускоренных испытаний пластичных деформированных металлов на коррозионное растрескивание. *Заводская лаборатория*. 1992;58(3):44–46.
17. Krzhizhanovskaya M.G., Firsova V.A., Bubnova R.S. Application of the Rietveld Method for Solving Problems of Powder Diffractometry: Textbook. Saint Petersburg University; 2016:67.
Кржижановская М.Г., Фирсова В.А., Бубнова Р.С. Применение метода Ритвельда для решения задач порошковой дифрактометрии: Учебное пособие. Санкт-Петербургский университет; 2016:67.
18. Umanskii Ya.S., Skakov Yu.A., Ivanov A.N., Rastorguev L.N. Crystallography, Radiography and Electron Microscopy. Moscow: Metallurgiya; 1980.
Уманский Я.С., Скаков Ю.А., Иванов А.Н., Расторгуев Л.Н. Кристаллография, рентгенография и электронная микроскопия. Москва: Металлургия; 1980.
19. Gorelik S.S., Skakov Yu.A., Rastorguev L.N. Radiographic and Electron-Optical Analysis. Moscow: MISIS; 1994:328.
Горелик С.С., Скаков Ю.А., Расторгуев Л.Н. Рентгенографический и электронно-оптический анализ. Москва: МИСИС; 1994:328.
20. Speidel M.O. Nitrogen containing austenitic stainless steels. *Materialwissenschaft und Werkstofftechnik*. 2006; 37(10):875–880. <https://doi.org/10.1002/mawe.200600068>
21. Rashev Ts.V., Eliseev A.V., Zhekova L.Ts., Bogeve P.V. High nitrogen steels. *Izvestiya. Ferrous Metallurgy*. 2019;62(7):503–510. (In Russ.).
<https://doi.org/10.17073/0368-0797-2019-7-503-510>
Рашев Ц.В., Елисеев А.В., Жекова Л.Ц., Богев П.В. Высокоазотистые стали. *Известия вузов. Черная металлургия*. 2019;62(7):503–510.
<https://doi.org/10.17073/0368-0797-2019-7-503-510>
22. Oldfield J.W. Crevice corrosion resistance of commercial and high purity experimental stainless steels in marine environments – the influence of N, Mn, and S. *Corrosion*. 1990;46(7):574–581. <https://doi.org/10.5006/1.3585151>
23. Bannykh O.A., Blinov V.M. Dispersion-Hardening Non-Magnetic Vanadium-Containing Steels. Moscow: Nauka; 1980:189.
Баных О.А., Блинов В.М. Дисперсионно-твердеющие немагнитные ванадийсодержащие стали. Москва: Наука; 1980:189.
24. Goikhenberg Yu.N., Mirzaev D.A., Mirmel'stein V.A., Vnukov V.Yu., Lobanova T.G. Structure and corrosion-mechanical properties of high-nitrogen Cr–Mn steels with vanadium hardened by aging and cold deformation. *Fizika metallov i metallovedenie*. 1991;(8):176–182.
Гойхенберг Ю.Н., Мирзаев Д.А., Мирмельштейн В.А., Внук В.Ю., Лобанова Т.Г. Структура и коррозионно-механические свойства высокоазотистых Cr–Mn сталей с ванадием, упрочненных старением и холодной деформацией. *Физика металлов и металловедение*. 1991;(8):176–182.

Information about the Authors

Сведения об авторах

Yurii N. Goikhenberg, Dr. Sci. (Eng.), Senior Researcher, Prof. of the Chair of Materials Science and Physical Chemistry of Materials, South Ural State University

E-mail: goikhenbergyn@susu.ru

Dmitrii S. Polukhin, Cand. Sci. (Eng.), Executive Director, LLC "Scientific and Technical Centre KONAR"

E-mail: polukhin.dmitriy@konar.ru

Юрий Нафтулович Гойхенберг, д.т.н., старший научный сотрудник, профессор кафедры «Материаловедение и физико-химия материалов», Южно-Уральский государственный университет

E-mail: goikhenbergyn@susu.ru

Дмитрий Сергеевич Полухин, к.т.н., исполнительный директор, ООО «Научно-технический центр КОНАР»

E-mail: polukhin.dmitriy@konar.ru

Received 20.03.2024

Revised 02.04.2024

Accepted 23.08.2024

Поступила в редакцию 20.03.2024

После доработки 02.04.2024

Принята к публикации 23.08.2024



UDC 669.017: 669.162.275.12

DOI 10.17073/0368-0797-2024-5-579-592



Original article

Оригинальная статья

MICROHETEROGENEOUS STRUCTURE OF LIQUID CAST IRONS IChKh28N2 AND ICh310Kh24M2F4TR

V. S. Tsepelev¹, N. I. Sinitsin¹, O. A. Chikova¹✉,M. G. Potapov², V. V. V'yukhin¹

¹Ural Federal University named after the first President of Russia B.N. Yeltsin (19 Mira Str., Yekaterinburg 620002, Russian Federation)

²Nosov Magnitogorsk State Technical University (38 Lenina Ave., Magnitogorsk, Chelyabinsk Region 455000, Russian Federation)

✉ chik63@mail.ru

Abstract. The paper presents original experimental data on the viscosity and electrical resistivity of liquid cast irons IChKh28N2 and ICh310Kh24M2F4TR.

The authors discuss the measurement results within the framework of the concept of metal melts microheterogeneity. Liquid cast iron in a microheterogeneous state is considered as a dispersed system consisting of dispersed Fe – 30 % Cr particles distributed in a Fe – 3 % C dispersion medium. The concept of colloidal microheterogeneity (microheterogeneity) of Fe–C melts was first formulated by Wertman & Samarin more than 80 years ago and found another confirmation in this work. The introduction of theoretical approaches to the rheology of dispersed systems into the analysis of the temperature dependences of the viscosity of microheterogeneous melts made it possible to estimate the parameters of microheterogeneity: the volume fraction and size of dispersed particles. The volume fraction of dispersed particles was determined using the Taylor equation for the viscosity of dispersed systems and size of dispersed particles – within the framework of the theory of absolute reaction rates. Analysis of the temperature dependences of microheterogeneous melts electrical resistivity within the framework of the theory of transport phenomena (in this case, conductivity) in inhomogeneous media (microheterogeneous melts) made it possible to estimate the volume fraction of dispersed particles. The volume fraction of dispersed particles based on data on the electrical resistivity of liquid cast iron was determined using the Odelevsky equation for the inhomogeneous media conductivity. The cluster size was determined by the ratio of the melt electrical resistivity at the liquidus temperature and the analysis temperature, taking into account the known data for the mean free path and the electron scattering coefficient of liquid iron. The volume fraction of dispersed particles in liquid cast iron was 0.2 – 0.1 at the liquidus temperature. With increasing temperature, the volume fraction of dispersed particles decreases. The cluster size in liquid cast iron was about 3 nm at the liquidus temperature, and with increasing temperature the cluster size decreased to 1 – 2 nm. The results obtained are of practical importance: increasing the performance properties of cast iron castings is possible by high-temperature melt treatment (HTMT) in order to change the crystallization conditions and obtain a modified structure. Studies of the microheterogeneous structure of liquid cast irons and assessment of microheterogeneity parameters make it possible to substantiate and propose the optimal HTMT mode in order to improve the performance characteristics of products made of wear-resistant cast irons alloyed with chromium.

Keywords: melt, cast iron, microheterogeneity, conductivity of inhomogeneous media, viscosity of dispersions, dispersed particles, melt temperature treatment, kinematic viscosity, electrical resistivity

Acknowledgements: The article was performed within the framework of state assignment No. FEUZ-2023-0015.

For citation: Tsepelev V.S., Sinitsin N.I., Chikova O.A., Potapov M.G., V'yukhin V.V. Microheterogeneous structure of liquid cast irons IChKh28N2 and ICh310Kh24M2F4TR. *Izvestiya. Ferrous Metallurgy*. 2024;67(5):579–592. <https://doi.org/10.17073/0368-0797-2024-5-579-592>

МИКРОГЕТЕРОГЕННОЕ СТРОЕНИЕ ЖИДКИХ ЧУГУНОВ ИЧХ28Н2, ИЧ310Х24М2Ф4ТР

В. С. Цепелев¹, Н. И. Синицин¹, О. А. Чикова¹✉,
М. Г. Потапов², В. В. Вьюхин¹

¹ Уральский федеральный университет имени первого Президента России Б.Н. Ельцина (Россия, 620002, Екатеринбург, ул. Мира, 19)

² Магнитогорский государственный технический университет им. Г.И. Носова (Россия, 455000, Челябинская обл., Магнитогорск, пр. Ленина, 38)

✉ chik63@mail.ru

Аннотация. Приведены оригинальные экспериментальные данные о вязкости и удельном электросопротивлении жидких чугунов ИЧХ28Н2, ИЧ310Х24М2Ф4ТР. Результаты измерений рассмотрены в рамках представлений о микрогетерогенности металлических расплавов. Жидкий чугун в микрогетерогенном состоянии понимался как дисперсная система, состоящая из дисперсных частиц Fe – 30 % Cr, распределенных в дисперсионной среде Fe – 3 % C. Представления о коллоидной микронеоднородности (микрогетерогенности) расплавов Fe–C впервые сформулированы А.А. Вертманом и А.М. Самариным более 80 лет назад и нашли еще одно подтверждение в данной работе. Привнесение теоретических подходов реологии дисперсных систем в анализ температурных зависимостей вязкости микрогетерогенных расплавов позволило оценить параметры микрогетерогенности: объемную долю и их размер. Определение объемной доли дисперсных частиц проводилось по уравнению Тейлора для вязкости дисперсных систем и размера дисперсных частиц в рамках представлений теории абсолютных скоростей реакций. Анализ температурных зависимостей удельного электросопротивления микрогетерогенных расплавов в рамках теории явлений переноса (в данном случае проводимости) в неоднородных средах (микрогетерогенных расплавах) дал возможность оценки объемной доли дисперсных частиц. Объемную долю дисперсных частиц по данным об удельном электросопротивлении жидких чугунов определяли из уравнения Оделевского для проводимости неоднородных сред. Установлены размер кластера из соотношения величин удельного электросопротивления расплава при температуре ликвидус и температуре анализа с учетом известных данных для длины свободного пробега и коэффициент рассеяния электронов жидкого железа. Величина объемной доли дисперсных частиц в жидких чугунах составила 0,2 – 0,1 вблизи температуры ликвидус. С повышением температуры объемная доля дисперсных частиц уменьшается. Размер кластера в жидком чугуне составил около 3 нм вблизи температуры ликвидус, с повышением температуры размер кластера снижается до 1 – 2 нм. Полученные результаты имеют практическое значение: повышение эксплуатационных свойств отливок из чугунов возможно путем высокотемпературной обработки расплава (ВТОР) с целью изменения условий кристаллизации и получения модифицированной структуры. Исследования микрогетерогенного строения жидких чугунов и оценка параметров микрогетерогенности позволит обосновать и предложить оптимальный режим ВТОР с целью повышения эксплуатационных характеристик изделий из износостойких чугунов, легированных хромом.

Ключевые слова: расплав, чугуны, микрогетерогенность, проводимость неоднородных сред, вязкость дисперсий, дисперсные частицы, температурная обработка расплава, кинематическая вязкость, удельное электросопротивление

Благодарности: Статья выполнена в рамках государственной работы № FEUZ-2023-0015.

Для цитирования: Цепелев В.С., Синицин Н.И., Чикова О.А., Потапов М.Г., Вьюхин В.В. Микрогетерогенное строение жидких чугунов ИЧХ28Н2, ИЧ310Х24М2Ф4ТР. *Известия вузов. Черная металлургия.* 2024;67(5):579–592.

<https://doi.org/10.17073/0368-0797-2024-5-579-592>

INTRODUCTION

The development of concepts regarding the microinhomogeneous structure of complex alloyed metallic melts is relevant from a practical perspective for the scientific justification of selecting temperature-time treatment modes. The discussion of structural transitions related to the irreversible destruction of microinhomogeneities when heating a melt to a specific temperature T^* for each composition makes this justification possible. Measuring the temperature dependencies of viscosity, density, electrical resistivity, and surface tension of the melt allows determining the temperature T^* , explaining it through a structural transition caused by the destruction of microinhomogeneities. Numerous experiments have shown that after the structural transition, upon subsequent cooling and crystallization, an ingot with a modified-like structure is formed, which exhibits better mechanical

properties. The mechanism of structural transitions in complex alloyed metallic melts involves the destruction of microinhomogeneity not only in structure but also in chemical composition. Anomalies in the temperature and concentration dependencies of the structurally sensitive properties of metallic melts – viscosity, density, electrical resistivity, and surface tension – are caused by changes in the melt structure. Microinhomogeneities, which arise due to the predominant interaction of atoms of the same or different types, correspond to the disruption of short-range order (SRO) in the atomic arrangement and range between 2 – 5 Å. The microinhomogeneous state of metallic melts, which is due to the segregation of atoms of a fluctuational nature without clear interfacial boundaries (clusters), is associated with the disruption of medium-range order (MRO) and ranges between 5 – 20 Å. The microheterogeneous state of the melt, characterized by the presence of dispersed particles

enriched with one component suspended in a surrounding medium of a different composition with a distinct interphase surface, corresponds to the disruption of long-range order (LRO) and a range of more than 20 Å [1]. In work [2], the primary focus is on studying impurity effects corresponding to SRO in complex alloyed melts, including investigations of the structure and properties of iron-based melts aimed at improving cast iron and steel production technologies. From a methodological point of view, alongside direct diffraction studies of the structure, a large amount of information is provided by measuring physical properties such as magnetic susceptibility, electrical resistivity, viscosity, and density. For example, magnetic susceptibility together with electrical resistivity forms a pair of electron-sensitive properties that allow assessing the character of short-range order in the system, the distribution of impurities, and alloying effects. Studying the entire set of properties makes it possible to influence the melt by applying small additives. The oscillatory nature of their influence facilitates achieving significant effects through small concentration changes. Moreover, the possibility arises to control the melt structure and the primary crystallization process.

The results of calculations of the radii of microgroupings around carbon atoms in iron and the electronic characteristics of diluted Fe–C–O alloys are presented [2]. Concepts of the cluster structure of metallic liquids, which are due to the segregation of atoms of a fluctuational nature without distinct interphase boundaries (clusters), associated with the disruption of MRO and a range of 5 – 20 Å, are consistently developed by G.V. Tyagunov. The cluster structure of metallic liquids can be described in physical terms if the quantity, composition, and size of clusters, the number of atoms in the clusters, the lifetime of clusters, etc., are known. In this case, the clusters have significant sizes $R_{cl} \geq (10 - 25) \cdot 10^{-10}$ m [3].

The concept of colloidal, i.e., microheterogeneous, structure of liquid melts, characterized by the presence of dispersed particles enriched with one of the components suspended in a medium of a different composition with a clear interphase surface, corresponds to LRO and a range of more than 20 Å, and has been consistently developed by P.S. Popel concerning eutectic and monotectic melts [4]. The idea of the colloidal structure of eutectic melts was first proposed by Yu.A. Klyachko [5], and later developed by V.M. Zalkin, A.A. Wertman, and A.M. Samarin with colleagues [6 – 9]. They considered eutectic melts as classic colloidal systems with particle dispersity on the order of 1 – 10 nm. In this case, from the perspective of physical chemistry, the melt represents a microheterogeneous system. The terms “*microstratified*” and “*colloidal state*” are also used in the same sense. V.M. Zalkin understood eutectic alloys in the liquid state as a thermodynamically stable two-phase state (microemulsions)

caused by the slow dissolution of one of the components, gradually transitioning into a state of true (homogeneous) solution, i.e., as lyophilic two-phase systems [7]. The transition from the microemulsion state in this case is reversible: when cooling a true solution, the original microheterogeneity is restored. The existence of a stable two-phase region caused objections from A.A. Wertman due to the violation of the phase rule at the eutectic point [6]. However, the unsoundness of this assertion was pointed out by Ya.I. Frenkel [10]. In the case where one of the phases is dispersed to colloidal scale, an additional degree of freedom arises – the pressure inside the dispersed particles or their radius [11].

The hypothesis of the colloidal microinhomogeneity (microheterogeneity) of Fe – C melts was formulated based on sedimentation experiments by A.A. Wertman and A.M. Samarin. The centrifugation experiments on liquid cast iron conducted by A.A. Wertman, A.M. Samarin, and A.M. Yakobson showed that the radius of carbon atom groupings is close to 10 nm [12]. In the works of A.A. Wertman and A.M. Samarin, colloidal microinhomogeneity (microheterogeneity) of the melt is associated with the presence of a nonequilibrium dispersed phase that gradually dissolves into the dispersion medium [6]. This dynamic (fluctuational) microinhomogeneity has an inherited short-range order structure of solid eutectic phases, with its lifetime comparable to the relaxation time in the arrangement of atoms. The study of the microinhomogeneous (colloidal) state of liquid cast irons led A.A. Wertman and A.M. Samarin to conclude the nonequilibrium nature of this state, which explained the branching of the temperature dependencies of their physical properties obtained in heating and subsequent cooling modes of the melt [13]. V.M. Zalkin proposed limited solubility of carbon in liquid iron, not exceeding 6.5 – 8.5 at. % [7]. At higher carbon concentrations in the melt, spontaneously formed carbon-rich ordered groupings of different types of atoms, structurally similar to cementite, appear as distinct phases. The formation of dispersed cementite particles in liquid alloys occurs within this temperature range during the melting of alloys containing cementite and graphite in their initial structure, as well as during the dissolution of graphite in liquid iron. A rise in carbon content in the melt above 12.4 – 14.2 at. % results in the formation of submicron carbon atom clusters, arranged in a structure similar to graphite [14]. Subsequent development of the understanding of the microheterogeneous state of Fe–C melts views it as a temporary, nonequilibrium state, gradually transitioning into the equilibrium state of a true solution [15]. The concepts of Fe–C melt microheterogeneity enable analyzing the causes for the divergence in the temperature dependencies of their kinematic viscosity and electrical resistivity based on the theory of transport phenomena in inhomogeneous media. Experiments have shown that

the size of microregions enriched with like atoms reaches tens of nanometers, significantly exceeding the scale of short-range ordering in melts, allowing the application of known dependencies from the theory of transport phenomena in inhomogeneous media to the calculation of microheterogeneous melt properties [16]. The authors previously used this approach to determine the transition temperatures of Fe–Mn–C melts from the model of isolated inclusions to the model of interpenetrating inclusions [17], as well as the transition temperatures from a heterogeneous system to a homogeneous solution [18].

Based on the concept of the microheterogeneous structure of melts, the theory of suspension viscosity can be applied to analyze the temperature dependencies of kinematic viscosity. The viscosity of a medium containing dispersed inclusions exceeds the viscosity of a pure liquid due to the stresses that arise during particle movement. In this case, one speaks of the effective viscosity of the medium. For dilute dispersed systems, it can be assumed that the interfacial interaction force under slow flow conditions represents Stokes force multiplied by the number of particles in a given volume. This approach was used by Einstein [19; 20] to determine the viscosity of dilute dispersed systems containing solid particles, and by Taylor [19] for dispersions of droplets and bubbles. In another limiting case, when the particle concentration is so high that a close packing regime is realized, filtration theory methods are applied, based on Darcy's law [21; 22].

Einstein's theory was first applied to liquid metals to analyze the phenomenon following melting [23]. The Einstein equation has been used multiple times in discussions of viscometric experiments with metallurgical melts. The author of [24] notes that the increase in viscosity upon cooling can be attributed to the enlargement of viscous flow units and crystallization. The viscosity of a suspension is determined by the size of the dispersed phase particles and their quantity in the melt. In the case of liquid steels and cast irons, it has been found that the presence of inclusions in the melt significantly affects its viscosity [25] and resistivity [26].

Alloys with high carbon (up to 4 %) and chromium (up to 30 %) content are characterized by increased strength properties, while parts made from these alloys exhibit higher resistance to wear and oxidation, placing them in the class of wear-resistant cast irons. The high properties of these alloys are due to the presence of a large number of chromium carbides, which are extremely hard. The size, type, and morphology of these carbides determine the wear resistance and impact toughness. The required microstructural characteristics of wear-resistant cast irons are achieved by altering the chemical composition, the crystallization rate, or through special heat treatment [27].

Studies on the influence of vanadium and chromium on the microstructures of white cast irons alloyed with Cr, V, Mn, and Ni have shown that vanadium and chromium increase the overall carbide fraction and the amount of austenite in the matrix, with vanadium carbides (VC) serving as nucleation centers for carbide eutectics [28]. Research on the effect of alloy processing temperature led the authors of [29] to conclude that raising the temperature to 850 °C promotes the formation of secondary carbides and martensite in the microstructure, providing high hardness values. The authors of [30] demonstrated the feasibility of using time-temperature treatment of steel and cast iron in a liquid state for the production of critical castings with high resistance to abrasive and impact-abrasive wear. Specifically, for steel grade 4Kh5V2FSL, high-temperature melt treatment increased the strength properties by 36 %, while maintaining high wear resistance. However, for cast iron IChKh28N2, the alloy with the highest abrasive and impact-abrasive wear resistance was obtained by holding at 1420 °C. Holding at 1520 °C resulted in a reduction of the microhardness of the matrix and eutectics, but increased the microhardness of individual chromium carbides by 400 HV.

A rational processing mode for obtaining IChKh28N2 cast iron was proposed: heating the melt to 1470 °C, holding for 15 min, cooling to the pouring temperature, followed by the introduction of (Ca, Sr)CO₃ and BFT-1 ligature in amounts of 3 and 4 kg/ton, respectively. The application of the developed cast iron melt treatment method also positively influenced fluidity, a key casting property. The effect of boron on the crystallization conditions of heat-resistant and wear-resistant cast irons in the Fe–C–Cr–Mn–Ni–Ti–Al–Nb system was studied [31].

It was found that the hardness of the matrix of high-chromium cast irons increased after heat treatment due to the combined effect of secondary carbide precipitation $Me_{23}C_6$ during destabilization and the austenite-martensite transformation during quenching. Kinetic calculations of the destabilization process showed that secondary carbides Me_7C_3 precipitate first, reaching a maximum at 850 °C. Upon further heating to 980 °C and holding at this temperature, they are fully transformed into $Me_{23}C_6$ [32]. As the destabilization temperature increases to 1000 °C, the number, volume, and size of secondary carbides (up to 2.22 μm) increase. At 1050 °C and a 3 h holding time, the size of secondary carbides significantly decreases, with a high density of distribution in the matrix phase. At this stage, the samples exhibit better corrosion resistance [33]. The carbon content in the matrix, depending on the destabilization temperature and the subsequent dissolution of eutectic carbides, controls the martensite formation onset temperature and has a dominant effect on bulk hardness [34].

The work [35] presents data on the phase composition and structure formation of alloys and oxide layers, the distribution of elements across the structural components of the alloy and the oxidation surface to the depth of the oxide and sub-oxide layers, as well as changes in wear resistance, oxidation resistance, stability, and mechanical properties of cast irons in the Cr–Mn–Ni–Ti–Al–Nb system, depending on the aluminum and niobium content and the heat retention capacity of the casting mold.

Overheating liquid cast iron above 1500 °C reduces the size of primary carbides. Within the temperature range between the liquidus and solidus lines, recrystallization of primary carbides (Cr, Fe)₇C₃ was observed, significantly reducing chromium content and increasing iron content in them [36]. Structural and property changes in hypereutectic chromium cast irons after heat treatment were found, which, according to the authors of [36], are associated with the existence of compositionally stable clusters in the melt from the melting point to approximately 1500 °C. This is due to the high affinity of chromium and carbon and the presence of refractory carbide Cr₇C₃. It was found that heat treatment of the melt in the temperature range of 1260 – 1320 °C (between the liquidus and solidus lines) increases wear resistance, while increasing the treatment temperature leads to a decrease in the wear resistance of the ingots. Heat treatment of fine-grained castings from hypereutectic chromium iron in the temperature range between the liquidus and solidus causes recrystallization of primary carbide crystals (Cr, Fe)₇C₃, altering their composition, shape, and slightly increasing their size. In this case, the fraction of primary carbides increases, and the fraction of eutectic carbides decreases as the temperature of heat treatment is reduced.

The microstructure of Fe–Cr–C ingots includes primary and secondary dendrites of the Fe–Cr solid solution, decorated with complex Me₂₃C₆ and Me₇C₃ [37]. The microstructure of the Fe–34Cr–4.5C alloy consists of a chromium-rich austenitic matrix with Me₇C₃ carbides, which persists at temperatures slightly above 1150 °C and is metastable in nature [38]. Based on this, it is assumed that in the liquid state, the Fe–Cr–C melt, in the context of microheterogeneous structure, can be understood as Fe–Cr dispersed particles distributed in an Fe–C dispersion medium.

Thus, liquid cast iron can be considered a colloidal system consisting of a dispersion medium and inclusions. In this case, the concepts of the theory of transport phenomena in inhomogeneous media and the theory of suspension viscosity are applicable to such systems. The objective of this work is to analyze experimental data on kinematic viscosity and electrical resistivity to determine the volume fraction of dispersed particles in IChKh28N2 and ICh310Kh24M2F4TR cast iron melts. To determine the volume fraction of dispersed particles, it is proposed to use established concepts from the theory of viscous flow of suspensions and the theory of transport phenomena in inhomogeneous media.

RESEARCH METHODS

Experimental methods

The objects of the study were selected samples of industrial wear-resistant cast iron alloys IChKh28N2, alloyed with Cr and Ni, as well as ICh310Kh24M2F4TR, alloyed with Cr, Mo, V, and Ti, produced under laboratory conditions while adhering to the technology of casting wear-resistant cast irons. The chemical composition of the samples was determined using a spark source spectrometer (SPECTROMAXx, SPECTRO Analytical Instruments GmbH, Germany) and is presented in Table. Under laboratory conditions, the electrical resistivity and kinematic viscosity of these samples were studied.

The electrical resistivity ρ of the wear-resistant cast iron alloys in the liquid state was measured using Regel's method, which involves the twist angle of a container with the test sample under the influence of a rotating magnetic field, with a sample height-to-diameter ratio of $h/d \approx 1$. A.R. Regel demonstrated that the twist angle φ of the suspended system is proportional to the electrical conductivity of the metal if the radius of the cylindrical sample is comparable to its height [39 – 41]. Measurements of the electrical resistivity were conducted using an original setup described in [42].

The kinematic viscosity ν of the wear-resistant cast irons in the liquid state was measured using the method of torsional oscillations of a crucible containing the melt in a single-ended configuration [43; 44]. The kinematic viscosity was determined by observing the damping of the torsional oscillations of the crucible with the melt,

Chemical composition of the samples

Химический состав образцов

Sample	Contents of elements, wt. %								
	C	Si	Mn	Cr	Mo	Ni	V	Fe	Rest.
IChKh28N2	3.8	0.6	0.7	25.1	<0.01	2.0	<0.01	66.5	1.3
ICh310Kh24M2F4TR	2.8	0.6	0.3	23.5	0.4	<0.01	3.7	68.0	0.7

recording the oscillation period and the logarithmic decrement of the damping. The kinematic viscosity of the melt was then calculated. The height of the liquid alloy must be $2H \geq 1.85R$ relative to the radius of the crucible, to ensure full damping of the viscous waves propagating from the bottom of the crucible to the free surface.

Measurements of electrical resistivity and kinematic viscosity were performed over a temperature range from T_L to 1650 °C. The working chamber was pre-evacuated to 0.001 Pa, after which helium was introduced to a pressure of $\sim 10^5$ Pa. The samples were held in an inert atmosphere for 10 – 15 min at the liquidus temperature T_L , followed by heating to 1650 °C in increments of 30 – 40 °C. The systematic error in the measurement of ρ and ν was 3 %, while the random error, determining the scatter of points in a single experiment with a confidence probability of $p = 0.95$ did not exceed 1.5 %.

The liquidus temperature was determined based on viscometric studies by the sharp change in the logarithmic decrement of the damping torsional oscillations of the crucible with the melt, according to the method described in [45].

Calculation of the volume fraction of microheterogeneous inclusions

To determine the volume fraction of inclusions in liquid cast irons, an approach was used based on the theory of conductivity in inhomogeneous media and theoretical models of suspension viscosity. In this case, the liquid cast iron was considered a microheterogeneous system, in which dispersed particles are distributed in a dispersion medium. For the IChKh28N2 and ICh310Kh24M2F4TR alloys in the liquid state, the dispersion medium is assumed to be the Fe – 3 % C melt, while the dispersed particles consist of the Fe – 30 % Cr melt.

In analyzing the results of the viscometric experiment on liquid cast irons to estimate the volume fraction φ of the dispersed phase in the melts, Taylor’s equation [19] for dispersions of droplets and bubbles was applied:

$$\eta_\varphi = \eta_2 \left[1 + 2,5\varphi \left(\frac{\eta_1 + 0,4\eta_2}{\eta_1 + \eta_2} \right) \right], \quad (1)$$

where η_φ is the effective viscosity of the dispersion; η_1 and η_2 are the viscosities of the dispersed phase and the continuous phase, respectively.

Based on the experimental data on the temperature dependence of kinematic viscosity ν , the dynamic viscosity η of the liquid cast iron was determined from the equation $\eta = \nu d$. The density d of the liquid cast iron was determined from an additive dependence on the content of each component in the melt X_i and its temperature-dependent density d_i .

In the liquid state, the melt was understood as a microheterogeneous system consisting of Fe – 30 % Cr dispersed particles and an Fe – 3 % C dispersion medium. The dynamic viscosity of such a system can be estimated using Taylor’s equation (1)

$$\eta_{ef} = \eta_{Fe-C} \left[1 + 2,5\varphi \left(\frac{\eta_{Fe-Cr} + 0,4\eta_{Fe-C}}{\eta_{Fe-C} + \eta_{Fe-Cr}} \right) \right], \quad (2)$$

where η_{ef} is the viscosity of the liquid cast iron; η_{Fe-C} is the viscosity of the Fe–C melt, and η_{Fe-Cr} is the viscosity of the Fe–Cr melt.

Experimental data on the viscosity of Fe–C melts with carbon content up to 5 % were obtained by the authors of [46] and modeled using molecular dynamics in [47]. The viscosity of Fe–Cr melts up to 40 at. % and $Fe_{85-x}Cr_{15}C_x$ ($x = 10 - 17$ at. %) was studied in [48; 49]. The known experimental data on the temperature dependence of the viscosity of Fe–C, Fe–Cr melts, and liquid cast irons were approximated by an exponential expression of the form

$$\eta = A \exp\left(\frac{b}{T}\right). \quad (3)$$

To determine the volume fraction of dispersed Fe–Cr particles in the liquid cast iron, the following equation was derived

$$\eta_{ef} - \eta_{Fe-C} \left[1 + 2,5\varphi \left(\frac{\eta_{Fe-Cr} + 0,4\eta_{Fe-C}}{\eta_{Fe-C} + \eta_{Fe-Cr}} \right) \right] = 0. \quad (4)$$

In analyzing the results of the resistometric experiment on liquid cast irons, to estimate the volume fraction φ of the dispersed phase in the melts, the Odelevsky equation [50] was applied, which relates the conductivity σ of a two-phase system to the conductivities of the solvent σ_s and the dispersed particles σ_p :

$$\sigma = \frac{2\sigma_s - \sigma_p + \varphi(3\sigma_p + \sigma_s)}{4} + \sqrt{\left(\frac{2\sigma_s - \sigma_p + \varphi(3\sigma_p + \sigma_s)}{4} \right)^2 + \frac{\sigma_s \sigma_p}{2}}. \quad (5)$$

Experimental data on the resistivity of Fe–C melts with carbon content up to 4.2 % were obtained by the authors of [51]. The experimental data on the resistivity of Fe–Cr melts over a wide range of compositions were studied in [52]. The known experimental data on the temperature dependence of the resistivity of the melts were approximated by linear dependencies.

To determine the volume fraction of Fe–Cr dispersed particles in the liquid cast iron, the following equation was derived

$$\sigma_{ef} - \frac{2\sigma_s - \sigma_p + \varphi(3\sigma_p + \sigma_s)}{4} + \sqrt{\left(\frac{2\sigma_s - \sigma_p + \varphi(3\sigma_p + \sigma_s)}{4}\right)^2 + \frac{\sigma_s \sigma_p}{2}} = 0, \quad (6)$$

where $\sigma_{ef} = \frac{1}{\rho_{ef}}$ is the conductivity of the liquid cast iron; $\sigma_s = \frac{1}{\rho_{Fe-C}}$ is the conductivity of the Fe–C melt; $\sigma_p = \frac{1}{\rho_{Fe-Cr}}$ is the conductivity of the Fe–Cr melt.

Equations (4) and (6), given the known properties of the binary systems Fe–C (η_{Fe-C}, σ_s), Fe–Cr (η_{Fe-Cr}, σ_p) and the liquid cast iron (η_{ef}, σ_{ef}) were solved for the volume fraction of inclusions (φ) using the `fsolve` function from the `SciPy` library within the temperature range of 1310 – 1650 °C.

The molar fraction of the dispersed particles was determined from the obtained data on the volume fraction of inclusions using the expression

$$m_i = \frac{n_i}{n_\Sigma}, \quad n_i = \frac{\varphi_i}{M_i} d_i, \quad (7)$$

where $m_i, n_i, \varphi_i, M_i, d_i$ are the molar fraction, the number of moles per unit volume, the volume fraction, the molar mass, and the density of the i^{th} component, respectively.

RESULTS AND DISCUSSION

The results of the experimental investigation of kinematic viscosity in the temperature range from T_L to 1650 °C for IChKh28N2 and ICh310Kh24M2F4TR liquid cast irons are presented in Fig. 1. The values of kinematic viscosity obtained in this study are consistent with the viscosity data of the Fe – 15 at. % Cr – 10 at. % C melt reported by the authors of [48]. On the right axis of the same graph (Fig. 1) the dynamic viscosity values are shown. Under the temperature dependence of kinematic viscosity, the experimental and calculated data on the volume (right axis of the graph) and molar (left axis of the graph) fractions of heterogeneous inclusions in the liquid cast irons are presented. Based on the viscometric study, the liquidus temperatures for the liquid cast irons were determined using the method described in [45]. The liquidus temperatures are indicated on the temperature dependencies of kinematic viscosity.

In analyzing the results of the viscometric experiment on liquid cast irons to estimate the volume fraction φ of the dispersed phase in the melts, the approach proposed by A. Einstein for describing the viscosity of dispersed systems was applied [19; 20]. A. Einstein considers the case of constrained flow around a system of spherical particles by a liquid flow and introduces the concept of the effective viscosity of the medium. The velocity of particle movement in a constrained flow depends not

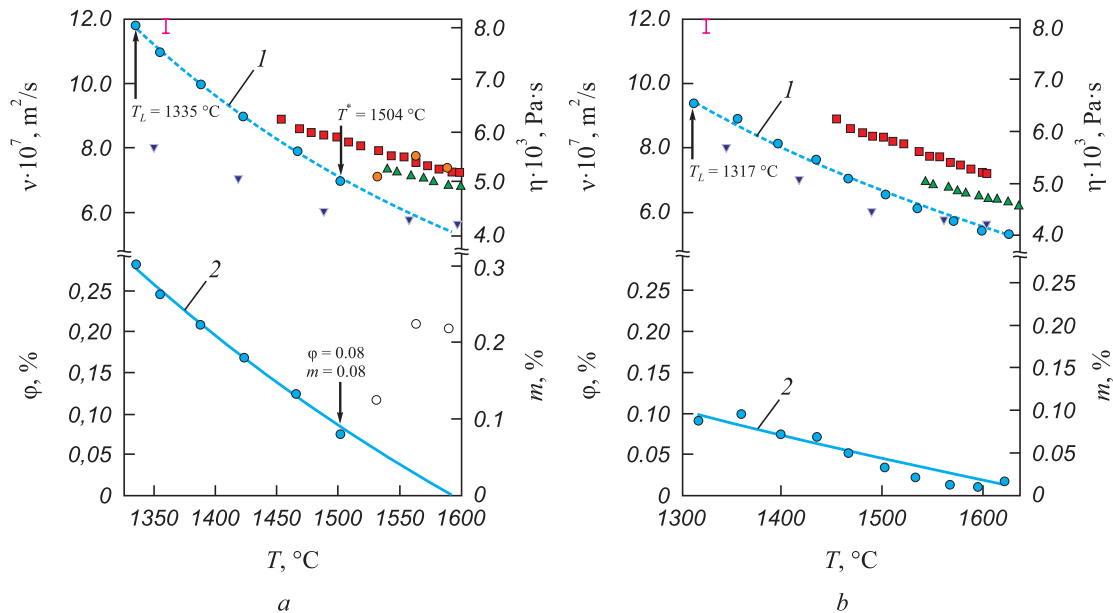


Fig. 1. Temperature dependences of kinematic viscosity (v), dynamic viscosity (η), volumetric (φ) and molar fraction (m) of heterogeneous inclusions in liquid cast irons IChKh28N2 (a) and ICh310Kh24M2F4TR (b): ● – this work; ■ – Fe – 15 % Cr – 4 % C [49]; ▲ – Fe – 30 % Cr [48]; ▼ – Fe – 3 % C [46; 47]; 1 – approximation; 2 – calculation by equation (4)

Рис. 1. Температурные зависимости кинематической вязкости (v), динамической вязкости (η), объемной (φ) и мольной доли (m) гетерогенных включений в жидких чугунах ИЧХ28Н2 (a) и ИЧ310Х24М2Ф4ТР (b): ● – данная работа; ■ – Fe – 15 % Cr – 4 % C [49]; ▲ – Fe – 30 % Cr [48]; ▼ – Fe – 3 % C [46; 47]; 1 – аппроксимация; 2 – расчет по уравнению (4)

only on their size, shape, and the physicochemical properties of the medium but also on the volume concentration φ . The dependence on the volume concentration is caused by hydrodynamic interactions between the particles. The velocity of a particle in a constrained flow is generally lower than that of an isolated particle. The viscosity of a medium containing dispersed inclusions exceeds the viscosity of a pure liquid due to the stresses that arise during particle movement. In this case, the term “effective viscosity of the medium” is used. A strict description of the laws governing constrained particle motion in a viscous flow does not yet exist. For the case of dilute dispersed systems, this approach was used by Einstein [19] to determine the effective viscosity of a medium containing solid particles, and by Taylor [19] for determining the dispersion of droplets and bubbles. The melt, as a microheterogeneous system, was understood as dispersed particles enriched with Cr (Fe – 30 % Cr), distributed in a dispersion medium of Fe – 3 % C. Based on the known values of the viscosities of Fe–Cr and Fe–C melts [46 – 48] and the experimental data on the viscosity of the dispersed system, the values of the volume fraction of the dispersed particles (Fe – 30 % Cr) in liquid cast irons were obtained by solving equation (4). The calculated values of the volume fraction of inclusions (Fig. 1) were derived from the temperature dependencies of the kinematic viscosity of Fe – 3 % C, Fe – 30 % Cr and liquid cast irons, approximated by equation (3). The values of the volume fraction of dispersed particles, marked with the symbol ● in Fig. 1, were obtained from the experimental data on the kinematic viscosity of liquid cast irons and the approximated values of the kinematic viscosity of the dispersed particles (Fe – 30 % Cr) and the dispersion medium (Fe – 3 % C) from equation (3). The molar fraction of the dispersed particles was determined from the obtained data on the volume fraction using equation (7).

The dependence of the kinematic viscosity on temperature for the liquid cast iron IChKh28N2 in the range from T_L to 1504 °C follows an exponential law and is consistent with the Arrhenius equation. In the same temperature range, the volume and molar fractions decrease from 0.28 (0.30) to 0.08 (0.08). However, at temperatures above 1504 °C, an anomalous increase in kinematic viscosity with rising temperature (marked by the symbol ○ in Fig. 1, a) was observed, which was also accompanied by an abnormal increase in the volume fraction of dispersed particles in the liquid cast iron, deviating from the calculated curve. This behavior may be related to structural changes in the melt. As the dispersed particles dissolve, the melt transitions into a more homogeneous solution, changing the chemical composition of the dispersed phase, which leads to the anomalous increase in viscosity. In this case, equation (4) is not applicable for describing the viscous flow of a homogeneous system.

The kinematic viscosity for the liquid cast iron ICh310Kh24M2F4TR decreases monotonically with increasing temperature, and the volume (molar) fraction of heterogeneous inclusions in the liquid cast iron also decreases monotonically, from 0.10 (0.10) at the liquidus temperature to 0.01 (0.01). This indicates the dissolution of heterogeneous inclusions in the melt as the temperature rises.

Based on the data from the viscometric experiment, an estimate of the size of the structural unit responsible for viscous flow in the melts of IChKh28N2 and ICh310Kh24M2F4TR cast irons was made. The method proposed in [53] was used to determine the size of the structural unit of viscous flow. The temperature dependence of the kinematic viscosity is expressed as

$$\nu = \frac{BT^{1/2}}{s^{1/2}} \exp\left(\frac{\varepsilon}{kT}\right), \quad (8)$$

where $B = \frac{\pi}{4} \left(\frac{k}{3d}\right)^{1/2}$; s is the size of the dispersed particles.

It was found that for the IChKh28N2 melt, $s = 1.3$ nm, and for the ICh310Kh24M2F4TR melt, $s = 1.4$ nm, which is of the same order of magnitude as the data obtained for the liquid steel 110G13L in [54].

The results of the resistometric study of the liquid cast irons IChKh28N2 and ICh310Kh24M2F4TR are presented in Fig. 2. The values of electrical resistivity are shown on the left axis of the graph, while the values of electrical conductivity of the liquid cast irons are shown on the right axis. Below the experimental data on resistivity (conductivity), the obtained values of the volume (left axis) and molar (right axis) fractions of dispersed particles in the liquid cast irons are presented.

The analysis of the resistivity measurements was based on the theory of conductivity in inhomogeneous media. The liquid cast iron was considered as dispersed particles enriched with Cr (Fe – 30 % Cr), distributed in a dispersion medium of Fe – 3 % C. Using the framework of conductivity in inhomogeneous media, the volume fraction of dispersed particles in the liquid cast irons was determined by solving equation (6), based on the known data on the conductivity ($1/\rho$) of dispersed particles (Fe – 30 % Cr) [52], the dispersion medium (Fe – 3 % C) [51], and the experimental data on the conductivity of the liquid cast iron. The calculated values of the volume fraction (Fig. 2) were obtained from the linear approximation of the known experimental data on the temperature dependencies of the conductivity of Fe – 3 % C, Fe – 30 % Cr, and the liquid cast irons. The volume fractions of dispersed particles in Fig. 2, were derived from the experimental data on

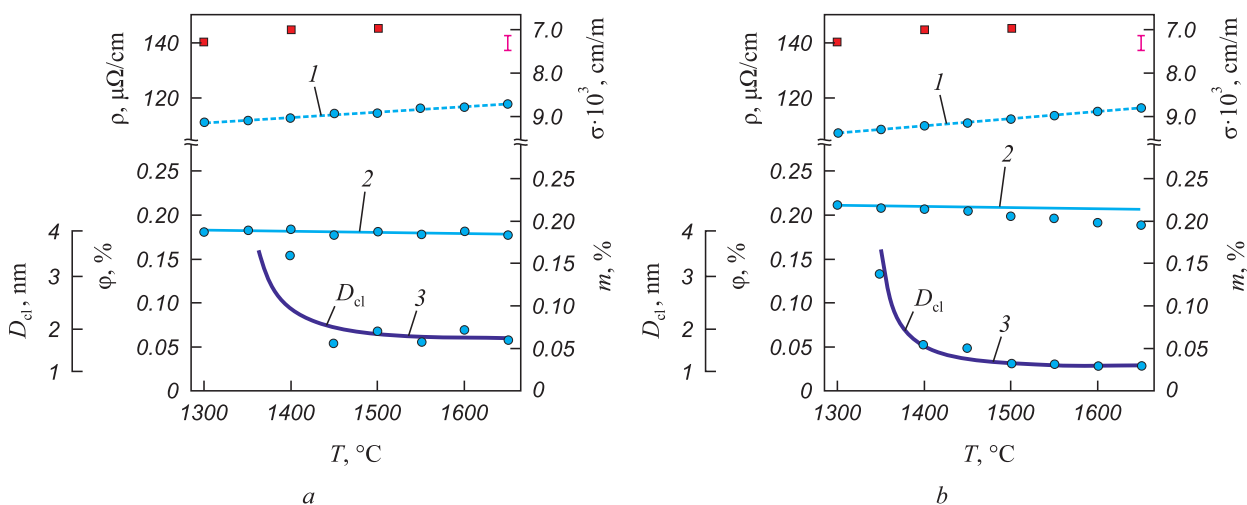


Fig. 2. Temperature dependences of electrical resistivity (ρ), conductivity (σ), volume (φ) and molar fraction (m) of heterogeneous inclusions, as well as the cluster size determined by equation (8) in liquid cast irons IChKh28N2 (a) and ICh310Kh24M2F4TR (b):

● – this work; ■ – Fe – 3 % C; 1 – approximation; 2 – calculation by equation (6); 3 – calculation by equation (8)

Рис. 2. Температурные зависимости удельного электросопротивления (ρ), удельной проводимости (σ), объемной (φ) и мольной (m) доли гетерогенных включений, а также размер кластера, определенный по уравнению (8) в жидких чугунах ИЧХ28Н2 (a) и ИЧ310Х24М2Ф4ТР (b):

● – данная работа; ■ – Fe – 3 % C [51]; 1 – аппроксимация; 2 – расчет по уравнению (6); 3 – расчет по уравнению (8)

the conductivity of the liquid cast irons and the linear approximation of the conductivity values of the dispersed particles (Fe – 30 % Cr) [52] and the dispersion medium (Fe – 3 % C) [51]. Near the melting temperature, the volume (molar) fraction of dispersed particles is 0.18 (0.19) for IChKh28N2 and 0.21 (0.22) for ICh310Kh24M2F4TR. As the temperature increases, the volume (molar) fraction of dispersed particles decreases slightly.

In [55], the following expression was proposed for microinhomogeneous metallic melts:

$$\ln\left(\frac{\rho}{\rho_L}\right) = \frac{l_{\text{ж}}}{D_{\text{кл}}} \ln\left(\frac{1}{r}\right), \quad (9)$$

where ρ_L and ρ are the specific resistivity of liquid iron at the liquidus temperature and the analysis temperature, respectively; $l_{\text{ж}}$ is the mean free path of electrons in liquid iron; $D_{\text{кл}}$ is the cluster diameter; r is the electron scattering coefficient.

The mean free path of electrons in liquid iron decreases from 4.63 to 4.28 Å when the melt is heated from 1400 to 1600 °C. Since the scattering coefficient varies within the range $0 < r < 1$, equation (4) implies that as the cluster size decreases, the resistivity of the melt should increase. Calculations showed that at $t = 1600$ °C, $r = 0.97$, and at $t = 1800$ °C $r = 0.86$, meaning that as the temperature rises, r decreases, and ρ increases. The cluster size determined by equation (8) (Fig. 2) for IChKh28N2 is 3.4 nm at 1400 °C and decreases to 1.7 nm at temperatures above 1600 °C. For ICh310Kh24M2F4TR, the cluster size is

1.7 nm at 1400 °C and decreases to 1.2 nm at temperatures above 1600 °C. Therefore, the experimentally observed increase in the resistivity of liquid iron with increasing temperature is likely not related to changes in the melt structure at the atomic level, but rather to a decrease in the number of conduction electrons. This is explained by the increased number of electrons participating in the strengthening of interatomic bonds and ensuring the stability of the clusters as they become smaller with increasing temperature.

In conclusion, based on the results of viscometric and resistometric studies, it was established that liquid cast irons represent a dispersed system, containing, near the melting temperature, a volume fraction of dispersed particles of 0.28 and 0.10, according to viscometry, for liquid cast irons IChKh28N2 and ICh310Kh24M2F4TR, respectively, corresponding to particle sizes ranging from 100 to 10 nm. According to resistometry data, the volume fraction of dispersed particles is about 0.20 for the liquid cast irons and does not significantly change with increasing temperature. A volume fraction of 0.20 corresponds to dispersed particles with a size of about 10 nm. According to estimates made by the authors of [56] within the framework of the quasi-chemical model of microinhomogeneous structure for complex-alloyed melts [1], the molar fraction of clusters in the liquid cast irons IChKh28N2 and ICh310Kh24M2F4TR is 0.43 at the liquidus temperature, which is significantly higher than the values obtained in this study. Based on this, liquid cast iron can be considered a microheterogeneous system. Increasing the temperature leads to a reduction in

the volume fraction of dispersed particles, consistent with the concept of the breakdown of the microheterogeneous state as the liquid melt is overheated beyond a certain temperature.

CONCLUSIONS

The study presents experimental data on the temperature dependencies of kinematic viscosity and electrical resistivity of liquid cast irons in the range from the liquidus temperature T_L to 1650 °C. Liquid cast iron in the molten state was understood as a microheterogeneous system, characterized by the presence of dispersed particles enriched with one of the components.

Based on the data on the kinematic viscosity of liquid cast irons, the volume fraction of heterogeneous inclusions was determined using the concept of viscous flow in dilute dispersed systems. It was found that the volume fraction of dispersed particles in liquid cast irons near the melting point is 0.28 for IChKh28N2 and 0.1 for ICh310Kh24M2F4TR. A volume fraction of 0.28 corresponds to dispersed particle sizes of ~100 nm, while 0.1 corresponds to particle sizes of ~10 nm. The obtained particle sizes align with the concept of the microheterogeneous structure of liquid cast irons. As the temperature increases, the volume fraction of dispersed particles decreases monotonously to values of 0.08 – 0.01.

The volume fraction of dispersed particles was also determined based on the data on the electrical resistivity of liquid cast irons, which amounted to 0.18 for IChKh28N2 and 0.21 for ICh310Kh24M2F4TR. The obtained volume fractions correspond to dispersed particle sizes of ~10 nm. With increasing temperature, the volume fraction of dispersed particles decreases only slightly.

It is known that heat treatment of the melt, aimed at breaking down the microheterogeneous structure, leads to a modification of the crystallized ingot's structure by altering the crystallization conditions. However, the authors of [30; 36] found that overheating of chromium cast iron melts reduces the wear resistance of the ingots. The authors of [36] discovered that overheating the melt above 1500 °C leads to the destruction of compositionally stable clusters in the melt, which results in changes in the structure and properties of hypereutectic chromium cast irons after heat treatment. To improve the performance properties, the authors of [30] propose the introduction of additional modifiers before casting the iron after time-temperature melt treatment, while the authors of [36] found that wear resistance can be enhanced by heat treatment between the liquidus and solidus temperatures. Thus, the study of chromium cast iron melts in the liquid state from the perspective of their microinhomogeneous structure will help to advance the understanding of processes occurring in the liquid state and develop

an optimal melt heat treatment mode to improve the performance characteristics.

REFERENCES / СПИСОК ЛИТЕРАТУРЫ

- Chikova O.A. Structural transitions in complexly alloyed melts. *Izvestiya. Ferrous Metallurgy*. 2020;63(3–4): 261–270. (In Russ.).
<https://doi.org/10.17073/0368-0797-2020-3-4-261-270>
Чикова О.А. О структурных переходах в сложнорегированных расплавах. *Известия вузов. Черная металлургия*. 2020;63(3–4):261–270.
<https://doi.org/10.17073/0368-0797-2020-3-4-261-270>
- Sidorov V.E., Son L.D. Research of melts as a basis for improvement of technologies of ferrous metallurgy. *Chernye Metally*. 2023;(3):58–64. (In Russ.).
<https://doi.org/10.17580/chm.2023.03.10>
Сидоров В.Е., Сон Л.Д. Исследование расплавов как основа совершенствования технологий черной металлургии. *Черные металлы*. 2023;(3):58–64.
<https://doi.org/10.17580/chm.2023.03.10>
- Tyagunov G.V., Baryshev E.E., Tyagunov A.G., Mushnikov V.S., Kostina T.K. On some structuring features of metallic fluids. *Bulletin of South Ural state university. Series "Metallurgy"*. 2018;18(3):16–25. (In Russ.).
<https://doi.org/10.14529/met180302>
Тягунов Г.В., Барышев Е.Е., Тягунов А.Г., Мушников В.С., Костина Т.К. О некоторых особенностях структурирования металлических жидкостей. *Вестник Южно-Уральского государственного университета. Серия: Металлургия*. 2018;18(3):16–25.
<https://doi.org/10.14529/met180302>
- Popel P.S. Metastable microheterogeneity of melts in systems with eutectic and monotectic and its effect on the alloy structure after solidification. *Rasplavy*. 2005(1):22–48. (In Russ.).
Попель П.С. Метастабильная микрорегерогенность расплавов в системах с эвтектикой и монотектикой и ее влияние на структуру сплава после затвердевания. *Расплавы*. 2005;(1):22–48.
- Klyachko Yu.A. Experience of Colloidal Chemical Research of Metals. Moscow: Publishing House of the Voroshilov Academy; 1935:92. (In Russ.).
Клячко Ю.А. Опыт коллоидно-химического исследования металлов. Москва: Издательство Академии им. К.Е. Ворошилова; 1935:92.
- Vertman A.A. Microheterogeneity of metal melts regulation of castings properties. *Fizika i khimiya obrabotki materialov*. 1967;(3):132–141. (In Russ.).
Вертман А.А. Микрорегерогенность металлических расплавов и проблема регулирования свойств отливок. *Физика и химия обработки материалов*. 1967;(3):132–141.
- Zalkin V.M. Nature of Eutectic Alloys and Effect of Contact Melting. Moscow: Metallurgiya; 1987:52. (In Russ.).
Залкин В.М. Природа эвтектических сплавов и эффект контактного плавления. Москва: Металлургия; 1987:152.
- Zalkin V.M. On two theories describing the initial stage of contact melting. *Rasplavy*. 2004;(2):93–95. (In Russ.).
Залкин В.М. О двух теориях начальной стадии контактного плавления. *Расплавы*. 2004;(2):93–95.

9. Zalkin V.M. On microheterogeneous structure of eutectic alloys (solutions) in liquid state (on the 120th anniversary of the term “eutectic”). *Journal of Physical Chemistry*. 2005;79(4):763–765. (In Russ.).
Залкин В.М. О микрогетерогенном строении эвтектических сплавов (растворов) в жидком состоянии. *Журнал физической химии*. 2005; 79(4):763–765.
10. Frenkel' Ya.I. Statistical Physics. Moscow: Publishing House of the USSR Academy of Sciences; 1948:760. (In Russ.).
Френкель Я.И. Статистическая физика. Москва: Издательство АН СССР; 1948:760.
11. Morozov D.I., Trusov L.I., Lapovok V.N. Physical Phenomena in Ultrafine Media. Moscow: Energoatomizdat; 1984:224. (In Russ.).
Морохов Д.И., Трусов Л.И., Лаповок В.Н. Физические явления в ультрадисперсных средах. Москва: Энергоатомиздат; 1984:224.
12. Vertman A.A., Samarin A.M., Yakobson A.M. On structure of liquid eutectic. *Izv. AS USSR. OTN. Metallurgiya i toplivo*. 1960;(3):17–21. (In Russ.).
Вертман А.А., Самарин А.М., Якобсон А.М. О строении жидких эвтектик. *Известия АН СССР. ОТН. Metallurgiya i toplivo*. 1960;(3):17–21.
13. Vertman A.A., Samarin A.M., Turovskii B.M. Structure of liquid alloys of iron-carbon system. *Izv. AS USSR. OTN. Metallurgiya i toplivo*. 1960;(6):123–129. (In Russ.).
Вертман А.А., Самарин А.М., Туровский Б.М. Структура жидких сплавов системы железо-углерод. *Известия АН СССР. ОТН. Metallurgiya i toplivo*. 1960;(6):123–129.
14. Vertman A.A., Samarin A.M. Properties of Iron Melts. Moscow: Nauka; 1969:197. (In Russ.).
Вертман А.А., Самарин А.М. Свойства расплавов железа. Москва: Наука; 1969:197.
15. Brodova I.G., Zamyatin V.M., Popel' P.S., Esin V.O., Baum B.A., Moiseev A.I., Korshunov I.P., Topchii A.L., Tikhomirov Y.G., Polents I.V. Conditions of metastable phases formation during solidification of Al-Zr alloys. *Raspplavy*. 1988;(6–2):23–27. (In Russ.).
Бродова И.Г., Замятин В.М., Попель П.С., Есин В.О., Баум Б.А., Моисеев А.И., Коршунов И.П., Топчий А.Л., Тихомиров Ю.Г., Поленц И.В. Условия формирования метастабильных фаз при кристаллизации сплавов Al-Zr. *Расплавы*. 1988;(6–2):23–27.
16. Dul'nev G.N., Novikov V.V. Transfer Processes in Inhomogeneous Media. Leningrad: Energoatomizdat; 1991:248. (In Russ.).
Дульнев Г.Н., Новиков В.В. Процессы переноса в неоднородных средах. Ленинград: Энергоатомиздат; 1991:248.
17. Sinitsin N.I., Chikova O.A., V'yukhin V.V. Resistivity of Fe–Mn–C melts. *Inorganic Materials*. 2021;57(1):86–93.
<https://doi.org/10.1134/S002016852101012X>
Синицин Н.И., Чикова О.А., Вьюхин В.В. Удельное электросопротивление расплавов Fe–Mn–C. *Неорганические материалы*. 2021;57(1):89–97.
<https://doi.org/10.31857/S0002337X21010127>
18. Chikova O.A., Sinitsin N.I., V'yukhin V.V. Electrical resistivity of liquid Fe–Mn alloys. *Russian Physics Journal*. 2021;64:1039–1046.
<https://doi.org/10.1007/s11182-021-02426-y>
- Чикова О.А., Синицин Н.И., Вьюхин В.В. Электросопротивление сплавов Fe–Mn в жидком состоянии. *Известия вузов. Физика*. 2021;64(6):68–75.
<https://doi.org/10.17223/00213411/64/6/68>
19. Bibik E.E. Rheology of Dispersed Systems. Leningrad: Leningrad University; 1981:172. (In Russ.).
Бибик Е.Е. Реология дисперсных систем. Ленинград: Издательство Ленинградского университета; 1981:172.
20. Happel J., Brenner H. Low Reynolds Number Hydrodynamics. Springer Dordrecht; 1983:553.
<https://doi.org/10.1007/978-94-009-8352-6>
Хаппель Дж., Бреннер Г. Гидродинамика при малых числах Рейнольдса. Москва: Мир; 1976:630.
21. Ur'ev N.P., Highly Concentrated Dispersed Systems. Moscow: Khimiya; 1980:149. (In Russ.).
Урьев Н.П. Высококонцентрированные дисперсные системы. Москва: Химия; 1980:149.
22. Rheology. Theory and Applications. Eirich F.R. ed. Vol. 1. New York: Acad. Press; 1956:540.
Реология: Теория и приложения. Пер. с англ. / Под ред. Ф. Эйриха; Под общ. ред. Ю.Н. Работнова и П.А. Ребиндера. Москва: Издательство иностранной литературы; 1962:824.
23. Glazov V.M., Timoshenko V.I. Analysis of the phenomenon of post-melting in semiconductor melts based on the cluster model. *Journal of Physical Chemistry*. 1981;55(6):1148–1452. (In Russ.).
Глазов В.М., Тимошенко В.И. Анализ явления послеплавания в расплавах полупроводников на основе кластерной модели. *Журнал физической химии*. 1981;55(6):1148–1452.
24. Morozov A.A. Technological properties and structure of titanate melts. *Tsvetnye metall*. 2002;(8):60–63. (In Russ.).
Морозов А.А. Технологические свойства и строение титанатных расплавов. *Цветные металлы*. 2002;(8):60–63.
25. Borovykh M.A., V'yukhin V.V., Chikova O.A., Tsepelev V.S. The influence of defects on the ductility of liquid steel 32G1 and 32G2. *Izvestiya. Ferrous Metallurgy*. 2015;58(6):402–406. (In Russ.).
<https://doi.org/10.17073/0368-0797-2015-6-402-406>
Борových М.А., Вьюхин В.В., Чикова О.А., Цепелев В.С. О влиянии дефектов на вязкость жидких сталей 32Г1 и 32Г2. *Известия вузов. Черная металлургия*. 2015;58(6):402–406. <https://doi.org/10.17073/0368-0797-2015-6-402-406>
26. Borovykh M.A., Chikova O.A., Tsepelev V.S., V'yukhin V.V. Effect of heat treatment conditions on electrical resistivity of 35KhGF molten steel. *Izvestiya. Ferrous Metallurgy*. 2018;61(3):237–243. (In Russ.).
<https://doi.org/10.17073/0368-0797-2018-3-237-243>
Борových М.А., Чикова О.А., Цепелев В.С., Вьюхин В.В. О влиянии режима термообработки на удельное электросопротивление расплава стали 35ХГФ. *Известия вузов. Черная металлургия*. 2018;61(3):237–243.
<https://doi.org/10.17073/0368-0797-2018-3-237-243>
27. Abdel-Aziz K., El-Shennawy M., Omar A. Microstructural characteristics and mechanical properties of heat treated high-Cr white cast iron alloys. *International Journal of Applied Engineering Research*. 2017;12(14):4675–4686.
28. Efremenko V.G., Shimizu K., Cheiliakh A.P., Kozarevskaya T.V., Kusumoto K., Yamamoto K. Effect of vanadium

- and chromium on the microstructural features of V-Cr-Mn-Ni spheroidal carbide cast irons. *International Journal of Minerals Metallurgy and Materials*. 2014;21(11):1096–1108. <https://doi.org/10.1007/s12613-014-1014-6>
29. Karantzalis A.E., Lekatou A., Kapoglou A., Mavros H., Dracopoulos V. Phase transformations and microstructural observations during subcritical heat treatments of a high-chromium cast iron. *Journal of Materials Engineering and Performance*. 2012;21(6):1030–1039. <https://doi.org/10.1007/s11665-011-9995-z>
 30. Kolokoltsev V.M., Mikhalkina I.V., Shevchenko A.V. High temperature treatment of special steel and cast iron melts. *Liteishchik Rossii*. 2016;(9):18–23. (In Russ.).
Колокольцев В.М., Михалкина И.В., Шевченко А.В. Высокотемпературная обработка расплавов специальных сталей и чугунов. *Литейщик России*. 2016;(9):18–23.
 31. Kolokol'tsev V.M., Petrochenko E.V., Molochkova O.S. Influence of boron modification and cooling conditions during solidification on structural and phase state of heat- and wear-resistant white cast iron. *Izvestiya. Ferrous Metallurgy*. 2019;62(11):887–893. (In Russ.). <https://doi.org/10.17073/0368-0797-2019-11-887-893>
Колокольцев В.М., Петроченко Е.В., Молочкова О.С. Влияние бора и температурных режимов охлаждения металла в литейной форме на структурно-фазовое состояние жароизносостойких белых чугунов. *Известия вузов. Черная металлургия*. 2019;62(11):887–893. <https://doi.org/10.17073/0368-0797-2019-11-887-893>
 32. Guitar M.A., Nayak U.P., Britz D., Mücklich F. The effect of thermal processing and chemical composition on secondary carbide precipitation and hardness in high-chromium cast irons. *International Journal of Metalcasting*. 2020;14(3):755–765. <https://doi.org/10.1007/s40962-020-00407-4>
 33. Quyen Hoang Thi Ngoc, Ngoc Tran Vu Diem, Viet Nguyen Hoang, Hai Nguyen Hong, Ha Le Thu, Nam Nguyen Duong. Effect of residual stress distribution on the formation, growth and coalescence of voids of 27Cr white cast iron under impact loading. *Materials Transactions*. 2022;63(2):170–175. <https://doi.org/10.2320/matertrans.MT-M2021161>
 34. Le Nué C., Corujeira Gallo S., Vahid A., Wang J., Taherishargh M., Attar H., Fabijanic D., Barnett M. Destabilization treatment and its influence on microstructure and matrix hardness of high-Cr cast iron. *Metallurgical and Materials Transactions A*. 2023;54(12):4952–4965. <https://doi.org/10.1007/s11661-023-07216-4>
 35. Kolokoltsev V.M., Petrochenko E.V., Molochkova O.S. Influence of aluminium and niobium alloying on phase composition, structure and properties of heat- and wear-resistant cast iron of Cr-Mn-Ni-Ti system. *CIS Iron and Steel Review*. 2021;(2):55–60. <https://doi.org/10.17580/cisr.2021.02.10>
 36. Panichkin A., Wieleba W., Kenzhegulov A., Uskenbayeva A., Mamaeva A., Imbarova A., Kvyatkovskii S., Kasenova B. Effect of thermal treatment of chromium iron melts on the structure and properties of castings. *Materials Research Express*. 2023;10(8):086502. <https://doi.org/10.1088/2053-1591/acead7>
 37. Wiczczak K.K., Bała P., Stepień M., Cios G., Kozieł T. The Characterization of Cast Fe-Cr-C Alloy. *Archives of Metallurgy and Materials*. 2015;60(2):779–782. <https://doi.org/10.1515/amm-2015-0206>
 38. Svensson L.-E., Grefot B., Ulander B., Bhadeshia H.K.D.H. Fe-Cr-C hardfacing alloys for high-temperature applications. *Journal of Materials Sci*. 1986;21(3):1015–1019. <https://doi.org/10.1007/BF0117388>
 39. Tsepelev V.S. Physics of Amorphous and Nanocrystalline Metallic Melts: Methodology of Analysis: Monography. Yekaterinburg: Ural Publishing House university; 2023:208. (In Russ.).
Цепелев В.С. Физика аморфных и нанокристаллических металлических расплавов: методология анализа: Монография. Екатеринбург: Издательство Уральского университета; 2023:208.
 40. Regel A.R. An electrodeless method for measuring electrical conductivity and possibility of its application to problems of physico-chemical analysis. *Journal of Inorganic Chemistry*. 1956;1(6):1271–1277. (In Russ.).
Регель А.Р. Безэлектродный метод измерения электропроводности и возможности его применения для задач физико-химического анализа. *Журнал неорганической химии*. 1956;1(6):1271–1277.
 41. Ryabina A.V., Kononenko V.I., Razhabov A.A. Nonelectrode method of measurement electrical resistivity of metals in solid and liquid states and installation for its realization. *Rasplavy*. 2009(1):36–42. (In Russ.).
Рябина А.В., Кононенко В.И., Ражабов А.А. Безэлектродный метод измерения электросопротивления металлов в твердом и жидком состояниях и установка для его реализации. *Расплавы*. 2009(1):36–42.
 42. Tyagunov G.V., Baum B.A., Tsepelev V.S., Tyagunov A.G., Vlokh A.N. Measurement of electrical resistivity by rotating magnetic field method. *Zavodskaya laboratoriya*. 2003;69(2):36–38. (In Russ.).
Тягунов Г.В., Баум Б.А., Цепелев В.С., Тягунов А.Г., Влох А.Н. Измерение удельного электрического сопротивления методом вращающегося магнитного поля. *Заводская лаборатория*. 2003;69(2):36–38.
 43. Shvidkovskii E.G. Some Issues of Molten Metals Viscosity. Moscow: Gostekhizdat; 1955:206. (In Russ.).
Швидковский Е.Г. Некоторые вопросы вязкости расплавленных металлов. Москва: Гостехиздат; 1955:206.
 44. Konashkov V.V., Tsepelev V.S., V'yukhin V.V., Povodator A.M., Podol'skaya A.I. A computer-aided plant for studying the kinematic viscosity of high-temperature metallic melts. *Instruments and Experimental Techniques*. 2011; 54(2):284–285. <https://doi.org/10.1134/S0020441211020187>
Конашков В.В., Цепелев В.С., Вьюхин В.В., Поводатор А.М., Подольская А.И. Автоматизированная установка для изучения кинематической вязкости высокотемпературных металлических расплавов. *Приборы и техника эксперимента*. 2011;(2):149–150.
 45. Chikova O.A., Shmakova K.Yu., Tsepelev V.S. Determination of phase equilibrium temperatures of high-entropy metal alloys by the viscometric method. *Metaly*. 2016;(2):54–59. (In Russ.).
Чикова О.А., Шмакова К.Ю., Цепелев В.С. Определение температур фазовых равновесий высокоэнтропийных металлических сплавов вискозиметрическим методом. *Металлы*. 2016;(2):54–59.

46. Tanaka T., Hara S. Surface tension and viscosity of liquid iron alloys. *Materia Japan*. 1997;36(1):47–54.
47. Feng G., Jiao K., Zhang J., Gao S. High-temperature viscosity of iron-carbon melts based on liquid structure: The effect of carbon content and temperature. *Journal of Molecular Liquids*. 2021;330:115603. <https://doi.org/10.1016/j.molliq.2021.115603>
48. Kamaeva L.V., Sterkhova I.V., Lad'yanov V.I. Viscosity and supercooling of Fe-Cr (≤ 40 at % Cr) melts. *Inorganic Materials*. 2012;48(3):318–324. <https://doi.org/10.1134/S0020168512030089>
49. Sterkhova I.V., Kamaeva L.V., Lad'yanov V.I. Viscosity of the eutectic $Fe_{85-x}Cr_{15}C_x$ ($x = 10-17$) melts. *Physics and Chemistry of Liquids*. 2020;58(5):559–565. <https://doi.org/10.1080/00319104.2019.1616194>
50. Odelevskii V.I. Calculation of generalized conductivity of heterogeneous systems. *Journal of Technical Physic*. 1951;21(6):667–685. (In Russ.).
Оделевский В.И. Расчет обобщенной проводимости гетерогенных систем. *Журнал технической физики*. 1951;21(6):667–685.
51. Ono Y., Hirayama K., Furukawa K. Electric resistivity of molten Fe-C, Fe-Si, and Fe-C-Si alloys. *Tetsu-to-Hagane*. 1974;60(14):2110–2118. https://doi.org/10.2355/tetsutohagane1955.60.14_2110
52. Kudryavtseva E.D., Singer V.V., Radovskii I.Z. Electronic structure of liquid alloys of iron with manganese, chromium and vanadium. *Izvestiya vuzov. Fizika*. 1983;(1):55–58. (In Russ.).
Кудрявцева Е.Д., Сингер В.В., Радовский И.З. Электронная структура жидких сплавов железа с марганцем, хромом и ванадием. *Известия вузов. Физика*. 1983;(1):55–58.
53. Chikova O.A., Tsepelev V.S., Moskovskikh O.P. Estimating the parameters of the microheterogeneous structure of metal melts according to viscometric experimental data in terms of the absolute reaction rate theory. *Russian Journal of Physical Chemistry A*. 2017;91(6):979–983. <https://doi.org/10.7868/S0044453717060073>
Чикова О.А., Цепелев В.С., Московских О.П. Оценка параметров микрогетерогенной структуры металлических расплавов из результатов вискозиметрического эксперимента на основе представлений теории абсолютных скоростей реакций. *Журнал физической химии*. 2017;91(6):925–930.
54. Chikova O.A., Sinitsin N.I., V'yukhin V.V. Parameters of the microheterogeneous structure of liquid 110G13L steel. *Russian Journal of Physical Chemistry A*. 2019;93(8):1435–1442. <https://doi.org/10.1134/S0044453719080065>
Чикова О.А., Синицин Н.И., Вьюхин В.В. Параметры микрогетерогенной структуры жидкой стали 110Г13Л. *Журнал физической химии*. 2019;93(8):1138–1146. <https://doi.org/10.1134/S0044453719080065>
55. Tyagunov G.V., Baryshev E.E., Vandysheva I.V., Zaitseva N.V., Khomenko A.O. Structure and properties of liquid iron. *Bulletin of SUSU. Series "Metallurgy"*. 2019;19(3):13–23. (In Russ.).
Тягунов Г.В., Барышев Е.Е., Вандышева И.В., Зайцева Н.В., Хоменко А.О. Структура и свойства жидкого железа. *Вестник ЮУрГУ. Серия "Металлургия"*. 2019;19(3):13–23.
56. Potapov M.G., Babaev A.A., Gulyaev Yu.E. Classification of complex-alloyed cast irons by the temperature of melt clusters disordering during development of TTM. *Actual problems of modern science, technology and education*. 2022;13(1):31–35. (In Russ.).
Потапов М.Г., Юмабаев А.А., Гуляев Ю.Е. Классификация комплексно-легированных чугунов по температуре разупорядочения кластеров расплава при разработке режимов ВТОР. *Актуальные проблемы современной науки, техники и образования*. 2022;13(1):31–35.

Information about the Authors

Сведения об авторах

Vladimir S. Tsepelev, Dr. Sci. (Eng.), Prof., Director of the Research Center of Physics of Metallic Liquids, Ural Federal University named after the first President of Russia B.N. Yeltsin

ORCID: 0000-0003-4195-9042

E-mail: v.s.tsepelev@urfu.ru

Nikolai I. Sinitsin, Cand. Sci. (Phys.-Math.), Assist. Prof. of the Chair of Physics, Senior Researcher of the Research Center of Physics of Metallic Liquids, Ural Federal University named after the first President of Russia B.N. Yeltsin

ORCID: 0000-0002-6264-6523

E-mail: n.i.sinitsin@urfu.ru

Ol'ga A. Chikova, Dr. Sci. (Phys.-Math.), Prof. of the Chair of Physics, Ural Federal University named after the first President of Russia B.N. Yeltsin

ORCID: 0000-0002-3347-9148

E-mail: chik63@mail.ru

Mikhail G. Potapov, Cand. Sci. (Eng.), Assist. Prof. of the Chair "Foundry Processes and Materials Science", Nosov Magnitogorsk State Technical University

ORCID: 0000-0002-2818-6535

E-mail: potapovmg@mail.ru

Владимир Степанович Цепелев, д.т.н., профессор, директор Исследовательского центра физики металлических жидкостей, Уральский федеральный университет имени первого Президента России Б.Н. Ельцина

ORCID: 0000-0003-4195-9042

E-mail: v.s.tsepelev@urfu.ru

Николай Иванович Синицин, к.ф.-м.н., доцент кафедры физики, старший научный сотрудник Исследовательского центра физики металлических жидкостей, Уральский федеральный университет имени первого Президента России Б.Н. Ельцина

ORCID: 0000-0002-6264-6523

E-mail: n.i.sinitsin@urfu.ru

Ольга Анатольевна Чикова, д.ф.-м.н., профессор кафедры физики, Уральский федеральный университет имени первого Президента России Б.Н. Ельцина

ORCID: 0000-0002-3347-9148

E-mail: chik63@mail.ru

Михаил Геннадьевич Потапов, к.т.н., доцент кафедры литейных процессов и материаловедения, Магнитогорский государственный технический университет им. Г.И. Носова

ORCID: 0000-0002-2818-6535

E-mail: potapovmg@mail.ru

Vladimir V. Vyukhin, Senior Researcher of the Research Center of Physics of Metallic Liquids, Ural Federal University named after the first President of Russia B.N. Yeltsin
ORCID: 0000-0002-0772-8155
E-mail: v.v.vyukhin@urfu.ru

Владимир Викторович Вьюхин, старший научный сотрудник Исследовательского центра физики металлических жидкостей, Уральский федеральный университет имени первого Президента России Б.Н. Ельцина
ORCID: 0000-0002-0772-8155
E-mail: v.v.vyukhin@urfu.ru

Contribution of the Authors

Вклад авторов

V. S. Tsepelev – theoretical justification for the study of liquid metal melts, methodology for studying the kinematic viscosity and specific electrical resistance of liquid cast iron, experimental planning, analysis and interpretation of results, provision of financial resources and necessary materials for conducting high-temperature experiments, scientific editing of the text.

N. I. Sinitsin – conducting an experimental study of liquid cast iron using a unit for measuring specific electrical resistance, primary processing of the obtained data.

O. A. Chikova – theoretical substantiation of the study of liquid chromium cast iron from the point of their micro-heterogeneous structure, writing the text.

M. G. Potapov – initiating the research, formulating the research goal and objectives, preparation and certification of materials.

V. V. Vyukhin – conducting an experimental study of liquid cast iron using a unit for measuring kinematic viscosity, primary processing of the obtained data.

В. С. Цепелев – теоретическое обоснование исследования металлических расплавов в жидком состоянии, методология исследований кинематической вязкости и удельного электросопротивления жидких чугунов, планирование эксперимента, анализ и интерпретация полученных результатов, предоставление финансовых ресурсов и необходимых материалов для проведения высокотемпературных экспериментов, научное редактирование текста статьи.

Н. И. Сеницин – проведение экспериментального исследования жидких чугунов на установке по измерению удельного электросопротивления, первичная обработка полученных данных.

О. А. Чикова – теоретическое обоснование исследования расплавов хромистых чугунов в жидком состоянии с точки зрения их микрооднородного строения, написание статьи.

М. Г. Потанов – инициатива проведения исследования, формулирование цели и задач исследования, подготовка и аттестация материалов.

В. В. Вьюхин – проведение экспериментального исследования жидких чугунов на установке по измерению кинематической вязкости, первичная обработка полученных данных.

Received 28.02.2024

Revised 19.03.2024

Accepted 23.08.2024

Поступила в редакцию 28.02.2024

После доработки 19.03.2024

Принята к публикации 23.08.2024

INNOVATION IN METALLURGICAL
INDUSTRIAL AND LABORATORY EQUIPMENT,
TECHNOLOGIES AND MATERIALSИННОВАЦИИ В МЕТАЛЛУРГИЧЕСКОМ
ПРОМЫШЛЕННОМ И ЛАБОРАТОРНОМ
ОБОРУДОВАНИИ, ТЕХНОЛОГИЯХ И МАТЕРИАЛАХ

UDC 621.74.045:53.09

DOI 10.17073/0368-0797-2024-5-593-603



Original article

Оригинальная статья

INFLUENCE OF COMPRESSION MODES OF WAXY POWDERS ON STRESS-STRAIN STATE OF COMPACTS USED IN PRECISION CASTING

N. A. Bogdanova[✉], S. G. Zhilin

Institute of Metallurgy and Mechanical Engineering of the Khabarovsk Federal Research Center, Far-Eastern Branch of the Russian Academy of Sciences (1 Metallurgov Str., Komsomolsk-on-Amur, Khabarovsk Territory 681005, Russian Federation)

✉ joyful289@inbox.ru

Abstract. The high demands placed on the surface quality and geometric complexity of metal products, structures and parts produced from a wide range of non-ferrous and ferrous alloys determine the demand for investment casting as a method that provides a range of critical products for the needs of aircraft, ship building and mechanical engineering industries. A number of “bottlenecks” in the implementation of investment casting processes include a significant number of technological operations, each of them is accompanied by phenomena of a thermophysical nature that require correction, and it ultimately determines the high cost of casting. The difficulties arise from phenomena such as shrinkage of the pattern material, its thermal expansion during melting from a ceramic mold, which determines penetration of pattern mass into ceramic pores and can affect the appearance of surface defects, the chemical composition and structure of the alloy of future casting. The process of forming a porous surface on wax patterns without shrinkage defects by pressing powders of waxy materials is aimed at eliminating the noted shortcomings, which ensures the required geometry of the compacts and absence of deformation effects on ceramics of the model material at the stage of its melting. Widespread use of the method is hampered by the lack of information about the features of stress control in the compact body determining the magnitude of elastic response of the compacted material, which is an order of magnitude less than thermal shrinkage. The paper presents the results of an experimental study of influence of the compression rate of powder materials on the stress-strain state of pressed wax patterns formed in a closed matrix, as well as on the strength of these compacts.

Keywords: experimental modeling, mechanical engineering processes, investment casting, stress-strain state, pressing, porosity, elastic response, strength

Acknowledgements: The work was performed within the framework of a state assignment of the Khabarovsk Federal Research Center, Far-Eastern Branch of the Russian Academy of Sciences. The authors used photos by Firsov S.V.

For citation: Bogdanova N.A., Zhilin S.G. Influence of compression modes of waxy powders on stress-strain state of compacts used in precision casting. *Izvestiya. Ferrous Metallurgy*. 2024;67(5):593–603. <https://doi.org/10.17073/0368-0797-2024-5-593-603>

ВЛИЯНИЕ РЕЖИМОВ УПЛОТНЕНИЯ ВОСКОБРАЗНЫХ ПОРОШКОВ НА НАПРЯЖЕННО-ДЕФОРМИРОВАННОЕ СОСТОЯНИЕ ПРЕССОВОК, ПРИМЕНЯЕМЫХ В ТОЧНОМ ЛИТЬЕ

Н. А. Богданова[✉], С. Г. Жилин

Институт машиноведения и металлургии Хабаровского Федерального исследовательского центра Дальневосточного отделения РАН (Россия, 681005, Хабаровский край, Комсомольск-на-Амуре, ул. Металлургов, 1)

✉ joyful289@inbox.ru

Аннотация. Высокие требования, предъявляемые к качеству поверхности и сложности геометрии металлоизделий, конструкций и узлов деталей, получаемых из широкой линейки цветных и черных сплавов, определяют востребованность литья по выплавляемым моделям (ЛВМ) как метода, обеспечивающего номенклатуру изделий ответственного назначения для нужд авиа-, судо-, и машиностроения. К ряду «узких» мест в реализации процессов ЛВМ можно отнести значительное число технологических операций, каждая из которых сопровождается явлениями теплофизической природы, требующих коррекции, что в конечном итоге определяет высокую стоимость литья. Сложность представляют такие явления, как усадка модельного материала, его температурное расширение на стадиях выплавки из керамической формы, определяющее проникновение модельной массы в поры керамики и способное повлиять на появление поверхностных дефектов, химический состав и структуру сплава будущей отливки. На устранение отмеченных недостатков направлен процесс

формирования пористой поверхности выплавляемой модели без усадочных дефектов путем прессования порошков воскообразных модельных материалов, что обеспечивает требуемую геометрию прессовок и отсутствие деформационного воздействия на керамику модельного материала на стадии его выплавления. Широкому распространению метода препятствует недостаток сведений об особенностях управления напряжениями в теле прессовки, определяющими величину упругого отклика уплотняемого материала, который на порядок меньше, чем тепловая усадка. В работе представлены результаты экспериментального определения влияния скорости уплотнения порошковых модельных материалов на напряженно-деформированное состояние прессованных выплавляемых моделей, формируемых в закрытой матрице, а также на прочность таких прессовок.

Ключевые слова: экспериментальное моделирование, машиностроительные процессы, литье по выплавляемым моделям, напряженно-деформированное состояние, прессовка, пористость, упругий отклик, прочность

Благодарности: Работа выполнена в рамках государственного задания Института машиноведения и металлургии Хабаровского Федерального исследовательского центра ДВО РАН. В работе использованы фото Фирсова С.В.

Для цитирования: Богданова Н.А., Жилин С.Г. Влияние режимов уплотнения воскообразных порошков на напряженно-деформированное состояние прессовок, применяемых в точном литье. *Известия вузов. Черная металлургия*. 2024;67(5):593–603.

<https://doi.org/10.17073/0368-0797-2024-5-593-603>

INTRODUCTION

A key feature of modern industrial enterprises specializing in the production of products for the automotive, aircraft, and shipbuilding industries is the high demand for metals and the increased production of high-quality cast products with the required set of characteristics, driven by the use of energy- and material-efficient technologies [1 – 4].

In these sectors, it is crucial to reduce costs at all stages of the technological cycle, especially in the formation of castings for high-precision and complex-shaped parts made from a wide range of alloys [5].

One of the most in-demand methods for obtaining precision cast blanks from a variety of structural steels and alloys is investment casting (IC), which allows the creation of complex-shaped products by combining separate parts into all-cast assemblies [6; 7]. The versatility of this method makes it suitable for producing both thin-walled castings of relatively small mass and cast products with linear dimensions of up to 500 mm [8 – 10].

The surface of such castings can achieve a roughness of up to $R_a = 1.25 \mu\text{m}$, meet quality grades 11 – 16, and achieve mold cavity dimensional tolerances of no more than grades 8 – 9 according to GOST 25347–82 “Basic norms of interchangeability. Unified system of tolerances and fits. Tolerance fields and recommended fits”.

Like any technological sequence, IC has its drawbacks, largely due to the large number of operations involved, which are characterized by a certain degree of irreparable defects. These factors ultimately increase the cost of the final product and complicate the calculation and modeling of the IC process outcomes [11].

The most widely used sequence in IC processes includes the following operations [12]:

- manufacturing of wax models and elements of the gating and feeding systems by injection of the model composition (melt or paste) into the corresponding mold, followed by the assembly of all elements into model clusters;

- layer-by-layer application of ceramic coating to the model cluster and drying of the ceramic shell;

- melting of the pattern material from the ceramic shell, followed by its firing and pouring of molten metal.

A significant problem is the negative impact of thermophysical phenomena, which result in changes in material volume due to thermal expansion or shrinkage. These phenomena accompany many of the technological operations mentioned above. Combatting shrinkage defects, characteristic of IC processes, which manifest both in the alloy of the casting body [13; 14] and during the production of wax models [15; 16], presents several technological challenges. The solution primarily involves ensuring a narrow pouring temperature range and controlling the solidification conditions of both the molten metal and the model mass.

For instance, during the cooling phase of the wax mass in the formation of the wax pattern, volumetric shrinkage can reach 14 %, manifesting on the surface in the form of sink marks, wrinkles, and waviness, requiring additional resources to correct these defects [17]. Preventing such defects is only partially achieved by optimizing processes at the design stage, strictly controlling the injection temperature of the pattern materials, and improving their compositions, which helps reduce the thermal expansion coefficient [18 – 21]. Geometrical distortion in castings can also occur due to the poor wettability of the wax model surface by the materials forming the ceramic shell [22]. The thermal expansion of the pattern material during its melting from the shell is also a cause of shell integrity violations [23]. The issue of low crack resistance in ceramics is sometimes addressed by reinforcing them with various materials and inserts [24]. After achieving the required ceramic thickness, shell molds are often subjected to a de-waxing process, typically performed by autoclaving. This operation also carries certain risks of damage to the inner layers due to the thermal expansion of the pattern material, which penetrates the pores of the ceramic during melting [25]. Residual wax material in the ceramic layers can affect the structure and sur-

face properties of the casting. These issues necessitate increased allowances for mechanical processing, leading to higher metal consumption.

The researchers from the Laboratory of Problems of Creation and Processing of Materials and Products at the Khabarovsk Federal Research Center of the Far Eastern Branch of the Russian Academy of Sciences have proposed a comprehensive solution to the aforementioned problems related to the thermal expansion of pattern materials. The solution involves forming wax patterns either entirely or their surface (in the case of producing wax patterns for bimetallic castings, where the surface is formed by pressing pattern material powder onto a steel frame) through cold pressing of fractions of waxy pattern materials. This approach allows for the creation of a pressed structure with porosity of up to 12 %, with the outer surface configuration corresponding to the shaping cavity of the mold [26; 27].

This method of forming wax patterns ensures that the pattern material penetrates complex shaping cavities of the press matrix and achieves the required density in sections of the compact [28; 29]. Pressed wax patterns are distinguished by the absence of such casting defects as shrinkage, waviness, or geometric distortion. During the stage of model removal from the ceramic mold, these models do not deform the shell, and the pattern material does not penetrate its structure, thereby ensuring its crack resistance. The absence of pattern material in the pores of the ceramic ensures predictable structure and surface properties of the final casting.

A drawback of the presented process is the potential for dimensional changes in the compact due to the unloading of the pattern material and the release of air trapped during compaction. The magnitude of the elastic response of the compacted material after the load is removed can reach 0.7 – 1.2 % in the pressing axis direction and 0.4 – 0.5 % in the transverse direction, which, although significantly lower than the values of volumetric shrinkage, still requires a special approach to eliminate this phenomenon [30]. The mechanical strength of porous pressed wax patterns is lower than that of traditional models but is compensated by higher thermal stability.

The magnitude of the elastic unloading of the compacted material largely depends on its rheological characteristics: elasticity, plasticity, strength, viscosity, etc. During the compaction of a plastic powder body without external heat sources, the temperature in local sections of the compact material increases. Thus, reducing the values of elastic unloading depends on both the compaction speed and the stress relaxation time [31; 32]. In view of the aforementioned, the production of pressed wax patterns or their elements with predictable dimensions and minimal geometric distortions relative

to the press mold cavity appears to be a relevant task in the pressing of waxy pattern material powders.

In previous works [33; 34], various solutions were proposed for addressing the issues related to the pressing modes that ensure stress relaxation in the compacts, and consequently, a reduction in the elastic after-effect of the compacted material. However, the comprehensive study of the influence of compaction speed modes of waxy powder materials in a closed press mold on the stress-strain state of the compacts, as well as the final strength and nature of their failure, is presented here for the first time.

Thus, the purpose of the present work is to determine the influence of the movement speed of the press punch during the deformation of powder bodies composed of waxy pattern materials on the stress-strain state of the compacts formed in a closed matrix.

To achieve this goal, the following tasks were addressed in the study:

- experimental determination of the stress dependencies accompanying the stages of compaction and unloading of compacts with porosity ranging from 0 to 10 %, as a function of time, at various press punch movement rates and fractions of waxy powder materials;
- experimental determination of the ultimate compression strength as a function of the porosity of samples formed from fractions of waxy powder materials at various press punch movement rates, and evaluation of the influence of pressing conditions on the nature of compact failure.

METHODS FOR CONDUCTING THE STUDY

In the experimental part of the study, which involved forming the compacts and recording stresses during their compaction and failure, the reliability of the measured stress values was ensured by using the Shimadzu AG-X Plus testing machine. The specified characteristics of this machine, as regulated by the manufacturer, include a permissible deviation of 0.03 % at a load of 100 kN and a deformation of 10 mm. Fig. 1 shows the working area of the testing machine, located between the stationary lower support 1, which holds the press matrix 2 (fitted with a punch), and the moving rod 3. The press matrix is made of steel grade 45 in the form of a hollow blind-bottom cylinder with an inner diameter of $d = 44$ mm and a wall thickness of 4 mm, which, within the scope of this experiment, allows it to be considered non-deformable. The mold cavity was filled with a calculated dose of waxy powder material required for each experiment. For the experimental tasks, waxy powders commonly used in investment casting processes, corresponding to the first classification group of model compositions, were employed [6]:

– refined paraffin of grade T1, with a melting point of 60 °C and a density of $\rho_{T1} = 0.86 \text{ g/cm}^3$ in the cast state;

– PS50/50 (a paraffin-stearin alloy in a 1:1 ratio), with a melting point of 52 °C and a density of $\rho_{PS50/50} = 0.935 \text{ g/cm}^3$ in the cast state.

The melting point and density of the materials in their cast state are essential for ensuring the accuracy of the experimental data. These values slightly differ from the characteristics specified by relevant GOST standards (for example, “Petroleum solid paraffins. Specifications. GOST 23683–89”) and were determined experimentally. The melting points of T1 and PS50/50 were preliminarily determined using the Shimadzu DTG-60H differential thermal analyzer during the heating of these materials at a rate of 2 °C/min [17]. Since the materials used in the study are low-melting, the experiments were conducted at ambient temperatures of $20 \pm 2 \text{ °C}$. The powder fractions of the waxy materials mentioned above were obtained by sieving through model 026 sieves in the technologically preferred standard size range of 0.63 to 2.5 mm [33]. Using smaller fractions is impractical due to the high tendency of the material to cake, and using fractions larger than 2.5 mm may, in some cases, lead to the formation of “arches” in the inner sections of complex-shaped molds, causing uneven material distribution and, as a result, compacts with zones of local over-compaction. The bulk density values (ρ_{bulk}) depend on the type

and fraction of the materials and are as follows: for T1 with a fraction of 2.5 mm, $\rho_{\text{bulk}} = 0.360 \text{ g/cm}^3$; for T1 with a fraction of 0.63 mm, $\rho_{\text{bulk}} = 0.320 \text{ g/cm}^3$; for PS50/50 with a fraction of 2.5 mm, $\rho_{\text{bulk}} = 0.340 \text{ g/cm}^3$; and for PS50/50 with a fraction of 0.63 mm, $\rho_{\text{bulk}} = 0.310 \text{ g/cm}^3$.

To reduce the effect of friction between the material and the inner surface of the press mold on the stress values that occur during compaction, the mold cavity was treated with kerosene. The uniform distribution of the material within the volume of the powder body placed in the press mold was achieved by pre-vibrating it for 5 min at a frequency of 3.5 Hz. After the vibration process, the experimental materials were compacted at press punch movement speeds of 0.5 mm/s and 1.5 mm/s, which were controlled by the movement of the crosshead of the universal testing machine AG-X Plus Shimadzu. As a result of the uniaxial movement of the punch, a compact was formed in the lower part of the press mold, with final dimensions satisfying the condition: $d = h = 0.44 \text{ m}$ (where h is the final height of the compact).

The dose of waxy powder material was determined by the final porosity of the compacts, which in the experiment varied in increments of 2 % within the range $0 \% \leq P \leq 10 \%$, depending on the mechanical characteristics of the compacts. For example, in preliminary experiments, it was found that compacts with porosity $P > 10 \%$ exhibited reduced strength.

The porosity of the compact was calculated using the formula

$$P = \left(1 - \frac{\rho_p}{\rho_c}\right) 100 \%, \quad (1)$$

where ρ_p is the density of the compact, kg/m^3 , and ρ_c is the density of the cast material, kg/m^3 .

It is evident that compacts with a porosity of $P = 0 \%$ will have a density equal to the density of the material in its freely cast state, which for materials of grades T1 and PS50/50 $\rho_{cT1} = 0.86 \text{ g/cm}^3$ and $\rho_{cPS50/50} = 0.935 \text{ g/cm}^3$.

The mass M of the waxy powder material required to form a compact with the desired porosity was determined based on the condition

$$M = h\rho_c \left(1 - \frac{P}{100}\right) \left(\frac{\pi d^2}{4}\right). \quad (2)$$

The Table presents the values of the mass and bulk density of the powdered materials of grades T1 and PS50/50 used in the experiment to form compacts with final porosity in the range of $0 \% \leq P \leq 10 \%$.

From the data presented in the Table, it is evident that the values of the final porosity of the compacts, in this case confined within the volume of a cylindrical cavity with a diameter and height of 44 mm, determine the mass and bulk

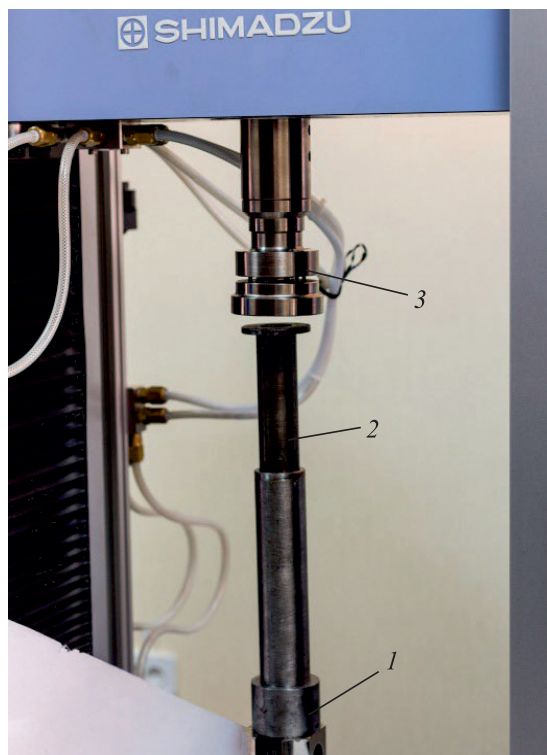


Fig. 1. Press matrix and working area of the testing machine

Рис. 1. Пресс-матрица и рабочая зона тестовой машины

Values of masses and bulk density of waxy materials powders

Значения масс и насыпной плотности порошков воскообразных материалов

Porosity, %	Filling mass, g / Bulk density, g/cm ³	
	T1	ПС 50/50
0	57.51/0.8600	62.52/0.9350
2	56.36/0.8428	61.27/0.9163
4	55.21/0.8256	60.02/0.8976
6	54.06/0.8084	58.77/0.8789
8	52.91/0.7912	57.52/0.8602
10	51.76/0.7740	56.27/0.8415

density values of the powdered materials used in the experiment. These factors, combined with the material fractions, account for the varying heights of the powder filling in the shaping cavity of the press matrix and, consequently, the differences in the deformation values of the compacted powder bodies. Thus, it is clear that at equal press punch movement rates, the time required to obtain compacts with different final porosity values will vary.

Fig. 2 presents the experimental dependencies of the deformation of powder bodies composed of T1 and PS50/50 materials with fractions of 0.63 and 2.5 mm, as a function of the compaction time to achieve porosity values of $0\% \leq P \leq 10\%$, with press punch movement rates of 1.5 mm/s (a) and 0.5 mm/s (b). These dependencies are shown in different colors. The equations corresponding to each curve are displayed in the same color scheme on the graph. For each curve shown in Fig. 2, the porosity values decrease from 10 to 0% as the compaction time increases (i.e., from left to right).

It can be seen from Fig. 2 that the deformation magnitude of the compacted powder bodies for compacts with all porosity values does not exceed 60%. Additionally, larger fractions of homogeneous materials exhibit higher bulk density values and, consequently, slightly lower final deformation values.

Once the height *h* was reached, the crosshead of the testing machine was fixed, and the stresses were recorded. One of the factors affecting the geometry of the resulting porous wax patterns is the magnitude of residual stresses in the compact material. Therefore, after the compaction process was completed, the samples were held under load with the press mold elements closed for 15 min. Preliminary experiments established that this amount of time is sufficient for stress relaxation to 90% or more [33].

Next, to determine the maximum stresses corresponding to the failure of the samples and the nature of their

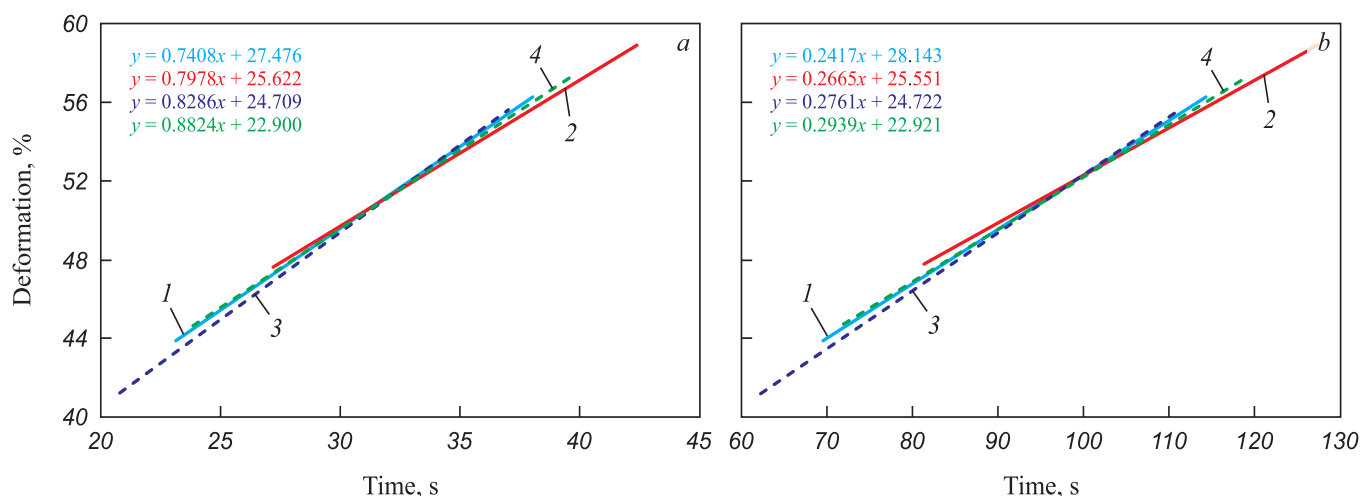


Fig. 2. Dependence of powder body deformation on time of its compaction when moving the press punch at a rate of 1.5 mm/s (a) and 0.5 mm/s (b):

1 – T1, fraction 0.63 mm; 2 – PS50/50, fraction 0.63 mm; 3 – T1, fraction 2.5 mm; 4 – PS50/50, fraction 2.5 mm

Рис. 2. Зависимости деформации порошкового тела от времени его уплотнения при перемещении пресс-пуансона со скоростью 1,5 мм/с (a) и 0,5 мм/с (b):

1 – Т1, фракция 0,63 мм; 2 – ПС50/50, фракция 0,63 мм; 3 – Т1, фракция 2,5 мм; 4 – ПС50/50, фракция 2,5 мм

failure, the resulting compacts were subjected to a compression test, as shown in Fig. 3.

The stresses arising during the determination of the compressive strength of the experimental cylindrical compacted samples were also recorded using the AG-X Plus Shimadzu testing machine. Since waxy powder materials are not structural materials and there are no standards for this type of testing, the movement speed of the testing machine's crosshead was selected at 22 mm/min, in accordance with GOST 4651–2014 "Plastics. Compression testing method".

Based on the data obtained from the series of experiments, the dependencies of the stresses accompanying the stages of material compaction and unloading on time, as well as the stresses arising during compression tests as a function of the porosity of the samples formed at various deformation rates, were plotted.

RESULTS AND DISCUSSION

The waxy model compositions used in the present experiment have a relatively high yield point [34], which naturally influences the nature of the compaction process of the powder body and the formation of the final properties of the compact. During the forming of materials with significant plasticity, the stages of the pressing process occur simultaneously, and the sections of the curves characterizing the compaction stages overlap with each other. Thus, in the case under consideration, the stages of the forming process in a closed press matrix (typical of the sequential stages of ideal compaction), such as structural deformation of the powder body, pressure increase without an increase in compact density, and subsequent plastic deformation distributed throughout its volume, have no clear boundaries.



Fig. 3. Placing an experimental cylindrical sample in the testing machine during a compression test

Рис. 3. Размещение экспериментального цилиндрического образца в тестовой машине при испытании на сжатие

As a result of the experiment, the stress dependencies accompanying the compaction and unloading stages of the compacts, with final porosity values of $P = 0 - 10\%$, were determined as a function of time, using various press punch movement speeds for fractions of waxy powder materials.

Fig. 4 shows the stress dependencies accompanying the compaction stages up to a porosity value of 0% and the unloading stages as a function of time for compacts made from T1 and PS50/50 materials with fractions of 0.63 mm (a) and 2.5 mm (b). Fig. 5 shows similar stress dependencies for the processes of forming compacts with a porosity of $P = 10\%$.

The sections of the dependencies shown in Figs. 4 and 5 that lie in the region of negative time values characterize the compaction processes of waxy powder bodies.

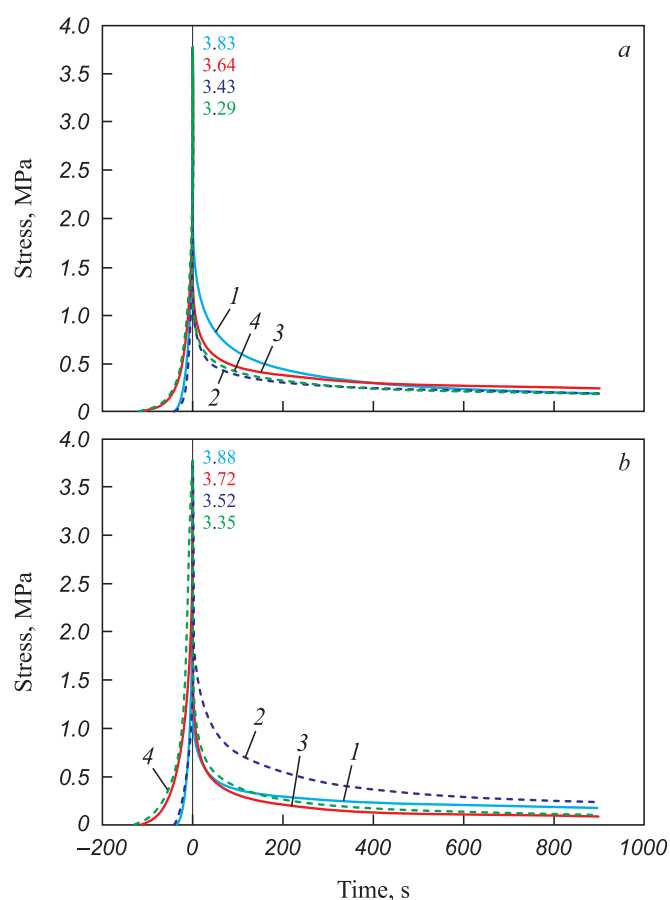


Fig. 4. Dependences of the stresses accompanying the stages of compaction to a porosity of 0% and outloading of compacts from materials of grades T1 and PS50/50 with a fraction of 0.63 mm (a) and 2.5 mm (b) on time:
1 – T1, rate 1.5 mm/s; 2 – PS50/50, rate 1.5 mm/s;
3 – T1, rate 0.5 mm/s; 4 – PS50/50, rate 0.5 mm/s

Рис. 4. Зависимости напряжений, сопровождающих стадии уплотнения до значения пористости 0% и разгрузки от времени прессовок из материалов марок Т1 и ПС50/50 фракций 0,63 мм (а) и 2,5 мм (б):
1 – Т1, скорость 1,5 мм/с; 2 – ПС50/50, скорость 1,5 мм/с;
3 – Т1, скорость 0,5 мм/с; 4 – ПС50/50, скорость 0,5 мм/с

The peak stress values arising during the compaction of powder bodies are indicated by numbers on the graph.

It can be seen from Fig. 4 that an increase in the press punch movement rate leads to an increase in the stress values required for forming the compacts. Moreover, the compaction of the T1 powder material is characterized by slightly higher stress values compared to the compaction of the paraffin-stearin material PS50/50, which exhibits greater plasticity. The material fraction of the pattern material (at the press punch movement rates used in this experiment) significantly influences the stress values arising during the compaction of the powder body, primarily under conditions of pressing bodies with low porosity. Thus, the largest stress values arising during the compaction of the powder bodies examined in this experiment are determined by conditions where the powder body con-

sists of the largest fraction, compaction occurs at higher press punch movement rates, and the required final porosity value is minimal.

It is evident that at higher press punch movement rates, the deformation time is reduced. However, the reduction in residual stress values does not directly depend on the press punch movement rate during the compaction of the experimental powder bodies.

A combined analysis of the data presented in Figs. 4 and 5 shows that as the porosity increases to 10 %, the stresses required for compacting the compacts decrease. The changes in the stress values presented in Fig. 5, depending on the material, press punch movement rate, and powder fraction, follow a pattern similar to the dependencies shown in Fig. 4. It is also apparent that residual stress relaxation of more than 90 % is characteristic of all compaction variations after just 10 min of holding in a confined state. Overall, it should be noted that the residual stress values after 15 min of holding the compacts under load do not exceed 0.25 MPa for compacts with $P = 0 \%$ and 0.12 MPa for compacts with final porosity $P = 10 \%$.

According to previously obtained experimental results [33], which aimed to determine the stress values arising during the failure of experimental samples as a function of their porosity, it was established that the stresses at failure are higher the lower the porosity and the larger the fraction of the material from which the compacts are formed. However, the effects of compaction speed during the production of the compacts and material fraction on compressive strength and the nature of sample failure were not addressed.

In the experiment aimed at determining the ultimate compression strength, it was necessary to establish the dependence of this parameter on the porosity of the samples formed by the deformation of powder bodies composed of fractions of the waxy materials T1 and PS50/50 at various press punch movement speeds in a fixed mold. Fig. 6 shows the third-order polynomial dependencies of the determined parameter as a function of the porosity of samples formed at various press punch movement speeds. The reliability values of the polynomial approximation of the ultimate compression strength of the samples are indicated by the symbols R_f^2 .

Analysis of the data presented in Fig. 6 reveals that the stresses arising during the failure of experimental samples under compression are dependent on the maximum stress values required for compacting the samples. Thus, the higher the press punch movement rate and the larger the material fraction (with identical pre-set values of final compact porosity), the higher the stress value during pressing and, consequently, the higher the compressive strength at sample failure.

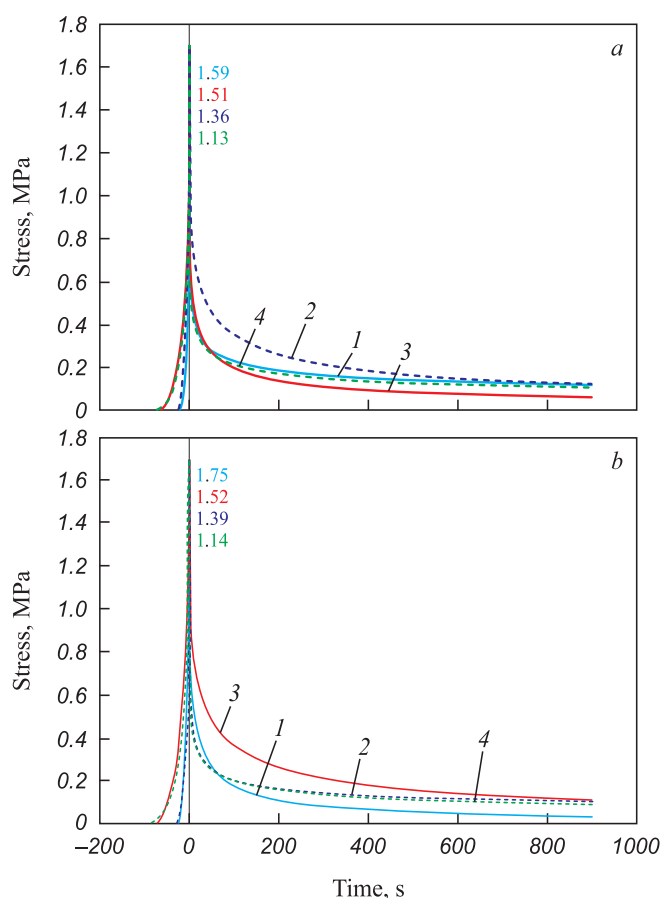


Fig. 5. Dependences of the stresses accompanying the stages of compaction to a porosity of 10 % and outloading of compacts from materials of grades T1 and PS50/50 with a fraction of 0.63 mm (a) and 2.5 mm (b) on time:
 1 – T1, rate 1.5 mm/s; 2 – PS50/50, rate 1.5 mm/s;
 3 – T1, rate 0.5 mm/s; 4 – PS50/50, rate 0.5 mm/s

Рис. 5. Зависимости напряжений, сопровождающих стадии уплотнения до значения пористости 10 % и разгрузки от времени прессовок, формируемых из материалов марок Т1 и ПС50/50 фракций 0,63 мм (а) и 2,5 мм (б):
 1 – Т1, скорость 1,5 мм/с; 2 – ПС50/50, скорость 1,5 мм/с;
 3 – Т1, скорость 0,5 мм/с; 4 – ПС50/50, скорость 0,5 мм/с

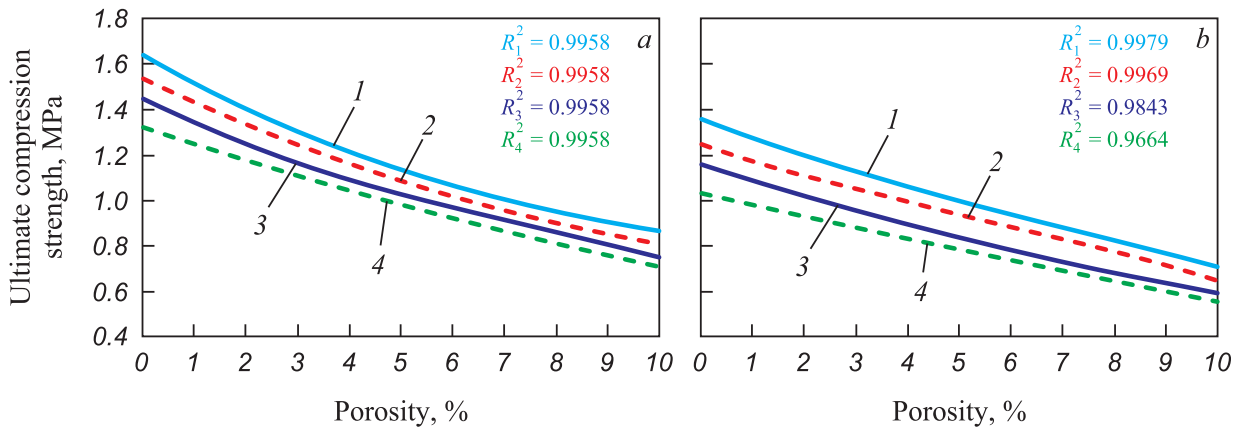


Fig. 6. Dependences of ultimate compression strength on porosity of the samples from fractions of materials of grades T1 (a) and PS50/50 (b) at different rate of press punch movement: 1 – fraction 2.5 mm, rate 1.5 mm/s; 2 – fraction 0.63 mm, rate 1.5 mm/s; 3 – fraction 2.5 mm, rate 0.5 mm/s; 4 – fraction 0.63 mm, rate 0.5 mm/s

Рис. 6. Зависимости предела прочности на сжатие от пористости образцов, сформированных из фракций материалов марок Т1 (а) и ПС50/50 (b) при различных скоростях перемещения пресс-пуансона: 1 – фракция 2,5 мм, скорость 1,5 мм/с; 2 – фракция 0,63 мм, скорость 1,5 мм/с; 3 – фракция 2,5 мм, скорость 0,5 мм/с; 4 – фракция 0,63 мм, скорость 0,5 мм/с

During the experiment, a visual assessment of the failure patterns of the experimental compacts was also conducted, and the influence of factors such as pressing speed, material fraction used in the experiment, and final compact porosity was determined. It is worth noting that, during visual observation of the compacts' deformation under compression, the material fraction and press punch movement rate during their formation had a minimal impact on the failure process. Fig. 7 shows the most typical failure patterns of compacts with minimal and maximal porosity values formed from PS50/50 material.

As shown in Fig. 7, samples with 0 % porosity typically exhibit barrel-shaped deformation under compression, indicating a more ductile type of failure. In contrast,

samples with 10 % porosity tend to fail in a trapezoidal shape, with cracks forming at angles of approximately 60° to the horizontal base, suggesting a more brittle failure.

Overall, it can be concluded that while compacts made from T1 material demonstrate better resistance to compression compared to those made from PS50/50, the PS50/50 compacts still possess sufficient strength to withstand compressive loads during the application of the initial (uncured) layers of the refractory shell. The experimental data on the failure patterns of the compacts are intended to assist in determining the design, mass, and dimensions of wax patterns and/or their components produced using powder material molding techniques.

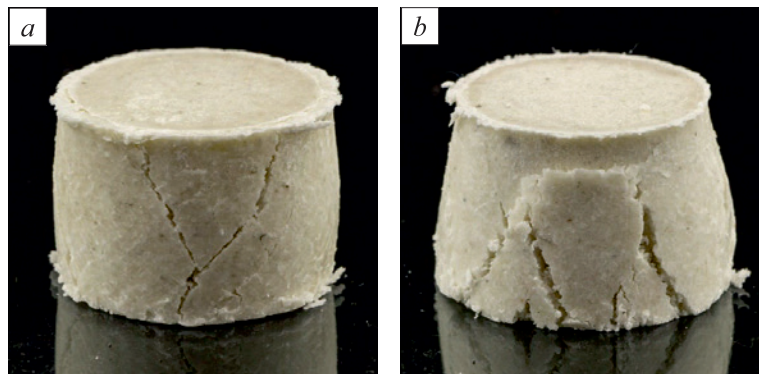


Fig. 7. Nature of destruction of compacts formed at a rate of press punch movement of 0.5 mm/sec: a – PS50/50, P = 0 %, fraction 0.63; b – PS50/50, P = 10 %, fraction 0.63

Рис. 7. Характер разрушения образцов прессовок, сформированных при скорости перемещения пресс-пуансона 0,5 мм/с: а – ПС50/50, П = 0 %, фракция 0,63 мм; б – ПС50/50, П = 10 %, фракция 0,63 мм

CONCLUSIONS

As a result of a series of experiments involving the loading of waxy powder materials, holding the formed compacts in a confined state, and their failure, the influence of the press punch movement rate on the stress-strain state of the compacts formed in a closed mold was determined.

Through experimental determination of the stress dependencies accompanying the stages of compaction and unloading of compacts with a porosity of 0 – 10 % over time, at various press punch movement rates and material fractions of waxy powder materials, the following was established:

- reducing the specified values of the final compact porosity leads to an increase in the stresses arising during the compaction of waxy powder bodies and is also determined by the use of larger material fractions and compaction at higher pressing rates;

- the press punch movement rate plays a less significant role in the magnitude of the residual stresses of compacts in a confined state after compaction than the final porosity of the compacts. As a result, in the compaction of experimental powder bodies, the residual stress values after 15 min of holding the compact in a loaded state do not exceed 0.25 MPa for compacts with $P = 0\%$ and 0.12 MPa for compacts with final porosity $P = 10\%$.

The analysis of the experimental data showed that increasing the press punch movement rate and increasing the fraction of the material being pressed leads to higher stress values at the failure of the experimental samples under compression. The final porosity of the compacts and the nature of the compacted material have a greater influence on whether the compacts fail in a ductile or brittle manner than the material fraction and pressing rate.

The results of this research are intended to help determine the design, mass, and dimensions of wax patterns and/or their components produced using powder material molding methods, ultimately leading to improved dimensional and geometric accuracy of the castings.

REFERENCES / СПИСОК ЛИТЕРАТУРЫ

1. Wang B., Zhang Z., Xu G., Zeng X., Hu W., Matsubae K. Wrought and cast aluminum flows in China in the context of electric vehicle diffusion and automotive lightweighting. *Resources, Conservation and Recycling*. 2023;191:106877. <https://doi.org/10.1016/j.resconrec.2023.106877>
2. Lim S.S., Mun J.C., Kim T.W., Kang C.G. Development of low-temperature high-strength integral steel castings for offshore construction by casting process engineering. *International Journal of Naval Architecture and Ocean Engineering*. 2014;6(4):922–934. <https://doi.org/10.2478/IJNAOE-2013-0222>
3. Yang X., Zhang C., Li X., Cao Z., Wang P., Wang H., Liu G., Xia Z., Zhu D., Chen W.Q. Multinational dynamic steel cycle analysis reveals sequential decoupling between material use and economic growth. *Ecological Economics*. 2024;217:108092. <https://doi.org/10.1016/j.ecolecon.2023.108092>
4. Sata A., Ravi B. Bayesian inference-based investment-casting defect analysis system for industrial application. *International Journal of Advanced Manufacturing Technology*. 2017;90(9–12):3301–3315. <https://doi.org/10.1007/s00170-016-9614-0>
5. Rodriguez A., López de Lacalle L.N., Calleja A., Lami-kiz A.F. Maximal reduction of steps for iron casting one-of-a-kind parts. *Journal of Cleaner Production*. 2012;24:48–55. <https://doi.org/10.1016/j.jclepro.2011.11.054>
6. Garanin V.F., Ivanov V.N., Kazennov S.A., etc. Investment Casting. Ozerov V.A. ed. Moscow: Mashinostroenie; 1994:448. (In Russ.).
Гаранин В.Ф., Иванов В.Н., Казеннов С.А. и др. Литье по выплавляемым моделям. Под общ. ред. В.А. Озерова. 4-е издание, переработанное и дополненное. Москва: Машиностроение; 1994:448.
7. Dong R.Z., Wang W.H., Zhang T.R., Jiang R.S., Yang Z.N., Cui K., Wan Y.B. Ensemble learning-enabled early prediction of dimensional accuracy for complex products during investment casting. *Journal of Manufacturing Processes*. 2024;113:291–306. <https://doi.org/10.1016/j.jmapro.2024.01.072>
8. Pattnaik S., Karunakar D.B., Jha P.K. Developments in investment casting process – A review. *Journal of Materials Processing Technology*. 2012;212(11):2332–2348. <https://doi.org/10.1016/j.jmatprotec.2012.06.003>
9. Kapranos P., Carney C., Pola A., Jolly M. Advanced casting methodologies: investment casting, centrifugal casting, squeeze casting, metal spinning, and batch casting. *Reference Module in Materials Science and Materials Engineering. Comprehensive Materials Processing*. 2014;5:39–67. <https://doi.org/10.1016/B978-0-08-096532-1.00539-2>
10. Yarlagadda P.K.D.V., Hock T.S. Statistical analysis on accuracy of wax patterns used in investment casting process. *Journal of Materials Processing Technology*. 2003;138(1–3):75–81. [https://doi.org/10.1016/S0924-0136\(03\)00052-9](https://doi.org/10.1016/S0924-0136(03)00052-9)
11. Zhilin S.G., Komarov O.N., Bogdanova N.A. Production of the steel casting with improved dimensional and geometrical accuracy using complex models. *IOP Conference Series: Materials Science and Engineering*. 2020;709(3):033104. <https://doi.org/10.1088/1757-899X/709/3/033104>
12. Vidyarthi G., Gupta N. New development in investment casting process. *International Journal of Scientific & Engineering Research*. 2017;8(12):529–540.
13. Huang P.H., Shih L.K.L., Lin H.M., Chu C.I., Chou C.S. Novel approach to investment casting of heat-resistant steel turbine blades for aircraft engines. *The International Journal of Advanced Manufacturing Technology*. 2019;104:2911–2923. <https://doi.org/10.1007/s00170-019-04178-z>
14. Chen T.Y., Wang Y.C., Huang C.F., Liu Y.C., Lee S.C., Chan C.W., Fuh Y.K. Formation mechanism and improved remedy of thermal property of cold shut surface defects in Vortex Flow Meters: Numerical simulation and experimental verification in investment casting of 316 L stainless steel.

- Journal of Manufacturing Processes*. 2024;120:542–554. <https://doi.org/10.1016/j.jmapro.2024.04.052>
15. Chica E., Agudelo S., Sierra N. Lost wax casting process of the runner of a propeller turbine for small hydroelectric power plants. *Renewable Energy*. 2013;60:739–745. <https://doi.org/10.1016/j.renene.2013.06.030>
 16. Thakre P., Chauhan A.S., Satyanarayana A., Kumar E.R., Pradyumna R. Estimation of shrinkage & distortion in Wax-Injection using Moldex3D simulation. *Materials Today: Proceedings*. 2018;5(9–3):19410–19417. <https://doi.org/10.1016/j.matpr.2018.06.301>
 17. Zhilin S.G., Bogdanova N.A., Komarov O.N. Influence of granulometric composition and extrusion ratio of the waxy materials on the geometry of extended compact by extruding forming. *Bulletin of the Yakovlev Chuvash State Pedagogical University. Series: Mechanics of Limit State*. 2018;(4(38)): 54–64. <https://doi.org/10.37972/chgpu.2020.11.35.024>
Жилин С.Г., Богданова Н.А., Комаров О.Н. Влияние гранулометрического состава и скорости выдавливания воскообразной композиции на геометрию длинномерной прессовки при мундштучном экструдировании. *Вестник Чувашского государственного педагогического университета им. И.Я. Яковлева. Серия: Механика предельного состояния*. 2018;(4(38)):54–64. <https://doi.org/10.37972/chgpu.2020.11.35.024>
 18. Tacioglu S., Akar N. Conversion of an investment casting sprue wax to a pattern wax by chemical agents. *Materials and Manufacturing Processes*. 2003;18(5):753–768. <https://doi.org/10.1081/AMP-120024973>
 19. Abualigah L., Abd Elaziz M., Khasawneh A.M., Alshinwan M., Ibrahim R.A., Al-qaness M.A.A., Mirjalili S., Sumari P., Gandomi A.H. Meta-heuristic optimization algorithms for solving real-world mechanical engineering design problems: A comprehensive survey, applications, comparative analysis, and results. *Neural Computing & Applications*. 2022;34:4081–4110. <https://doi.org/10.1007/s00521-021-06747-4>
 20. Xu M., Lekakh S.N., Richards V.L. Thermal property database for investment casting shells. *International Journal of Metalcasting*. 2016;10:329–337. <https://doi.org/10.1007/s40962-016-0052-4>
 21. Perry M.C. Investment casting. *Advanced Materials & Processes*. 2008;166(6):31–33.
 22. Foggia M.D., D’Addona D.M. Identification of critical key parameters and their impact to zero-defect manufacturing in the investment casting process. *Procedia CIRP*. 2013;12: 264–269. <https://doi.org/10.1016/j.procir.2013.09.046>
 23. Dubrovin V.K., Zaslavskaya O.M., Karpinskii A.V. Casting production from non-ferrous alloys in bulk molds of consumable patterns. *Izvestiya vuzov. Tsvetnaya metallurgiya*. 2011;(2):34–39. (In Russ.).
Дубровин В.К., Заславская О.М., Карпинский А.В. Производство отливок из цветных сплавов в объемные формы по выплавляемым моделям. *Известия вузов. Цветная металлургия*. 2011;(2):34–39.
 24. Harun Z., Kamarudin N.H., Badaruzaman N.A., Wahab M.S. Shell mould composite with rice husk. *Key Engineering Materials*. 2011;471–472:922–927. <https://doi.org/10.4028/www.scientific.net/KEM.471-472.922>
 25. Aguilar J., Schievenbusch A., Kättlitz O. Investment casting technology for production of TiAl low pressure turbine blades – Process engineering and parameter analysis. *Intermetallics*. 2011;19(6):757–761. <https://doi.org/10.1016/j.intermet.2010.11.014>
 26. Sosnin A.A., Bogdanova N.A., Zhilin S.G., Komarov O.N. Finite element modeling of the stress-strain state of waxy compacts. *AIP Conference Proceedings*. 2019;2176(1):030017. <https://doi.org/10.1063/1.5135141>
 27. Bogdanova N.A., Zhilin S.G., Komarov O.N. Method for producing bimetallic casting. Patent RF 2696118, Publ. 07/31/2019. Bulletin no. 22. (In Russ.).
Богданова Н.А., Жилин С.Г., Комаров О.Н. Способ получения биметаллической отливки. Патент на изобретение RU 2696118, опубл. 31.07.2019. Бюллетень № 22.
 28. Zhilin S.G., Komarov O.N., Bogdanova N.A., Amosov O.S. Mathematical modelling of forming processes in the conditions of uniaxial compaction of powder wax-like materials. In: *CEUR Workshop Proceedings. 6 ITHPC 2021 – Short Paper Proceedings of the 6th Int. Conf. on Information Technologies and High-Performance Computing*. 2021:148–154.
 29. Vinokurov G.G., Popov O.N. Statistical modeling of the correlation of local macrostructure density during one-sided pressing of powder materials. *Izvestiya Samarskogo nauchnogo tsentra RAN*. 2011;13(1–3):553–557. (In Russ.).
Винокуров Г.Г., Попов О.Н. Статистическое моделирование корреляции локальной плотности макроструктуры при одностороннем прессовании порошковых материалов. *Известия Самарского научного центра РАН*. 2011;13(1–3):553–557.
 30. Zhilin S.G., Bogdanova N.A., Komarov O.N., Sosnin A.A. Decrease in the elastic response in compacting a paraffin–stearin powder composition. *Russian Metallurgy (Metally)*. 2021;2021(4):459–463. [10.1134/S0036029521040376](https://doi.org/10.1134/S0036029521040376)
 31. Krairi A., Matouš K., Salvadori A. A poro-viscoplastic constitutive model for cold compacted powders at finite strains. *International Journal of Solids and Structures*. 2018;135: 289–300. <https://doi.org/10.1016/j.ijsolstr.2017.11.027>
 32. Malkin A.Ya., Isaev A.I. Rheology. Concepts, Methods, Applications. Moscow: Professiya; 2007:560. (In Russ.).
Малкин А.Я., Исаев А.И. Реология. Концепции, методы, приложения. Москва: Профессия; 2007:560.
 33. Zhilin S.G., Bogdanova N.A., Komarov O.N. Porous wax patterns for high-precision investment casting. *Izvestiya. Non-Ferrous Metallurgy*. 2023;29(3):54–66. <https://doi.org/10.17073/0021-3438-2023-3-54-66>
Жилин С.Г., Богданова Н.А., Комаров О.Н. Исследование процессов формирования пористых выплавляемых моделей, применяемых для изготовления высокоточного литья. *Известия вузов. Цветная металлургия*. 2023; 29(3):54–66. <https://doi.org/10.17073/0021-3438-2023-3-54-66>
 34. Zhilin S.G., Bogdanova N.A., Komarov O.N. Experimental simulation of volumetric compacts formation from spherical waxy elements. *Izvestiya. Ferrous Metallurgy*. 2022;65(11):758–768. (In Russ.). <https://doi.org/10.17073/0368-0797-2022-11-758-768>
Жилин С.Г., Богданова Н.А., Комаров О.Н. Экспериментальное моделирование процессов формирования объемных прессовок из сферических воскообразных элементов. *Известия вузов. Черная металлургия*. 2022;65(11):758–768. <https://doi.org/10.17073/0368-0797-2022-11-758-768>

Information about the Authors

Сведения об авторах

Nina A. Bogdanova, Junior Researcher of the Laboratory of Problems of Creation and Processing of Materials and Products, Institute of Metallurgy and Mechanical Engineering of the Khabarovsk Federal Research Center, Far-Eastern Branch of the Russian Academy of Sciences

ORCID: 0000-0002-8769-8194

E-mail: joyful289@inbox.ru

Sergei G. Zhilin, Cand. Sci. (Eng.), Assist. Prof., Leading Researcher of the Laboratory of Problems of Creation and Processing of Materials and Products, Institute of Metallurgy and Mechanical Engineering of the Khabarovsk Federal Research Center, Far-Eastern Branch of the Russian Academy of Sciences

ORCID: 0000-0002-0865-7109

E-mail: zhilin@imim.ru

Нина Анатольевна Богданова, младший научный сотрудник лаборатории проблем создания и обработки материалов и изделий, Институт машиноведения и металлургии Хабаровского Федерального исследовательского центра Дальневосточного отделения РАН

ORCID: 0000-0002-8769-8194

E-mail: joyful289@inbox.ru

Сергей Геннадьевич Жилин, к.т.н., доцент, ведущий научный сотрудник лаборатории проблем создания и обработки материалов и изделий, Институт машиноведения и металлургии Хабаровского Федерального исследовательского центра Дальневосточного отделения РАН

ORCID: 0000-0002-0865-7109

E-mail: zhilin@imim.ru

Received 11.07.2024

Revised 22.07.2024

Accepted 28.08.2024

Поступила в редакцию 11.07.2024

После доработки 22.07.2024

Принята к публикации 28.08.2024

INNOVATION IN METALLURGICAL
INDUSTRIAL AND LABORATORY EQUIPMENT,
TECHNOLOGIES AND MATERIALSИННОВАЦИИ В МЕТАЛЛУРГИЧЕСКОМ
ПРОМЫШЛЕННОМ И ЛАБОРАТОРНОМ
ОБОРУДОВАНИИ, ТЕХНОЛОГИЯХ И МАТЕРИАЛАХ

UDC 539.374

DOI 10.17073/0368-0797-2024-5-604-611



Original article

Оригинальная статья

INFLUENCE OF COMBINED THERMAL EFFECT OF ELECTRIC ARC WELDING WITH ALUMINOTHERMIC BACKFILL ON INTERNAL STRESSES IN A STEEL PLATE

A. V. Tkacheva , E. E. Abashkin

Institute of Metallurgy and Mechanical Engineering of the Khabarovsk Federal Research Center, Far-Eastern Branch of the Russian Academy of Sciences (1 Metallurgov Str., Komsomolsk-on-Amur, Khabarovsk Territory 681005, Russian Federation)

 4nansi4@mail.ru

Abstract. The paper is devoted to automatic electric arc welding under a flux layer using filler material in the form of aluminothermic backfill for joining thick-plate structures. The plate material is assumed to be elastic-plastic, the deformations are small and consist of elastic and plastic. Reversible (elastic) deformations are associated with stresses by the Duhamel-Neumann law, irreversible (plastic) ones arise and grow due to plastic flow within the framework of the associated law of plastic flow. The modified Mises condition, which takes into account viscosity, is adopted as the condition of plastic flow. The heat source from automatic electric arc welding is modeled by a double ellipsoid proposed by John A. Goldak, and heat from chemical reaction in the region of aluminothermic combustion front is specified by the heat flux value. Elastic moduli and yield strength depend on temperature. Plates with thicknesses of 12, 14, 16, 18 mm were considered. Comparing the intensity of residual stresses in the upper and lower layers of the plates and by their thicknesses, it can be stated that with increasing thickness, the areas of distribution of residual stresses high intensity increase and their values increase too. These areas are located inside the material in the near-weld zone in the area of blue brittleness. Analyzing straightening of temperature fields, for the case of electric arc welding with filler material in the form of aluminothermic backfill and without it, it was found that as a result of a chemical reaction, the temperature in the weld zone increases by 500 °C, this makes it possible to use this technology for welding at low climatic temperatures.

Keywords: powder filler material, aluminothermy, electric arc welding, elasticity, plasticity, filling, low temperature

Acknowledgements: The work was performed within the framework of the state assignment of the Khabarovsk Federal Research Center, Far Eastern Branch of the Russian Academy of Sciences.

For citation: Tkacheva A.V., Abashkin E.E. Influence of combined thermal effect of electric arc welding with aluminothermic backfill on internal stresses in a steel plate. *Izvestiya. Ferrous Metallurgy*. 2024;67(5):604–611. <https://doi.org/10.17073/0368-0797-2024-5-604-611>

ВЛИЯНИЕ КОМБИНИРОВАННОГО ТЕПЛООВОГО ВОЗДЕЙСТВИЯ ЭЛЕКТРОДУГОВОЙ СВАРКИ С АЛЮМОТЕРМИТНОЙ ЗАСЫПКОЙ НА ВНУТРЕННИЕ НАПРЯЖЕНИЯ В СТАЛЬНОЙ ПЛАСТИНЕ

А. В. Ткачева , Е. Е. Абашкин

Институт машиноведения и металлургии Хабаровского Федерального исследовательского центра Дальневосточного отделения РАН (Россия, 681005, Хабаровский край, Комсомольск-на-Амуре, ул. Металлургов, 1)

 4nansi4@mail.ru

Аннотация. Работа посвящена автоматической электродуговой сварке под слоем флюса с применением присадочного материала в виде алюмотермитной засыпки для соединения толстолистовых конструкций. Материал пластины принимается упругопластическим, деформации малыми и состоящими из упругих и пластических. Обратимые (упругие) деформации связаны с напряжениями законом Дюамеля-Неймана, необратимые (пластические) зарождаются и растут благодаря пластическому течению в рамках ассоциированного закона пластического течения. За условие пластического течения принято модифицированное условие Мизеса, в котором учитывается вязкость. Источник тепла от автоматической электродуговой сварки моделируется двойным эллипсоидом, предложенным Джон А. Голдаком, а тепло от химической реакции в области фронта горения алюмотермита задается значением теплового потока. Упругие модули и предел

текутести зависят от температуры. Рассматривались пластины с толщинами 12, 14, 16, 18 мм. Сравнивая интенсивность остаточных напряжений в верхнем и нижнем слоях пластин и по их толщинам, можно утверждать, что с повышением толщины возрастают области распространения высокой интенсивности остаточных напряжений и увеличиваются их значения. Эти области располагаются внутри материала в околосшовной зоне на участке синеломкости. Анализируя распрямления полей температур для случая электродуговой сварки с присадочным материалом в виде алюмотермитной засыпки и без него, установлено, что в результате химической реакции температура в зоне шва повышается на 500 °С. Это дает возможность для применения данной технологии проведения сварочных работ при низких климатических температурах.

Ключевые слова: порошковый присадочный материал, алюмотермия, электродуговая сварка, упругость, пластичность, засыпка, низкая температура

Благодарности: Работа выполнена в рамках государственного задания Хабаровского федерального научного центра Дальневосточного отделения Российской академии наук.

Для цитирования: Ткачева А.В., Абашкин Е.Е. Влияние комбинированного теплового воздействия электродуговой сварки с алюмотермитной засыпкой на внутренние напряжения в стальной пластине. *Известия вузов. Черная металлургия*. 2024;67(5):604–611. <https://doi.org/10.17073/0368-0797-2024-5-604-611>

INTRODUCTION

With the growth of production, there emerged a need for the assembly of large metal structures. This is generally achieved through welding, which negatively affects the base metal, creating irreversible deformations and increased stresses in the weld zone due to localized thermal overheating. To reduce stresses in the area affected by temperature, preheating and concurrent heating are applied [1 – 4], reducing the temperature gradient, or post-weld heat treatment is used. Mechanical impact in the weld zone by means of forging is also employed to reduce the negative effects of welding. When it comes to extended welds in thick-walled metal plates, the aforementioned methods become difficult to implement, making it more appropriate to use a filler material to perform welding in a single pass.

Automatic electric arc welding under flux using powder filler material (PFM) is intended for welding thick-walled structures with a thickness of up to 60 mm. The use of PFM increases the thermal efficiency of the process and improves the quality of the weld joint. Traditionally, filler material is used in the form of granules, which are small fragments cut from welding wire with a diameter of 0.8 – 2.0 mm. PFM is supplied to the welding zone either by pre-filling it into the gap or groove before welding, or it is fed along the electrode extension using a metering device, provided the material is ferromagnetic [5]. The key advantages of the process are higher efficiency, higher productivity, and better weld joint quality. Possible variations of electric arc multi-wire welding and surfacing with the addition of metal powder have been discussed in works [6 – 9]. PFM is also used in laser welding [10 – 13].

In the present study, aluminothermic backfill is investigated as PFM, as an aluminothermic filler in powder wire, consisting of a mixture of metal scale fractions and aluminum alloy with the addition of alloying components, has demonstrated the best performance [14 – 17]. Its use ensures uniform subsequent heating of the weld due to the combination of electric arc thermal effects and the exothermic redox reaction, during which iron

is reduced from scale [18]. The slag formed as a result of the reaction has insulating properties, reducing heat dissipation from the surface of the weld and increasing the time for uniform solidification, which contributes to the formation of a fine-grained structure in the material.

Mathematical modeling allows optimizing the electric arc welding process without incurring significant costs [19 – 21].

Objective: to establish the effect of the combined thermal impact of aluminothermic backfill during the welding of thick-plate structures on the distribution of residual stress intensity and assess the possibility of using this welding technology at low ambient temperatures.

BASIS OF THE MATHEMATICAL MODEL

We assume that at the initial moment, there are no irreversible deformations in the plate material. Deformations are considered small d_{ij} and consist of reversible e_{ij} and irreversible p_{ij} components:

$$d_{ij} = 0.5(u_{i,j} + u_{j,i}) = e_{ij} + p_{ij}. \quad (1)$$

The Duhamel-Neumann relationship describes the connection between stress, elastic deformation, and temperature:

$$\sigma_{ij} = [\lambda e_{kk} - 3\alpha K(T - T_0)]\delta_{ij} + 2\mu e_{ij}, \quad (2)$$

where λ , μ , $K = \frac{2}{3}\mu + \lambda$ are the elastic moduli; α is the coefficient of linear expansion.

The elastic moduli depend on temperature. In this case, we use their linear dependence

$$\begin{aligned} E(x, y, z, t) &= E_p - (E_p - E_0)\theta(x, y, z, t); \\ \nu(x, y, z, t) &= 0.5 - (0.5 - \nu_0)\theta(x, y, z, t); \\ \mu &= \frac{E}{2(1 + \nu)}; \lambda = \frac{\nu E}{(1 + \nu)(1 - 2\nu)}; \theta = \frac{T_p - T}{T_p - T_0}, \end{aligned} \quad (3)$$

where E_0 and E_p are the Young's moduli at room temperature T_0 and at the melting point T_p respectively; and ν is the Poisson's ratio and ν_0 is the Poisson's ratio at room temperature.

When the stress state reaches the yield surface in stress space, irreversible deformations begin to grow. We express the associated flow law

$$\varepsilon_{ij}^p = dp_{ij} = d\varphi \frac{\partial f(\sigma_{ij}, \eta)}{\partial \sigma_{ij}}, \quad d\varphi > 0. \quad (4)$$

The Mises plastic flow condition is adopted as the yield surface

$$\sqrt{\frac{3}{2}(\tau_{ij} - \eta \varepsilon_{ij}^p) \cdot (\tau_{ij} - \eta \varepsilon_{ij}^p)} = k, \quad (5)$$

where $\tau_{ij} = \sigma_{ij} - \delta_{ij} \sigma_0$, δ_{ij} – Kronecker index, if $i = j$, then $\delta_{ij} = 1$, and if $i \neq j$, then $\delta_{ij} = 0$; $\sigma_0 = \frac{1}{3} \sigma_{ii} = \frac{1}{3} \delta_{ij} \sigma_{ij}$; k is the yield strength dependent on temperature $k = k_0 \theta^2$; at $T = T_p$ $k = 0.10$ Pa; η is the material viscosity.

The system of equations (1) – (5) is supplemented by the equilibrium equation

$$\sigma_{ij,j} = 0. \quad (6)$$

The boundary conditions model the free surface. The mechanical problem (1), (2), (4) – (6) is solved numerically for a given temperature field.

PROBLEM SETUP

A plate made of low-carbon and low-alloy steel (St3 grade) at room temperature in an unstressed state (free-standing) is filled with a powder filler material consisting of an aluminothermic composition (backfill geometry: 40×20 mm) (Fig. 1, a) along the length of the future weld. At a speed of 20 m/h, the welding machine follows the designated path (as shown in Fig. 1, b), activating the chemical reaction in the filler material by the heat of the electric arc. The combustion front of the aluminothermic backfill moves at the same speed, slightly ahead of the welding process. The plate thickness varies from 12 to 18 mm. The diameter of the Sv-08 electrode wire is 3 mm.

During arc welding, the process of heat distribution in a solid body is described by a nonlinear heat conduction equation considering the active heat source

$$c(T)\rho \frac{\partial T}{\partial t} = \text{div}[\lambda(T)\text{grad}T] + q, \quad (7)$$

where $\lambda(T)$ is thermal conductivity, (W/m·°C); $c(T)$ is specific heat capacity (J/kg·°C); ρ is density (kg/m³); q is the volumetric power density of the heat source (W/m³).

The heat source from electric arc welding is modeled using a double ellipsoid proposed by John A. Goldak [22]. Fig. 2, b shows the shape of the heat flux in the plate during welding.

$$\begin{aligned} q_s &= f_s \frac{6\sqrt{3Q}}{a_s b c \pi^{1.5}} e^{-3\left[\left(\frac{x+\nu(\tau-t)}{a_s}\right)^2 + \left(\frac{y}{b}\right)^2 + \left(\frac{z}{c}\right)^2\right]}; \\ q_l &= f_l \frac{6\sqrt{3Q}}{a_l b c \pi^{1.5}} e^{-3\left[\left(\frac{x+\nu(\tau-t)}{a_l}\right)^2 + \left(\frac{y}{b}\right)^2 + \left(\frac{z}{c}\right)^2\right]}, \end{aligned} \quad (8)$$

where Q is the effective thermal power of the heating source (for arc welding $Q = \eta IU$, in W); τ is the time since the source started, in s; t is the current time, in s; ν is the welding speed, in m/s; x, y, z are the semi-axes of the ellipsoid in the OX, OY , and OZ directions, in m; f_s and f_l are coefficients defining the ratios for heat introduced into the front and rear parts of the ellipsoid; a_s, a_l, b, c are the respective radii of the normal distribution. Based on the above, the relationship between coefficients f_s and f_l is as follows:

$$f_s = \frac{2a_s}{a_s + a_l}; \quad f_l = \frac{2a_l}{a_s + a_l}; \quad f_s + f_l = 2.$$

At the front of the aluminothermic combustion zone, the boundary conditions are given as

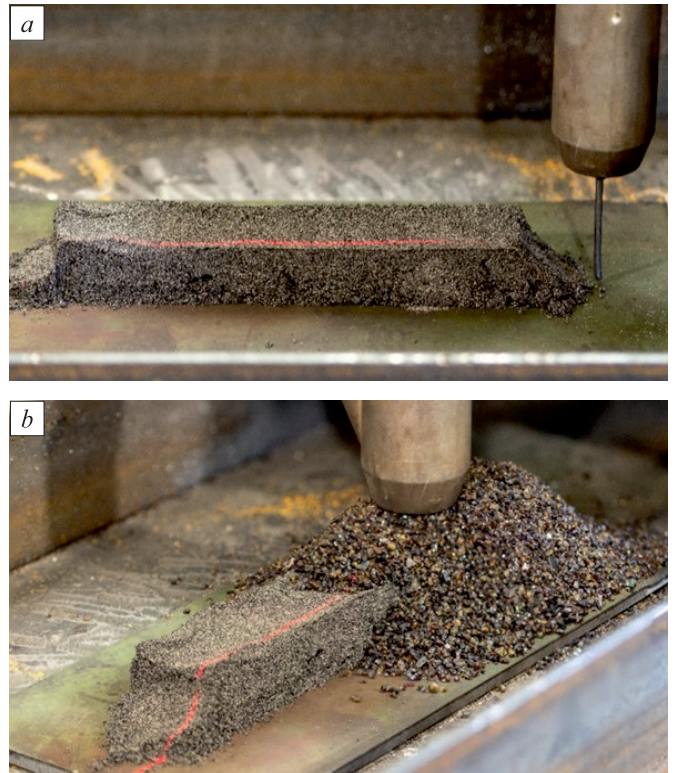


Fig. 1. Experimental setup

Рис. 1. Постановка эксперимента

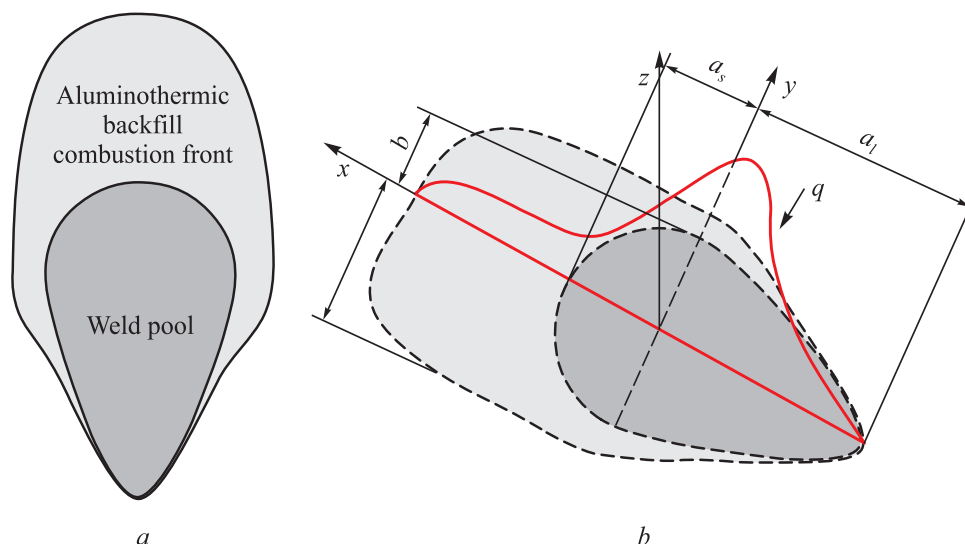


Fig. 2. Task outline

Рис. 2. Схема задачи

$$-\lambda \left(\frac{\partial T}{\partial z} \right) = q_w(x, y, z), \quad (9)$$

where $q_w(x, y, z)$ is the heat flux from the chemical reaction, amounting to 58 W.

On surfaces free from the heat source, boundary conditions model heat dissipation into the surrounding environment:

$$\lambda \frac{\partial T}{\partial x_i} = kof(T - T_0), \quad (10)$$

where kof is the heat transfer coefficient with the surrounding medium, equal to 6 W/(m²·°C). In the weld area, the slag formed by the welding process reduced heat dissipation from the plate surface to 3.5 W/(m²·°C).

Since λ and c are constants, the system of equations (7) – (10) is solved using the sweep method.

CALCULATION RESULTS

We consider steel plates measuring 500×150 mm with thicknesses of 12, 14, 16, and 18 mm and the following physical-mechanical characteristics: density $\rho = 785$ kg/m³; Young’s modulus $E_0 = 210$ GPa at room temperature and $E_p = 0.3$ GPa at the melting point $T_p = 1400$ °C; Poisson’s ratio of 0.27; yield strength of 255 MPa at room temperature; coefficient of linear thermal expansion of $11.1 \cdot 10^{-6}$ 1/°C; thermal conductivity 55.5 W/m·°C; specific heat capacity of 482 J/kg·°C; source efficiency of 90 %; current of 300 A; and voltage of 35 V.

To analyze the effect of powder backfill, we will compare the thermal fields. Fig. 3 shows the distribution

of the temperature field resulting from automatic electric arc welding using aluminothermic backfill and without it. The voltage-current characteristics and welding speed are identical in both cases. As can be seen, in the area of the welding arc, the temperature field with the filler material is increased by 500 °C. This allows the use of aluminothermic backfill in low ambient temperatures as preheating.

If we take the cooling time of the weld obtained by electric arc welding at room temperature as the basis for assessing the quality of the joint, then this time can also be achieved at sub-zero temperatures. Fig. 4 shows

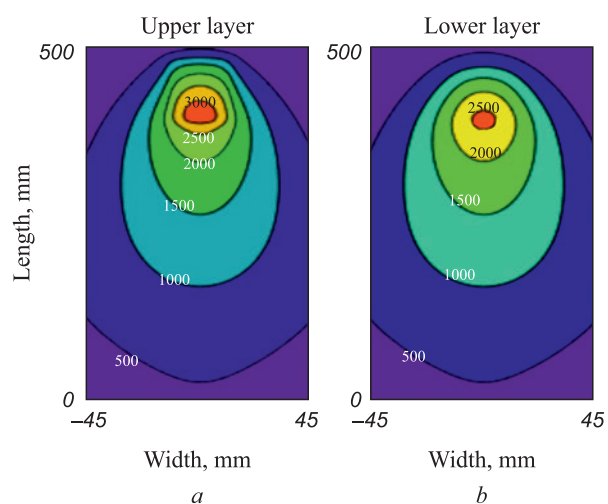


Fig. 3. Temperature distribution in the upper layer of a steel plate formed as a result of electric arc welding with (a) and without filler material (b)

Рис. 3. Распределение температуры в верхнем слое стальной пластины, образованное в результате электродуговой сварки с применением присадочного материала (а) и без него (б)

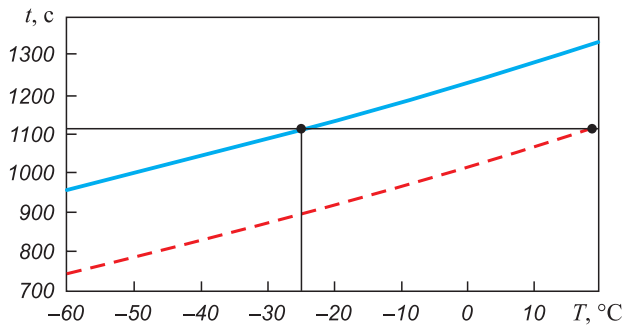


Fig. 4. Cooling time of a 12 mm thick plate

Рис. 4. Время остывания пластины толщиной 12 мм

the cooling time for a plate with a thickness of 12 mm, depending on the ambient temperature. The solid line represents the use of filler material, while the dashed line represents welding without it.

The cooling time of the weld obtained by automatic electric arc welding at 20 °C is the same as at –25 °C with the use of aluminothermic backfill, making it possible to apply this welding process at sub-zero ambient temperatures.

Next, let us consider the effect of plate thickness on the intensity of residual stresses formed as a result of electric arc welding at room temperature using filler material in the form of aluminothermic backfill. Fig. 5 shows the residual stress fields in the upper and lower layers of the plate. It can be seen that as the plate thickness increases, the intensity of residual stresses in the material also increases. Looking in the transverse direction at the center of the plate, the highest intensity of residual stresses is located in the area of blue brittleness and increases with plate thickness, while in the center of the weld the values are small (Fig. 6).

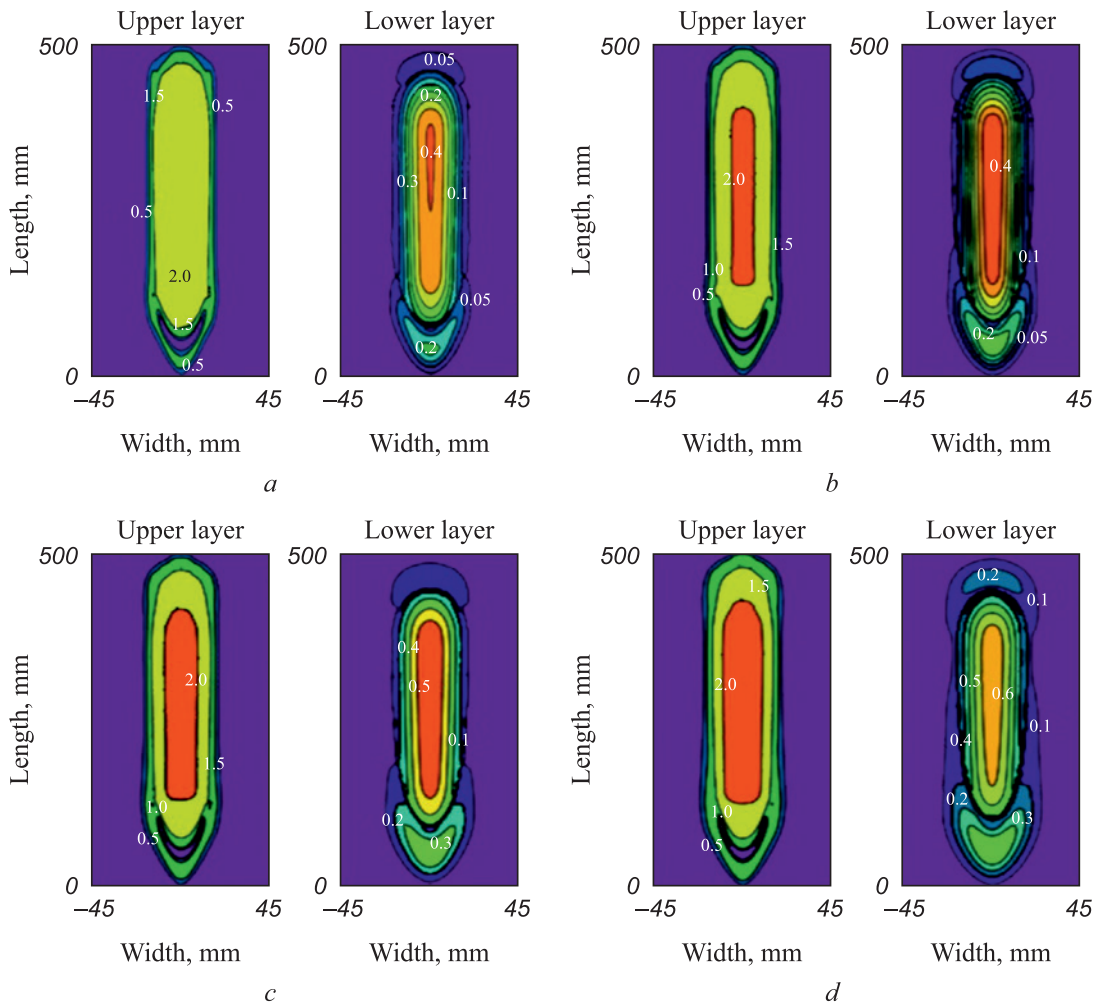


Fig. 5. Distribution of residual stresses intensity depending on plate thickness, formed as a result of automatic electric arc welding with filler material in the form of aluminothermic backfill: 12 mm (a); 14 mm (b); 16 mm (c); 18 mm (d)

Рис. 5. Распределение интенсивности остаточных напряжений, образованных в результате автоматической электродуговой сварки с присадочным материалом в виде алюмотермитной засыпки, в зависимости от толщины пластины: 12 мм (a); 14 мм (b); 16 мм (c); 18 мм (d)

To demonstrate that the use of aluminothermic backfill during electric arc welding reduces areas with high intensity of residual stresses, we compare Fig. 6, *a* with Fig. 7, which shows the distribution of residual stress intensity in a weld obtained without filler material in a 12 mm thick plate. The positive effect of aluminothermic backfill is evident, as the weld obtained without filler material shows a high level of residual stress intensity covering a large area, almost half the thickness of the weld, and decreasing towards the periphery. This cannot be said for the weld made using filler material in the form of aluminothermic backfill, where the small area of high residual stress intensity is located away from the weld zone in the area of blue brittleness. The pattern

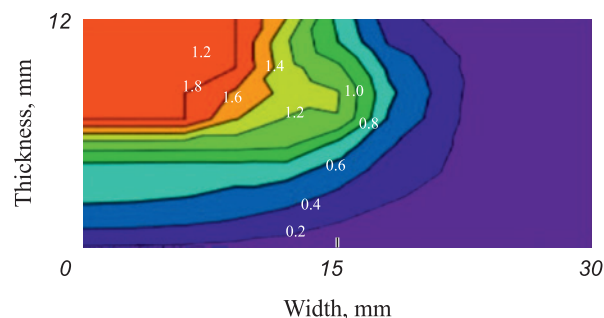


Fig. 7. Distribution of intensity of residual stresses located along the plate center thickness and formed as a result of automatic electric arc welding without filler material

Рис. 7. Распределение интенсивности остаточных напряжений, расположенных по толщине в центре пластины и образованных в результате автоматической электродуговой сварки без присадочного материала

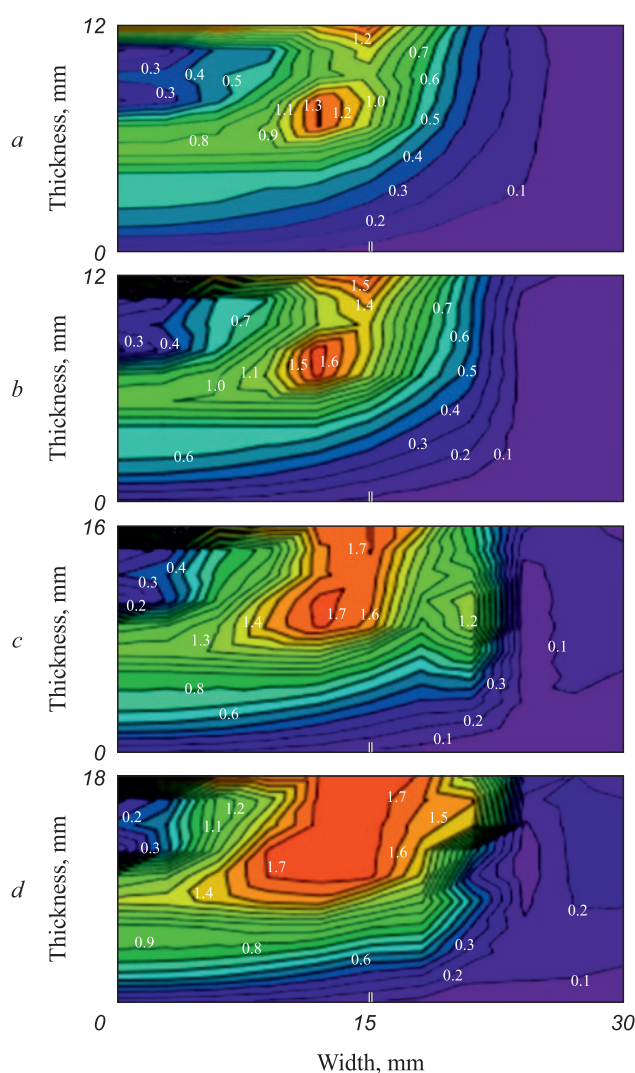


Fig. 6. Distribution of intensity of residual stresses located along the plate center thickness and formed as a result of automatic electric arc welding with aluminothermic backfill as filler material: 12 mm (*a*); 14 mm (*b*); 16 mm (*c*); 18 mm (*d*)

Рис. 6. Распределение интенсивности остаточных напряжений, расположенных по толщине в центре пластины и образованных в результате автоматической электродуговой сварки с присадочным материалом в виде алюмотермитной засыпки при толщине пластин: 12 мм (*a*); 14 мм (*b*); 16 мм (*c*); 18 мм (*d*)

(effect) of this arrangement can be compared to preheating, with the regions of high-temperature gradient located on the sides of the weld zone in the fusion area.

CONCLUSIONS

Studies were conducted on automatic electric arc welding under a flux layer using filler material in the form of aluminothermic backfill for joining thick-plate structures. It was found that the use of aluminothermic backfill reduces the intensity of residual stresses compared to traditional welding. As the plate thickness increases, both the intensity of residual stresses and the area of their distribution expand.

Due to the additional heat generated during the chemical reaction, the temperature in the material during automatic electric arc welding with aluminothermic backfill increases by 500 °C compared to welding without this filler material. This indicates that welding operations can be carried out at low ambient temperatures, while ensuring the same quality of the weld joint as would be achieved at room temperature.

REFERENCES / СПИСОК ЛИТЕРАТУРЫ

- Li L., Mi G., Wang Ch. A comparison between induction preheating and induction post-heating of laser-induction hybrid welding on S690QL steel. *Journal of Manufacturing Processes*. 2019;43(A):276–291. <https://doi.org/10.1016/j.jmapro.2019.05.003>
- Charkhi M., Akbari D. Experimental and numerical investigation of the effects of the pre-heating in the modification of residual stresses in the repair welding process. *International Journal of Pressure Vessels and Piping*. 2019;171:79–91. <https://doi.org/10.1016/j.ijpvp.2019.02.006>
- Ji Sh., Li Zh., Ma L. Joint formation and mechanical properties of back heating assisted friction stir welded Ti–6Al–4V alloy. *Materials & Design*. 2017;113:37–46. <http://dx.doi.org/10.1016/j.matdes.2016.10.012>

4. Tkacheva A.V., Abashkin E.E. Effect of preheating of the edge of a steel plate on the intensity of residual stresses formed as a result of electric arc welding. *Marine Intelligent Technologies*. 2023;(2–1(60)):304–314. (In Russ.). <https://doi.org/10.37220/MIT.2023.60.2.038>
Ткачева А.В., Абашкин Е.Е. Влияние предварительного подогрева кромки стальной пластины на интенсивность остаточных напряжений, образованных в результате электродуговой сварки. *Морские интеллектуальные технологии*. 2023;(2–1(60)):304–314. <https://doi.org/10.37220/MIT.2023.60.2.038>
5. Instructions for Automatic Submerged Arc and Electroslag Welding with Powder Filler Material (PMM) VSN 375–77. Moscow: Central Bureau of Scientific and Technical Information; 1978. (In Russ.).
6. Gorokhova M.N., Churilov D.G. Influence of polar effect and electrode material on transfer of filler powder material using the electric pulse method. *Trudy GOSNITI*. 2012;109(2): 51–56 (In Russ.).
Горохова М.Н., Чурилов Д.Г. Влияние полярного эффекта и материала электродов на перенос присадочного порошкового материала при электроимпульсном способе. *Труды ГОСНИТИ*. 2012;109(2):51–56.
7. Ranjan R., Das A.K. Protection from corrosion and wear by different weld cladding techniques: A review. *Materials Today: Proceedings*. 2022;57(4):1687–1693. <https://doi.org/10.1016/j.matpr.2021.12.329>
8. Tusek J., Suban M. High-productivity multiple-wire submerged-arc welding and cladding with metal-powder addition. *Journal of Materials Processing Technology*. 2003;133(1):207–213.
9. Zhilin P.L., Gavrilov G.N., Melnichenko O.P. Welding and cladding with pre-heated additional filler wire. *Materials Today: Proceedings*. 2021;38(4):1622–1626. <https://doi.org/10.1016/j.matpr.2020.08.168>
10. Shishov A.Yu., Tretyakov R.S., Tretyakov E.S., Staverty A.Ya. Prospects for the development of laser-plasma welding technology for large-thickness products in shipbuilding using powder filler material. *Bulletin of the Bauman Moscow State Technical University*. 2012;(6(6)):15–22. (In Russ.).
Шишов А.Ю., Третьяков Р.С., Третьяков Е.С., Ставертй А.Я. Перспективы разработки технологии лазерно-плазменной сварки изделий больших толщин в судостроении с использованием порошкового присадочного материала. *Вестник московского государственного технического университета им. Н.Э. Баумана*. 2012;(6(6)):15–22.
11. Zhang Zh., Zhao Y., Shan J., Wu A., Sato Y.S., Tokita Sh., Kadoi K., Inoue H., Tang X. The role of shot peening on liquation cracking in laser cladding of K447A nickel superalloy powders over its non-weldable cast structure. *Materials Science and Engineering: A*. 2021;823:141678. <https://doi.org/10.1016/j.msea.2021.141678>
12. Zhu Y., Cai Y., Wang Y. Effects of He content in shielding gases on high-efficient hybrid laser arc welding with C-276 filler metal. *Journal of Materials Processing Technology*. 2022;299:117367. <https://doi.org/10.1016/j.jmatprotec.2021.117367>
13. Alvarães C.P., Jorge C.F., Souza L., Araújo L.S., Mendes M.C., Farneze H.N. Microstructure and corrosion properties of single layer Inconel 625 weld cladding obtained by the electroslag welding process. *Journal of Materials Research and Technology*. 2020;9(6):16146–16158. <https://doi.org/10.1016/j.jmrt.2020.11.048>
14. Sergejevs D., Mikhaylovs S. Analysis of factors affecting fractures of rails welded by aluminothermic welding. *Transport Problems*. 2008;3(4–2):33–37.
15. Kargin V.A., Tikhomirova L.B., Galay M.S. Improving service properties of welded joints produced by aluminothermic welding. *Welding International*. 2015;29(2):155–157. <https://doi.org/10.1080/09507116.2014.897809>
16. Manakov A.L., Abramov A.D., Ilinykh A.S., Galay M.S. Improvement of aluminothermic welding on the basis of the experimentally-theoretical research of welding seam cooling process. *Journal of Physics: Conference Series*. 2018;1050:012051. <https://doi.org/10.1088/1742-6596/1050/1/012051>
17. Tkacheva A.V., Abashkin E.E. The effect of preheating the edge of a plate made of steel 30KhGSA on the distribution of residual stresses in the electric arc process. *Marine Intelligent Technologies*. 2023;(3–1(61)):188–199. (In Russ.). <https://doi.org/10.37220/MIT.2023.61.3.019>
Ткачева А.В., Абашкин Е.Е. Воздействие предварительного подогрева кромки пластины из стали 30ХГСА на распределение остаточных напряжений при электродуговом процессе. *Морские интеллектуальные технологии*. 2023;(3–1(61)):188–199. <https://doi.org/10.37220/MIT.2023.61.3.019>
18. Tkacheva A.V., Abashkin E.E. Effect of local combined thermal action on the magnitude and distribution of residual stresses in a steel plate 20. *Metallurg*. 2023;(6):85–93. (In Russ.). https://doi.org/10.52351/00260827_2023_06_85
Ткачева А.В., Абашкин Е.Е. Влияние локального комбинированного теплового воздействия на величину и распределение остаточных напряжений в пластине из стали 20. *Металлург*. 2023;(6):85–93. https://doi.org/10.52351/00260827_2023_06_85
19. Franks J., Wheatley G., Zamani P., Nejad R.M., Macek W., Branco R., Samadi F. Fatigue life improvement using low transformation temperature weld material with measurement of residual stress. *International Journal of Fatigue*. 2022;164:107137. <https://doi.org/10.1016/j.ijfatigue.2022.107137>
20. Huang W., Wang Q., Ma N., Kitano H. Characteristics of residual stress distribution in wire-arc additive manufactured layers of low transformation temperature material. *International Communications in Heat and Mass Transfer*. 2023;148:107066. <https://doi.org/10.1016/j.icheatmasstransfer.2023.107066>
21. Feng Z., Aung T.L., Shao Ch., Lu F., Tsutsumi S., Ma N. A design method of tensile triangles and low transformation temperature weld metal for reduction of stress concentration and residual stress of welded joints. *Marine Structures*. 2020;72:102759. <https://doi.org/10.1016/j.marstruc.2020.102759>
22. Goldak J.A., Akhlagi M. *Computational Welding Mechanics*. New York: Springer Science & Business Media; 2006:322.

Information about the Authors

Сведения об авторах

Anastasiya V. Tkacheva, *Cand. Sci. (Phys.-Math), Senior Researcher*, Institute of Metallurgy and Mechanical Engineering of the Khabarovsk Federal Research Center, Far-Eastern Branch of the Russian Academy of Sciences

ORCID: 0000-0003-1795-0021

E-mail: 4nansi4@mail.ru

Evgenii E. Abashkin, *Cand. Sci. (Eng.), Senior Researcher*, Institute of Metallurgy and Mechanical Engineering of the Khabarovsk Federal Research Center, Far-Eastern Branch of the Russian Academy of Sciences

ORCID: 0000-0002-9308-1326

E-mail: abashkine@mail.ru

Анастасия Валерьевна Ткачева, *к.ф.-м.н., старший научный сотрудник*, Институт машиноведения и металлургии Хабаровского Федерального исследовательского центра Дальневосточного отделения РАН

ORCID: 0000-0003-1795-0021

E-mail: 4nansi4@mail.ru

Евгений Евгеньевич Абашкин, *к.т.н., старший научный сотрудник*, Институт машиноведения и металлургии Хабаровского Федерального исследовательского центра Дальневосточного отделения РАН

ORCID: 0000-0002-9308-1326

E-mail: abashkine@mail.ru

Received 31.07.2024

Revised 12.09.2024

Accepted 14.10.2024

Поступила в редакцию 31.07.2024

После доработки 12.09.2024

Принята к публикации 14.10.2024

INNOVATION IN METALLURGICAL
INDUSTRIAL AND LABORATORY EQUIPMENT,
TECHNOLOGIES AND MATERIALSИННОВАЦИИ В МЕТАЛЛУРГИЧЕСКОМ
ПРОМЫШЛЕННОМ И ЛАБОРАТОРНОМ
ОБОРУДОВАНИИ, ТЕХНОЛОГИЯХ И МАТЕРИАЛАХ

UDC 621.926.22

DOI 10.17073/0368-0797-2024-5-612-615



Short Report

Краткое сообщение

IMPROVING THE EFFICIENCY OF RAW MATERIAL PREPARATION FOR METALLURGICAL PROCESSING

A. G. Nikitin¹, I. A. Bazhenov², N. M. Kurochkin¹¹ Siberian State Industrial University (42 Kirova Str., Novokuznetsk, Kemerovo Region – Kuzbass 654007, Russian Federation)² Ural Federal University named after the first President of Russia B.N. Yeltsin (19 Mira Str., Yekaterinburg, 620002, Russian Federation)✉ nikitin1601@yandex.ru

Abstract. In the metallurgical industry, approximately 40 % of the energy spent on raw material preparation for further processing accounts for the processes of brittle materials destruction in crushing machines. From the analysis of operation of crushing machines, differing in the method of creating stresses in a destructible piece of brittle material, it follows that the best, from the point of view of energy efficiency, is the one in which tangential stresses (shear deformation) are generated in the processed material. The authors describe the design of a crushing machine which ensures that during the crushing process only tangential stresses arise in the piece, causing shear deformations.

Keywords: metallurgical processes, raw material preparation, crusher, energy efficiency, brittle material, shear

For citation: Nikitin A.G., Bazhenov I.A., Kurochkin N.M. Improving the efficiency of raw material preparation for metallurgical processing. *Izvestiya. Ferrous Metallurgy*. 2024;67(5):612–615. <https://doi.org/10.17073/0368-0797-2024-5-612-615>

ПОВЫШЕНИЕ ЭФФЕКТИВНОСТИ ПОДГОТОВКИ СЫРЬЯ ДЛЯ МЕТАЛЛУРГИЧЕСКИХ ПЕРЕДЕЛОВ

А. Г. Никитин¹, И. А. Баженов², Н. М. Курочкин¹¹ Сибирский государственный индустриальный университет (Россия, 654007, Кемеровская обл. – Кузбасс, Новокузнецк, ул. Кирова, 42)² Уральский федеральный университет имени первого Президента России Б.Н. Ельцина (Россия, 620002, Екатеринбург, ул. Мира, 19)✉ nikitin1601@yandex.ru

Аннотация. В металлургической промышленности примерно 40 % энергии, затрачиваемой на подготовку сырья для дальнейшего передела, приходится на процессы разрушения хрупких материалов. Измельчение осуществляется на дробильных машинах. Из проведенного анализа работы дробильных машин, отличающихся по способу создания в разрушаемом куске хрупкого материала напряжений, следует, что оптимальным, с точки зрения энергоэффективности, является способ дробления, при котором в перерабатываемом материале путем генерации возникают касательные напряжения (деформация сдвига). Авторы приводят описание конструкции дробильной машины, обеспечивающей в процессе дробления в куске возникновение только касательных напряжений, вызывающих сдвиговые деформации.

Ключевые слова: металлургические процессы, подготовка сырья, дробилка, энергоэффективность, хрупкий материал, сдвиг

Для цитирования: Никитин А.Г., Баженов И.А., Курочкин Н.М. Повышение эффективности подготовки сырья для металлургических переделов. *Известия вузов. Черная металлургия*. 2024;67(5):612–615. <https://doi.org/10.17073/0368-0797-2024-5-612-615>

The rapid growth in the production of metallurgical products necessitates an increase in the volume of mineral raw materials prepared for metallurgical processes. Typically, the primary reserve for improving the performance of metallurgical units is enhancing the quality of raw material preparation. Therefore, mineral processing is one of the key stages in preparing mineral resources for further use.

The productivity of metallurgical units depends on the quality of charge materials, including their particle size distribution. Therefore, charge preparation is a priority for boosting productivity and improving the quality of finished products in the metallurgical industry at its current stage of development. For example, to produce high-quality coke, coal undergoes preliminary preparation, while iron ores are processed into pellets used in blast furnace iron smelting. Loose fluxes containing limestone are essential in the preparation of sinter and in the smelting process in steelmaking furnaces (converters, electric arc furnaces). The initial stages of mineral raw material preparation for smelting include crushing to achieve the required particle size for further processing [1].

In the metallurgical industry, approximately 40 % of the energy spent on raw material preparation for further processing is dedicated to the destruction of brittle materials in crushing machines. This makes energy conservation a pressing concern. Additionally, the demand for processed (size-reduced) raw materials is increasing by about 7 % annually [2; 3], as metallurgical processes require lump materials of specific sizes, which are achieved through the use of crushing equipment. One of the key indicators of the crushing process is its energy efficiency. Crushers that operate based on compression, such as roll crushers [4], cone crushers [5], and high-performance jaw crushers [6], are commonly used for brittle materials. However, it is well known that compression-based crushing is the most energy-intensive method [7].

To reduce energy consumption in the crushing of brittle materials, it is essential to create conditions in which only tangential stresses act within the material, leading to shear deformations. In this case, the strength of the processed material is minimized, reaching a value that is half of what it would be under normal stresses that occur during compression.

In this study, a design of a jaw crusher (see Figure) is proposed, which ensures that the forces acting on the crushed piece are distributed in such a way that only tangential stresses are generated, causing shear deformations [8]. The developed crusher design consists of the crusher's bed (1), to which a support hinge (2) is attached on the lower plate, and a movable jaw (3) is

installed. The jaw is driven by a crank-connecting rod mechanism, allowing it to perform a swinging motion around the vertical axis. In the upper crossbar of the crusher's bed (1), there is a loading spout (6) for feeding lump material into the crushing zone. The size of the discharge opening of the spout corresponds to the size of the crushed piece (7), and the spout's axis aligns with the vertical axis of the support hinge (2). To ensure the crusher remains operational during use, it is necessary to meet the condition that the upper edge of the movable jaw does not touch the lower edge of the discharge opening of the loading spout during the swinging motion.

The operation proceeds as follows: pieces of material to be crushed are fed one by one into the crushing zone through the loading spout under the influence of gravity. The crushing zone is formed by the surface of the movable jaw and the lower edge of the spout's opening. When a piece enters the crushing zone, it contacts one side along line B with the edge of the loading spout and the other side along line A with the movable jaw.

As the movable jaw moves, it presses the crushed piece against the lower edge of the spout's discharge opening, causing forces to act upon it. One of these forces, com-

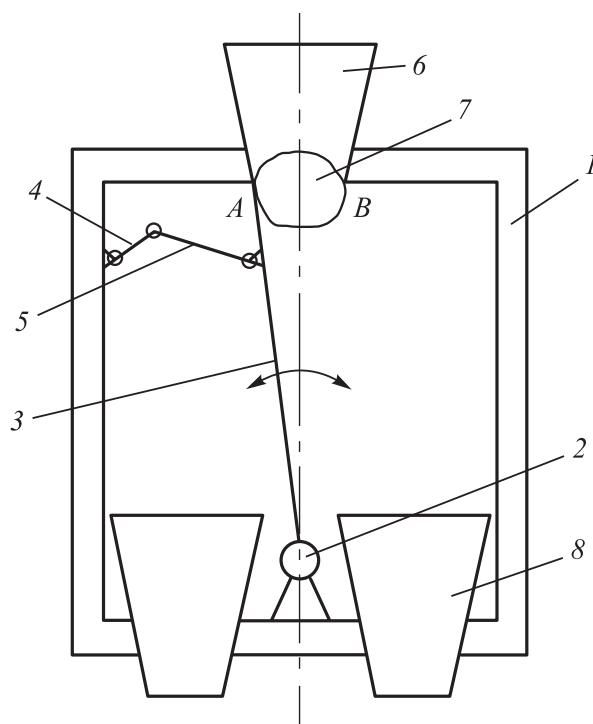


Diagram of a jaw crushing machine operating in shear:
 1 – crusher's bed; 2 – support hinge; 3 – movable jaw;
 4 – crank; 5 – connecting rod; 6 – loading spout; 7 – crushed piece;
 8 – unloading spout

Схема щековой дробильной машины, работающей на сдвиг:
 1 – станина дробилки; 2 – опорный шарнир; 3 – подвижная щека;
 4 – кривошип; 5 – шатун; 6 – загрузочная течка;
 7 – дробимый кусок; 8 – разгрузочная течка

ing from the upper edge of the movable jaw, is directed tangentially to the trajectory of point *A*'s movement. The other force, from the lower edge of the spout, is directed horizontally away from point *B*, passing through the lower edge of the spout. With this force distribution acting on the crushed piece, only tangential stresses arise due to the opposing directions of the force vectors in the same plane. In this case, the fracture of the brittle material occurs as a result of shear deformation generated in the piece.

After the initial fracture, the detached part of the material is ejected toward the discharge spout, while the remaining part is removed from the crushing zone as the movable jaw changes its direction. During the reverse stroke of the movable jaw, the crushing process is repeated.

In the jaw crusher under consideration, the fragmentation of the brittle piece is achieved due to the generation of tangential stresses and the formation of shear deformations. The energy consumption for crushing is reduced by nearly half compared to jaw crushers operating on compression.

CONCLUSIONS

An analysis of the operation of crushing machines (which use various methods to generate stresses in the crushed piece of brittle material) shows that the most energy-efficient method is one where fragmentation of the original piece is achieved by generating tangential stresses in the processed material, resulting in shear deformation.

A crushing machine design has been developed that ensures only tangential stresses, causing shear deformations, occur in the crushed piece during operation. This design reduces energy consumption for crushing by nearly half compared to crushers that operate based on compression.

REFERENCES / СПИСОК ЛИТЕРАТУРЫ

- Gzogyan T.N., Gubin S.L. Improvement of ore crushing technology at the Mikhailovskii GOK. *Ferrous Metallurgy. Bulletin of Scientific, Technical and Economic Information*. 2002;(7):25–26. (In Russ.).
Гзогян Т.Н., Губин С.Л. Совершенствование технологии дробления руд на Михайловском ГОКе. *Черная металлургия: Бюллетень научно-технической и экономической информации*. 2002;(7):25–26.
- Poltoratskii L.M., Barnaev I.A. Competitiveness of Ferrous Metallurgy in the Context of Crisis Phenomena. Novokuznetsk: Poligrafist; 2009:129. (In Russ.).
Полторацкий Л.М., Барнаев И.А. Конкуренентность черной металлургии в условиях кризисных явлений. Новокузнецк: Полиграфист; 2009:129.
- De la Vergne J. *Hard Rock Miner's Handbook*. Edmonton, Alberta, Canada: Stantec Consulting; 2008:330.
- Egbe E.A.P., Olugboji O.A. Design, fabrication and testing of a double roll crusher. *International Journal of Engineering Trends and Technology (IJETT)*. 2016;35(11):511–515. <https://doi.org/10.14445/22315381/IJETT-V35P303>
- Johansson M., Quist J., Evertsson M., Hulthen E. Cone crusher performance evaluation using DEM simulations and laboratory experiments for model validation. *Minerals Engineering*. 2017;103–104:93–101. <http://doi.org/10.1016/j.mineng.2016.09.015>
- Legendre D.A. Numerical and Experimental Optimization Analysis of a Jaw Crusher and a Bubble Column Reactor. Turku, Finland: Åbo Akademi University; 2019:78.
- Maslennikov V.A. Crushers that destroy material by compression. *Gornyi zhurnal*. 1996;(10-11):124–138. (In Russ.).
Масленников В.А. Дробилки, разрушающие материал сжатием. *Известия вузов. Горный журнал*. 1996;(10-11):124–138.
- Nikitin A.G., Kurochkin N.M. The method of crushing lump materials in a jaw crusher. Pat. RF 2785676. *Byulleten' izobretenii*. 2022;(35). (In Russ.).
Пат. РФ 2785676. Способ дробления кусковых материалов в щековой дробилке / А.Г. Никитин, Н.М. Курочкин; *Открытия. Изобретения*. Заявл. 24.05.2022. Опубл. 12.12.2022. Бюл. № 35.

Information about the Authors

Сведения об авторах

Aleksandr G. Nikitin, Dr. Sci. (Eng.), Prof. of the Chair of Mechanics and Machine Engineering, Siberian State Industrial University
ORCID: 0000-0001-9198-6386
E-mail: nikitin1601@yandex.ru

Igor' A. Bazhenov, Cand. Sci. (Eng.), Assist. Prof. of the Chair of Marketing, Ural Federal University named after the first President of Russia B.N. Yeltsin
ORCID: 0000-0002-0099-483X
E-mail: bazhenovmta@yandex.ru

Nikita M. Kurochkin, Postgraduate of the Chair of Mechanics and Machine Engineering, Siberian State Industrial University
E-mail: k_nikitos@mail.ru

Александр Григорьевич Никитин, д.т.н., профессор кафедры механики и машиностроения, Сибирский государственный индустриальный университет
ORCID: 0000-0001-9198-6386
E-mail: nikitin1601@yandex.ru

Игорь Алексеевич Баженов, к.т.н., доцент кафедры маркетинга, Уральский федеральный университет им. первого Президента России Б.Н. Ельцина
ORCID: 0000-0002-0099-483X
E-mail: bazhenovmta@yandex.ru

Никита Максимович Курочкин, аспирант кафедры механики и машиностроения, Сибирский государственный индустриальный университет
E-mail: k_nikitos@mail.ru

Contribution of the Authors / Вклад авторов

A. G. Nikitin – formation of the basic concept, formulation of conclusions, scientific guidance.

I. A. Bazhenov – development of the crusher design, writing the text.

N. M. Kurochkin – revision of the text, correction of conclusions, discussion of results.

А. Г. Никитин – формирование основной концепции, формулирование выводов, научное руководство.

И. А. Баженов – разработка конструкции дробилки, написание текста.

Н. М. Курочкин – доработка текста, корректировка выводов, обсуждение результатов.

Received 23.04.2024

Revised 26.04.2024

Accepted 21.08.2024

Поступила в редакцию 23.04.2024

После доработки 26.04.2024

Принята к публикации 21.08.2024



UDC 669.017:517

DOI 10.17073/0368-0797-2024-5-616-624



Original article

Оригинальная статья

TYPE OF GENERALIZED MATHEMATICAL MODEL FOR DESCRIBING LARGE HOT DEFORMATIONS

M. Yu. Belomyttsev

National University of Science and Technology “MISIS” (4 Leninskii Ave., Moscow 119049, Russian Federation)

myubelom@yandex.ru

Abstract. The relationship between temperature-strain-force parameters in hot deformation processes is important in the forming practice. Of the two options for searching and describing such relationships (based on physical laws and mathematical techniques), in some cases the method of mathematical search for the desired dependence turns out to be simpler. This is exactly the path implemented in the abstracted message. For this propose, a matrix of initial data was created from digitized strain diagrams of the samples made of heat-resistant 1Cr12Ni3Mo2VNbN 12 % Cr steel deformed to a true deformation degree of ~1 at 1253 – 1453 K and a compression rate of 0.01 – 10 s⁻¹ in true coordinates (φ and S). In this matrix, for each point of the experimental deformation diagram the stress S , the deformation degree φ , the deformation rate φ' , and the temperature T were indicated. The required mathematical model has a multiplicative form, which made it possible to bring it into a linear form by taking logarithms and to search for coefficients with the factors (and after logarithm, with terms in a polynomial) to use standard Mathcad operators with calculation algorithms based on the least squares method. The quality of the model was assessed quantitatively by calculating Q – the sum of squared differences between the calculated and experimental stress values with its normalization to the average stress value S from the entire array. For the found best form of relationship $S = f(\varphi, \varphi', T)$ as $\log(S) = A + B \log(\varphi) + C[\log(\varphi)]^2 + D[\log(\varphi)]^3 + E \log(\varphi') + F \log(\varphi) \log(\varphi') + G \frac{\varphi}{\varphi'} + \frac{H + K\varphi + M \log(\varphi) + N \log(\varphi') + P \log(\varphi) \log(\varphi')}{T}$ the Q value was 6 % of $S_{av} = 130$ MPa. It was established that the found type of mathematical description of hot deformation is applicable to the analysis of hot deformation processes of a wide variety of metal materials, while the accuracy of the predictive characteristics of the deformation stress is 3 – 11 %.

Keywords: hot deformation, mathematical model, Arrhenius equation, heat-resistant high-chromium steel, least squares method

For citation: Belomyttsev M.Yu. Type of generalized mathematical model for describing large hot deformations. *Izvestiya. Ferrous Metallurgy*. 2024;67(5):616–624. <https://doi.org/10.17073/0368-0797-2024-5-616-624>

ВИД ОБОБЩЕННОЙ МАТЕМАТИЧЕСКОЙ МОДЕЛИ ДЛЯ ОПИСАНИЯ БОЛЬШИХ ГОРЯЧИХ ДЕФОРМАЦИЙ

М. Ю. Беломытцев

Национальный исследовательский технологический университет «МИСИС» (Россия, 119049, Москва, Ленинский пр., 4)

myubelom@yandex.ru

Аннотация. Взаимосвязь температурно-деформационно-силовых параметров в процессах горячей деформации имеет важное значение в практике обработки давлением. Из двух вариантов поиска и описания таких связей (основанных на физических закономерностях и математических приемах) в некоторых случаях оказывается более простым способ математического поиска искомой зависимости. Именно такой путь реализован в данной работе. Для этого из оцифрованных диаграмм деформации образцов жаропрочной 12 %-ной хромистой стали 1Cr12Ni3Mo2VNbN, продеформированных до истинной степени деформации ~1 при 1253 – 1453 К и скорости сжатия 0,01 – 10 с⁻¹ в истинных координатах (φ и S) создавали матрицу исходных данных, в которой для каждой точки экспериментальной диаграммы деформации указывались напряжение S , степень деформации φ , скорость деформации φ' и температура T . Проведен поиск математической модели в мультипликативной форме, что позволило логарифмированием привести ее к линейному виду, а для поиска коэффициентов при сомножителях (а после логарифмирования – при слагаемых) использовать стандартные операторы программы Mathcad, использующие алгоритмы расчетов на основе метода наименьших квадратов. Качество модели оценивали количественно через расчет Q – суммы квадратов разностей между расчетными и экспериментальными значениями напряжений с нормировкой ее на среднее значение напряжения S от всего массива. Для найденной наилучшей формы связи $S = f(\varphi, \varphi', T)$ вида $\log(S) = A + B \log(\varphi) + C[\log(\varphi)]^2 + D[\log(\varphi)]^3 + E \log(\varphi') + F \log(\varphi) \log(\varphi') + G \frac{\varphi}{\varphi'} + \frac{H + K\varphi + M \log(\varphi) + N \log(\varphi') + P \log(\varphi) \log(\varphi')}{T}$ значение Q

составило 6 % от $S_{cp} = 130$ МПа. Установлено, что найденный вид математического описания горячей деформации применим к анализу процессов горячей деформации самых разнообразных металлических материалов, при этом точность прогнозных характеристик напряжения деформирования составляет 3 – 11 %.

Ключевые слова: горячая деформация, математическая модель, уравнение Аррениуса, жаропрочная высокохромистая сталь, метод наименьших квадратов

Для цитирования: Беломятцев М.Ю. Вид обобщенной математической модели для описания больших горячих деформаций. *Известия вузов. Черная металлургия.* 2024;67(5):616–624. <https://doi.org/10.17073/0368-0797-2024-5-616-624>

INTRODUCTION

Pressure processing is the primary method for obtaining metal products of a specified grade and size. From the perspective of production efficiency (balance of equipment and billet heating costs), hot deformation has an undeniable advantage. Cold deformation is used to impart high mechanical properties at the final stage of pressure processing through the mechanism of cold work hardening (sheet, wire, strip, rod, etc.).

The ability to control hot deformation processes is determined by knowledge of the relationships between such variable factors as pressure, deformation, strain rate, and temperature. Understanding these patterns allows for the introduction of computer control over hot deformation processes (such as controlled rolling for automobile body sheet) to regulate the structure and mechanical properties of the final product.

Basic equations relating variables of the Hollomon type (H) [1; 2], exponential-power law (ES) [3], Ludwigson (L) [4], Zener-Hollomon (Z and Z1) [5; 6], Bird–Mukherjee–Dorn (BMD) [7], the modified Zener-Hollomon equation (ZM) [5], and Johnson-Cook (DK) [8] are known. These equations mathematically appear as follows:

$$S = S_0 \varphi^n; \quad (H)$$

$$\sigma = A \varepsilon^n \exp(k\varepsilon); \quad (ES)$$

$$S = K_0 \varphi^n + \exp(K_1 + K_2 \varphi); \quad (L)$$

$$\sigma = (A + B \varepsilon^n) \left[1 + C \ln \left(\frac{\varepsilon'}{\varepsilon'_0} \right) \right] \left(1 - \frac{T - T_r}{T_m - T_r} \right)^m; \quad (DK)$$

$$Z = \dot{\varepsilon} \exp \left(\frac{Q}{RT} \right); \quad (Z)$$

$$\dot{\varepsilon} = AF(\sigma) \exp \left(-\frac{Q}{RT} \right), \quad (Z1)$$

where S is the true stress, МПа; S_0 , K_0 , K_1 , K_2 , A , α , n are material constants, $\alpha = \beta/n$; φ is the true strain, dimensionless; σ is the flow stress, МПа; ε is strain, dimensionless; Z is the Zener-Hollomon parameter; $\dot{\varepsilon}$ is the strain rate, s^{-1} ; Q is the activation energy of hot deformation, kJ/mol; R is

the universal gas constant, 8.314 J/mol·K; T is the absolute temperature, K; $F(\sigma) = \sigma^\alpha$, $\alpha \sigma < 0.8$; $F(\sigma) = \exp(\beta\sigma)$, $\alpha \sigma > 1.2$; $F(\sigma) = [\sinh(\alpha\sigma)]^n$ for all other $\alpha\sigma$.

The replacement of the hyperbolic law $F(\sigma)$ in equation (Z1) gives

$$\dot{\varepsilon} = A [\sinh(\alpha\sigma)]^n \exp \left(-p \frac{Q}{RT} \right), \quad (A)$$

where p is a constant.

Equation (A) – the Arrhenius equation in the form of the hyperbolic sine [9; 10] – can better describe the dependence of stress on temperature and strain rate during steady-state flow. According to the definition of the hyperbolic law, the flow stress can be expressed as a function of the Zener-Hollomon parameter in the form:

$$\sigma = \frac{1}{\alpha} \ln \left\{ \left(\frac{Z}{A} \right)^{1/n} + \left[\left(\frac{Z}{A} \right)^{2/n} + 1 \right]^{1/2} \right\}; \quad (Z)$$

$$\dot{\varepsilon} = D_0 E b A \frac{\sigma}{E} \frac{b}{d} \exp \left(-\frac{Q}{RT} \right) \frac{1}{kT}; \quad (BMD)$$

$$\sigma = \frac{\beta_0}{\alpha} \varepsilon^{\beta_1} \exp(-\beta_2 \varepsilon) \ln \left[\left(\frac{Z}{A} \right)^{1/n} + \left(\frac{Z}{A} + 1 \right)^{1/2} \right]. \quad (ZM)$$

The above equations are not universal. The Hollomon-type equation (H) is used to determine the parameters of the cold and warm deformation curve, where, until the point of plastic flow instability (most often until the onset of necking), the strain hardening coefficient $d\sigma/d\varepsilon$ is positive (i.e., the curve continuously rises, although with a constantly decreasing slope). The exponential-power equation (ES) describes well the hot deformation curve, where there is a stage with a constantly decreasing load (although quite slowly) as deformation increases, not associated with the onset of necking (at this stage, processes are controlled by dynamic polygonization), but it poorly describes the stage of dynamic recrystallization. The first two types of equations do not account for temperature and strain rate. The Zener-Hollomon (ZM) equations and their variants are used to describe those hot deformation curves where the stage with a constant strain rate is pronounced (at this stage, the curve runs parallel to the abscissa axis, which may be

due to dynamic polygonization or dynamic recrystallization), and the found equations allow predicting the relationship between strain rate at this stationary stage with temperature and stress, but without considering the degree of deformation.

The number of generalized mathematical dependencies (i.e., considering all four factors – strain ε , strain rate $\dot{\varepsilon}$, temperature T , and stress σ) that various researchers aim to derive from experimental results is limited. These include the general Arrhenius-type dependencies

$$\sigma = A\varepsilon^n \dot{\varepsilon}^m \exp\left(\frac{Q}{RT}\right),$$

the Zerilli-Armstrong dependency

$$\sigma = C_0 + C_2 \varepsilon^{1/2} \exp[-C_3 T + C_4 \ln(\dot{\varepsilon})],$$

and the combined equation

$$\sigma = A\varepsilon^n \exp(k\varepsilon) \dot{\varepsilon}^m \exp\left(\frac{Q}{RT}\right),$$

where C_0, C_2, C_3, C_4 are constants.

The relationship between all four variables ($\sigma, \varepsilon, \dot{\varepsilon}, T$) can be represented by generalized model equations (GM) [1; 11]

$$\sigma = A\varepsilon^n \dot{\varepsilon}^m \exp\left(\frac{Q}{RT}\right) \quad (1.1)$$

or after logarithmization

$$\log(\sigma) = A + B \log(\varepsilon) + C \log(\dot{\varepsilon}) + \frac{D}{T}. \quad (1.1a)$$

Combining equations (ES – exponential-power law) and (GM – generalized model) [12] gives

$$\sigma = A\varepsilon^n \exp(k\varepsilon) \dot{\varepsilon}^m \exp\left(\frac{Q}{RT}\right)$$

or after logarithmization

$$\log(\sigma) = A + B \log(\varepsilon) + C(\varepsilon) + D \log(\dot{\varepsilon}) + \frac{E}{T}.$$

The generalized Zerilli-Armstrong equation [13] is also known

$$\sigma = C_0 + C_2 \varepsilon^{1/2} \exp[-C_3 T + C_4 \ln(\dot{\varepsilon})],$$

after logarithmization of which (assuming $C_0 = 0$ at the initial cycle), the relationship between variables can be expressed as a functional dependence in the form

$$\log(\sigma) = A + B \log(\varepsilon) + C \log(\dot{\varepsilon}) + DT.$$

All these equations are used both to describe deformation processes and to predict (calculate) the parameters required by engineers or researchers – stress, strain, or strain rates.

Some researchers introduce structural parameters (grain size, dislocation density, etc.) into deformation models. Such models include the Bird–Mukherjee–Dorn (BMD) and Johnson-Cook (DK) models [7; 8]. However, the application of such methods requires preliminary determination of a large number of structural parameters for each deformation curve (up to three), so the total number of determined variables can amount to several dozen.

The experimental part of hot deformation research is conducted on small-sized test samples. The parameters of hot pressure processing are simulated by varying temperature, strain rate, and deformation degree while recording the load on the sample. The purpose of such tests is to obtain a set of deformation curves constructed in the coordinates “strain ε – stress σ ” while varying the test temperature T and the nominal strain rate $\dot{\varepsilon}$, which are kept constant in a single experiment, and then to find a formula that links all the variables (both dependent and independent). This is the procedure for constructing a generalized mathematical model of hot deformation. For an adequate comparison of the mechanical behavior of samples in such tests with the evolution of the structure, the experiments are conducted in a manner that maintains a constant true strain rate ϕ' throughout the entire test, and the recorded force on the sample is converted into true stress S . When using “true coordinates” S and ϕ , the change in the dimensions of the samples during deformation is taken into account (when using “nominal coordinates” σ and ε , all the calculated mechanical characteristics are related to the initial dimensions of the samples).

Analysis of mathematical methods used to obtain coefficients for various dependencies leads to the conclusion that the simplest ones are the “one-step” methods, which, through logarithmization or other mathematical transformations, reduce the original model (chosen as a hypothesis to test its quality) to a linear form. After this, determining the coefficients of such a model becomes trivial (the procedure for finding the coefficients of linear equations in typical calculation programs such as Excel, Mathcad, Origin, MATLAB, Statistica, and the like is extremely simple and formalized). In contrast, the procedure for determining the coefficients for variables in the Z1 deformation law, which is most often used by researchers, is multistep, with several intermediate stages of analysis. The authors of [14; 15], based on the ideology of simplifying the search for a deformation law, developed a method for analyzing the creep process, in which the number of experimental variables

was limited to three (stress, temperature, and strain rate). The analysis, carried out using such a simplified model, showed that the first step in such a process should be the experimental or theoretical (or hypothesized) search for the form of the model that is convenient for mathematical transformations. For the case of creep analysis, the following was demonstrated:

– two main methods used in practice – Hollomon’s method (or its special case, the Larson-Miller method) and the Arrhenius approximation – allowed models to be obtained with similar predictive accuracy;

– in the factors of both models, which account for the influence of deformation temperature, it is advisable to also consider the level of applied stresses (which, according to creep test methodology, are always initial);

– accounting for the previous point inevitably leads to the appearance of a “cross” influence of independent factors in the generalized deformation equation (such as “stress $\sigma(1/T)$ ”).

These results led to the idea of applying the same procedures to find the generalized mathematical law of hot deformation, in which the fourth variable – degree of deformation – inevitably appears.

The aim of this work is to develop a generalized mathematical equation to describe large hot plastic deformations, taking into account the simultaneous influence of strain φ , strain rate $\dot{\varphi}$, and temperature T ,

without relying on the structural-mechanical constants of the material.

DESCRIPTION OF THE ANALYSIS OBJECT AND THE PROCESSING METHODOLOGY

All researchers conducting multifactor analysis of hot deformation use the results of compression tests on cylindrical samples with a diameter of about 10 mm and a height-to-diameter ratio of ~ 1 to 2. In this study, the analysis was carried out using the results described in [12]. Yang-Hong Xiao and Cheng Guo, in their report, presented data from compression tests up to true strain values of ~ 1 at 1253 – 1453 K and compression rates of $0.01 - 10 \text{ s}^{-1}$ on samples of heat-resistant 12 % chromium steel 1Cr12Ni3Mo2VNbN. The shape of the initial deformation curves is shown in Fig. 1.

By digitizing these curves using the Grafula program, an array of experimental data was obtained in the form of a table containing approximately 800 rows. In four columns, the table recorded data on deformation, stress, strain rate, and temperature for each experimental point (approximately 40 points for each of the 20 experimental curves). The independent variables were true strain φ' , and temperature T (in K). The dependent variable was true stress S . A fragment of the initial data table is shown in Table.

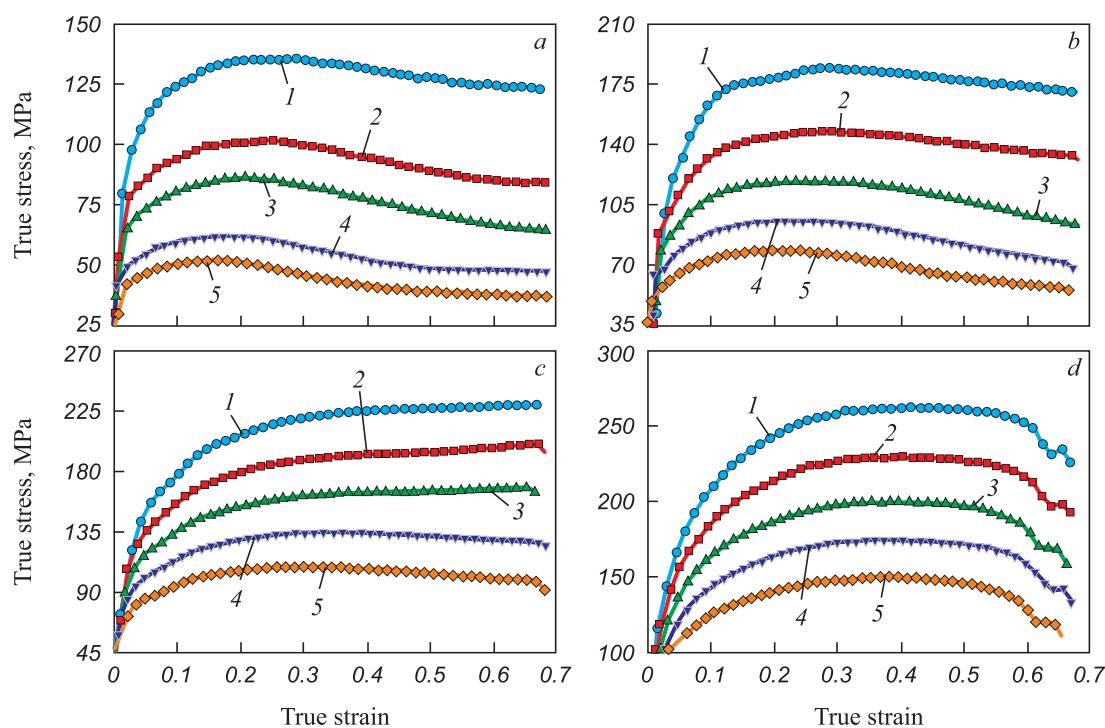


Fig. 1. Curves of hot compressive deformation in true coordinates according to [12] at deformation rate, s^{-1} : 0.001 (a); 0.1 (b); 1 (c); 10 (d) and temperature, K: 1 – 1253; 2 – 1303; 3 – 1353; 4 – 1403; 5 – 1453

Рис. 1. Кривые горячей деформации сжатием в истинных координатах по данным работы [12] при скорости деформации, с^{-1} : 0,001 (a); 0,1 (b); 1 (c); 10 (d) и температуре, К: 1 – 1253; 2 – 1303; 3 – 1353; 4 – 1403; 5 – 1453

RESULTS AND DISCUSSION

Taking into account the results of studies described above, the first step was to base the analysis on the generalized Arrhenius-type dependency (GM). Using the regress function from the Mathcad program, the values of the coefficients A , B , C , D were obtained in equation (1.1a). After reversing the logarithmic form of equation (1.1a) to the direct form (1.1b) the following equation was derived

$$\sigma = 5.633 \cdot 10^{-4} \varepsilon^{0,077} \dot{\varepsilon}^{0,127} \exp\left(-\frac{66.487}{RT}\right) \quad (R = 8.315 \text{ J/mol}\cdot\text{K}). \quad (1.1b)$$

A visual assessment of the model’s quality was conducted by comparing the experimental values of S with the values calculated using the derived equation (1.1b) (Fig. 2).

To quantitatively assess the quality of the mathematical model, the sum of squared differences between the calculated and experimental stress values was computed, normalized to the mean stress value S using the formula

$$Q = \frac{n}{\sum S} \sqrt{\sum \frac{(S_{\text{calc}} - S_{\text{exp}})^2}{n - 5}}. \quad (2)$$

For the model in the form (1.1b), this value was approximately 14 %.

The comparison of the visual and quantitative assessments shows that, despite the small average deviation of the predicted values from the experimental ones, the model (1.1b) provides poor predictions for high-stress intervals (the final sections of the compression curves with large degrees of deformation) (Fig. 2).

Fragment of initial data array for analysis of 1Cr12Ni3Mo2VNbN steel hot deformation

Фрагмент массива исходных данных для анализа горячей деформации стали 1Cr12Ni3Mo2VNbN

Number	S , MPa	φ , fraction of 1	φ' , s ⁻¹	T , K
1	79.5	0.08876	0.010	1453
2	97.7	0.02500	0.010	1453
3	106.8	0.03700	0.010	1453
4	114.3	0.05100	0.010	1453
5	117.8	0.06700	0.010	1453
6	121.9	0.08000	0.010	1453
7	124.2	0.09400	0.010	1453
...
889	120.3	0.61200	10	1253

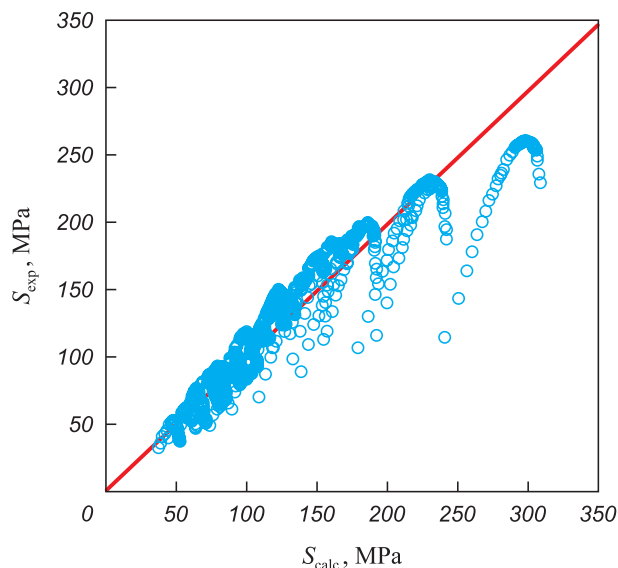


Fig. 2. Comparison of calculated and experimental stress values according to the model (GM)

Рис. 2. Сопоставление расчетных и экспериментальных значений напряжений по модели (ОВ)

In order to refine the assumed model, an analysis of individual deformation curves was conducted. Since the primary mathematical method for determining coefficients for the variables was linear regression analysis using the least squares method, the focus of the analysis was on linear equations with a logarithmic form of the variables. Preliminary trials (where “trial” refers to various mathematical formulations of the relationships between the variables) for determining equations that describe individual deformation curves (each of these curves was obtained at constant values of temperature and strain rate) showed that for most deformation curves, the equation of the form

$$S = A(\varphi)^B 10^{C(\varphi)} \quad (3)$$

or, after logarithmization

$$\log(S) = A_1 + B_1 \log(\varphi) + C_1(\varphi) \quad (3a)$$

provides a good description. This representation allows obtaining Q values for individual curves in the range of 1.5 to 5 % (Fig. 3).

The accuracy of the prediction improves even further when the expression (3a) is modified by including a multiplier in the form of the ratio of the strain degree φ to the logarithm of this value:

$$\log(S) = A2 + B2 \log(\varphi) + C2(\varphi) + \frac{D2(\varphi)}{\log(\varphi)}. \quad (4)$$

The quality of such equations, evaluated by the parameter Q ranges from 0.5 to 1.7 % (Fig. 3), and the rela-

tionship between variables in its direct form (without logarithms) is described by the equation

$$S = \varphi^{B3} \exp \left[A3 + C3(\varphi) + \frac{D3(\varphi)}{\log(\varphi)} \right]. \quad (4a)$$

Further development of this model followed the next steps. In the deformation curves obtained from tests conducted at low temperatures and/or high strain rates, there is an extended section of significant stress increase after the yield point on the graphs, with a high strain hardening coefficient $D = dS/d\varphi$. Such a feature of the curve shape can be accounted for by introducing a third-degree polynomial of strain φ . Based on this logic, quadratic and cubic terms of the strain degree φ were added to the model in its logarithmic form:

$$\log(S) = A4 + B4 \log(\varphi) + C4 \log(\varphi)^2 + D4 \log(\varphi)^3 + E4(\varphi) + \frac{F4(\varphi)}{\log(\varphi)}. \quad (4c)$$

In its direct form, this expression is described by the equation

$$S = \exp \frac{A5 + E5(\varphi) + \frac{F5(\varphi)}{\log(\varphi)}}{\varphi^{B5 + C5 \log(\varphi) + D5 [\log(\varphi)]^2}}. \quad (4d)$$

With this representation, the parameter Q for individual curves decreases from 0.3 to 1.0 %.

Taking all of the above into account, a modified mathematical model was developed to describe the complete dataset. The modifications to the model (1.1) in its logarithmic form (1.1a) were as follows:

– terms accounting for the degree of deformation φ and the strain rate φ' were introduced (under the exponen-

tial sign) into the multiplier that accounts for the effect of deformation temperature;

– the mutual influence of independent factors on each other was accounted for by adding a multiplier $(\varphi\varphi')$;

– dependencies on the square and cube of the strain degree φ were introduced through corresponding multipliers.

The general form of the equation for the relationship between variables, after being reduced to a linear form by logarithmization, looks as follows:

$$\log(S) = A + B \log(\varphi) + C [\log(\varphi)]^2 + D [\log(\varphi)]^3 + E \log(\varphi') + F \log(\varphi) \log(\varphi') + G \left(\frac{\varphi}{\varphi'} \right) + \frac{H + K\varphi + M \log(\varphi) + N \log(\varphi') + P \log(\varphi) \log(\varphi')}{T}. \quad (5)$$

Finding the coefficients $A - P$ for equation (5), which ensures the minimum sum of squared differences between the calculated S_{calc} and experimental S_{exp} values, conducted using the Mathcad program, made it possible to obtain the desired equation for the relationship in the following form

$$\log(S) = -0.738 - 1.311 \log(\varphi) - 0.564 [\log(\varphi)]^2 - 0.13 [\log(\varphi)]^3 + 0.584 \log(\varphi') - 8.779 \cdot 10^{-4} \log(\varphi) \log(\varphi') - 1.18 \cdot 10^{-3} \left(\frac{\varphi}{\varphi'} \right) + \frac{3.727 \cdot 10^3 + 82.351\varphi + 1.096 \cdot 10^{-3} \log(\varphi)}{T} + \frac{593.8 \log(\varphi') + 76.6 \log(\varphi) \log(\varphi')}{T}, \quad (6)$$

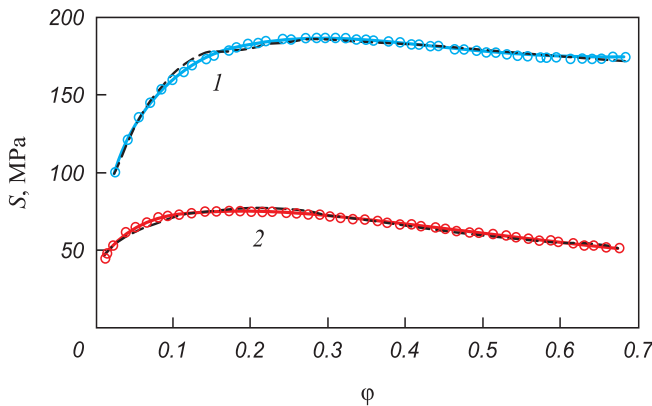


Fig. 3. Description of $S - \varphi$ dependences with formula (3):
 ○, ○ – experiment, dashed lines – calculated values;
 1 – $T = 1253 \text{ K}$, $\varphi' = 0.1 \text{ s}^{-1}$; 2 – $T = 1453 \text{ K}$, $\varphi' = 0.1 \text{ s}^{-1}$

Рис. 3. Описание зависимостей $S - \varphi$ формулой (3):

○, ○ – эксперимент, штриховые линии – расчетные значения;
 1 – $T = 1253 \text{ K}$, $\varphi' = 0,1 \text{ c}^{-1}$; 2 – $T = 1453 \text{ K}$, $\varphi' = 0,1 \text{ c}^{-1}$

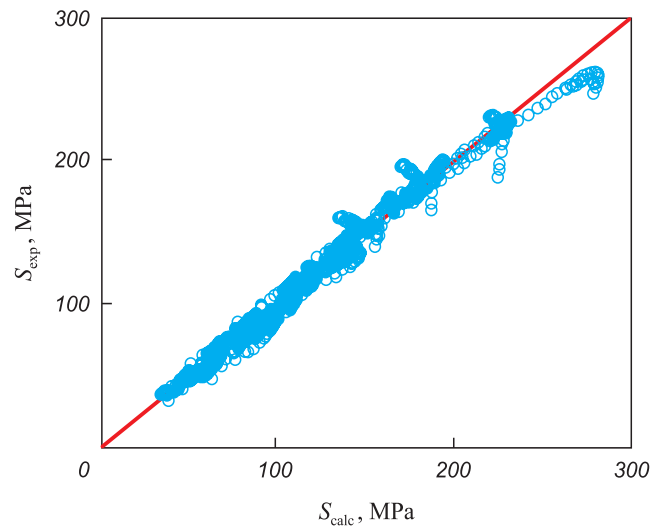


Fig. 4. Comparison of calculated and experimental stress values according to model (6a)

Рис. 4. Сопоставление расчетных и экспериментальных значений напряжений по модели (6a)

which can be transformed into its direct form:

$$S = 10^{-0.738} (\varphi')^{0.584} \times \varphi^{-1.311-0.564\log(\varphi)-0.131[\log(\varphi)]^2-8.779\cdot 10^{-4}\log(\varphi')} \times \exp\left[\frac{8583.3+198.7\varphi+2524\log(\varphi)}{T} - \frac{1367.5\log(\varphi') + 176.4\log(\varphi)\log(\varphi')}{T} - 2.718 \cdot 10^{-3} \left(\frac{\varphi}{\varphi'}\right)\right], \quad (6a)$$

or with the temperature component separated:

$$S = 10^{-0.738} (\varphi')^{0.584} \times \varphi^{-1.311-0.564\log(\varphi)-0.131[\log(\varphi)]^2-8.779\cdot 10^{-4}\log(\varphi')} \times \exp\left[-2.718 \cdot 10^{-3} \left(\frac{\varphi}{\varphi'}\right)\right] \times \exp\left[\frac{8583.3+198.7\varphi+2524\log(\varphi)}{T} - \frac{1367.5\log(\varphi') + 176.4\log(\varphi)\log(\varphi')}{T}\right]. \quad (6b)$$

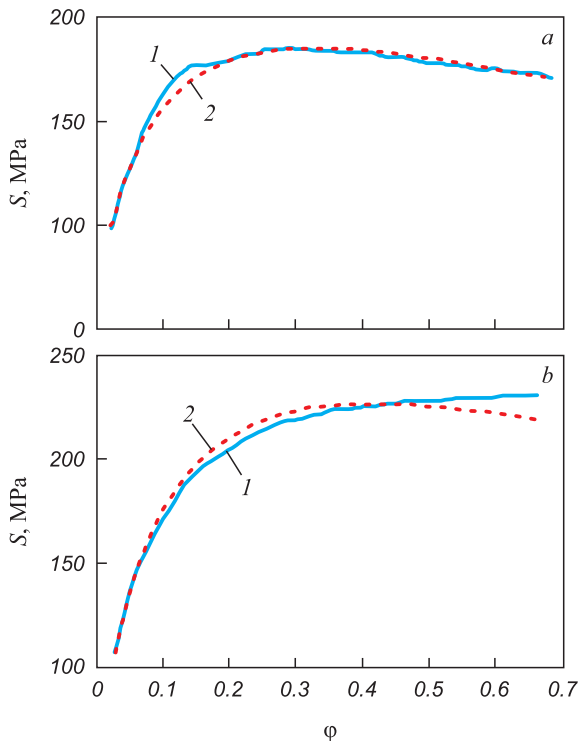


Fig. 5. Comparison of experimental (1) deformation curves and dependencies constructed according to equation (6a) (2).

Deformation modes:

a – 1253 K, 0.1 s⁻¹; b – 1253 K, 1.0 s⁻¹

Рис. 5. Сопоставление экспериментальных кривых деформации (1) и зависимостей, построенных по уравнению (6а) (2) при режимах деформации:

a – 1253 К, 0,1 с⁻¹; b – 1253 К, 1,0 с⁻¹

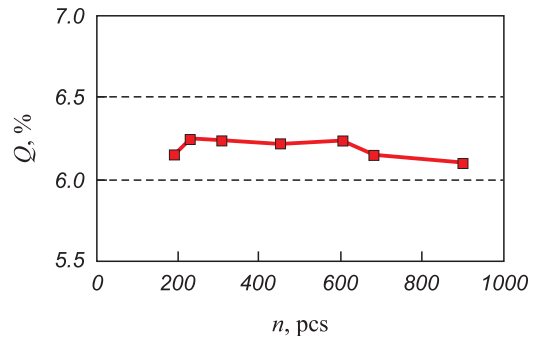


Fig. 6. Change in Q index of the generalized deformation model in the form (6a) depending on sample size (Y axis marks the range of observed values of Q)

Рис. 6. Изменение показателя Q обобщенной модели деформации в форме (6а) в зависимости от объема выборки (по оси Y отмечен диапазон наблюдавшихся значений Q)

A graphical illustration of the agreement between the calculated and experimental values of S is shown in Fig. 4. The quality indicator of this model, $Q = 6.1\%$, is significantly better than that of the original model, both qualitatively and quantitatively (compare with Fig. 2).

The obtained equation (6a) allows for predicting the shape of the deformation curve for various combinations of φ , φ' and T . Examples of such graphs, compared with experimental curves, are shown in Fig. 5. The presented graphs illustrate both “good” and “not-so-good” agreement between the calculated and experimental curves.

It is known from statistical theory [16] that increasing the sample size of experimental data can lead to improved accuracy in the description of a mathematical model (reducing its variance). To test this hypothesis, the number of original data points (the number of rows in the full matrix) was artificially reduced sequentially from ~900 to ~200, and the model quality indicator Q was recalculated. The results of these calculations are presented in Fig. 6. It can be seen that reducing the size of the experimental data sample by approximately 4 times (from 900 to 200) does not significantly affect the predictive quality of model (6a).

This unexpected result may reflect the fact that only a few characteristic points are decisive in shaping the modeled curve (in this respect, the methodology is similar to the aforementioned Johnson-Cook method).

An important test of the developed model’s functionality is its validation on other datasets. Using the methodology described above, the results of hot compression tests of materials from other groups were processed: heat-resistant nickel alloy $\text{Ni}_{33}\text{Cr}_{27}\text{Fe}_{35}\text{Mo}_{3.5}\text{Mn}_1\text{Cu}_{0.6}$ from the Inconel group [17], heat-resistant nickel alloys [18], and the $\text{Ni}_{56}\text{Cr}_{24}\text{Co}_{14}\text{Mo}_{0.5}\text{W}_1\text{Nb}_{1.5}\text{Al}_{1.5}\text{Ti}_{1.5}$ alloy from the Nimonic group [19], cobalt alloys [20; 21], ferritic heat-resistant Cr12 – Cr27 steels [22], heat-resistant 9 % chromium DUO steel [23], and steel 20Cr13 [24]. It was

found that the developed type of mathematical model is applicable to these cases as well. It is implied that for all these cases, the nomenclature and form of the multipliers in the relationship formula are unified across all studied alloys, though the coefficients for these multipliers, naturally, differ. The predictive quality, evaluated by the Q , indicator ranged from 3 to 11 %.

CONCLUSIONS

A generalized mathematical model in multiplicative form has been proposed, which describes the relationship between stress, strain, strain rate, and temperature during large hot deformations (up to a true strain degree of 0.8), at temperatures ranging from 0.6 to $0.85T/T_{\text{melt}}$ and strain rates between 0.01 and 10 s^{-1} . The model predicts deformation force with an accuracy of approximately 6 %, without relying on a priori (tabulated) or pre-determined structural, mechanical, or energy characteristics.

The multipliers used in the developed mathematical model reflect experimentally observed interdependencies between the independent variables (φ , φ' , T) and the specific features of the deformation curves.

It has been established that this mathematical model is applicable to a wide range of metallic materials undergoing hot deformation, with predictive accuracy for deformation stress characteristics ranging from 3 to 11 %.

The obtained data allow for the analysis of not only test results with a fixed true strain rate φ' – which is methodologically complex – but also results from experiments conducted using the traditional method with a constant nominal strain rate $\dot{\varepsilon}$, where the true strain rate φ' is not constant.

REFERENCES / СПИСОК ЛИТЕРАТУРЫ

- Shtremel' M.A. Alloy Strength. Part 2. Deformation. Moscow: MISIS; 1997:527. (In Russ.).
Штремель М.А. Прочность сплавов. Ч. 2. Деформация. Москва: МИСИС; 1997:527.
- Hollomon J.H. Tensile deformation. *Trans AIME*. 1945; 162:268–290.
- Rosenberg V.M. Fundamentals of Heat Resistance of Metallic Materials. Moscow: Metallurgiya; 1973:328. (In Russ.).
Розенберг В.М. Основы жаропрочности металлических материалов. Москва: Металлургия; 1973:328.
- Ludwigson D.C. Modified stress-strain relation for FCC metals and alloys. *Metallurgical Transactions A*. 1971;2(10): 2825–2828. <https://doi.org/10.1007/BF02813258>
- Bershtein M.L., Zaimovskii V.A. Mechanical Properties of Metals. Moscow: Metallurgiya; 1979:496. (In Russ.).
Берштейн М.Л., Займовский В.А. Механические свойства металлов. Москва: Металлургия; 1979:496.
- Zener C., Hollomon J. H. Effect of strain rate upon plastic flow of steel. *Journal of Applied Physics*. 1944;15(1):22–32. <https://doi.org/10.1063/1.1707363>
- Bird J.E., Mukherjee A.K., Dorn J.E. Experimental correlations between high-temperature creep behavior and structure. In: *Quantitative Relation Between Properties and Microstructure*. Brandon D.G., Rosen A. eds. Jerusalem University Press; 1969:255–342.
- Johnson G.R., Cook W.H. Fracture characteristics of three metals subjected to various strains, strain rates, temperatures and pressures. *Engineering Fracture Mechanics*. 1985;21(1):31–48. [https://doi.org/10.1016/0013-7944\(85\)90052-9](https://doi.org/10.1016/0013-7944(85)90052-9)
- Sellars C.M., McTegart W.J. Cavity growth mechanisms during creep. *Acta Metallurgical*. 1966;14:1136–1138.
- Sun C., Liu G., Zhang Q., Li R., Wang L. Determination of hot deformation behavior and processing maps of IN 028 alloy using isothermal hot compression test. *Materials Science and Engineering: A*. 2014;595:92–98. <https://doi.org/10.1016/j.msea.2013.10.051>
- Fang B., Ji Z., Liu M., Tian G., Jia C., Zeng T., Benfu HU, Wang C. Study on constitutive relationships and processing maps for FGH96 alloy during two-pass hot deformation. *Materials Science and Engineering: A*. 2014;590:255–261. <https://doi.org/10.1016/j.msea.2013.10.034>
- Xiao Y.-H., Guo C. Constitutive modeling for high temperature behavior of 1Cr12Ni3Mo2VNbN martensitic steel. *Materials Science and Engineering: A*. 2011;528(15): 5081–5087. <https://doi.org/10.1016/j.msea.2011.03.050>
- Zerilli F.J., Armstrong R.W. Dislocation-mechanics-based relations for material dynamics calculations. *Journal of Applied Physics*. 1987;61(5):1816–1825. <https://doi.org/10.1063/1.338024>
- Belomyttsev M.Yu. Experimental analysis of creep regularities of high-temperature ferritic-martensitic steel. *Deformatsiya i razrushenie materialov*. 2019;(10):31–41. (In Russ.).
Беломытцев М.Ю. Экспериментальный анализ закономерностей ползучести жаропрочной ферритно-мартенситной стали. *Деформация и разрушение материалов*. 2019;(10):31–41.
- Belomyttsev M.Yu., Molyarov V.G. Creep resistance of ferritic-martensitic steel 16Cr12MoWSiVNbB (EP-823). *Izvestiya. Ferrous Metallurgy*. 2019;62(4):290–302. (In Russ.). <https://doi.org/10.17073/0368-0797-2019-4-290-302>
Беломытцев М.Ю., Моляров В.Г. Исследование сопротивления ползучести ферритно-мартенситной стали 16X12MBCФБР (ЭП-823). *Известия вузов. Черная металлургия*. 2019;62(4):290–302. <https://doi.org/10.17073/0368-0797-2019-4-290-302>
- Melnichenko A.S. Statistical Analysis in Metallurgy and Materials Science: Textbook. Moscow: MISIS; 2009:268. (In Russ.).
Мельниченко А.С. Статистический анализ в металлургии и материаловедении: Учебник. Москва: Издательский Дом МИСИС; 2009:268.
- Wang L., Liu F., Cheng J.J., Zuo Q., Chen C.F. Hot deformation characteristics and processing map analysis for Nickel-based corrosion resistant alloy. *Journal of Alloys and Compounds*. 2015;623:69–78. <https://doi.org/10.1016/j.jallcom.2014.10.034>
- Pan Q.L., Li B., Wang Y., Zhang Y.W., Yin Z.M. Characterization of hot deformation behavior of Ni-base superalloy

- Rene'41 using processing map. *Materials Science and Engineering: A*. 2013;585:371–378.
<https://doi.org/10.1016/j.msea.2013.07.066>
19. Wu Y., Zhang M., Xie X., Dona J., Lin F., Zhao S. Hot deformation characteristics and processing map analysis of a new designed nickel-based alloy for 700 °C A-USC power plant. *Journal of Alloys and Compounds*. 2016;656:119–131.
<https://doi.org/10.1016/j.jallcom.2015.09.219>
 20. Kumar V.A., Gupta R.K., Murty S.V.S. Narayana, Prasad A.D. Hot workability and microstructure control in Co20Cr15W10Ni cobalt based superalloy. *Journal of Alloys and Compounds*. 2016;676:527–541.
<https://doi.org/10.1016/j.jallcom.2016.03.186>
 21. Kartica Ika, Matsumoto H., Chiba A. Deformation and microstructure evolution in Co-Ni-Cr-Mo superalloy during hot working. *Metallurgical and Materials Transactions A*. 2009;40:1457–1468.
<https://doi.org/10.1007/s11661-009-9829-x>
 22. Mehtonen S.V., Karjalainen L.P., Porter D.A. Modeling of the high temperature flow behavior of stabilized 12 – 27wt% Cr ferritic stainless steels. *Materials Science and Engineering: A*. 2014;607:44–52.
<https://doi.org/10.1016/j.msea.2014.03.124>
 23. Zhang G., Zhou Z., Sun H., Zou L., Wang M., Li S. Hot deformation behavior and processing map of a 9Cr ferritic/martensitic ODS steel. *Journal of Nuclear Materials*. 2014;455(1-3):139–144.
<https://doi.org/10.1016/j.jnucmat.2014.05.043>
 24. Akhmed'anov A.M., Rushchits S.V., Smirnov M.A. Physical and numerical modeling of hot deformation behaviour of 20Kh13 steel. *Bulletin of SUSU. Series "Metallurgy"*. 2013;13(2):116–124. (In Russ.).
 Ахмедьянов А.М., Рушиц С.В., Смирнов М.А. Физическое и математическое моделирование горячей деформации стали 20Х13. *Вестник ЮУрГУ. Серия «Металлургия»*. 2013;13(2):116–124.

Information about the Author

Сведения об авторе

Mikhail Yu. Belomytsev, Dr. Sci. (Eng.), Prof. of the Chair "Metallography and Physics of Strength", National University of Science and Technology "MISIS"

E-mail: myubelom@yandex.ru

Михаил Юрьевич Беломятцев, д.т.н., профессор кафедры металловедения и физики прочности, Национальный исследовательский технологический университет «МИСИС»

E-mail: myubelom@yandex.ru

Received 27.02.2024
 Revised 29.06.2024
 Accepted 22.08.2024

Поступила в редакцию 27.02.2024
 После доработки 29.06.2024
 Принята к публикации 22.08.2024

Над номером работали:

Л.И. Леонтьев, главный редактор

Е.В. Протопопов, заместитель главного редактора

Е.А. Ивани, ответственный секретарь

Л.П. Башенко, заместитель ответственного секретаря

Е.Ю. Потапова, заместитель главного редактора по развитию

О.А. Долицкая, научный редактор

Е.М. Запольская, ведущий редактор

А.О. Гашникова, ведущий редактор

В.В. Расенец, верстка, иллюстрации

Г.Ю. Острогорская, менеджер по работе с клиентами

Подписано в печать 20.10.2024. Формат 60×90 ¹/₈. Бум. офсетная № 1.
Печать цифровая. Усл. печ. л. 16,75. Заказ 20701. Цена свободная.

Отпечатано в типографии Издательского Дома МИСИС.
119049, Москва, Ленинский пр-кт, д. 4, стр. 1.
Тел./факс: +7 (499) 236-76-17



History and current state of metallurgy in St. Petersburg

Recent development in powder metallurgy of high entropy alloys for high-temperature applications. Brief review

Assessment of the effectiveness of technological measures to extend the campaign of blast furnace No. 5 of PJSC Severstal (2006 – 2024) based on an examination of its working space during a first-category overhaul

A study on processing of blast furnace dust and sludge using reduction roasting and magnetic separation

Mineralogical and granulometric composition of soils formed on the surface of iron ore tailings dumps

Formation of non-metallic inclusions in production of O8Kh18N10T corrosion-resistant steel

Deformation and fracture of heat treated ribbon of amorphous Co – Fe – Cr – Si – B alloy during indentation

Structural-phase states and properties of high-speed surfacing after tempering and electron beam processing

Simulation of structural changes in metal under high-intensity external influence

Effect of silicon and vanadium on corrosion-mechanical properties of high-nitrogen Cr – Mn steels

Microheterogeneous structure of liquid cast irons IChKh28N2 and ICh310Kh24M2F4TR

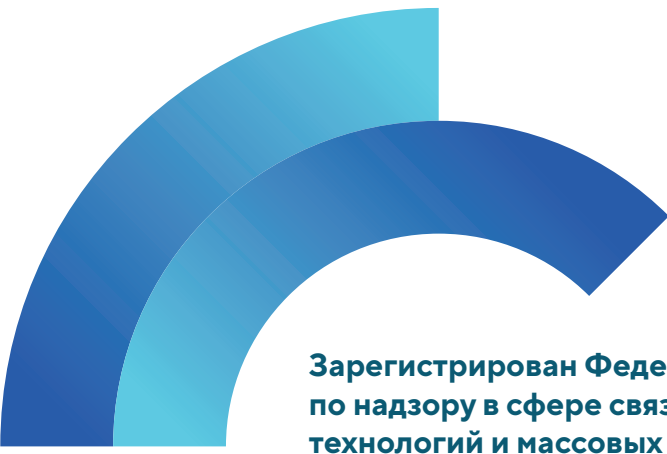
Influence of compression modes of waxy powders on stress-strain state of compacts used in precision casting

Influence of combined thermal effect of electric arc welding with aluminothermic backfill on internal stresses in a steel plate

Improving the efficiency of raw material preparation for metallurgical processing

Type of generalized mathematical model for describing large hot deformations

To the 75th Anniversary of Nikolai Aleksandrovich Spirin



**Зарегистрирован Федеральной службой
по надзору в сфере связи, информационных
технологий и массовых коммуникаций.
Свидетельство о регистрации
ПИ № ФС77-35456.**

Подписной индекс 70383.

